Quantum Simulation of Renormalized Quantum Field Theory Hamiltonians

A dissertation

submitted by

Carter Mulford Gustin

In partial fulfillment of the requirements
for the degree of

Doctor of Philosophy

in

Physics

TUFTS UNIVERSITY

May 2026

ADVISORS: Prof. Gary R. Goldstein

Prof. Peter J. Love

DOCTORAL COMMITTEE: Prof. Timothy Atherton

Prof. Mark Hertzberg

Prof. Martin Savage

Abstract

Quantum Simulation of Renormalized Quantum Field Theory Hamiltonians

Carter Mulford Gustin

ADVISOR: Prof. Gary R. Goldstein

ADVISOR: Prof. Peter J. Love

We are beginning to enter the 'Early Fault Tolerant Quantum Computing' (EFTQC) era which promises *quantum advantage* – useful problem instances that can be solved more efficiently on quantum architecture in comparison to its classical counterparts. One prospective field that may lead to the first demonstrations of quantum advantage is quantum simulation. To this end, this thesis aims to formalize quantum simulation of quantum field theories in the EFTQC era, which serve as a source of potential quantum advantage.

Through newly developed quantum algorithms, we propose an end-to-end framework for computing relevant physical properties from quantum field theories that can be compared to experiment and lattice QCD. Quantum field theory Hamiltonians, renormalized via the Renormalization Group Procedure for Effective Particles, serve as the input, while the output is any interesting observable – hadronic mass spectrum, parton distribution functions, etc.

Throughout this thesis, we answer the question of how do we assemble this framework, and additional questions, such as: "When will quantum computers be big enough to solve these problems", and "Can we accelerate timelines to quantum advantage for quantum simulation of quantum field theories in this new framework?"

For Papa

Acknowledgments

I consider myself extremely lucky to be in the position I am in. Had it not been for the people I've surrounded myself with, I would not be writing and defending this thesis.

I first thank my best friend, my fiancée Deanna. I would not be at Tufts, and likely would not be writing a thesis at all, if it wasn't for her. The love and care she gives me every day, along with our two cats, Sullivan and Kenmore, fueled me throughout my Ph.D. They are the reason I get out of bed in the morning, and not just because the cats need to be fed.

I would not be here without the support of my parents. My education is directly a result of my mother reading with us every night growing up, and my father waking up at 4 a.m. to put us through college. I will never be able to repay what they have given to me. I also thank my best friend, my brother, Brett. Brett is three years younger than I am; however, I look up to him in a way that is typical of a younger brother aspiring to be like his older brother. I thank his girlfriend Martine who I didn't know before I started grad school, but has become one of the most important people in my life over the last four years. Lastly, I thank my family for supporting me throughout my Ph.D. – my papa, who passed away during my first year, my nana, my grandma, and my Aunt Linda and Uncle Woody, as well as Deanna's immediate family – Ron, Denise, Danielle, and Sean.

I have made some lifelong friends during my Ph.D., in particular Drs. Alexis Ralli, Michael Dolce, Jack Thomas, and Anuja Jayasekara. I thank the four of them for the many pints of beer we've shared, as well as being some of the biggest supporters of my work. While I cannot thank the entirety of the Tufts physics and astronomy graduate student body by name, I specifically must thank three current

graduate students, Ian Descamps, Udathari Kumarasinghe, and Rebecca Sipen for our close friendship.

I attribute the quality of my thesis largely to my research group (both past and present), but in particular to Dr. Kamil Serafin and (soon to be Dr.) William Simon. They both taught me more about quantum field theory and quantum algorithms respectively, than anyone else. In addition to my research group, I must thank my two advisors, Prof. Gary Goldstein and Prof. Peter Love for their patience and interest they put into my work. They both pushed me to become the scientist I am today, and for that I will be forever grateful. I thank the rest of my doctoral committee – Prof. Tim Atherton and Prof. Mark Hertzberg at Tufts for supporting my work and being fantastic educators throughout my coursework at Tufts. I also thank my external committee member, Prof. Martin Savage for taking time out of his busy schedule to read my thesis.

External to Tufts, I thank Prof. James Vary and Dr. Michael Kreshchuk, both who had strong influences over my work, and cared about my success in this field, with no external motivation to do so. Lastly, I thank NuHaQ (nuclei and hadrons for quantum computing), and the Burlingame Fellowship for financial support throughout my Ph.D.

This thesis contains work previously published [SGS+25, SGL25, GSS+26].

Carter Mulford Gustin

TUFTS UNIVERSITY

May 2026

Contents

List of Tables

List of Figures

Chapter 1

Introduction

Quantum simulation, that is using quantum computers to simulate phenomena in quantum physics, was the original motivation for quantum computing [Fey18a]. Today, quantum simulation is used to probe "*quantum advantage*" – useful problem instances that can be solved more efficiently on quantum architecture. Determining problems in fundamental physics where quantum computers may give quantum advantage over their classical counterparts has lead to the rapid expansion of this field. The most 'fundamental' physics problems arguably arise in high energy particle and nuclear physics, making these problems ideal candidates for quantum advantage.

The genesis of quantum field theories as a problem instance of quantum simulation comes from a ~ 15 year old paper by Stephen Jordan, Keith Lee, and John Preskill [JLP12]. Since then, this field has rapidly expanded with the overwhelming majority of work done using the framework proposed by Jordan, Lee, and Preskill.

The work in this thesis follows an alternative framework proposed by Kreshchuk et al. in [KKG$^+$22]. The main criticism of this work is that the results all come from *bare* (unrenormalized) Hamiltonians, and do not lead to physical observables. This thesis aims to quell this criticism and answer the question: "Are renormalized Hamiltonians in the light-front formalism prohibitively more expensive for quantum simulation than the corresponding bare unphysical Hamiltonians?" Furthermore, this dissertation aims to formalize quantum simulation of quantum field theories in the early fault-tolerant quantum computing era using a renormalization procedure

called the Renormalization Group Procedure for Effective Particles to produce physical, finite results. Aided by novel quantum algorithms based on a technique known as block-encoding in which we have reduced the necessary computational cost, we propose an end-to-end framework to compute physical observables from quantum field theories. We attempt to answer an additional question: "Can we accelerate timelines to achieve quantum advantage for quantum simulation of quantum field theories?"

In this introductory Chapter, we discuss the history and basic mathematical principles of quantum information and quantum computing. From here, we discuss early fault-tolerant quantum computers and relevant quantum algorithms that are the pillars of this era.

1.1 An Introduction to Quantum Computation

The conceptual birth of quantum computation has been largely attributed to a 1981 lecture given by Richard Feynman [Fey18a] at a physics conference at MIT [ACM24]. Feynman's proposal revolved around a simple principle: the quantum wavefunction lives in an exponentially large Hilbert space, so representing a wavefunction on a classical processor, with classical bits, requires *exponential* overhead (e.g. number of bits). Alternatively, given a processor that is instead built with quantum bits (qubits), one can represent the same complex wavefunction with a *linear* number of qubits. This exponential reduction in memory stems from quantum states obeying the superposition principle and their ability to become entangled. As an important and relevant historical note, quantum computation was postulated concurrently to Feynman independently by both Yuri Manin [Man80] and Pauli Benioff [Ben79].

Fifteen years after Feynman's original lecture on this subject, Seth Lloyd proved Feynman's conjecture in [Llo96]. In his work, Lloyd states simulation is "a process by which one system is made to mimic another". Today, *quantum* simulation colloquially refers to two broad categories: the estimation of static properties, e.g. energy estimation, or simulating quantum dynamics, e.g. time evolution of

a quantum state. Within the last ten years, we have seen experimental results of quantum advantage for quantum simulation. These claims of advantage first came from models such as the Ising chain [CMN$^+$18] and the Hubbard model [DBK$^+$22].

The first experimental realizations of quantum computers arose less than 10 years after Feynman/Manin/Benioff by Kazuhiro Igeta and Yoshihisa Yamamoto [IY88]. The first demonstration of a quantum gate was performed by Chris Monroe et al. [MMK$^+$95], in which they entangled two qubits through a controlled-NOT gate. In 2000, David DiVincenzo proposed his "DiVincenzo" criteria [DiV00] of what is needed for a physical quantum computer:

1. A scalable physical system with well-characterized qubits
2. The ability to initialize the qubits to a simple fiducial state
3. Long decoherence times
4. A universal set of quantum gates to approximate the action of any qubit operation
5. A qubit-specific measurement capability

In order to thoroughly understand this criteria, we discuss the basics of quantum information and computation by describing quantum bits, quantum gates and measurement.

1.1.1 Qubits

The fundamental unit of classical computation is the bit – a logical state that takes on values of 0 *or* 1. The quantum analog to the bit is the qubit, which is the fundamental memory unit of quantum computation. Qubits are represented by quantum state vectors whose state can be expressed as linear superpositions of the basis states $|0\rangle$ *and* $|1\rangle$, with coefficients $\in \mathbb{C}$:

$$|\psi\rangle = \alpha\,|0\rangle + \beta\,|1\rangle = \alpha \begin{pmatrix} 1 \\ 0 \end{pmatrix} + \beta \begin{pmatrix} 0 \\ 1 \end{pmatrix} = \begin{pmatrix} \alpha \\ \beta \end{pmatrix}, \tag{1.1}$$

subject to the constraint $\langle\psi|\psi\rangle = 1$, which for a single qubit implies $|\alpha|^2 + |\beta|^2 = 1$. An arbitrary pure quantum state lives at a point on the surface of the Bloch sphere, depicted in Fig. 1.1 and can be written as

$$|\psi\rangle = \cos\Big(\frac{\theta}{2}\Big)|0\rangle + e^{i\phi}\sin\Big(\frac{\theta}{2}\Big)|1\rangle, \tag{1.2}$$

where $\theta \in [0, \pi]$ and $\phi \in [0, 2\pi)$.

The quantum state of a two-qubit system arises from taking the tensor product of the two individual qubit states:

$$\begin{aligned} |\psi\rangle \otimes |\phi\rangle &= \Big(\alpha_0 |0\rangle + \beta_0 |1\rangle\Big) \otimes \Big(\alpha_1 |0\rangle + \beta_1 |1\rangle\Big) \\ &= \alpha_0\alpha_1 |00\rangle + \alpha_0\beta_1 |01\rangle + \beta_0\alpha_1 |10\rangle + \beta_0\beta_1 |11\rangle = \begin{pmatrix} \alpha_0\alpha_1 \\ \alpha_0\beta_1 \\ \beta_0\alpha_1 \\ \beta_0\beta_1 \end{pmatrix}. \end{aligned} \tag{1.3}$$

We can also represent the above state in compact notation by mapping each binary qubit state to its corresponding integer, i.e. $\alpha_0\alpha_1 |0\rangle + \alpha_0\beta_1 |1\rangle + \beta_0\alpha_1 |2\rangle + \beta_0\beta_1 |3\rangle$. In general, an n-qubit state can be represented by this compact notation

$$|\psi\rangle = \sum_{l=0}^{2^n-1} \alpha_l |l\rangle . \tag{1.4}$$

We define the basis of states of the form $\Big\{ |l\rangle : l \in \mathbb{Z}\Big\}$ as the *computational basis*.

States of the form $|\psi\rangle \otimes |\phi\rangle$ are said to be *separable*: the overall quantum state can be separated into a tensor product of individual quantum states of its constituents. Any quantum state that is not separable is called *entangled*. For example the normalized superposition of the computational basis states $|00\rangle$ and $|11\rangle$, called a Bell state, is an entangled state, i.e.

$$\frac{1}{\sqrt{2}}\Big(|00\rangle + |11\rangle \Big) \neq |\psi\rangle \otimes |\phi\rangle , \tag{1.5}$$

for any $|\phi\rangle$ or $|\psi\rangle$.

If two states differ simply by a global phase, they will be indistinguishable from each other, that is no experiment can be performed to distinguish one from the other. For example, the basic superposition of the single qubit computational basis states $\alpha|0\rangle + \beta|1\rangle$ is indistinguishable from the state: $e^{i\varphi}\Big(\alpha|0\rangle + \beta|1\rangle\Big)$, where $e^{i\varphi}$ is a global phase. The differences in these states cannot be resolved by experiment because Born's rule will lose the phase information.

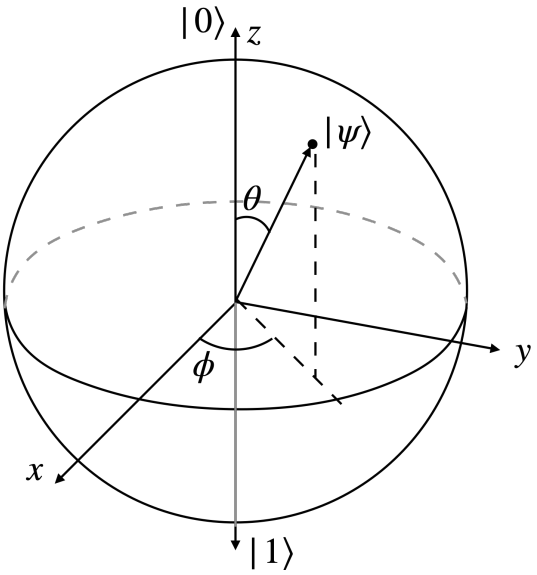

Figure 1.1: **Bloch Sphere**: An arbitrary pure quantum state lives on the surface of the Bloch sphere and can be written $|\psi\rangle = \cos\left(\frac{\theta}{2}\right)|0\rangle + e^{i\phi}\sin\left(\frac{\theta}{2}\right)|1\rangle$.

1.1.2 Gates

Qubits are manipulated by action of quantum gates, analogous to classical logical gates changing the state of a bit (or bits):

$$|\psi'\rangle = U|\psi\rangle\,. \tag{1.6}$$

All gates in quantum computation must be unitary:

$$U^\dagger U = UU^\dagger = \mathbb{1}. \tag{1.7}$$

This is a strict requirement as it maintains the normalization of the wavefunction (i.e. it satisfies the constraint outlined above that $\langle\psi|\,\psi\rangle = 1$.):

$$\langle\psi|\psi\rangle = \langle\psi|\,U^\dagger U\,|\psi\rangle = 1 \iff U^\dagger U = UU^\dagger = \mathbb{1}. \tag{1.8}$$

An example of a unitary gate is the quantum analog of the classical **NOT** gate, the Pauli X gate, which switches $|0\rangle \leftrightarrow |1\rangle$:

$$\begin{cases} X\,|0\rangle = |1\rangle \\ X\,|1\rangle = |0\rangle\,. \end{cases}$$

In the computational basis (which all matrices in this Section will be written in), the matrix form of Pauli X is

$$X = \begin{pmatrix} 0 & 1 \\ 1 & 0 \end{pmatrix}.$$

Similarly, one can define the gates Pauli Y and Pauli Z:

$$Y = \begin{pmatrix} 0 & -i \\ i & 0 \end{pmatrix} \qquad Z = \begin{pmatrix} 1 & 0 \\ 0 & -1 \end{pmatrix} \tag{1.9}$$

The Pauli gates can be interpreted about reflections of the qubit state around the corresponding axis. The Pauli operators are n-fold tensor products of the Pauli matrices ($\{I, X, Y, Z\}$) on n qubits.

Another useful gate is the Hadamard gate, which maps the qubit basis states to superpositions over the basis:

$$\begin{cases} H\,|0\rangle = \frac{1}{\sqrt{2}}\Big(\,|0\rangle + |1\rangle\,\Big) \\ H\,|1\rangle = \frac{1}{\sqrt{2}}\Big(\,|0\rangle - |1\rangle\,\Big). \end{cases}$$

The Hadamard gate also generates uniform superpositions over the computational

basis states:

$$H^{\otimes n}|0\rangle^{\otimes n} = \frac{1}{\sqrt{2^n}} \sum_{l=0}^{2^n-1} |l\rangle. \tag{1.10}$$

There also exists a class of unitary gates which rotate the state vector around the x, y, and z axes of the Bloch sphere, called arbitrary Pauli rotation gates:

$$R_x(\theta) = \begin{pmatrix} \cos\frac{\theta}{2} & -i\sin\frac{\theta}{2} \\ -i\sin\frac{\theta}{2} & \cos\frac{\theta}{2} \end{pmatrix} \qquad R_y(\theta) = \begin{pmatrix} \cos\frac{\theta}{2} & -\sin\frac{\theta}{2} \\ \sin\frac{\theta}{2} & \cos\frac{\theta}{2} \end{pmatrix} \tag{1.11}$$

$$R_z(\theta) = \begin{pmatrix} e^{-i\theta/2} & 0 \\ 0 & e^{i\theta/2} \end{pmatrix}. \tag{1.12}$$

Sometimes, the $R_z(\theta)$ gate is written instead in the form $\mathrm{diag}(1, e^{i\theta})$, which is the same up to an arbitrary global phase. This alternative way of writing it is nice because it is simple to define two more useful gates from this: the S and T gates:

$$S = \begin{pmatrix} 1 & 0 \\ 0 & i \end{pmatrix} \qquad T = \begin{pmatrix} 1 & 0 \\ 0 & e^{i\pi/4} \end{pmatrix}. \tag{1.13}$$

It should be obvious from this definition that $S = R_z(\pi/2) = \sqrt{Z}$ and $T = R_z(\pi/4) = Z^{1/4}$.

Another class of gates are n-qubit gates. A canonical example of these is the **CNOT** or controlled-X gate. The controlled-X gate acts on two qubits: a control qubit and a target qubit. The gate itself is designed to flip the target qubit from $|0\rangle \leftrightarrow |1\rangle$ if the control qubit is in the $|1\rangle$ state. In matrix form:

$$\textbf{CNOT} = \begin{pmatrix} 1 & 0 & 0 & 0 \\ 0 & 1 & 0 & 0 \\ 0 & 0 & 0 & 1 \\ 0 & 0 & 1 & 0 \end{pmatrix} \tag{1.14}$$

The **CNOT** gate forms entangled states from separable states, which will become obvious when we discuss the Bell state below. The **CNOT** is explicitly a

controlled-X gate, which leads one to define arbitrary controlled unitaries. These unitaries are applied to target qubit(s) if the control qubit is in the $|1\rangle$ state. In matrix form:

$$\text{controlled} - U = \begin{pmatrix} \mathbb{1} & 0 \\ 0 & U \end{pmatrix}. \tag{1.15}$$

We close this section on quantum gates with some common definitions about groups of quantum gates [RWL25].

Definition 1.1.1 *The Pauli group on n qubits, $\mathcal{P}_n$, is the set of all Pauli operators with coefficients $\{\pm 1, \pm i\}$*

Definition 1.1.2 *The Clifford group on n qubits, $\mathcal{C}_n$, is the normalizer of the Pauli group, that is conjugation of any operator $O \in \mathcal{P}_n$ with a member of the Clifford group returns an element of the Pauli group.*

Definition 1.1.3 *The stabilizer group on n qubits $\mathcal{S}_n$ is a subset of the Pauli group whose members all commute with each other and $-I \notin \mathcal{S}_n$.*

From the last definition, we can define a state $|\psi\rangle$ as a stabilizer state if $S|\psi\rangle = |\psi\rangle$ $\forall S \in \mathcal{S}_n$. By the Gottesman-Knill theorem [NC10], stabilizer states can be efficiently reached by the state $|0\rangle^{\otimes n}$ using only gates from the Clifford group. This implies that stabilizer states can be efficiently simulated classically.

A set of quantum gates is *universal* if the set can approximate any unitary up to some error. A common example of a universal gate set is $\{H, S, T, \mathbf{CNOT}\}$, commonly referred to as "Clifford + T". This is a popular choice for quantum computing architectures which utilize the surface code.

1.1.3 The Circuit Model

The actions of gates on qubits can be realized diagrammatically by the quantum circuit model. Each qubit in a quantum circuit is represented by a single wire in which time progresses from left to right. Gates are represented by boxes or circles and act on one or more qubits that live on the corresponding wire(s). A quantum

$$|q_n\rangle \text{ ——}$$
$$|q_n \dots q_0\rangle \leftrightarrow \quad \vdots \tag{1.16}$$
$$|q_0\rangle \text{ ——}$$

Figure 1.2: **State vector-circuit correspondence**. Note this choice is convention only and is referred to as big-endian notation.

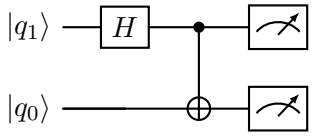

Figure 1.3: **Example Circuit Diagram**: Circuit diagram that creates the Bell state: $\frac{1}{\sqrt{2}}\Big(|00\rangle + |11\rangle\Big)$. The rightmost gates are measurement gates which collapse the wavefunction to a classical bitstring via measurement.

register is a collection of one of more wires, and generally are grouped based on their function. The ordering of the qubit wires and relation to the qubit states is a notational choice. In this thesis qubits are numbered from q_0 to q_n, where q_n is the top-most qubit in the circuit model and the left-most qubit in the state ket, see Fig. 1.2.

In the case of multiple qubits, sometimes subscripts are given to the unitaries to dictate which qubits they act one, while other times this is obvious from context. For example, the operation

$$(\mathbf{CNOT}_{0,1})(\mathbb{1}_1 \otimes H_0)\,|00\rangle$$

first applies a Hadamard gate to qubit 0 (while applying nothing to qubit 1), followed by a **CNOT** gate (with subscript (control qubit, target qubit)). In the circuit model, this is represented by the circuit in Fig. 1.3. In general, the qubits start in the $|0\rangle$ state, unless otherwise stated.

The Toffoli gate extends the **CNOT** gate to include an additional control

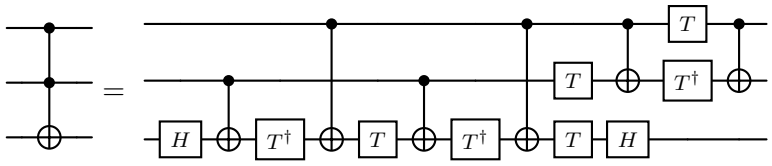

Figure 1.4: **Toffoli decomposition**: An aribtrary Toffoli gate can be decomposed using seven T-gates, six CNOT's, and two Hadamard gates.

qubit (i.e. two controls, one target). In matrix form the Toffoli gate is given by

$$\mathbf{Toff} = \begin{pmatrix} 1 & 0 & 0 & 0 & 0 & 0 \\ 0 & 1 & 0 & 0 & 0 & 0 \\ 0 & 0 & 1 & 0 & 0 & 0 \\ 0 & 0 & 0 & 1 & 0 & 0 \\ 0 & 0 & 0 & 0 & 0 & 1 \\ 0 & 0 & 0 & 0 & 1 & 0 \end{pmatrix}. \tag{1.17}$$

The Toffoli gate must be decomposed into Hadamard and T-gates, where an explicit decomposition is given in Fig. 1.4.

For controlled operations, it is often common that one will want to control a gate on the condition that the control qubit is in a state other than the $|1\rangle$ state. We can define 0-controlled gates to be controlled gates whose application on the target state is contingent on the control qubit being in the $|0\rangle$ state. In the circuit model, an open circle control (rather than the closed dot in Fig. 1.3) signifies a control gate acting on the target if the control qubit is in the state $|0\rangle$.

In many algorithms throughout this thesis, multiple qubits will be used as controls. For example, a controlled-U gate, controlled by the computational basis state $|101\rangle$ is shown as an example in Fig. 1.5. Decomposing multi-controlled gates into elementary gates is a challenging endeavour and the focus of much current research. A further discussion on this decomposition will be done in Chapter 3.

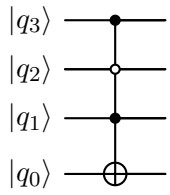

Figure 1.5: **Multi-controlled Gate**: The target qubit, q_0 is controlled by the qubits q_3, q_2, q_1 being in the computational basis state $|101\rangle$.

1.1.4 Measurement

Measurement is performed by the addition of measurement operations (rightmost boxes in Fig. 1.3), generally at the end of a quantum circuit. Measurement collapses the wavefunction onto a classical bitstring. Running multiple shots (state preparation, circuit execution, and measurement) builds up a classical probability distribution over computational basis states which gives insight into the final wavefunction after the action of the unitaries in the circuit. Measurement probabilities are calculated via Born's rule: $p(m) = |\langle\psi| M_m^\dagger M_m |\psi\rangle|^2$, where M_m is a measurement operator [NC10]. Measurement in a single basis is not sufficient to fully reconstruct the final state vector.

For example, consider the Bell-state prepared by the circuit in Fig. 1.3. Right before measurement, the quantum state is $\frac{1}{\sqrt{2}}\Big(|00\rangle + |11\rangle\Big)$. In the computational basis, the possible measurement outcomes are the bitstrings 00 or 11. Performing 'shots' of the circuit, that is running the circuit and measuring the output multiple times, allows one to build up statistics which can give information on the bitstring makeup of the state. Given a noiseless circuit that prepares this Bell state, one should only ever measure either 00 or 11 If you built a histogram of these results, as the number of shots approach infinity, these measurements should become equally likely by Born's rule.

These measurements alone however do not tell you that the statevector before measurement was $\frac{1}{\sqrt{2}}\Big(|00\rangle + |11\rangle\Big)$. If you instead prepared a different Bell-state $\frac{1}{\sqrt{2}}\Big(|00\rangle - |11\rangle\Big)$, you would obtain the same measurements in the computational basis. In other words, measurements only in a single basis cannot fully reconstruct

the final state vector. In other words, the information about the -1 phase in front of the basis state $|11\rangle$ is lost upon measurement.

1.2 Fault Tolerant Quantum Computing

Today's quantum computers are plagued by noise – unwanted effects that affect a quantum state and cause it to decohere. Quantum gates are never perfect and lead to small errors in the quantum states. Even though these are small, when you have a circuit with thousands to hundreds of thousands of operations, or if you need thousands of circuit shots, these errors can dramatically affect the results of the computation. We are currently in the *Noisy Intermediate Scale Quantum* (NISQ) era of quantum computing, a phrase coined by John Preskill [Pre18]. This is characterized by noisy quantum computers with upwards of a couple hundred physical qubits and relatively shallow circuit depths. NISQ devices rely on error mitigation, which is a post-processing technique to improve measurement results by removing the effects of noise after the computation has been run.

The ultimate goal of quantum computers is to have them to realize *quantum error correction*(QEC) [Sho95], which corrects errors concurrently while the computation is running, rather than mitigating them at the end. QEC is necessary for any quantum simulation due to decoherence of the wavefunction, and gates with small, but nonzero error rates. Originally, QEC was thought to be impossible for three main reasons [NC10]:

- No–cloning theorem: Classical error correction is based on repetition codes which copy classical bits to introduce redundancy. Quantum states, however, cannot be copied.

- Continuous errors: Classical errors occur by bit flips: $0 \longleftrightarrow 1$, but quantum errors can occur by bit flips *and/or* phase flips, e.g. $|\phi\rangle \rightarrow -|\phi\rangle$.

- Destruction of quantum information under measurement: Measurement explicitly collapses the wavefunction. One cannot measure the wavefunction to

find out which error(s) occurred without losing the quantum information and reducing it to classical information.

Despite this incorrect intuition, the field of quantum error correction has tackled these problems and developed topological QEC codes such as the surface code [FMMC12] and the color code [LBH$^+$25], both of which utilize the stabilizer framework proposed in Daniel Gottesman's Ph.D. thesis [Got97].

Following NISQ, is the *early fault-tolerant* quantum computing era with "MegaQuop" machines, also coined by Preskill [Pre25]. A fault tolerant quantum computer is one characterized by collections of physical qubits which encode a single logical qubit, with the property that the error rate of the single logical qubit is less than the individual error rates of the physical qubits. One possible encoding of physical qubits to a logical qubit is given as:

$$\begin{cases} |0\rangle_L = |000\ldots\rangle \\ |1\rangle_L = |111\ldots\rangle. \end{cases}$$

These are called *codewords*. This necessitates the definition of logical qubit gates, e.g. $X \to X_L$. *Transversal* operators are those whose action onto logical qubits is 'simple' – the logical qubit gate can be preformed by applying the same gate on every physical qubit. Under the surface code, Clifford gates are transversal. Different quantum error correction codes define different transversal gates and codewords, and are chosen dependent on the physical topology of the architecture.

By the Eastin-Knill Theorem [EK09], it is impossible for every operator in a universal gate set to be transversal. Under the surface code, the T gate must be implemented non-transversally, and is thus the "difficult" gate to apply in fault tolerant quantum computing. Since Clifford gates can be efficiently simulated classicaly by the Gottesman-Knill Theorem [NC10], the introduction of a T gate into a gate set brings in the 'magic' of quantum computation.

Since T gates are non-transversal under the surface code architecture, an alternative method based around '*magic states*' can be used, which accomplishes

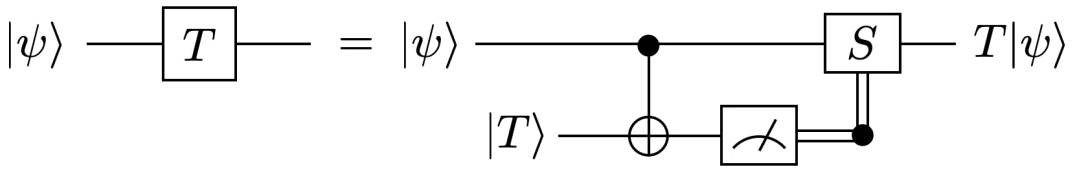

Figure 1.6: **Magic State Injection** is the most efficient way to apply T gates under the surface code architecture. Here, magic states ($|T\rangle$) are prepared ahead of time through magic state distillation and are injected into the circuit by this procedure. If the ancilla qubit (storing $|T\rangle$) is measured in the 0 state, $T|\psi\rangle$ has been properly applied to the system register. Otherwise, one must apply an S gate to the system register, leading to the state $e^{i\pi/4}T|\psi\rangle$ which implies the T-gate has been applied up to an irrelevant global phase.

the same effect as applying a T gate. A magic state is formally defined as

$$|T\rangle = T|+\rangle = \frac{1}{\sqrt{2}}\Big(|0\rangle + e^{i\pi/4}|1\rangle\Big). \tag{1.18}$$

Magic states encode the non-Clifford action of the T-gates onto states which can be prepared ahead of time and 'stored' to be used whenever a T-gate is needed in the computation. By preparing magic states ahead of time, in a sense the problems from a non-Clifford gate has been evaded.

The act of 'preparing' and 'using' magic states are processes known as magic state distillation and magic state injection respectively. Magic state distillation is an algorithm which takes multiple noisy states that are close to a magic state and purifies, or distills, them into a state which is arbitrary close to a perfect magic state. Magic state distillation can be performed in advance of any computation so that anytime a T gate is needed, a magic state can be injected into the circuit via magic state injection Fig. 1.6. This is currently the most efficient way of applying T gates in fault tolerant quantum computing under the surface code and has been experimentally demonstrated within the last year [SRRJ$^+$25]. A cheaper alternative to distillation is through magic state cultivation [RGR$^+$25] which reduces the cost of a T-gate to roughly the same cost as a CNOT.

1.3 Quantum Algorithms for Quantum Simulation

As quantum computers started to be formalized as a method of computation, people began to develop quantum algorithms to assist in the goal of quantum simulation. Two of the groundbreaking algorithms in quantum computing were (Peter) Shor's algorithm which factors a large integer N [Sho94], and (Lov) Grover's search algorithm which searches for a binary string x that satisfies some condition $f(x) = 1$ [Gro96]. Famously, both Shor's and Grover's algorithms have a reduction in complexity when compared to their classical counterparts, shown in Table 1.1.

	Classical	Quantum
Factoring	$\mathcal{O}\left(e^{N^{1/3}\log^{2/3} N}\right)$	$\mathcal{O}\left(N^2 \log N \log\log N\right)$
Search	$\mathcal{O}(N)$	$\mathcal{O}(\sqrt{N})$

Table 1.1: **Algorithmic Complexity**: Number of operations on N (qu)bits to solve factoring and search problems both classically and with a quantum computer. Quantum search complexity comes from [NC10]. The best classical factoring algorithm is 'number field sieve' [LL93]. Quantum factoring complexity comes from [Sho94]. This table was adapted from William Kirby's Ph.D. Thesis [Kir23].

Some other foundational algorithms that arose early in the development of the field are Trotterization [Suz76, HS05, Tro59], and the quantum fourier transform [Cop02], which is an important subroutine in quantum phase estimation (QPE) [Kit95]. Trotterization is a broad category of approximation schemes that allows one to simulate approximate time evolution of a quantum wavefunction under a Hamiltonian. QPE is an efficient algorithm for estimating the eigenvalues of a unitary operator.

The field in the last decade has built off these foundational algorithms to design new techniques. Block-encodings [CW12a, BC09] are a class of approaches that allow one to 'unitarize' operators that are not themselves unitary. This is useful because quantum computers explicitly take unitary operators as their input, but in general, interesting operators, such as the Hamiltonian, are not unitary. Qubitization [LC19b] is an extension of block-encodings, which modifies the standard block-encoding, allowing one to faithfully encode the spectrum of a block-encoded

operator within the spectrum of the block-encoded unitary.

Quantum Signal Processing (QSP) [LC17a] and the Quantum Singular Value Transform (QSVT) [GSLW19] are algorithms that construct block-encodings of polynomials of operators. A 2021 paper by John Martyn et. al [MRTC21a] unifies QSP & QSVT under a general umbrella of all quantum algorithms.

In this section, we give an overview of three quantum algorithms which are the foundation of the work in this thesis. We begin with block-encodings, followed by quantum phase estimation. We then end with qubitization, and describe how all three of these algorithms works in concert.

1.3.1 Block-Encoding

As noted by Eq. 1.6, quantum computers take in unitary operators as an input as these operators preserve the norm of quantum states. Many interesting operators one may want to study with quantum algorithms are non-unitary, such as a Hamiltonian. One must encode properties of the non-unitary operator of interest into a unitary operator. One way to achieve this is by constructing the 'time evolution operator':

$$U_H(t) = e^{-iHt}, \tag{1.19}$$

which is unitary since exponentiated anti-Hermitian operators (iH is anti-Hermitian if H is Hermitian) are unitary by Lie theory. $U_H(t)$ must be decomposed into a universal gate set, and in general requires some approximation scheme. The main class of techniques to accomplish this is by Trotterization [Tro59] which aims to approximate operators of this form by

$$e^{-i(A+B)t} \approx \prod_l e^{-iC_l t}. \tag{1.20}$$

This field is extensively studied; however, we do not consider these approaches in this thesis.

Rather we study block-encodings, which are a category of algorithms that

'unitarize' non-unitary operators by embedding them in a unitary occupying a larger Hilbert space. For a non-unitary operator A, a block-encoded operator for A is:

$$U_A = \begin{pmatrix} A/\alpha & \star \\ \star & \star \end{pmatrix}, \tag{1.21}$$

where $\star$ represents sub-blocks of U_A that maintain the unitarity of U_A, but are otherwise arbitrary. The scalar α rescales A such that all the eigenvalues of U_A have magnitude 1. Unless stated otherwise, U_A will specifically refer to a block-encoding, rather than an arbitrary unitary encoding of A.

There are two registers in a block-encoding circuit: the system and ancillae registers. The system register belongs to the Hilbert space of the operator that is being block encoded, while the ancillae register are the additional qubits needed to increase in the overall Hilbert space and make U_A unitary. The action of U_A on an arbitrary quantum state in the system register $|\psi\rangle_s$ with Hilbert space dimension N_A, tensored with an ancilla state $|0\rangle_{anc}$, is

$$U_A |0\rangle_{anc.} |\psi\rangle_s = |0\rangle_{anc.} \left(A/\alpha |\psi\rangle_s \right) + \beta_\psi |\perp\rangle , \tag{1.22}$$

where the subscript s refers to the system register and *anc.* refers to the register of ancillae qubits. Equation 1.22 shows that, given a state $|\psi\rangle_s$, the block-encoded unitary of A acts in the subspace of $|\psi\rangle_s$ as $A/\alpha |\psi\rangle_s$ when the ancilla register is in the $|0\rangle_{anc.}$ state after U_A is applied. In general, there may be a contribution from a subspace that is orthogonal to the encoded subspace, which we define to be the subspace in which the ancilla register is in the all zero state. This orthogonal contribution all falls into the state $|\perp\rangle$. The factor β_ψ is a complex coefficient that depends on ψ. If it is not immediately obvious why $|\perp\rangle$ is unavoidable, it is easier when looking at Eq. 1.22 as matrix multiplication with $|0\rangle_{anc.} |\psi\rangle_s = \begin{pmatrix} \psi & 0 \end{pmatrix}^T$, then

$$\begin{pmatrix} A/\alpha & \star \\ \star & \star \end{pmatrix} \begin{pmatrix} \psi \\ 0 \end{pmatrix} = \begin{pmatrix} \frac{A}{\alpha}\psi \\ \star' \end{pmatrix}, \tag{1.23}$$

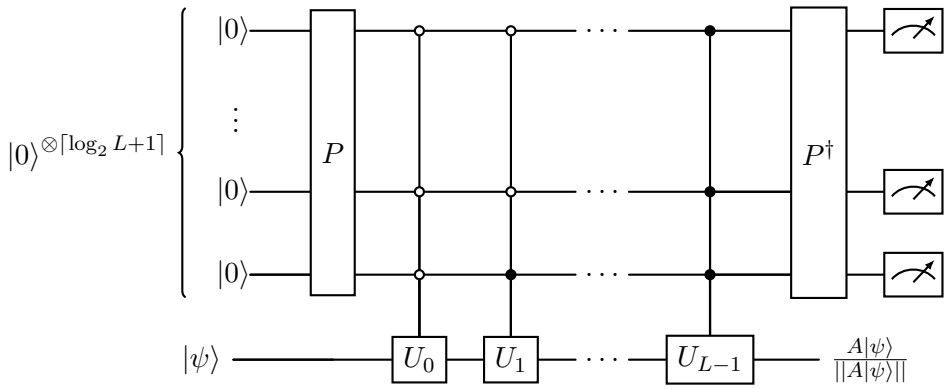

Figure 1.7: **LCU Block-Encoding Framework**

where $\star'$ is in general unknown and taken to be $\beta_\psi |\perp\rangle$.

Block-encodings can be interpreted as probabilistically applying non-unitary operators A to a state $|\psi\rangle$. After the block-encoding unitary is implemented in the circuit, the ancilla register is measured, and if the state $|0\rangle_{anc.}$ is measured then we are projected into the proper subspace in the system register, $\frac{A}{\alpha}|\psi\rangle_s$, and the block-encoding was applied successfully. If any other state (besides the all zero state) is measured in the ancillae register, we will be projected into the $|\perp\rangle$ subspace, and the block-encoding will be unsuccessful. The probability that the block-encoding is properly performed depends both on A and $|\psi\rangle$. The success probability is

$$P_{\text{success}} = \frac{|\langle\psi|_s A^\dagger A |\psi\rangle_s|}{|\alpha|^2} \tag{1.24}$$

The success probability also depends on $|\psi\rangle$. Take, for example, $A = |0\rangle\langle 0|$, then if $|\psi\rangle = |1\rangle$, the success probability will be zero [RLTC21]. In general, the success probability is actually irrelevant because very rarely are we interested in algorithms that actually post-select on the index register to probabilistically apply A to $|\psi\rangle$.

A common block-encoding framework produces a block-encoding for an operator written as a *linear combination of unitaries* (LCU) [CW12a], i.e.

$$A = \sum_{l=0}^{L} \alpha_l U_l. \tag{1.25}$$

Without loss of generality, we can assume $\alpha_l \in \mathbb{R}^{>0}$ since the phase of a coefficient can be absorbed into the unitary by $-i\alpha_l U_l = \alpha_l(-iU_l) = \alpha_l U_l'$. LCU is built of three unitaries: PREPARE (P), SELECT(S), and PREPARE† ($P^\dagger$), shown in Figure 1.7. The rescaling factor for LCU is the one-norm

$$\alpha = \sum_{i=0}^{N-1} |\alpha_i| \equiv ||\alpha||_1, \tag{1.26}$$

which ensures the unitarity of U_A.

The PREPARE unitary creates a superposition of computational basis states from 0 to $\lceil \log_2(L-1) \rceil$, weighted proportionally to the coefficient of the i^{th} unitary, U_i in the sum.

$$P|0\rangle_{anc.} = \sum_{l=0}^{L-1} \sqrt{\frac{\alpha_l}{||\alpha||_1}} |l\rangle \tag{1.27}$$

Implementing PREPARE can be achieved with the Grover-Rudolph algorithm [GR02] which creates an arbitrary superposition of computational basis states, weighted by coefficients from a probability distribution.

The SELECT unitary applies the l^{th} unitary on the system register when the ancilla register is in state $|l\rangle$. The way to implement SELECT can be seen explicitly in Fig. 1.7.

$$S = \sum_{l=0}^{L-1} |l\rangle \langle l| \otimes U_l. \tag{1.28}$$

In this thesis, whenever there is a sequence of controls in the same manner as SELSECT, it will be shown explicitly in circuit diagrams as it is in Fig. 1.8, where the gate In_l, denotes Indexing over l objects. All together,

$$U_A = P^\dagger S P. \tag{1.29}$$

Theorem 1.3.1 *$U_A = P^\dagger S P$ block-encodes $\bar{A} = A/||\alpha||_1$.*

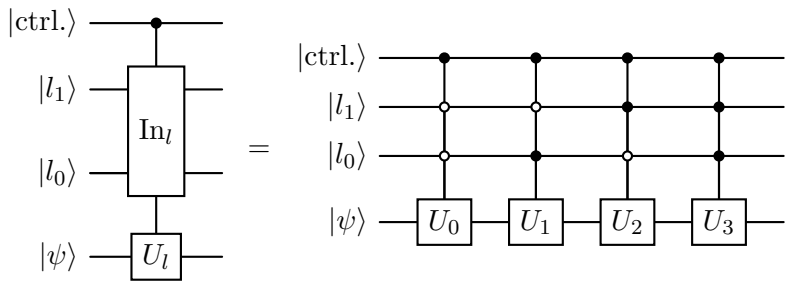

Figure 1.8: **Indexed controls over computational basis states.**

Proof For U_A to be a block-encoding of $\bar{A}$, we must show $\langle 0|_{anc.} P^\dagger SP |0\rangle_{anc.} = \bar{A}$.

$$
\begin{aligned}
&\langle 0|_{anc.}\, P^\dagger\ SP\, |0\rangle_{anc.} \\
&\quad = \left(\sum_{k'=0}^{L-1} \sqrt{\frac{\alpha_{k'}}{||\alpha||_1}}\, \langle k'|_{anc.} \right) \left(\sum_{l=0}^{L-1} |l\rangle_{anc.}\, \langle l|_{anc.} \otimes U_l \right) \left(\sum_{k=0}^{L-1} \sqrt{\frac{\alpha_k}{||\alpha||_1}}\, |k\rangle_{anc.} \right) \\
&\quad = \sum_{k,k',l=0}^{L-1} \frac{\sqrt{\alpha_{k'}\alpha_k \delta_{kl}\delta_{k'l}}}{||\alpha||_1} U_l \\
&\quad = \sum_{l=0}^{L-1} \frac{\alpha_l}{||\alpha||_1} U_l \\
&\quad \equiv \bar{A}
\end{aligned}
\tag{1.30}
$$

■

Implementing controlled block-encodings are ubiquitous in many quantum algorithms. Here, we describe an efficient way to compile them.

Lemma 1.3.2 *If $U = AB$ then controlled-U can be compiled as controlled-A $\cdot$ controlled-B.*

Proof

$$
\begin{aligned}
\mathrm{c}U &= \Big(|0\rangle\langle 0| \otimes \mathbb{1} + |1\rangle\langle 1| \otimes AB \Big) \\
&= \Big(|0\rangle\langle 0| \otimes \mathbb{1} + |1\rangle\langle 1| \otimes A \Big) \Big(|0\rangle\langle 0| \otimes \mathbb{1} + |1\rangle\langle 1| \otimes B \Big) \\
&= \mathrm{c}A \cdot \mathrm{c}B
\end{aligned}
\tag{1.31}
$$

By Lemma 1.3.2, it appears that to implement a controlled block-encoding, one must

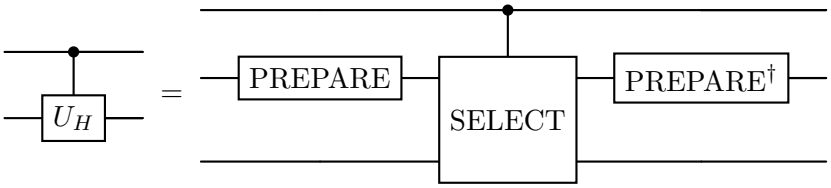

Figure 1.9: **An Efficient Controlled call to U_H**

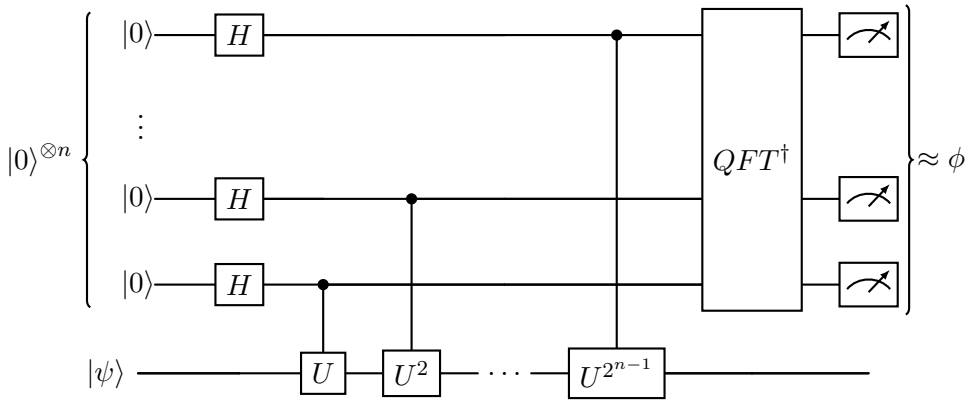

Figure 1.10: **The Quantum Phase Estimation Circuit**

implement controlled-PREPARE, controlled-SELECT, controlled-PREPARE†; however, there is a more efficient way.

Theorem 1.3.3 *A controlled call to $U_H = P^\dagger SP$ can be implemented by only controlling the SELECT unitary (see Fig. 1.9).*

Proof The circuit on the right hand side of Fig. 1.9 is

$$\begin{aligned}\Big(\mathbb{1}P\mathbb{1}\Big)\Big(|0\rangle\langle 0|\otimes\mathbb{1}+|1\rangle\langle 1|\otimes S\Big)\Big(\mathbb{1}P^\dagger\mathbb{1}\Big)&\\ =\Big(|0\rangle\langle 0|\otimes PP^\dagger+|1\rangle\langle 1|\otimes PSP^\dagger\Big)&\\ =\Big(|0\rangle\langle 0|\otimes\mathbb{1}+|1\rangle\langle 1|\otimes U_H\Big)&\end{aligned}\tag{1.32}$$

■

1.3.2 Quantum Phase Estimation

Given a unitary operator U and an eigenstate of this operator $|\lambda\rangle$, the Quantum Phase Estimation (QPE) algorithm computes an approximation to the corresponding eigenvalue, λ:

$$U|\lambda\rangle = \lambda|\lambda\rangle . \tag{1.33}$$

The eigenvalues of unitary operators explicitly have norm $|\lambda| = 1$, which implies that the eigenvalue can be represented as $e^{i\theta}$ for some θ. This mapping is not unique, however, since $e^{i\theta} = e^{i(2\pi+\theta)}$. Therefore, θ can be mapped to $\theta = 2\pi\phi$ with $\phi \in [0, 1]$, or any similar interval of period 2π. The convention we will use is $\theta = \pi\phi$ with $\phi \in [-1, 1]$.

Fig. 1.10 shows a circuit diagram for quantum phase estimation. Understanding the QPE algorithm requires some prerequisite knowledge.

1. **Binary Fractions**: Similarly to how a fraction can be represented in base-10 (e.g. $0.625 = 6 \times 10^{-1} + 2 \times 10^{-2} + 5 \times 10^{-3}$, a fraction can also be represented in base-2. For example, $0.625 = 0 \times 2^{-1} + 1 \times 2^{-2} + 0 \times 2^{-3} + 1 \times 2^{-4}$, which can be written as 0.0101. Therefore, we can represent a phase $0 \leq \phi \leq 1$ as a statevector such as $\phi = 0.625 \leftrightarrow 0.0101 \leftrightarrow |0101\rangle$.

2. **Phase Kickback**: A global phase ($e^{i\phi}|\phi\rangle$) of a quantum state is unmeasurable; however, relative phases (phases between superpositions of states such as $|0\rangle + e^{i\varphi}|1\rangle$) *can* be measured. Phase kickback is a technique that allows one to create interference and 'kickback' a relative phase to an ancilla register that, when measured, gives one access to the phase information [NC10]. For the same unitary described in Equation 1.33, the phase kickback circuit is shown in Figure 1.11. The final state (before measurement) is

$$|\pi\rangle = \Big(\frac{1 + e^{i\pi\phi}}{2}|0\rangle + \frac{1 - e^{i\pi\phi}}{2}|1\rangle\Big) \otimes |\psi\rangle .$$

   Measuring 0 in the ancilla register happens with probability $\cos^2(\pi\phi/2)$, while measuring 1 occurs with probability $\sin^2(\pi\phi/2)$. In general, this measurement

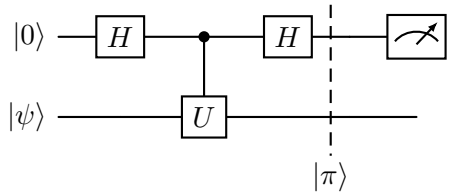

Figure 1.11: **Phase Kickback Circuit**

doesn't reveal exactly what ϕ is, but it does reveal some information about it. On the other hand, if one repeatedly measures this state and always measures $0(1)$, then one can be guaranteed that $\phi = 0(1)$.

3. **Quantum Fourier Transform**: The quantum Fourier transform is functionally a change of basis from the computational basis to the *Fourier basis*, and is analogous to the classical discrete fast Fourier transform. The algorithm creates a map $\vec{\boldsymbol{x}} = (x_0, \ldots, x_N) \in \mathbb{C}^N \to \vec{\boldsymbol{y}} = (y_0, \ldots, y_N) \in \mathbb{C}^N$, where $N = 2^n$ and

$$|j\rangle \to \frac{1}{\sqrt{N}} \sum_{k=0}^{N-1} e^{2\pi i jk/N} |k\rangle , \tag{1.34}$$

which is modeled after the discrete Fourier transform[1]. The action of this map can be summarized as

$$|j\rangle = \frac{\Big(|0\rangle + e^{2\pi i 0.\theta_n} |1\rangle\Big)\Big(|0\rangle + e^{2\pi i 0.\theta_{n-1}\theta_n} |1\rangle\Big) \ldots \Big(|0\rangle + e^{2\pi i 0.\theta_1 \ldots \theta_n} |1\rangle\Big)}{\sqrt{N}}.$$

Using binary fractions, phase kickback, and the quantum Fourier transform, the quantum phase estimation algorithm can be described.

There are three main parts of the QPE algorithm. The first part is state preparation. For the purpose of pedagogy, we assume one has access to an eigenstate of U, $|\lambda\rangle$. This seemingly restrictive constraint will be lifted at the end of the discussion of the algorithm, where it should become obvious that this constraint

[1]The discrete Fourier transform is given by

$$y_k \equiv \frac{1}{\sqrt{N}} \sum_{j=0}^{N-1} e^{2\pi i jk/N} x_j$$

is not necessary at all. The state preparation step involves acting on the all-zero ancilla register with $H^{\otimes n}$, creating a uniform superposition of computational basis states. At this point in the algorithm, the state is

$$|\pi_1\rangle = \frac{1}{\sqrt{2^n}} \sum_{l=0}^{n} |l\rangle \otimes |\lambda\rangle \,.$$

Next, phase kickback is used to compute the phase information about the eigenphase, and store it in the ancilla register. A cascading sequence of U^{2^j} for $j \in [0, n-1]$ allows one to store information about the different digits in the binary fractional expansion of ϕ, i.e. for $\phi = 0.\phi_1\phi_2 \ldots \phi_n$, U obtains information about ϕ_1, U^2 determines information on ϕ_2, etc.

After the controlled U^{2^j}'s, the state of both registers is

$$|\pi_2\rangle = \frac{1}{\sqrt{2^n}} \Big(\big(|0\rangle + e^{2\pi i 0.\phi_n} |1\rangle \big) \big(|0\rangle + e^{2\pi i 0.\phi_{n-1}\phi_n} |1\rangle \big) \ldots \big(|0\rangle + e^{2\pi i 0.\phi_1 \ldots \phi_n} |1\rangle \big) \Big) \otimes |\lambda\rangle \,.$$

The state at this point in the circuit looks like the action of the quantum Fourier transformation given above. Therefore, if one passes the ancilla register through an inverse quantum Fourier transform, denoted $\mathrm{QFT}^\dagger$ in the circuit, the Fourier basis state that the ancilla register appears to be in, will be transformed back to the computational basis, where the computational basis state that comes out is, by definition of the quantum Fourier transform, $|\phi_n \ldots \phi_1 \phi_0\rangle$. This tells exactly what the binary fractional decomposition of ϕ is, i.e. measuring the ancilla register gives a computational basis state, which is an approximation to the true ϕ. The number of ancilla qubits used is generally referred to as the bits of precision for ϕ since increasing n leads to a better approximation to ϕ.

While one can in theory measure phases to arbitrary precision with the phase kickback circuit (this is known as the Hadamard test) in Fig. 1.11, by taking products of U, this requires $\mathcal{O}(\epsilon^{-2})$ shots to reach precision ϵ. The quantum phase estimation algorithm requires $\mathcal{O}(\epsilon^{-1})$ shots to match the same precision [Lin22].

If the input state is not an eigenstate, all hope is not lost. Every state can

be written in the eigenbasis of the unitary:

$$|\psi\rangle = \sum_{\lambda} \langle\lambda|\psi\rangle \, |\lambda\rangle \, . \tag{1.35}$$

The QPE circuit acts on every eigenstate in superposition, and the readout in the phase register will give multiple peaks, one for each eigenstate.

1.3.3 Qubitization

A common goal in quantum simulation is estimating eigenvalues of a model Hamiltonian. Quantum phase estimation can be used to accomplish this only if the Hamiltonian, which is in general not unitary, is encoded into a unitary operator, U_H. An additional caveat is that the eigenvalues of the unitary which encode H must also encode the eigenvalues of H, i.e.

$$\text{spectrum}(U_H) = f\Big(\text{spectrum}(H)\Big). \tag{1.36}$$

This is necessary so that when one measures the eigenphases in QPE, the spectral information of the encoded Hamiltonian must be easily retrieved.

One way to achieve this is by constructing the time evolution operator $U_H = e^{-iHt}$, which has eigenvalues $e^{-i\lambda_n t}$. By running QPE on e^{-iHt}, and reading out the eigenphase, one can easily extract the eigenvalues of H through: $\lambda_n = \frac{\pi\phi^{(n)}}{t}$. We now consider the question: "Does a block-encoded U_H, which definitionally encodes H, also encode the spectrum of H."

To answer this question, assume one has access to a block-encoded unitary U_H with the additional property $U_H^2 = \mathbb{1}$. It turns out this is not a particularly restrictive condition because given a U_H which does not satisfy this, only a slight modification with minimal overhead is needed to satisfy this condition. We restrict ourselves at first to this case for pedagogical purposes, and then discuss the more general case in Chapter 3.

In the basis $\left\{ |0\rangle_{anc.} |\lambda\rangle_s , |\perp\rangle_{anc.,s} \right\}$, U_H is given by

$$U_H |0\rangle_{anc.} |\lambda\rangle_s = \bar{\lambda} |0\rangle_{anc.} |\lambda\rangle_s + \sqrt{1 - |\bar{\lambda}|^2} |\perp\rangle_{anc.,s} \tag{1.37}$$

$$U_H |\perp\rangle_{anc.,s} = \sqrt{1 - |\bar{\lambda}|^2} |0\rangle_{anc.} |\lambda\rangle_s - \bar{\lambda} |\perp\rangle_{anc.,s} . \tag{1.38}$$

The action of $U_H |\perp\rangle_{anc.,s}$ in the second line may not be obvious at first, but it's easy to determine if you apply a second action of U_H on $|0\rangle_{anc.} |\psi\rangle_s$:

$$\begin{aligned} U_H\Big(U_H |0\rangle_{anc.} |\lambda\rangle_s = \bar{\lambda} |0\rangle_{anc.} |\lambda\rangle_s + \sqrt{1 - |\bar{\lambda}|^2} |\perp\rangle_{anc.,s} \Big) \\ \mathbb{1} |0\rangle_{anc.} |\lambda\rangle_s - \bar{\lambda} U_H |0\rangle_{anc.} |\lambda\rangle_s = \sqrt{1 - |\bar{\lambda}|^2} U_H |\perp\rangle_{anc.,s} , \end{aligned} \tag{1.39}$$

where $U_H^2 = \mathbb{1}$ was used. This equation can now be written in terms of $U_H |\perp\rangle_{anc.,s}$ to obtain the lower line above.

In this basis, U_H has matrix form

$$U_H = \begin{pmatrix} \bar{\lambda} & \sqrt{1 - |\bar{\lambda}|^2} \\ \sqrt{1 - |\bar{\lambda}|^2} & -\bar{\lambda} \end{pmatrix} , \tag{1.40}$$

or on a general input written in its spectral decomposition it breaks up into a direct sum over the different eigenstates:

$$U_H = \bigoplus_i \begin{pmatrix} \bar{\lambda}_i & \sqrt{1 - |\bar{\lambda}_i|^2} \\ \sqrt{1 - |\bar{\lambda}_i|^2} & -\bar{\lambda}_i \end{pmatrix} . \tag{1.41}$$

The eigenvalues of U_H (in each block of fixed λ_i) are ± 1. This should be expected because U_H is unitary and self-inverse (and therefore Hermitian) so it's eigenvalues necessarily are ± 1[2]. In other words, the spectral information is lost in the eigenvalues of U_H, and therefore there is no map from the eigenvalues of U_H to the eigenvalues of H.

Consider what happens instead when we simply move the minus sign in the

[2]Eigenvalues of unitary matrices are complex numbers with norm 1. Eigenvalues of Hermitian matrices are real. Therefore, eigenvalues of matrices that are unitary and Hermitian must be ± 1.

matrix form of U_H from the bottom right to the top right. We will call this new matrix $\mathcal{W}_H$, which is colloquially referred to as the qubitization iterate [LC19a], or the walk operator, named after the *Szegedy quantum walk* [Sze04a, Sze04b, Chi09a, Chi09b]:

$$\mathcal{W}_H = \begin{pmatrix} \bar{\lambda} & -\sqrt{1-|\bar{\lambda}|^2} \\ \sqrt{1-|\bar{\lambda}|^2} & \bar{\lambda} \end{pmatrix}, \tag{1.42}$$

which also breaks up into a direct sum over eigenvalues on an arbitrary input:

$$\mathcal{W}_H = \bigoplus_i \begin{pmatrix} \bar{\lambda}_i & -\sqrt{1-|\bar{\lambda}_i|^2} \\ \sqrt{1-|\bar{\lambda}_i|^2} & \bar{\lambda}_i \end{pmatrix}. \tag{1.43}$$

The eigenvalues of $\mathcal{W}_H$ are $\bar{\lambda} \pm i\sqrt{1-|\lambda|^2}$. If we define $\cos(\theta) = \bar{\lambda}$, then the eigenvalues $\bar{\lambda} \pm i\sqrt{1-|\bar{\lambda}|^2}$ become $\cos(\theta) \pm i\sin(\theta)$, or more compactly $e^{\pm i\theta}$. Therefore, the eigenvalues of $\mathcal{W}_H$ are $e^{\pm i \arccos(\bar{\lambda})}$, which clearly encode $\bar{\lambda}$, and there is a well-defined map from the eigenphases when running QPE on $\mathcal{W}_H$ to λ.

The walk operator may be written as an R_y rotation about the angle $\theta = \arccos\Big(\bar{\lambda}\Big)$:

$$\mathcal{W}_H = \exp\Big(iY \arccos\Big(\bar{\lambda}\Big)\Big). \tag{1.44}$$

Furthermore, the walk operator has eigenvectors

$$|W\rangle = \frac{1}{\sqrt{2}}\Big(|0\rangle_{anc.} |\lambda\rangle_s \pm i\, |\perp\rangle_{anc.,s} \Big). \tag{1.45}$$

Powers of the walk operator generate Chebyshev polynomials [Lin22]:

$$W^k = \begin{pmatrix} T_k(\bar{\lambda}) & -\sqrt{1-|\bar{\lambda}|^2}U_{k-1}(\bar{\lambda}) \\ \sqrt{1-|\bar{\lambda}|^2}U_{k-1}(\bar{\lambda}) & T_k(\bar{\lambda}) \end{pmatrix}, \tag{1.46}$$

where $T_k(\bar{\lambda})$ and $U_{k-1}(\bar{\lambda})$ are Chebyshev polynomials of the first and second kind respectively, which are efficient polynomials for approximating any L_∞ function.

We know U_H does not encode spectral information while $\mathcal{W}_H$ does. Luckily, there is a simple transformation from U_H to $\mathcal{W}_H$. In other words, it is unnecessary

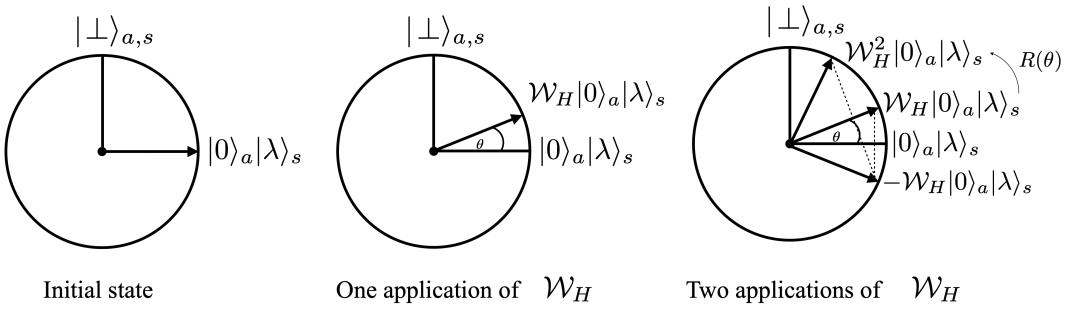

Figure 1.12: **Walk Operator as a rotation**: In the subspace defined by $\left\{ |0\rangle_{anc.} |\lambda\rangle_s , |\perp\rangle_{anc.,s} \right\}$ acts as a rotation by an angle $\theta = \arccos\left(\bar{\lambda}\right)$. This is analogous to Grover search [Gro96].

to completely disregard the block-encoding, but rather a simple modification to it is all that is needed. The map from U_H to $\mathcal{W}_H$ is accomplished by $\mathcal{W}_H = U_H V$. In the same basis that U_H and $\mathcal{W}_H$ is defined in, $V = \text{diag}(1, -1)$. The matrix V is generally written as a reflection about the ancillae register:

$$\mathcal{R}_a = 2 |0\rangle_{anc.} \langle 0|_{anc.} - \mathbb{1}. \tag{1.47}$$

Therefore, given a block-encoded unitary, the walk operator can be obtained by

$$\mathcal{W}_H = U_H \mathcal{R}_a, \tag{1.48}$$

which is formally a rotation in the subspace $\left\{ |0\rangle_{anc.} |\lambda\rangle_s , |\perp\rangle_{anc.,s} \right\}$, since the product of two reflections is rotation, and $U_H^2 = \mathbb{1}$ implies U_H acts as a reflection in this subspace , see Fig. 1.12.

In the LCU framework, U_H is self-inverse if the SELECT unitary is self-inverse. Furthermore, the SELECT unitary is automatically self-inverse if the unitaries $U_l's$ is indexes over are self-inverse (this will be proven in Ch. 3). Since the Pauli operators are self-inverse, a block-encoded Pauli-LCU satisfies $U_H^2 = \mathbb{1}$, and therefore, the walk operator can be constructed. Extending block-encodings to satisfy $U_H^2 = \mathbb{1}$ with minimal overhead when they do not natively satisfy this will be discussed in Chapter 3.

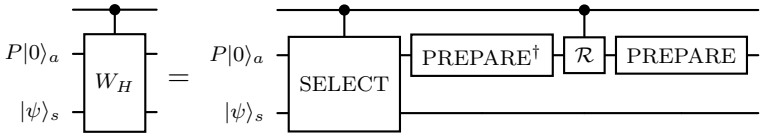

Figure 1.13: A construction for the walk operator built out of SELECT and PREPARE unitaries if the SELECT oracle indexes over self-inverse unitaries [BGB$^+$18]

We choose to compile the walk operator in a slightly different form:

$$\mathcal{W}_H = \mathcal{R}_a P^\dagger \cdot S, \tag{1.49}$$

which necessitates the ancillae register to be of the form $P\left|0\right\rangle_{anc.}$. This is a common compilation strategy for the walk operator when used in QPE [BGB$^+$18, PKS$^+$18], and is shown in Fig. 1.13. If the initial state is

$$\left|0\right\rangle_{\text{phase}} \otimes P|0\rangle_{anc.} \left|\lambda\right\rangle_s, \tag{1.50}$$

running QPE on the walk operator will output eigenvalues $e^{\pm i \arccos\left(\bar{\lambda}\right)}$ [PKS$^+$18]. The eigenvalue of interest can then be easily extracted by reading out ϕ from the phase register:

$$\lambda_n = \mp\alpha \cos\Big(\pi\phi^{(n)}\Big). \tag{1.51}$$

A plot of measurement results in QPE vs. ϕ will result in two peaks at $\pm \arccos\Big(\bar{\lambda}\Big)$ (note that there will be multiple peaks if the input of the system state is not an eigenstate). Table 1.2 summarizes two unitaries which encode H and how they can be used in QPE.

Method	**Unitary**	**Map $\phi^{(n)} \to \lambda_n$**	**Disadvantages**
Time Evolution	$U_H = e^{-iHt}$	$\lambda_n = -\frac{\pi\phi^{(n)}}{t}$	Trotter error.
Qubitization	Walk Operator $\left(W_H\right)$	$\lambda_n = \mp\alpha\cos\left(\pi\phi^{(n)}\right)$	Rescaling factor, ancilla overhead.

Table 1.2: Methods to encode a non-unitary operator within a unitary

1.4 Chapter 1 Summary

In this introductory chapter, we discussed the history of quantum computing from its conception to current day. Then we gave a short overview of quantum information and computation. Finally, relevant quantum algorithms for quantum simulation of quantum field theories were summarized.

The remainder of this thesis is organized as follows. Chapter 2 follows the introductory chapter about quantum computing with an introduction to quantum field theory, with an emphasis on light-front field theory and renormalization. Chapters 1 and 2 also provide historical context for the work presented. Chapter 3 develops an efficient quantum algorithm to simulate Hamiltonians that arise in light-front quantum field theories. Chapter 4 shows how this framework works for an interacting quantum field theory – Yukawa theory, and provides the first answer to the question about the costs of quantum simulation in our framework. Lastly, Chapter 5 produces estimates for how expensive this framework is to produce results, given a fault tolerant quantum computer, for quantum chromodynamics. We finish with a conclusion in which we summarize this thesis, and propose future work.

Chapter 2

Background

In this chapter, the relevant mathematics background on front-form quantum field theory will be reviewed. We begin with a historical introduction to quantum field theories, and describe common numerical approaches to solving these theories. Next, the front form approach to quantum field theories is described, starting with the definition of light-front coordinates, and then outlining the problems one can solve with this formalism. Lastly, we discuss our renormalization framework, the renormalization group procedure for effective particles. This scheme is a perturbative renormalization procedure that renders observables finite.

2.1 A Historical Summary of Quantum Field Theory

Quantum Field Theory (QFT) arose out of the attempted merging of quantum mechanics with special relativity. While conceptually and mathematically very demanding, QFT describes our world on the smallest of scales with greater accuracy than any other theory in physics. On top of technical complications, it is also computationally demanding, and requires the world's largest supercomputers to obtain accurate results and predictions.

The relevant energy scales of a given model determine the field theory that describes it. Fundamental indivisible particles are described by gauge theories with an underlying symmetry group. The first successful gauge theory studied in QFT was *Quantum Electrodynamics* (QED), described by the group $U(1)$, which underlies the interactions between charged leptons and photons. QED was propelled in a large part by Hans Bethe [Bet47], Freeman Dyson [Dys49], Sin-Itiro Tomonaga [Tom46], Julian Schwinger [Sch48a, Sch48b], and Richard Feynman [Fey50, Fey18b]. Tomonaga, Schwinger, and Feynman were jointly awarded the 1965 Nobel Prize in physics, for the development of a covariant formulation of QED, as well as developing techniques to compute observables at any order of perturbation theory. The claim that quantum field theories provide theoretical predictions that are in the strongest agreement with experiment is particularly true of QED [MTK$^+$23].

A few years after the advent of QED, many new composite particles were discovered [Fri12] leading Murray Gell-Mann to propose an underlying $SU(3)$ symmetry group describing these composite particles, called *hadrons*. A theory began to arise of indivisible particles called quarks which obey $SU(3)$ *color* symmetry, such that any given quark takes on one of three possible "colors": red (r), green (g), or blue (b). The wavefunctions of the quarks are assumed to be color singlets that fall into two categories: baryons with a color singlet wavefunction $rgb + brg + gbr - rbg - grb - bgr$, or mesons with a color singlet wavefunction $\bar{r}r + \bar{g}g + \bar{b}b$. By the 1970's, this symmetry began to be interpreted as a gauge group, similar to that of QED. The theory that arose out of this was Quantum

Chromodynamics (QCD), described by the gauge group $SU(3)$, which underlies the interactions between quarks via massless gauge bosons, called gluons. It is this theory that eventually began to describe hadronic composite particles coming out of colliders like CERN.

In 1973, David Gross and Frank Wilczek, as well as David Politizer independently, proposed one of the most important properties of QCD: confinement and asymptotic freedom [GW73, Pol73]. Confinement and asymptotic freedom are two sides of the same coin: they underlie the statement that at small distances (high energies), quarks and gluons can be approximated as free particles. Contrastingly, at large distances (weak energies), quarks and gluons are very tightly bounded. This implies that there is an energy scale in which perturbation theory works very well, but breaks down as the energy scale lowers. This is a fundamental property that all perturbative QCD calculations must take into account.

Many textbook calculations in QFT are done, in general, by computing scattering matrix (S-matrix) elements, or Green's functions, which can be used to determine cross sections of particular events. This is done perturbatively with Feynman diagrams. Corrections beyond 'tree-level' (lowest order) come from scattering diagrams containing loops, corresponding to integrals which in generally are formally divergent. These diagrams may lead one to believe this approach to QFT is incorrect, as it cannot make physical predictions beyond leading order. To resolve this problem, it is important to note that in an experiment, loops are not measurable. The measurable quantities are the n-particles in and out of the scattering experiment. Therefore, the mathematics describing the theory is not wrong, but just needs to take experiment into account. Renormalization is a systematic method that fixes the problem of loop divergences in scattering matrix elements, by fitting parameters at a particular scale in a given theory to experimental observables. This allows one to make non-trivial predictions of observables theoretically at a different scale

Techniques in renormalization came about largely due to the work by Murray Gell-Mann, Francis Low [GML54], Curtis Callan [Cal70], Kurt Symanzik [Sym70], and Kenneth Wilson [Wil71] [AEWHR24]. Ken Wilson, the so-called 'Father of the

Renormalization Group', connected the problem of scale dependencies in quantum field theories with phase transitions in condensed matter physics. This laid the way for the *Renormalization Group* [Wil83]. A derivative of Wilson's renormalization group, which aims to remove high-energy degrees of freedom, was developed jointly by Wilson and Stanisław Głazek. Coined the *Renormalization Group Procedure for Effective Particles* (RGPEP) [GW93], this approach removes large differences in energy in an interaction. This renormalization scheme will be described in detail in this thesis.

In a 1949 paper, Dirac [Dir49] suggested an alternative parameterization of space-time, rather than the standard equal-time parameterization, leading to a new Hamiltonian formulation of QFT. Dirac shows that this parameterization, called the front-form, along with the standard equal time frame and a lesser studied point-form, are the three unique parameterizations of space-time that cannot be accessed by a Lorentz transformation of one of the other. The main takeaway from this paper is that the front form (light-front) formalism of quantum field theory is a viable approach to QFT calculations. It turns out that the work of Sergio Fubini, Giuseppe Furlan [FF65], John Kogut, Davison Soper [KS70], and Stephen Weinberg [Wei66] all which studied the 'infinite momentum frame' is functionally the same framework proposed by Dirac. This was shown by Henrich Leutwyler [LS78, LKS70]. Stanley Brodsky, Hans-Christian Pauli, and Stephen Pinsky [BPP98] in their 1998 paper summarize all of these results, and show the benefits the front form provides, which will be discussed in length throughout this thesis.

The front form formalism is the backbone of Deep Inelastic Scattering (DIS) [Tay91, FK72], and Deeply Virtual Compton Scattering (DVCS) [Ji97, Die03], which collectively refer to processes to probe the subatomic structure of hadrons. DIS probes hadronic structure by scattering a charged lepton off a hadron: $lh \to l'X$. The process is 'deeply virtual' implying that the after the interaction with the lepton, the hadron breaks up to a collection of unmeasured quarks and gluons, collectively labeled X. Measuring the cross section at various scattering angles gives insight to the internal structure of hadrons. DVCS is a similar process, but is given by

$lH \to l'H'\gamma$, i.e. the hadron H doesn't break up into quarks and gluons but recoils with the incoming lepton and produces a photon. These experiments yield *structure functions*: Parton Distribution Functions (PDF), which come from DIS, and Generalized Parton Distribution Functions (GPD), which come from DVCS. PDFs describe the longitudinal momentum distribution carried by quarks and gluons within a hadron, while GPDs describe both the longitudinal and transverse momentum distributions.

PDFs and GPDs tie into renormalization groups via the Dokshitzer-Gribov-Lipatov-Alterelli-Parisi (DGLAP) evolution equations [Dok77, GL72, AP77, GBM98], which describe how these distributions change with a change in the relevant energy scale (determined by the invariant four-momentum of the 'probing' virtual photon, γ^*). These equations are based on the unproven, but experimentally consistent, property of *factorization*, which is a principle that states that the 'hard' (perturbative) part of the scattering process can be separated from the 'soft' (non-perturbative) part via a convolution. PDFs and GPDs describe the soft part of the cross section, implying that computing these distributions are necessary in reconstructing the full cross section.

2.2 Computational Methods for Quantum Field Theories

The large number of degrees of freedom in quantum field theories require powerful computational techniques to confirm theory and compare predictions with experiment. The leading computational method for classical calculations of QFTs is Lattice gauge theory. In particular, lattice QCD was developed by ideas from a paper by Wilson [Wil74], and further developed by work from Kogut and Leonard Susskind [KS75]. Today, there are multiple extensive collaborations who produce extremely precise results [Lin23, ABC$^+$26, DNB$^+$22, KBB$^+$22]. Formally lattice QCD calculations are done with varying lattice size L and lattice spacing a, and the results are extrapolated to $L \to \infty$ and $a \to 0$.

Current state-of-the-art calculations in lattice QCD have computed the proton mass as $960 \pm 13\ GeV$ [YLB$^+$18] in comparison to the experimental value of 938 GeV [NIS]. In this work, they also computed the proton mass decomposition and show that roughly 9% of the total proton mass comes from the up and down valence quarks. To decrease the computational time needed to perform these simulations, the pion mass is generally taken above the physical limit, and serves as another extrapolation, such that $m_\pi \to m_{\pi,\text{phys.}}$. This arises from the fact that in Monte Carlo-based algorithms, the inverse fermionic propagator $(i\gamma_\mu \partial^\mu - m_f)^{-1}$ needs to be computed. State-of-the-art calculations, however, are becoming increasingly more able to work at the physical pion mass, $m_\pi = 139\ MeV$ [ABC$^+$26].

An alternative classical computational approach uses light-front field theory. The light-front Hamiltonian corresponding to a particular theory is discretized via Discretized Light-cone Quantization (DLCQ) and/or Basis Light-front Quantization (BLFQ) developed by Pauli/Brodsky and James Vary et al. respectively.

The original work on quantum simulation of quantum field theories was done by Stephen Jordan, Keith Lee, and John Preskill [JLP12]. They employ a discrete lattice, in which the fields can be represented at each lattice point by a finite number of qubits. Since their original paper, this has become the preeminant quantum sim-

ulation of quantum field theories approach [PSCMAC21, EERS21, MTV20, BY06, AZL+21].

An alternative quantum simulation framework for quantum field theories was proposed by Michael Kreshchuk et al. in Refs. [KKG+22, KJK+21a, KJK+21b]. This work was based on a concept proposed by Wilson [Wil90], where he describes an interesting potential connection between quantum chemistry and quantum field theories by utilizing the front form. The extensive literature and research that has gone into quantum chemistry makes this a particularly auspicious framework for quantum simulation.

2.3 Light-front Field Theory

Quantum field theory courses are generally taught from a Lagrangian approach and compute physical predictions for experiments by computing S-matrix elements and feeding the results into a formula for a cross section. Mentions of a Hamiltonian are scant in most quantum field theory textbooks because it is not a Lorentz invariant quantity, but rather a component of a four-vector. The light-front approach to quantum field theory can be viewed as a Hamiltonian approach, and an alternative to the standard formalism. In this Section, we describe the light-front approach to quantum field theory, as well as its advantages and disadvantages.

2.3.1 An Introduction to the Front Form

The front form was proposed by Dirac [Dir49] as one of three possible parameterizations of Minkowski space-time. These three are unique in that there is not a possible Lorentz transformation that will take one to another. Most textbook QFT calculations are done in the equal-time coordinate system, but the front form has many useful features.

Any relativistically invariant quantum field theory must maintain the symmetries of the Poincaré group. The generators of the Poincaré group are the four-momentum vector P^μ and angular momentum tensor $M^{\mu\nu}$. The Poincaré algebra is [Ser19]

$$\Big[P^\mu, P^\nu\Big] = 0 \tag{2.1}$$

$$\Big[M^{\mu\nu}, P^\sigma\Big] = i\Big(g^{\nu\sigma}P^\mu - g^{\mu\sigma}P^\nu\Big) \tag{2.2}$$

$$\Big[M^{\mu\nu}, M^{\sigma\rho}\Big] = i\Big(g^{\nu\sigma}M^{\mu\rho} - g^{\mu\rho}M^{\nu\sigma} + g^{\nu\rho}M^{\sigma\mu} - g^{\sigma\mu}M^{\sigma\mu}\Big). \tag{2.3}$$

These are, what Dirac calls, ten fundamental quantities: P^0, the energy, P^i, the momentum, $J^i = \epsilon^{ijk}M^{jk}$ [BPP98], the angular momentum, and $K^i = M^{0i}$, the boost operators. Dirac also claims that no parameterization of space-time allows one to diagonalize more than seven of these ten operators simulateneously. The front

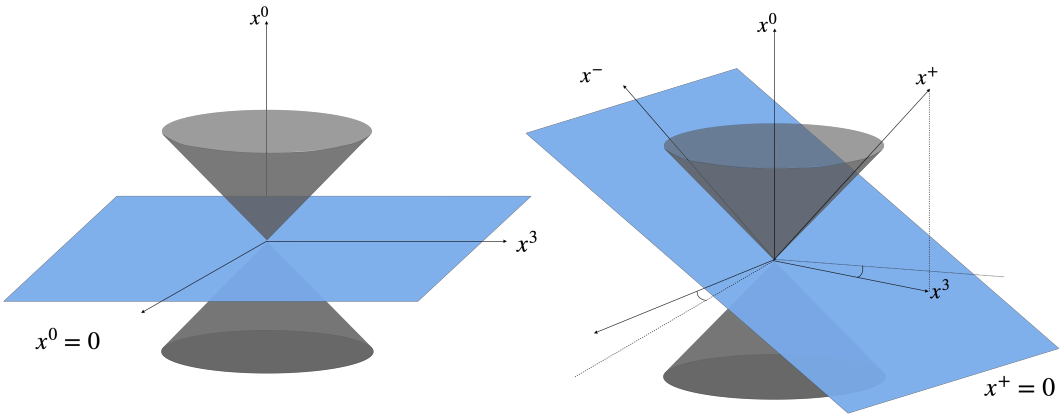

(a) Instant Form (b) Front Form

Figure 2.1: **Equal Time vs. Front Form**

form parameterization admits seven mutually commuting operators, the maximum possible that Dirac asserts. The operators P^i and M^{ij} are kinematical, that is their forms are the same in the free and interacting theories. P^0 and M^{0i} are dynamical, meaning their forms in the interacting case are complicated. In the front form, the kinematical components are: $P^+, \vec{P}^\perp, M^{-+}, M^{12}, M^{1+}$, and M^{2+}.

The front form is defined by a reparameterization of space-time coordinates. The light-front position vector is $x^\mu = (x^+, x^-, \vec{x}^\perp)$, where the light-front "time" is taken to be $x^+ \equiv x^0 + x^3$, light-front "space" is taken to be $x^- \equiv x^0 - x^3$, and the x^1 and x^2 are left untouched. Collectively, they are conventially referred to as $\vec{x}^\perp = (x^1, x^2)$. The metric in light-front coordinates is

$$g_{\mu\nu} = \begin{pmatrix} 0 & \frac{1}{2} & 0 & 0 \\ \frac{1}{2} & 0 & 0 & 0 \\ 0 & 0 & -1 & 0 \\ 0 & 0 & 0 & -1 \end{pmatrix} \qquad g^{\mu\nu} = \begin{pmatrix} 0 & 2 & 0 & 0 \\ 2 & 0 & 0 & 0 \\ 0 & 0 & -1 & 0 \\ 0 & 0 & 0 & -1 \end{pmatrix}. \tag{2.4}$$

The light-front four momentum is defined as $p^\mu = (p^+, p^-, \vec{p}^\perp)$, where the light-front 'momentum' is $p^+ = p^0 + p^3$, while the light-front 'energy' is $p^- = p^0 - p^3$.

For any massive particle, $p^+ > 0$ since

$$p^+ = p^0 + p^3 = \sqrt{m^2 - (p^1)^2 - (p^2)^2 - (p^3)^2} + p^3 \geq m.$$

The scalar dot product is

$$\begin{aligned} p^\mu x_\mu &= p^+ x_+ + p^- x_- - \vec{p}^\perp \cdot \vec{x}_\perp \\ &= \frac{1}{2} p^+ x^- + \frac{1}{2} p^- x^+ - \vec{p}^\perp \cdot \vec{x}^\perp. \end{aligned} \tag{2.5}$$

Throughout this thesis, capital P^μ refers to the four-momentum of a collection of particles, while lower-case p^μ refers to the four-momentum of a single particle. The representation of the Dirac algebra used in this thesis is:

$$\begin{aligned} \gamma^0 &= \begin{pmatrix} 0 & \mathbb{1} \\ \mathbb{1} & 0 \end{pmatrix}, & \gamma^3 &= \begin{pmatrix} 0 & -\mathbb{1} \\ \mathbb{1} & 0 \end{pmatrix} \\ \gamma^1 &= \begin{pmatrix} -i\sigma^2 & 0 \\ 0 & i\sigma^2 \end{pmatrix}, & \gamma^2 &= \begin{pmatrix} -i\sigma^1 & 0 \\ 0 & i\sigma^1 \end{pmatrix} \end{aligned} \tag{2.6}$$

Quantum fields are initially defined on the hypersurface in Fig. 2.1 tangential to the light cone at $x^+ = 0$. The light-front energy p^- generates translations in light-front time x^+. One can picture this as the hypersurface at $x^+ = 0$ moving in x^+ while remaining perpendicular to the x^+ axis.

Given the four-momentum of a collection of particles, P^μ, the invariant momentum squared is

$$P^\mu P_\mu = P^+ P^- - (\vec{P}^\perp)^2 = M^2 \tag{2.7}$$

When Equation 2.7 is quantized, such that P^+, P^-, and $\vec{P}^\perp$ become operators, this relation is interpreted as an eigenvalue equation:

$$\left(\hat{P}^- \hat{P}^+ - (\hat{\vec{P}}^\perp)^2\right) |\psi\rangle = M^2 |\psi\rangle \,, \tag{2.8}$$

where M^2 is the squared mass of the wavefunction $|\psi\rangle$. Recall that the kinematical

components of P^μ are P^+ and $\vec{P}^\perp$, and these two operators commute. This implies that there exists a basis for the wavefunction $|\psi\rangle$ in which $\hat{P}^+$ and $\hat{\vec{P}}^\perp$ are diagonal, i.e.

$$\hat{P}^+ |\psi\rangle = P^+ |\psi\rangle \tag{2.9}$$

$$\hat{\vec{P}}^\perp |\psi\rangle = \vec{P}^\perp |\psi\rangle \,. \tag{2.10}$$

After choosing a basis of fixed P^+ and $\vec{P}^\perp$ (the eigenvalues of the corresponding operators), one must diagonalize the 'Hamiltonian', $\hat{P}^-$ in this basis, giving the eigenvalues M^2, the squared mass of the bound states.

One of the main goals of the light-front approach should now be clear. One fixes the longitudinal and transverse momentum, and diagonalizes the following eigenvalue equation for the light-front Hamiltonian to determine bound state masses (M^2) and wavefunctions ($|\psi\rangle$):

$$\hat{P}^- |\psi\rangle = \frac{M^2 + (\vec{P}^\perp)^2}{P^+} |\psi\rangle \tag{2.11}$$

Since $\hat{P}^-$ is a component of a four-vector, it depends on the reference frame chosen; however, $\Big(\hat{P}^-\hat{P}^+ - (\hat{\vec{P}}^\perp)^2\Big)$ is Lorentz invariant. Therefore, when $\hat{P}^-$ is diagonalized, the resulting M^2 spectrum will be the same regardless of the choice of P^+ and $\vec{P}^\perp$. Lastly, the fact that the longitudinal boost operator is kinematic implies that boosting to different values of P^+ is simple, compared to in the instant form in which applying a boost to a wavefunction is as difficult as determining the wavefunction (by diagonalizing the Hamiltonian).

2.3.2 The Free Dirac Field

The Lagrangian corresponding to a free Dirac field is:

$$\mathcal{L}_{\rm D} = \bar{\psi}\Big(i\gamma^\mu\partial_\mu - m\Big)\psi. \tag{2.12}$$

The Euler-Lagrange equations lead to the form of the Dirac Equation:

$$\Big(i\gamma^\mu\partial_\mu - m\Big)\psi = 0, \tag{2.13}$$

whose solutions describe a free Dirac particle (a spin-1/2 fermion). The light-front gamma matrices, $\gamma^\mu = (\gamma^+, \gamma^-, \vec{\gamma}^\perp)$, satisfy the usual algebra: $\{\gamma^\mu, \gamma^\nu\} = 2g^{\mu\nu}$. Projectors ($\Lambda_i$) acting on the Dirac field must satisfy projector algebra:

1. **Completeness**

$$\sum_i \Lambda_i = \mathbb{1}$$

2. **Idempotency**

$$\Lambda_i\Lambda_j = \begin{cases} \Lambda_i, & i = j; \\ 0, & i \neq j \end{cases}$$

In equal-time coordinates, projectors can be defined by:

$$\Lambda_R = \frac{1+\gamma^5}{2} \qquad \Lambda_L = \frac{1-\gamma^5}{2}, \tag{2.14}$$

which project out the right and left-handed components of the Dirac spinor ψ respectively.

In light-front coordinates, a set of projectors can be defined by :

$$\Lambda_1 = \frac{1}{4}\gamma^-\gamma^+ = \frac{1}{2}\gamma^0\gamma^+ \qquad \Lambda_2 = \frac{1}{4}\gamma^+\gamma^- = \frac{1}{2}\gamma^0\gamma^-, \tag{2.15}$$

such that $\Lambda_1\psi \equiv \psi_1$ and $\Lambda_2\psi \equiv \psi_2$. Since $\Lambda_1 + \Lambda_2 = \mathbb{1}$, ψ can be written as a sum: $\psi = \psi_1 + \psi_2$.

In front-form coordinates, the free Dirac equation is:

$$\Big(\frac{i}{2}\gamma^+\partial^- + \frac{i}{2}\gamma^-\partial^+ - i\vec{\gamma}^\perp\cdot\vec{\partial}^\perp - m\Big)\psi = 0. \tag{2.16}$$

Multiplying Equation 2.16 by γ^0 gives:

$$\Big(i\Lambda_1\partial^- + i\Lambda_2\partial^+ - i\gamma^0\vec{\gamma}^\perp\cdot\vec{\partial}^\perp - \gamma^0 m\Big)\psi = 0. \tag{2.17}$$

To simplify, note that $\Lambda_1\gamma^0 = \gamma^0\Lambda_2$, $[\Lambda_i, \vec{\gamma}^\perp] = 0$, and that the ∂'s commute with all of the gamma matrices. Now, after multiplying Equation 2.17 by Λ_1, it reduces to:

$$i\partial^-\psi_1 = \gamma^0\Big(i\vec{\gamma}^\perp\cdot\vec{\partial}^\perp + m\Big)\psi_2. \tag{2.18}$$

Similarly, multiplying Equation 2.17 with Λ_2 gives:

$$i\partial^+\psi_2 = \gamma^0\Big(i\vec{\gamma}^\perp\cdot\vec{\partial}^\perp + m\Big)\psi_1. \tag{2.19}$$

The distinction between Equation 2.18 and Equation 2.19 is significant. Equation 2.18 gives the light-front 'time' evolution of the field ψ_1, while Equation 2.19 gives the light-front 'space' evolution of the field ψ_2. There is no 'time' derivative acting on ψ_2 which implies that ψ_2 is constrained by ψ_1. Contrastingly, ψ_1 is dynamical since it is being acted on by the 'time' derivative.

As an aside, a major difference between the instant form and the front form has now presented itself. In the instant form, the projectors one defines, Λ_L and Λ_R such that $\Lambda_R\psi = \psi_R$ and $\Lambda_L\psi = \psi_L$, project out two *dynamical* spinors [PS95]: $i\sigma\cdot\partial\psi_R = m\psi_L$, and $i\sigma\cdot\partial\psi_L = m\psi_R$ whose equations of motion are coupled. Notably, both ψ_R and ψ_L are acted on by ∂^0, the instant form time derivative, hence both ψ_R and ψ_L are dynamical. In the front form, the projectors one can define, Λ_1 and Λ_2, project out one dynamical spinor and one constrained spinor. This reduces the degrees of freedom in the Dirac spinors from 4 (in instant coordinates) to 2 (in light-front coordinates). A consequence of this comes from studying *interacting* theories. Higher order interaction diagrams will appear in the canonical Hamiltonian that don't appear in the canonical instant form Hamiltonian. These are referred to as 'instantaneous' interaction terms, which will be studied when discussing interacting theories. Eliminating fermion and gauge boson degrees of freedom leads to non-local

interaction terms.

Equations 2.18 and 2.19 are coupled differential equations so one field can be solved in terms of the other. Since ψ_1 is the dynamical field, ψ_2 should be solved in terms of ψ_1. To do this, an ansatz for the form of the free spinors is asserted [Hil16]:

$$\begin{aligned}\psi_1(x) &= w_1(p)e^{-ipx} \\ \psi_2(x) &= w_2(p)e^{-ipx},\end{aligned} \tag{2.20}$$

such that $\Lambda_i w_i(p) = w_i(p)$.

Plugging 2.20 into Equations 2.18 and 2.19 give equations for the spinors $w_i(p)$:

$$p^- w_1 = \gamma^0\Big(\vec{\gamma}^\perp \cdot \vec{p}^\perp + m\Big)w_2 \tag{2.21}$$

$$p^+ w_2 = \gamma^0\Big(\vec{\gamma}^\perp \cdot \vec{p}^\perp + m\Big)w_1. \tag{2.22}$$

The constraint equation can give the form of w_2 in terms of w_1:

$$w_2 = \frac{\gamma^0\Big(\vec{\gamma}^\perp \cdot \vec{p}^\perp + m\Big)}{p^+}w_1. \tag{2.23}$$

Now the full spinor ψ can be written purely in terms of the dynamical spinor, w_1:

$$\psi = \frac{1}{p^+}\Big(p^+ + \gamma^0(\vec{\gamma}^\perp \cdot \vec{p}^\perp + m)\Big)w_1(p). \tag{2.24}$$

The equation $\Lambda_1 w_1 = w_1$ implies that w_1 is an eigenvector of Λ_1 with eigenvalue $+1$. In the representation of the Dirac algebra chosen (Equation 2.6), the projector Λ_1 is given as:

$$\Lambda_1 = \begin{pmatrix} 1 & 0 & 0 & 0 \\ 0 & 1 & 0 & 0 \\ 0 & 0 & 0 & 0 \\ 0 & 0 & 0 & 0 \end{pmatrix}, \tag{2.25}$$

Two valid basis eigenvectors of this projector matrix can be taken $w_1^{(1)} = 2^{-1/2}(1,1,0,0)^T$ and $w_1^{(2)} = 2^{-1/2}(-1,-1,0,0)^T$, which can be used as a basis for ψ via Equation 2.24, i.e. a valid basis for ψ is

$$\psi^{(1)} = \frac{1}{p^+}\Big(p^+ + \gamma^0(\vec{\gamma}^\perp \cdot \vec{p}^\perp + m)\Big)w_1^{(1)} \tag{2.26}$$

$$\psi^{(2)} = \frac{1}{p^+}\Big(p^+ + \gamma^0(\vec{\gamma}^\perp \cdot \vec{p}^\perp + m)\Big)w_1^{(2)}. \tag{2.27}$$

By the fact $\{\gamma^0, \vec{\gamma}^\perp\} = 0$, and defining $\eta_\lambda = (\delta_{\lambda,+1}, \delta_{\lambda,-1})^T$:

$$\psi_\lambda^{(1)} = \frac{1}{p^+}\begin{pmatrix} p^+\eta_\lambda \\ (i\sigma^1 p^2 - i\sigma^2 p^1 + m)\eta_\lambda \end{pmatrix}. \tag{2.28}$$

Similarly,

$$\psi_\lambda^{(2)} = \frac{1}{p^+}\begin{pmatrix} -p^+\eta_\lambda \\ (i\sigma^2 p^1 - i\sigma^1 p^2 + m)\eta_\lambda \end{pmatrix}. \tag{2.29}$$

The spinor $\psi_\lambda^{(1)}$ is taken as the spinor $u_\lambda(p)$, while $\psi^{(2)}$ is taken as the spinor $v_\lambda(p)$. These spinors are not currently normalized in the standard way:

$$\bar{u}_\lambda(p)u_{\lambda'}(p) = -\bar{v}_\sigma(p)v_{\lambda'}(p) = 2m\delta_{\lambda\lambda'}. \tag{2.30}$$

To normalize the spinors u and v, define $\sigma_p = i\sigma^1 p^2 - i\sigma^2 p^1$ and compute:

$$\begin{aligned}\bar{u}_\lambda(p)u_{\lambda'}(p) &= \frac{|N|^2}{(p^+)^2}\begin{pmatrix} p^+\eta_\lambda & 0 & (-\sigma_p + m)\eta_\lambda & 0 \end{pmatrix}\begin{pmatrix} 0 & \mathbb{1} \\ \mathbb{1} & 0 \end{pmatrix}\begin{pmatrix} p^+\eta_{\lambda'} \\ 0 \\ (\sigma_p + m)\eta_{\lambda'} \\ 0 \end{pmatrix} \\ &= \frac{|N|^2}{(p^+)^2}\Big(2mp^+\delta_{\lambda,\lambda'}\Big).\end{aligned} \tag{2.31}$$

Similarly, the v spinor can be normalized. The full normalized form of the spinors

can be sumarized:

$$u_\lambda(p) = \frac{1}{\sqrt{p^+}} \begin{pmatrix} p^+\eta_\lambda \\ (i\sigma^1 p^2 - i\sigma^2 p^1 + m)\eta_\lambda \end{pmatrix} \tag{2.32}$$

$$v_\lambda(p) = \frac{1}{\sqrt{p^+}} \begin{pmatrix} -p^+\eta_{-\lambda} \\ (i\sigma^2 p^1 - i\sigma^1 p^2 + m)\eta_{-\lambda}. \end{pmatrix} \tag{2.33}$$

These spinors satisfy the Dirac equation:

$$(\gamma^\mu p_\mu - m)u_\lambda(p) = 0 \qquad (\gamma^\mu p_\mu + m)v_\lambda(p) = 0, \tag{2.34}$$

and are complete:

$$\sum_\lambda u_\lambda(p)\bar{u}_\lambda(p) = \gamma^\mu p_\mu + m \tag{2.35}$$

$$\sum_\lambda v_\lambda(p)\bar{v}_\lambda(p) = \gamma^\mu p_\mu - m. \tag{2.36}$$

The Dirac field for fixed helicity, color, and flavor can now be quantized:

$$\psi_{\lambda,c,f}(x) = \int \frac{dp^+ d^2\vec{p}^\perp}{16\pi^3 p^+} \Big(b_{\lambda,c,f}(p)u_\lambda(p)e^{-ipx} + d^\dagger_{\lambda,c,f}(p)v_\lambda(p)e^{ipx} \Big). \tag{2.37}$$

$$\bar{\psi}_{\lambda,c,f}(x) = \int \frac{dp^+ d^2\vec{p}^\perp}{16\pi^3 p^+} \Big(b^\dagger_{\lambda,c,f}(p)\bar{u}_\lambda(p)e^{ipx} + d_{\lambda,c,f}(p)\bar{v}_\lambda(p)e^{-ipx} \Big). \tag{2.38}$$

The 'ladder operators' $b_n(p), d_n(p), b^\dagger_n(p), d^\dagger_n(p)$ serve to create and annihilate particles with fixed quantum numbers, $n = \{\lambda, c, f\}$ and momentum, $p^+, \vec{p}^\perp$. These operators obey anticommutation relations:

$$\begin{aligned} \Big\{ b_n(q), b^\dagger_m(p) \Big\} = \Big\{ d_n(q), d^\dagger_m(p) \Big\} &= |q^+| 4\pi\delta(q^+ - p^+)(2\pi)^2\delta^{(2)}(\vec{q}^\perp - \vec{p}^\perp)\delta_{nm} \\ \Big\{ b_n(q), d_m(p) \Big\} = \Big\{ b^\dagger_n(q), d^\dagger_m(p) \Big\} = \Big\{ b_n(q), d^\dagger_m(p) \Big\} &= \Big\{ d_n(q), b^\dagger_m(p) \Big\} = 0, \end{aligned} \tag{2.39}$$

where n, m correspond to a set of discrete quantum numbers, and

$$\delta_{nm} = \delta_{\lambda,\lambda'}\delta_{c,c'}\delta_{f,f'}$$

A general field operator is the sum over all possible helicities, colors, and flavors, and is given as

$$\psi(x) = \sum_{\lambda,c,f} \psi_{\lambda,c,f}(x) \tag{2.40}$$

It is beneficial to work in momentum space. To accomplish this for the free Dirac field, $\psi(x)$ must be Fourier transformed to momentum space, $\psi(q)$. The Fourier pair is given as

$$\psi(q) = \int dx^- d^2\vec{x}^\perp e^{iqx}\psi(x) \tag{2.41}$$

$$\psi(x) = \int \frac{dq^+ d^2\vec{q}^\perp}{4\pi(2\pi)^2} e^{-iqx}\psi(q). \tag{2.42}$$

The conjugate field can also be transformed:

$$\bar{\psi}(x) = \int \frac{dq^+ d^2\vec{q}^\perp}{4\pi(2\pi)^2} e^{-iqx}\bar{\psi}(-q). \tag{2.43}$$

The $-q$ comes from taking the conjugate of $\psi(x)$ in its Fourier decomposition. This will now depend on e^{iqx}, rather than e^{-iqx}. Switching $q \to -q$ changes the exponential to e^{-iqx}, with the consequence of changing q in the conjugate field.

Now, to simplify $\psi(q)$, the quantized Dirac field in position space in Equation 2.37 can be substituted. Using

$$\begin{aligned}\int dx^- d^2\vec{x}^\perp e^{i(q-p)x} &= \int dx^- d^2\vec{x}^\perp e^{\frac{i}{2}(q^+-p^+)x^- - i(\vec{q}^\perp-\vec{p}^\perp)\cdot\vec{x}^\perp} \\ &= 4\pi\delta(q^+-p^+)(2\pi)^2\delta^{(2)}(\vec{q}^\perp-\vec{p}^\perp) \qquad (2.44)\\ &\equiv \delta(q-p), \qquad (2.45)\end{aligned}$$

the momentum-space Dirac fields are given as:

$$\psi_{c,f,\lambda}(q) = \frac{\theta(q^+)u_\lambda(q)b_{c,f,\lambda}(q) + \theta(-q^+)v_\lambda(-q)d^\dagger_{c,f,\lambda}(-q)}{|q^+|}, \tag{2.46}$$

where, again, the subscript q on the ladder operators refer to q^+ and $q^\perp$, while the subscript n refers to other relevant quantum numbers. The full fermionic field

operator is then

$$\psi(q) = \sum_{c,f,\lambda} \psi_{c,f,\lambda}(q). \tag{2.47}$$

2.3.3 Bosonic Fields

Spin-0 scalar bosonic fields are represented throughout this thesis by the field ϕ, whose plane wave front form position space representation is given by:

$$\phi(x) = \int \frac{dp^+ d^2\vec{p}^\perp}{16\pi^3 p^+} \theta(p^+) \Big(e^{-ipx} a(p) + e^{ipx} a^\dagger(p) \Big). \tag{2.48}$$

Here, the ladder operators $a^\dagger(p), a(p)$ create and annihilate respectively a boson in with momentum p. These operators satisfy bosonic statistics:

$$\Big[a_n(p), a_m(q)^\dagger \Big] = |q^+| 4\pi \delta(q^+ - p^+)(2\pi)^2 \delta^{(2)}(\vec{q}^\perp - \vec{p}^\perp)\delta_{nm} \tag{2.49}$$

In momentum space, $\phi(q)$ takes the form:

$$\phi(q) = \frac{\theta(q^+)a(q) + \theta(-q^+)a^\dagger(-q)}{|q^+|}. \tag{2.50}$$

The quantized vector potential for fields with integer spin > 0 in terms of its dynamical degrees of freedom in position space is

$$A^\mu_{a,\sigma}(x) = \int \frac{dp^+ d^2\vec{p}^\perp}{4\pi(2\pi)^2 p^+} \Big(a_{a,\sigma}(p) \varepsilon^\mu_\sigma(p) e^{-ipx} + a^\dagger_{a,\sigma}(p) \varepsilon^{\mu\star}_\sigma(p) e^{ipx} \Big), \tag{2.51}$$

where σ is the polarization, and the polarization vector $\varepsilon^\mu_\sigma(p)$ is given as:

$$\varepsilon^\mu_\sigma(p) = \Big(0, \frac{2\vec{p}^\perp \cdot \vec{\varepsilon}^\perp_\sigma}{p^+}, \vec{\varepsilon}^\perp_\sigma \Big), \tag{2.52}$$

where

$$\vec{\varepsilon}^\perp_\sigma = -\frac{1}{\sqrt{2}} \Big(\sigma \hat{x} + i\hat{y} \Big). \tag{2.53}$$

In momentum space, the vector field is

$$A^{\mu}_{a,\sigma}(q) = \frac{\theta(q^+)\varepsilon^{\mu}_{\sigma}(q)a_{a,\sigma}(q) + \theta(-q^+)\varepsilon^{\mu\star}_{\sigma}(-q)a^{\dagger}_{a,\sigma}(-q)}{|q^+|}. \tag{2.54}$$

The full vector field is

$$A^{\mu}(q) = \sum_{a,\sigma} A^{\mu}_{a,\sigma}(q) \tag{2.55}$$

2.3.4 Light-front Hamiltonians

The energy-momentum tensor in position space for the fields ϕ_r is

$$T^{\mu\nu} = \frac{\partial \mathcal{L}}{\partial(\partial_\mu \phi_r)}\partial^{\nu}\phi_r - g^{\mu\nu}\mathcal{L}. \tag{2.56}$$

For the free Dirac field:

$$\begin{aligned} T^{\mu\nu} &= i\bar{\psi}\gamma^{\mu}\partial^{\nu}\psi + \delta^{\mu\nu}\bar{\psi}(i\gamma^{\alpha}p_{\alpha} - m)\psi - g^{\mu\nu}\mathcal{L} \\ &= i\bar{\psi}\gamma^{\mu}\partial^{\nu}\psi. \end{aligned} \tag{2.57}$$

The energy-momentum tensor in momentum space can be calculated by taking a Fourier transform of $T^{\mu\nu}(x)$:

$$\begin{aligned} \tilde{T}^{\mu\nu}(q) &= \int dx^- d^2\vec{x}^{\perp} e^{iqx} T^{\mu\nu}(x) \\ &= \int dx^- d^2\vec{x}^{\perp} e^{iqx} i\bar{\psi}(x)\gamma^{\mu}\partial^{\nu}\psi(x) \\ &= \int dx^- d^2\vec{x}^{\perp} e^{iqx} \int_{q_1} e^{-iq_1 x}\bar{\psi}(-q_1)\gamma^{\mu}\int_{q_2} q_2^- e^{-iq_2 x}\psi(q_2) \\ &= \int_{q_1,q_2} \int dx^- d^2\vec{x}^{\perp} e^{i(q-q_1-q_2)x}\bar{\psi}(-q_1)\gamma^{\mu}q_2^-\psi(q_2) \\ &= \int_{q_1,q_2} \delta(q-q_1-q_2)\bar{\psi}(-q_1)\gamma^{\mu}q_2^-\psi(q_2), \end{aligned} \tag{2.58}$$

where

$$\int_q \equiv \int \frac{dq^+ d^2\vec{q}^{\perp}}{4\pi(2\pi)^2}.$$

The Hamiltonian can be easily computed by plugging in $q = 0$ into the

momentum-space energy momentum tensor:

$$H = \int dx^- d^2\vec{x}^\perp \mathcal{H}(x) = \int dx^- d^2\vec{x}^\perp \frac{1}{2} T^{+-}(x) = \frac{1}{2} T^{+-}(q=0). \tag{2.59}$$

For example, the free fermion Hamiltonian is:

$$\begin{aligned} H &= \frac{1}{2} T^{+-}(q=0) \\ &= \frac{1}{2} \int_{q_1,q_2} \delta(q_1+q_2) \bar{\psi}(-q_1) \gamma^\mu q_2^- \psi(q_2) \\ &= \int_q q^- \bar{\psi}(q) \frac{\gamma^+}{2} \psi(q) \end{aligned} \tag{2.60}$$

A similar calculation can be done for bosonic terms or interactions. When there are interactions present, the convention we use is the momenta q_i always point inwards towards the vertex, e.g.

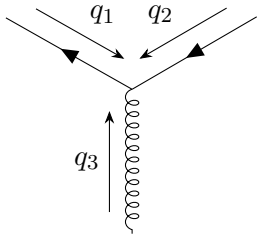

(2.61)

2.3.5 Invariant Mass, Momentum Transfer

A quantity that will appear a lot throughout this thesis is the square of the sum of two momentum four-vectors: $(q_1+q_2)^2$. This quantity is positive for a 'pair creation (or annihilation)' interaction term, but can be negative for a 'scattering' interaction term.

First, consider pair creation:

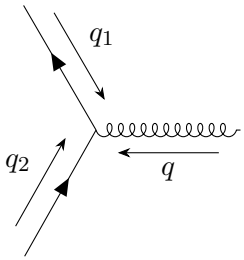

This corresponds to a term in the Hamiltonian $\sim \theta(-q_1^+)\theta(-q_2^+)\theta(q^+)\delta(q_1+q_2+q)$

which implies $q^+ = q_1^+ + q_2^+ > 0$ (i.e. q_1 and q_2 have the same sign). One can define a relative longitudinal momentum $x = q_1^+/q^+$, which with the momentum conservation implies $1 - x = q_2^+/q^+$ and $x \in (0, 1)$. From here, we can compute $(q_1 + q_2)^2$:

$$\begin{aligned}
(q_1 + q_2)^2 &= q_1^2 + q_2^2 + 2q_1 \cdot q_2 \\
&= m_1^2 + m_2^2 + q_1^+ q_2^- + q_1^- q_2^+ - 2q_1^\perp \cdot q_2^\perp \\
&= m_1^2\Big(1 + \frac{q_2^+}{q_1^+}\Big) + m_2^2\Big(1 + \frac{q_1^+}{q_2^+}\Big) + \frac{(q_1^+)^2(q_2^\perp)^2 + (q_2^+)^2(q_1^\perp)^2 - 2q_1^+ q_2^+ (q_1^\perp \cdot q_2^\perp)}{q_1^+ q_2^+} \\
&= \frac{m_1^2}{x} + \frac{m_2^2}{1-x} + \frac{\Big((1-x)q_1^\perp - xq_2^\perp\Big)^2}{x(1-x)} \\
&\geq (m_1 + m_2)^2
\end{aligned} \tag{2.62}$$

Therefore, for pair creation or annihilation, $(q_1 + q_2)^2 \geq (m_1 + m_2)^2$. Quite often, for pair creation or annihilation, we refer to $(q_1 + q_2)^2$ as the *invariant mass* of the two particles, and denote it $\mathcal{M}_{12}^2$. Furthermore, if we define $\kappa^\perp = (1-x)q_1^\perp - xq_2^\perp$, then

$$\mathcal{M}_{12}^2(x, \kappa) = \frac{m_1^2 + \kappa^2}{x} + \frac{m_2^2 + \kappa^2}{1-x}, \tag{2.63}$$

which will be a useful formula for computing loop integrals.

Next, consider a 'scattering' interaction term:

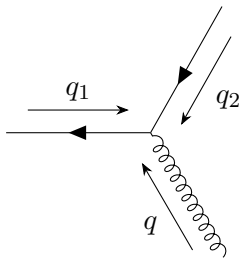

This corresponds to a term in the Hamiltonian $\sim \theta(-q_1)\theta(q_2)\theta(q)\delta(q_1+q_2+q)$ which

implies $q^+ = q_1^+ - q_2^+$ (and that $\mathrm{sgn}(q_1^+) = -\mathrm{sgn}(q_2^+)$). Therefore,

$$\begin{aligned}
(q_1+q_2)^2 &= q_1^2 + q_2^2 + 2q_1\cdot q_2 \\
&= m_1^2\Big(1+\frac{q_2^+}{q_1^+}\Big) + m_2^2\Big(1+\frac{q_1^+}{q_2^+}\Big) + \frac{(q_1^+)^2(q_2^\perp)^2 + (q_2^+)^2(q_1^\perp)^2 - 2q_1^+q_2^+(q_1^\perp\cdot q_2^\perp)}{q_1^+q_2^+} \\
&= m_1^2\Big(1+\frac{q_2^+}{q_1^+}\Big) + m_2^2\Big(1+\frac{q_1^+}{q_2^+}\Big) + \frac{\Big(q_2^+q_1^\perp - q_1^+q_2^\perp\Big)^2}{q_1^+q_2^+} \\
&\le m_1^2\Big(1+\frac{q_2^+}{q_1^+}\Big) + m_2^2\Big(1+\frac{q_1^+}{q_2^+}\Big) \\
&\le (m_1-m_2)^2. \qquad (2.64)
\end{aligned}$$

The last line can be easily computed in Mathematica by maximizing function $a(1+x/y)+b(1+y/x)$ subject to the constraint $\mathrm{sgn}(x) = -\mathrm{sgn}(y)$.

One last relationship that will be useful throughout this thesis is

$$\delta(q_1+q_2+q_3)\Big(q_1^- + q_2^- + q_3^-\Big) = \delta(q_1+q_2+q_3)\left(\frac{q_3^2-(q_1+q_2)^2}{q_3^+}\right). \qquad (2.65)$$

This is tedious and messy to prove, but the gist of the derivation is to write out explicitly $q_1^- + q_2^- + q_3^-$, substitute $q_3^\perp = -q_1^\perp - q_2^\perp$, which in q_3^- squares to give a term of the form $2q_1^\perp\cdot q_2^\perp$. We can make the substitution $2q_1^\perp\cdot q_2^\perp = q_1^2+q_2^2+q_1^+q_2^- + q_1^-q_2^+ - (q_1+q_2)^2$. From here, we group terms based on $q_1^2, q_2^2, (q_1^\perp)^2, (q_2^\perp)^2$ which leaves a term left over of the form $(q_3^2-(q_1+q_2)^2)(q_3^+)^{-1}$. For each of the terms that were grouped, the are each multiplied by an expression of the form $(q_1^+)^{-1} + (q_3^+)^{-1} + q_2^+(q_1^+q_3^+)^{-1}$, which simplifies to zero. Similarly,

$$\delta(q_1+q_2-q_3)\Big(q_1^- + q_2^- - q_3^-\Big) = \delta(q_1+q_2-q_3)\left(\frac{(q_1+q_2)^2-q_3^2}{q_3^+}\right). \qquad (2.66)$$

2.3.6 Advantages and disadvantages of light-front field theory

Quantum field theories are difficult conceptually and expensive computationally (both numerically and analytically). Any advantage one may find when studying these theories must be used. As the saying goes, "there is no free lunch" and so

with advantages come disadvantages. In this Section, we describe the pros and cons of light-front field theory.

We begin by discussing the advantages. In general, the form of canonical Hamiltonians in light-front field theory will be

$$H = H_0 + H_{int.}(g), \tag{2.67}$$

where H_0 is the kinetic energy, or free, part of the Hamiltonian with well-known eigenstates, and $H_{int.}$ is the non-trivial interacting part, whose strength is determined by the coupling parameter, g. This fact, paired with the fact that the eigenvalues of the light-front Hamiltonian (after fixing P^+ and $\vec{P}^\perp$) are M^2, makes the problem appear as a non-relativistic eigenvalue problem in standard quantum mechanics.

Another advantage is usually described as "the light-front vacuum is trivial/simple". This statement hides some relevant physics, but nevertheless has truth to it, which we will describe here. In the instant form, any state with zero longitudinal momentum couples to the vacuum, that is it has a non-zero matrix element. For example, $\langle 0| b^\dagger_{-p} b^\dagger_p |0\rangle \neq 0$. This implies vacuum fluctuations must be taken into account and complicate the theory. In the front form however, since massive particles have $p^+ > 0$, the vacuum can only couple to itself since, for example, $\langle 0| b^\dagger_{p^+} |0\rangle = 0$, implying all diagrams which generate vacuum fluctuations have a zero matrix element [BPP98]. Lastly, since the vacuum in the instant form is an eigenstate of the Hamiltonian in every sector, to compute the mass of a bound state, one needs to solve for the vacuum and an excited state and take the difference, whereas this is unnecessary in the front form.

The last advantage was an original proposition by Dirac for the utility of the front form [Dir49]. He states that the goal of any relativistic quantum theory is to mutually diagonalize as many of the 10 Poincaré generators as possible (by the commutation relations in Eqs. 2.1, 2.2, 2.3, it is not possible to mutually diagonalize all 10). According to Dirac, the front form admits the largest number of mutually

commuting operators – 7 out of 10 versus 6 out of 10 in the instant form. Additionally, the boost generators do not change when interactions are included, so boosting wavefunctions is 'easy', whereas in the instant form, boosting wavefunctions is as difficult as solving the eigenvalue problem.

The major disadvantage of the front form stems from the issue of zero modes – states with $p^+ = 0$ – which is only possible for massless particles (since $p^+ \geq m$ for a particle with mass m). Zero modes are a problem because of the energy-momentum dispersion relation

$$p^- = \frac{m^2 + (\vec{p}^{\perp})^2}{p^+}.$$

For a massless particle, p^+ can be zero which leads to infinitely large p^-. While all fermions we know of in the standard model have nonzero mass, two important gauge bosons (the photon and the gluon) have $m = 0$, which implies zero modes will be relevant in QED and QCD.

One way to mitigate zero modes is by imposing a vanishingly small, but nonzero, mass on theoretically massless gauge bosons. This appears at first to break gauge invariance of the theory since imposing $U(1)$ or $SU(3)$ symmetry of the fermion fields in QED and QCD respectively implies the existence of a gauge field A^μ with zero mass (note that Ward identities are preserved for $U(1)$, but not $SU(N)$). However, since we are working in a fixed gauge ($A^+ = 0$), this implies that we do not need explicit gauge invariance. In the end, we can look at a limit as the gauge boson mass goes to zero.

2.4 Probing Hadronic Substructure

A primary function of collider experiments is to understand the internal structure of hadrons. Different processes can be measured to learn different types of information about hadrons. In this section, we discuss two processes, deep inelastic scattering and deeply virtual compton scattering, which resolve longitudinal and transverse momentum distributions of quarks inside a hadron.

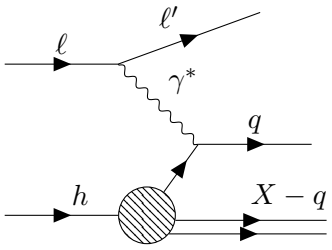

Figure 2.2: **Deep Inelastic Scattering**

2.4.1 Deep Inelastic Scattering and Parton Distribution Functions

The parton distribution function (PDF) of a hadron is a probability distribution that describes the probability of finding a quark (q) in the hadron (h) with momentum fraction x relative to the total hadronic momentum P^+. Formally, it is defined by [Sop97]

$$f_{q/h}(x) = \int \frac{dz^-}{4\pi} e^{-ixP^+z^-} \langle P| \bar{\psi}(z^-)\gamma^+\psi(0) |P\rangle , \tag{2.68}$$

where $|P\rangle$ is a bound state of the theory whose PDF one is interested in.

Collider experiments measure PDFs by studying the process $\ell h \to \ell' X$ via deep inelastic scattering (DIS), shown in Fig. 2.2, that is scattering a lepton with four momentum $\ell^\mu = (m_e, E)$ off a hadron with mass M. The PDF has a strong dependence on the four-momentum q of the exchanged virtual photon γ^*. One relevant Lorentz invariant quantity is the square of the virtual photon's four momentum, $Q^2 = -q^\mu q_\mu$. As Q^2 increases, the wavelength of the exchange boson decreases, refining the probe, which allows the structure inside the hadron to be resolved on a finer scale.

Besides Q^2, another important invariant quantity is "Bjorken x", given by $x_{Bj} = \frac{Q^2}{2M\nu}$, where $\nu = E - E'$ is the difference in the leptonic energy (which is also invariant). The physical interpretation of the Bjorken-x variable becomes obvious when looking at the momentum of the struck quark. Before the quark is struck by the virtual photon with four-momentum q, it carries a fraction of the total hadronic momentum x. In the parton model, $x \approx x_{Bj}$ [Gro].

The DIS cross section can be given as

$$d\sigma_{DIS} \sim L_{e^-}^{\mu\nu} W_{\mu\nu}^h, \tag{2.69}$$

where $L_\ell^{\mu\nu}$ is the leptonic tensor, which describes the coupling between the leptons and the exchange photon and depends on the lepton involved, and $W_{\mu\nu}^h$ is the hadronic tensor, which is formally given by

$$W_{\mu\nu}^h = \frac{1}{4\pi} \int d^4z e^{iq\cdot z} \Big\langle P,S \Big| \Big[J_\mu^\dagger(z), J_\nu(0) \Big] \Big| P,S \Big\rangle. \tag{2.70}$$

The leptonic tensor is calculable in perturbation theory; however, the hadronic tensor is not [Gro].

Since the hadronic tensor is not calculable, one must write down the most general form that it may take:

$$W_h^{\mu\nu} = W_1 \bigg(-g^{\mu\nu} + \frac{q^\mu q^\nu}{q^2} \bigg) + W_2 \bigg(-p^\mu + \frac{p\cdot q}{q^2} q^\mu \bigg) \bigg(-p^\nu + \frac{p\cdot q}{q^2} q^\nu \bigg), \tag{2.71}$$

where W_1 and W_2 are the *structure functions* of the hadron. These parameterize the behavior of the hadronic part of the interaction, and depend on Q^2 and ν[HM84].

Due to the complicated internal structure of hadrons consisting of quarks which are strongly bound, the total cross section of DIS cannot be exactly calculated. The principle of factorization, which is unproven but has strong experimental support, states that the cross section of DIS can be 'factorized' into a hard part (calculable in perturbation theory) and a soft part (one that must be extracted from experiment). That is, the factorization principle [CSS04] states

$$d\sigma_{DIS} = f_q(x) \otimes d\hat{\sigma}_{\ell\to\ell'\gamma^*}, \tag{2.72}$$

where $d\hat{\sigma}_{\ell\to\ell'\gamma^*}$ is the leptonic cross section and can be calculated with perturbation theory, and $f_q(x)$ is the parton distribution function. The symbol $\otimes$ is a Mellin convolution integral.

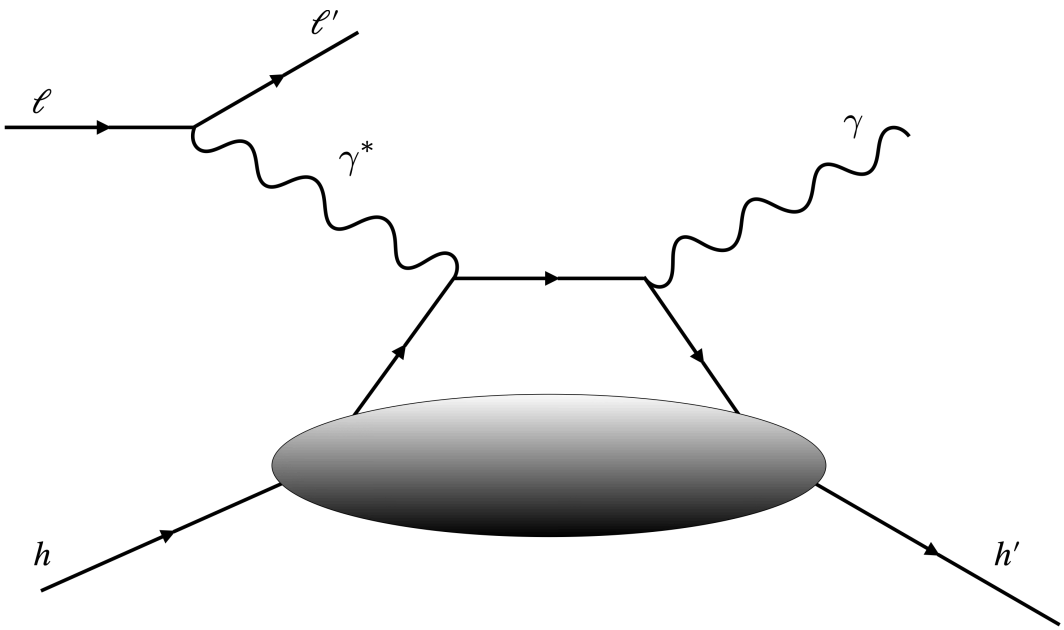

Figure 2.3: **DVCS** "Handbag Diagram" of the GPD

A major result in the theory of deep inelastic scattering is the DGLAP equation, which predicts the functional form of the PDF at various scales μ^2 (called the factorization scale) after an measurement at a particular scale, μ_0^2. The DGLAP equation is given as

$$\frac{\partial f_a}{\partial \ln \mu^2} \sim \frac{\alpha_s(\mu^2)}{2\pi} P_{ab} \otimes f_b, \tag{2.73}$$

where P_{ab} is a function that describes the probability that a parton of type b splits into a parton of type a.

2.4.2 Deeply Virtual Compton Scattering and Generalized Parton Distribution Functions

Notably, parton distribution functions measured by DIS do not give any information about transverse momentum distributions of quarks inside a hadron. To obtain this information, a new process must be studied – Deeply Virtual Compton Scattering (DVCS). DVCS measures the process $\ell h \to l'\gamma h'$ and is shown in Fig. 2.3 by what is colloquially referred to as a 'handbag diagram' [BDM$^+$20].

The formal defintion of the GPD [Mez22] for a quark is

$$H^q(x,\xi,t) = \int \frac{dz^-}{4\pi} e^{ixP^+z^-} \langle p'|\bar{\psi}(-z^-/2)\gamma^+\psi(z^-/2)|p\rangle, \tag{2.74}$$

where $|p\rangle$ and $|p'\rangle$ are initial and final hadronic states respectively. The two new parameters, $\xi = -(p'-p)^+/2P^+$ and $t = (p'-p)^2$ are invariant and describe momentum transfer in the transverse direction. The function H^q gives a three-dimensional view of the internal structure of the hadron in momentum space, and can describe both longitudinal and transverse momentum fractions. There are four unique GPD's that describe distributions for different polarizations combintations of the quarks relative to the hadron, but we only give the unpolarized helicity conserving GPD here (H^q) [Geo18].

2.5 The Renormalization Group Procedure for Effective Particles (RGPEP)

A well known hurdle of quantum field theories is the appearance of divergent observables calculated beyond leading order. At first, many thought this would invalidate the theory overall; however, today the technique of renormalization allows for finite observables to be calculated at any order of perturbation theory. There are many ways to do renormalization, and in this thesis we study the renormalization of Hamiltonians, which is the topic of this Section.

2.5.1 The Similarity Renormalization Group (SRG)

The similarity renormalization group (SRG) [SP00] is a very general method which can be adapted towards problems that arise in this thesis. SRG defines a unitary $U(s)$, which when conjugating a matrix A, results in a new matrix, parameterized by s:

$$A(s) = U^\dagger(s)AU(s). \tag{2.75}$$

The transformation in Eq. 2.75 is a *similarity* transformation, and defines the similarity renormalization "group" (technically it is a semi-group). Notably, similar matrices[1] share many properties: eigenspectra, trace, and determinant, to name a few.

The initial condition for Eq. 2.75 is $A(s=0) = A$, and s strictly increases towards infinity. Generally, one wishes to choose a $U(s)$ that leads to $A(s)$ to increase in 'diagonality' as s increases. There is not a clear definition of what is meant by increasing diagonality in the literature; however, we try to quantify it by the following definition

Definition 2.5.1 *A matrix $A(s)$ increases in diagonality with increasing s if*

$$\frac{d}{ds}\sum_i \Big|a_{ii}(s)\Big|^2 \geq 0 \tag{2.76}$$

$$\frac{d}{ds}\sum_{i\neq k} \Big|a_{ik}(s)\Big|^2 < 0 \tag{2.77}$$

The evolution of the matrix A with s is governed by the differential equation:

$$\begin{aligned}
\frac{d}{ds}A(s) &= \frac{d}{ds}\Big(U^\dagger(s)AU(s)\Big) \\
&= \frac{dU^\dagger(s)}{ds}AU(s) + U^\dagger(s)\frac{dA}{ds}U(s) + U^\dagger(s)A\frac{dU(s)}{ds} \\
&= \frac{dU^\dagger(s)}{ds}\Big(U(s)U^\dagger(s)\Big)AU(s) + U^\dagger(s)A\Big(U(s)U^\dagger(s)\Big)\frac{dU(s)}{ds} \\
&= \frac{dU^\dagger(s)}{ds}U(s)A(s) + A(s)U^\dagger(s)\frac{dU(s)}{ds}
\end{aligned}$$

Now, using the fact that

$$0 = \frac{d}{ds}\mathbb{1} = \frac{d}{ds}U^\dagger(s)U(s) = \frac{dU^\dagger(s)}{ds}U(s) + U^\dagger(s)\frac{dU(s)}{ds} \tag{2.78}$$

to get

$$\frac{d}{ds}A(s) = -U^\dagger(s)\frac{dU(s)}{ds}A(s) + A(s)U^\dagger(s)\frac{dU(s)}{ds}. \tag{2.79}$$

[1]Two matrices are similar if $\exists P$ whose inverse exists and $B \sim A \implies B = P^{-1}AP$. Here, we explicitly assume this "P" is unitary, but it does not have to be for similarity.

The evolution of $A(s)$ is now determined by the differential equation

$$\frac{dA(s)}{ds} = \Big[\mathcal{G}(s), A(s)\Big], \tag{2.80}$$

where $\mathcal{G}(s)$ is called the *generator* and is formally given by the differential equation:

$$\mathcal{G}(s) = -U^{\dagger}(s)\frac{dU(s)}{ds}, \tag{2.81}$$

which has the solution:

$$U(s) = T\exp\left(\int_0^s ds'\mathcal{G}(s')\right), \tag{2.82}$$

where T is the 'parameter-ordering' operator, which orders the operators in terms of increasing s. In practice, rather than choosing the unitary, $U(s)$, one chooses the generator, $\mathcal{G}(s)$.

The weakest constraint placed on $\mathcal{G}(s)$ such that Eq. 2.75 is satisfied is that it must be anti-Hermitian, that is $\mathcal{G}_{ij}(s) = -\mathcal{G}_{ji}(s)$, since exponentiating an anti-Hermitian operator generates a unitary. Satisfying this constraint alone, however, will not in general lead to a matrix which 'flows' towards the diagonal as intended.

Some common generators in the literature which do satisfy this 'flowing' behavior are the Wegner generator [Weg94], given as

$$\mathcal{G}(s) = \Big[\mathrm{diag}\Big(A(s)\Big), A(s)\Big], \tag{2.83}$$

and the Mielke generator [Mie98],

$$\mathcal{G}(s) = M \odot A(s), \tag{2.84}$$

where M is called the Mielke matrix, which has the form of -1's along the upper tridiagonal, and $+1$'s along the lower tridiagonal. The symbol $\odot$ is the standard Hadamard product between two matrices, that is element-wise multiplication, rather

than standard matrix multiplication.

Next, we prove that the Wegner generator increases the 'diagonality' of a matrix.

Theorem 2.5.1 *The flow of $A(s)$, under the Wegner generator monotonically increases the two-norm of the diagonal matrix elements of $A(s)$ and monotonically decreases the two-norm of the off-diagonal matrix elements of $A(s)$.*

Proof Defining $A(s) = \Big[a_{ij}(s)\Big]$, the ij^{th} component of the diagonal part of $A(s)$ is $\mathrm{diag}\Big(h(s)\Big)_{ij} = \delta_{ij}A_{ij}(s)$. The ij^{th} component of the generator is

$$\begin{aligned}\Big[G(s)\Big]_{ij} &= \Big[\mathrm{diag}\Big(A(s)\Big), A(s)\Big]_{ij} \\ &= \Big(\mathrm{diag}\Big(A(s)\Big)\cdot A(s)\Big)_{ij} - \Big(A(s)\cdot \mathrm{diag}\Big(A(s)\Big)\Big)_{ij}\end{aligned} \tag{2.85}$$

where

$$\begin{aligned}\Big(\mathrm{diag}\Big(A(s)\Big)\cdot A(s)\Big)_{ij} &= \sum_k \mathrm{diag}\Big(A(s)\Big)_{ik} a_{kj}(s) \\ &= \sum_k \delta_{ik}a_{ik}(s)a_{kj}(s) = a_{ii}(s)a_{ij}(s)\end{aligned} \tag{2.86}$$

and

$$\begin{aligned}\Big(A(s)\cdot \mathrm{diag}\Big(A(s)\Big)\Big)_{ij} &= \sum_k a_{ik}(s)\mathrm{diag}\Big(A(s)\Big)_{kj} \\ &= \sum_k a_{ik}(s)\delta_{kj}a_{kj}(s) = a_{ij}(s)a_{jj}(s).\end{aligned} \tag{2.87}$$

Put together,

$$g_{ij}(s) = \Big(a_{ii}(s) - a_{jj}(s)\Big)a_{ij}(s), \tag{2.88}$$

where $a_{ij}(s)$ and $a_{jj}(s)$ were commuted in the second product since $a_{mn}(s)$ are just matrix elements (scalars) which always commute.

The commutator between $g_{ij}(s)$ and $a_{ij}(s)$, which is the right hand side of

the Wegner flow equation, is

$$\left[\frac{dA(s)}{ds}\right]_{ij} = \Big[G(s), A(s)\Big]_{ij} = \sum_l \Big(g_{il}(s)a_{lj}(s) - a_{il}(s)g_{lj}(s)\Big)$$
$$= \sum_l \Big(a_{ii}(s) + a_{jj}(s) - 2a_{ll}(s)\Big)a_{il}(s)a_{lj}(s) \tag{2.89}$$

To show that the sum magnitude squared of the diagonal elements are increasing note that:

$$\frac{d}{ds}\Big|a_{ii}(s)\Big|^2 = \frac{d}{ds}\Big(a_{ii}(s)\Big)^2, \tag{2.90}$$

since A is Hermitian the magnitude squared of the diagonal matrix elements is just the square of the matrix elements (diagonal elements are real for Hermitian matrices). Now

$$\begin{aligned}
\frac{d}{ds}\sum_i \Big(a_{ii}(s)\Big)^2 &= 2\sum_i a_{ii}(s)\frac{da_{ii}(s)}{ds} \\
&= 2\sum_i a_{ii}(s)\Big[2a_{ii}(s)\Big(A^2(s)\Big)_{ii} - 2\sum_l a_{ll}(s)a_{il}(s)a_{li}(s)\Big] \\
&= 4\sum_{il}\Big(a_{ii}(s)a_{ii}(s)a_{il}(s)a_{li}(s) - a_{ii}(s)a_{ll}(s)a_{il}(s)a_{li}(s)\Big) \\
&= 4\sum_{il}\Big[a_{il}(s)a_{li}(s)a_{ii}(s)\Big(a_{ii}(s) - a_{ll}(s)\Big)\Big] \\
&= 4\sum_{i<l}\Big[|a_{il}(s)|^2 a_{ii}(s)\Big(a_{ii}(s) - a_{ll}(s)\Big) + |a_{li}(s)|^2 a_{ll}(s)\Big(a_{ll}(s) - a_{ii}(s)\Big)\Big],
\end{aligned}$$

where in the last line, the sum explicitly only goes over the upper triangle of $A(s)$, but still sums over the lower triangle by the addition of the second term in the last line. From here,

$$4\sum_{i<l}|a_{il}(s)|^2\Big(a_{ii}(s) - a_{ll}(s)\Big)^2 \geq 0. \tag{2.91}$$

Therefore,

$$\frac{d}{ds}\sum_i \Big|a_{ii}(s)\Big|^2 \geq 0, \tag{2.92}$$

i.e. the magnitude squared of the diagonal elements of $A(s)$ are monotonically

increasing. Since the two-norm is the square-root of magnitude squares of terms, and the square-root is a monotonic function, the two norm will be monotonically increasing.

The trace of $A(s)$ and $\Big(A(s)\Big)^2$ are invariant under $U(s)$:

$$\begin{aligned}\frac{d}{ds}\,\mathrm{Tr}\Big[A(s)\Big] &= \frac{d}{ds}\,\mathrm{Tr}\Big[U^\dagger(s)AU(s)\Big] \\ &= \frac{d}{ds}\,\mathrm{Tr}\Big[AU(s)U^\dagger(s)\Big] = \frac{d}{ds}\,\mathrm{Tr}\Big[A\Big] = 0 \end{aligned} \tag{2.93}$$

Similarly,

$$\begin{aligned}\frac{d}{ds}\,\mathrm{Tr}\Big[A^2(s)\Big] &= \frac{d}{ds}\,\mathrm{Tr}\Big[U^\dagger(s)AU(s)U^\dagger(s)AU(s)\Big] \\ &= \frac{d}{ds}\,\mathrm{Tr}\Big[U^\dagger(s)A^2U(s)\Big] = \frac{d}{ds}\,\mathrm{Tr}\Big[A^2\Big] = 0. \end{aligned} \tag{2.94}$$

Now from this,

$$\begin{aligned} 0 = \frac{d}{ds}\,\mathrm{Tr}\Big[A^2(s)\Big] &= \frac{d}{ds}\sum_i \Big[A^2(s)\Big]_{ii} \\ &= \frac{d}{ds}\sum_{i,k} a_{ik}(s)a_{ki}(s) = \frac{d}{ds}\sum_{i,k}|a_{ij}(s)|^2 \\ &= \frac{d}{ds}\Big[\sum_i |a_{ii}(s)|^2 + \sum_{i\neq k}|a_{ik}(s)|^2\Big]. \end{aligned} \tag{2.95}$$

It was previously proven that the first part of the sum in the last line monotonically increases (the diagonal part of $A(s)$). The second part of the sum is the magnitude of the off-diagonal elements. Since their sum must be zero, and the diagonal elements are monotonically increasing, the off-diagonal elements *must* decrease:

$$\frac{d}{ds}\sum_{i\neq k}|a_{ik}(s)|^2 < 0. \tag{2.96}$$

■

A similar proof for Mielke's generator can be found in the original paper, Ref. [Mie98].

2.5.2 The Renormalization Group Procedure for Effective Particles as an extension of SRG

The model, or canonical, Hamiltonians that come from quantum field theory Lagrangians are ill-defined, that is any observable calculated from these Hamiltonians will be divergent. In a sense, this is because we are asking too much from our Hamiltonians – we want them to describe a theory at any possible energy scale, and this is an unreasonable expectation. Their response to this is to return to us divergent observables.

Even though every matrix element of the QFT Hamiltonians are themselves finite, divergences still appear in the spectrum. One can see where the divergences come from by looking at the second-order perturbative correction to the energy eigenvalues:

$$E_n^{(2)} = \sum_{k \neq n} \frac{H_{nk} H_{kn}}{E_n^{(0)} - E_k^{(0)}}. \tag{2.97}$$

This sum runs over an entire column of the Hamiltonian matrix, which is formally infinitely large, and there is no guarantee of convergence of this sum. Therefore, the far off-diagonal matrix elements of H in general cause this correction to diverge, and thus this is what accounts for the divergent spectrum. By applying a similarity transformation to H such that it becomes band diagonal, this will force the sum in Eq. 2.97 to converge.

Before discussing renormalization, it is useful to discuss the preconditioning step to any renormalization procedure – regularization. Regularization implements a cutoff on the Hamiltonian such that any measured observables for the regularized Hamiltonian will come out finite. The catch is that the observables will be sensitive to the choice of cutoff, and thus this cutoff must be ultimately removed. Regularization produces a new Hamiltonian via:

$$H \to H(s_r), \tag{2.98}$$

which is formally the exact same Hamiltonian as H, but is only defined up to the

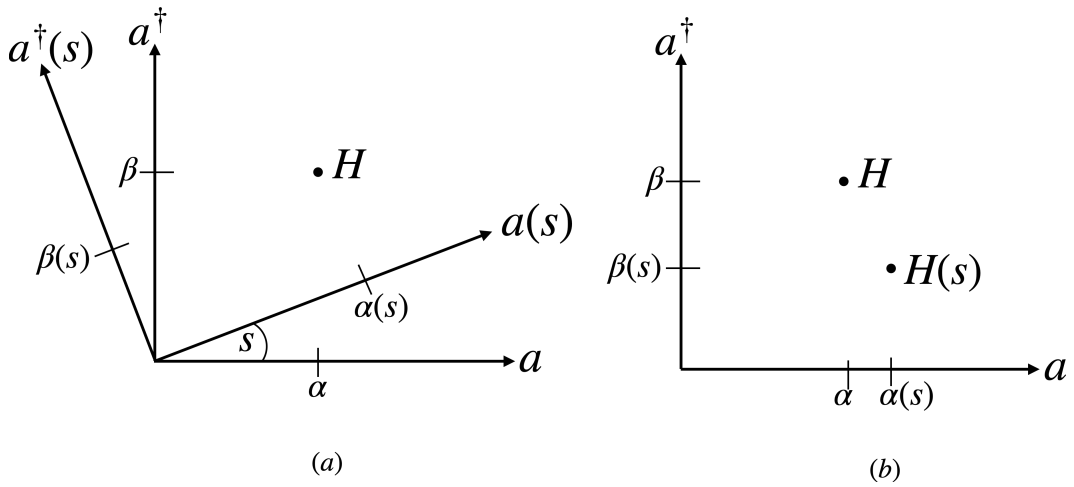

Figure 2.4: **RGPEP Illustration on an arbitrary operator space**: (a) A model Hamiltonian, H can be described in two different bases, (b) A new Hamiltonian can be defined which is unitarily equivalent to the model Hamiltonian.

cutoff, $s_r > 0$.

Renormalization is a systematic procedure which redefines a theory to be accurate in a limited energy range. In doing so, the observables one computes are finite and well-defined. The renormalization group procedure for effective particles (RGPEP) is a particular type of renormalization scheme that is designed for Hamiltonians written in terms of fermionic and bosonic creation and annihilation operators.

RGPEP applies a unitary transformation $U(s)$ to canonical QFT Hamiltonians analogous to what SRG does; however, the main difference is that while SRG acts in a matrix picture, RGPEP stays in the ladder operator picture. The scaling parameter s now has a physical intuition. s has units of L^4 and the more physical parameter $\lambda = s^{-1/4}$ (in $3+1D$) is roughly the width of the band. The parameter λ is interpreted as an energy scale.

To get a feel for what this means, consider the following toy model Hamiltonian described in a basis $\{a, a^\dagger\}$:

$$H = \alpha\ a + \beta\ a^\dagger. \tag{2.99}$$

The same Hamiltonian can also be described in a new basis $\{a(s), a^\dagger(s)\}$:

$$H = \alpha(s)\ a(s) + \beta(s)\ a^\dagger(s), \tag{2.100}$$

where the bases are related by

$$a(s) = U(s)aU^\dagger(s) \tag{2.101}$$

$$a^\dagger(s) = U(s)a^\dagger U^\dagger(s). \tag{2.102}$$

$$\tag{2.103}$$

This operator lives in a vector space shown in Fig. 2.4(a). Now, define a new operator, $H(s)$:

$$H(s) = \alpha(s)a + \beta(s)a^\dagger, \tag{2.104}$$

that is this operator is written in terms of the original basis, but with coefficients from the new basis. This operator lives at a different point in this vector space, see Fig. 2.4(b). Importantly, $H(s)$ is related to H via:

$$\begin{aligned} H(s) &= \alpha(s)a + \beta(s)a^\dagger \\ &= \alpha(s)\Big(U^\dagger(s)a(s)U(s)\Big) + \beta(s)\Big(U^\dagger(s)a^\dagger(s)U(s)\Big) \\ &= U^\dagger(s)\Big(\alpha(s)a(s) + \beta(s)a^\dagger(s)\Big)U(s) \\ &= U^\dagger(s)HU(s), \end{aligned} \tag{2.105}$$

that is they are unitarily equivalent. Although they are different operators, their spectra are identical.

It is important to note that since the spectrum of $H(s)$ is identical to that of H, the spectrum of $H(s)$ will also be divergent. The source if this divergence is different now however. Before, the divergence came from the far off-diagonal matrix elements causing the second order energy correction to diverge. Now that $U(s)$ causes H to become band diagonal, this cannot be the same source of the

divergence, since these matrix elements are zero (or vanishingly close such that the sum will converge). In $H(s)$ the divergence now appears in *matrix elements* along the diagonal which themselves are now divergent.

This is beneficial; however, because as it will be shown more explicitly throughout this thesis, constructing counterterms to cancel these divergences in the diagonal matrix elements is a relatively simple task. After conjugating the regularized Hamiltonian, $H(s_r)$ with $U(s)$, one obtains $H(s, s_r)$, which is band-diagonal, but contains matrix elements along the diagonal which diverge in the limit $s_r \to 0$.

From here, one can add in appropriate counterterms $X(s_r)$ that only depend on the regularization parameter. Each divergent parameter in the theory must have a counterterm. Here, $X(s_r)$ is meant to represent a sum of all counterterms. We now have a new operator:

$$\mathcal{H}(s) = H(s, s_r) + X(s_r), \tag{2.106}$$

the *effective* Hamiltonian, which will give an accurate representation of the true energy spectrum which is decoupled from the high energy degrees of freedom that cause divergences.

Lastly, we will discuss how $U(s)$ is constructed in RGPEP. Starting from the defining flow equation 2.80, in this thesis, we use what we call the kinetic energy generator:

$$\mathcal{G}(s) = \Big[H_0, H(s)\Big]. \tag{2.107}$$

The differential equation 2.80 with this choice of generator explicitly in the ladder operator picture will be colloquially referred to as the RGPEP equation.

In general for quantum field theories, the RGPEP equation governing the flow of $H(s)$ with the generator in Eq. 2.107 cannot be solved exactly, so it must be solved perturbatively by expanding $H(s)$ order-by-order in g:

$$H(s) = H^{(0)}(s) + gH^{(1)}(s) + g^2H^{(2)}(s) + \mathcal{O}(g^3). \tag{2.108}$$

Even if a theory admits canonical Hamiltonian terms up to a particular order, say n, the effective Hamiltonian also includes terms of order $n' > n$. While not immediately obvious why terms with orders greater than that in H are included in the $H(s)$ expansion, when the differential equation is solved order-by-order for physical theories in future chapters, it should become clear that these terms will naturally appear in the effective Hamiltonian.

Asserting this form of $H(s)$ in Equation 2.108, one obtains a differential equation at each order in the coupling:

$$\mathcal{O}(g^0) : \frac{dH^{(0)}(s)}{ds} = 0, \tag{2.109a}$$

$$\mathcal{O}(g^1) : g\frac{dH^{(1)}(s)}{ds} = \Big[\Big[H^{(0)}(s), gH^{(1)}(s)\Big], H^{(0)}(s)\Big], \tag{2.109b}$$

$$\mathcal{O}(g^2) : g^2\frac{dH^{(2)}(s)}{ds} = \Big[\Big[H^{(0)}(s), g^2H^{(2)}(s)\Big], H^{(0)}(s)\Big] + \Big[\Big[H^2(0)(s), gH^{(1)}(s)\Big], gH^{(1)}(s)\Big], \tag{2.109c}$$

$$\vdots$$

The solutions of each of these equations give the n^{th} order term in the effective Hamiltonian, $H^{(n)}(s)$. The n^{th} order RGPEP equation depends on solutions to all orders $< n$.

2.6 Chapter 2 Summary

In this Chapter, we reviewed the relevant background of light-front quantum field theory that is the basis of the remainder of this thesis. In specific, we describe light-front coordinates, their benefits, and their downsides. We give formulae for writing down Hamiltonians for any theory of interest in momentum space. Following this, we discuss hadronic distribution functions, which are natural to describe in light-front coordinates, which makes them important observables for quantum simulation. Lastly, we describe the Renormalization Procedure for Effective Particles which is the renormalization framework used in this thesis. The background in this Chapter, in addition to the quantum algorithms in Chapter 1 give a full theoretical basis for the novel work in this thesis.

Chapter 3

Ladder Operator Block Encoding

In this Chapter, the Ladder Operator Block Encoding (LOBE) framework is outlined. LOBE constructs efficient block-encodings for sums of (products of) ladder operators, which are the form that quantum field theory Hamiltonians in light-front coordinates naturally take. First, we describe the framework and give results compared to a standard block-encoding of the same operators transformed to the Pauli basis. Then we describe the extension from LOBE to block-encodings that are self-inverse. As we will show, this additional constraint comes at the cost of an additional ancilla qubit, and some Clifford gates. This extension, however, is the key to using LOBE in quantum phase estimation.

This Chapter is based on work which has been published in Quantum [SGS+25].

3.1 The Ladder Operator Block-Encoding Framework

In this section, we discuss the framework we developed for compiling block-encodings of linear combinations of *ladder operators*. Coined Ladder Operator Block-Encoding (LOBE) [SGS+25], LOBE generates a unitary which encodes a linear combination of operators of fermionic and bosonic creation and annihilation operators. This framework is particularly useful for this thesis because the Hamiltonians in the light-front formalism are built entirely out of these operators. Therefore, block-encodings of quantum field Hamiltonians with LOBE are more resource-efficient when compared to a more standard approach (mapping to the Pauli basis and using LCU).

3.1.1 Linear Combination of Operators

In our paper [SGS+25], and the works of [BCC+15, CKS17, GSLW19, Lin22, JLP+25], it is argued that the Linear Combination of Unitaries (LCU) block-encoding technique is a part of a larger framework. The linear combination of operators (LCO) framework block-encodes operators of the form

$$A = \sum_{l=0}^{L-1} \alpha_l O_l, \tag{3.1}$$

where O_l corresponds to an arbitrary operator, which is not necessarily unitary, and hence not an LCU. We again restrict $\alpha_l \in \mathbb{R}^{>0}$ without loss of generality.

The LCO framework is built upon a result from Ref. [GSLW19], that if one block-encodes each individual operator O_l such that

$$U_{O_l} |0\rangle_{anc.} |\psi\rangle_s = |0\rangle_{anc.} \frac{O_l}{\lambda_l} |\psi\rangle + \beta_\psi |\perp\rangle_{anc.,s}, \tag{3.2}$$

where each block-encoded U_{O_l} must use the same encoded subspace ($|0\rangle_{anc.}$), and has a rescaling factor λ_l, which depends on the structure of the O_l. From here, we

can define a new operator

$$\tilde{A} = \sum_{l=0}^{L-1} \tilde{\alpha}_l U_{O_l}, \qquad \tilde{\alpha}_l = \frac{\alpha_l \lambda_l}{\Lambda}, \tag{3.3}$$

where $\Lambda \geq \max \lambda_l$. Notably, a LCU block-encoding of $\tilde{A}$ ($U_{\tilde{A}}$) also block-encodes A:

$$\begin{aligned} U_{\tilde{A}} &= \begin{pmatrix} \tilde{A}/\lambda_{\text{LCO}} & \star \\ \star & \star \end{pmatrix} \propto \sum_l \begin{pmatrix} \tilde{\alpha}_l U_{O_l} & \star \\ \star & \star \end{pmatrix} \\ &= \sum_l \begin{pmatrix} \begin{pmatrix} \alpha_l O_l & \star \\ \star & \star \end{pmatrix} & \star \\ \star & \star \end{pmatrix}. \end{aligned} \tag{3.4}$$

We refer to this as a linear combination of operators (LCO). The rescaling factor of a LCO block-encoding is

$$\lambda_{\text{LCO}} = \sum_l^{L-1} |\tilde{\alpha}_l|, \tag{3.5}$$

which is worse (in general) than the rescaling factor of pure LCU. Each U_l will require m_l block-encoding ancillae (ancilla qubits needed to generate the block-encoding). If $m \equiv \max_l m_l$, then $U_{\tilde{A}}$ will require $m + \lceil \log_2(L) \rceil$ block-encoding ancillae.

3.1.2 An explicit LCO construction: Ladder Operator Block-Encoding

In this Subsection, explicit constructions of U_{O_l}'s are given when O_l is a ladder operator acting on fermionic and bosonic degrees of freedom. We have chosen to reduce primarily the number of non-Clifford operations and secondarily the number of block-encoding ancillae, at the expense of incurring "clean ancillae". Clean ancillae are what we define the ancilla qubits used as 'scrap paper' in our calculations, that is ancilla that start and end in the $|0\rangle$ state and can be reused throughout the circuit for different operations. Since many quantum algorithms (although not all) require *controlled* block encodings (such as quantum phase estimation) we show all compilations with an external control qubit.

Before giving explicit constructions, an encoding of the states from the Fock

basis to a qubit basis must be chosen. For fermions, the Jordan-Wigner encoding will be used to map fermionic Fock states to qubit states:

$$|n_{I_b-1}, \ldots, n_0\rangle \to |q_{I_b-1}, \ldots, q_0\rangle \tag{3.6}$$

where $n_i = q_i \in [0, 1]$, and I_b is the maximum fermionic mode number. If the i^{th} mode is occupied with a fermion, $|n_i\rangle = |1\rangle$, otherwise $|n_i\rangle = |0\rangle$.

Bosons are encoded such that each mode i can be occupied by ω_i bosons, where $\omega_i \in [0, \Omega_i - 1]$ (in general, each more can have a different maximum occupation, but for simplicity, throughout we assume that $\Omega_i = \Omega \; \forall i$.) The occupancy of a single bosonic mode is represented in the binary encoding [SMK+20], where the occupation of the i^{th} mode is written in binary on $\lceil \log_2(\Omega + 1) \rceil$ qubits. The total state is therefore the tensor product of each mode's occupation state.

3.1.2.1 Fermionic Ladder Operators

The action of a block-encoded fermionic creation/annihilation operator must obey Eq. 3.2. Therefore:

$$U_{b_j^\dagger} |n_j\rangle |0\rangle_a = b_j^\dagger |n_j\rangle |0\rangle_a + \beta |\perp\rangle \tag{3.7}$$

$$U_{b_j} |n_j\rangle |0\rangle_a = b_j |n_j\rangle |0\rangle_a + \beta |\perp\rangle \tag{3.8}$$

Fig. 3.1 shows our explicit construction of $U_{b_j^\dagger}$ (a) and U_{b_j} (b).

For the circuit in Fig. 3.1 (a), the bottom-right-most X gate flips the occupancy of $|n_j\rangle$, regardless if it is unoccpied or not. This is because if it is occupied, then the first Toffoli gate will cause the ancilla qubit to flip, putting it out of the encoded subspace. Therefore, if it is unoccpied, the ancilla will not flip since the $|n_j\rangle$ control doesn't fire, and the X gate will flip the qubit to its occupied state. The gate labeled $\vec{Z}$ corresponds to

$$\vec{Z} = \bigotimes_{i<j} Z_i, \tag{3.9}$$

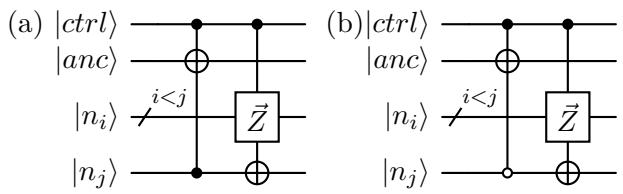

Figure 3.1: **Fermionic Ladder Operator Block Encoding**: (a)A block-encoded for a fermionic creation operator is given, $U_{b_j^\dagger}$. (b)A block-encoded for a fermionic annihilation operator is given, U_{b_j}.

and accounts for the parity of the occupancies of the preceding modes $i < j$. Conversely, for b_j, the logic is the same; however, the ancilla gets flipped out of the encoded subspace if $|n_j\rangle = |0\rangle$ to signify that the mode was zeroed out.

3.1.2.2 Products of Fermionic Ladder Operators

A naive block-encoding of a product of operators is based on a discussion in Gilyén et al. [GSLW19], where they state that given an operator written as a product of two operators, $A = BC$, with block-encodings of the individual operators U_B, U_C, then the product of U_B and U_C results in a block-encoding of A, with rescaling factor $\lambda_B \lambda_C$:

$$\begin{aligned} U_B U_C \left|\psi\right\rangle \left|0\right\rangle_{anc,C} \left|0\right\rangle_{anc,B} &= U_B \Big(\bar{C} \left|\psi\right\rangle \left|0\right\rangle_{anc,C} + \beta_{\psi,C} \left|\perp\right\rangle \Big) \left|0\right\rangle_{anc,B} \\ &= \bar{B}\bar{C} \left|\psi\right\rangle \left|0\right\rangle_{anc,C} \left|0\right\rangle_{anc,B} + \beta_{\psi,C,B} \left|\perp'\right\rangle . \end{aligned} \tag{3.10}$$

Alternatively, we define a construction for a block-encoding of products of fermionic creation and annihilation operators that doesn't utilize this native approach.

Consider the operator $b_l^\dagger b_k$. This operator acts non-trivially only on a Fock state with a fermion in mode k and no fermions in mode l. Therefore, we want the action of $U_{b_j^\dagger b_l}$ to encode the amplitude of a state it acts on in the encoded subspace iff the j^{th} mode is unoccupied and the l^{th} mode is occupied. A circuit that accomplishes this is in Fig. 3.2(a).

Fig. 3.2(c) uses "clean ancillae", i.e. ancillary qubits used as 'scrap paper'. These clean ancillae start and end in the $|0\rangle$ state and thus can be reused throughout

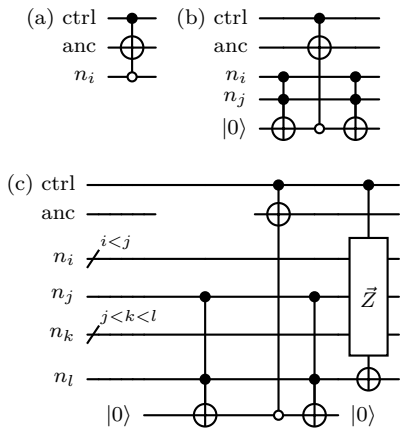

Figure 3.2: **Block-Encoding Products of Fermionic Ladder Operators** In (a), a block-encoding for the fermionic number operator acting on the i^{th} mode ($b_i^\dagger b_i$) is given. In (b), a block-encoding for the product of two fermionic number operators acting on the i^{th} and j^{th} modes ($b_i^\dagger b_i b_j^\dagger b_j$) is given. In (c), a block-encoding for the operator $b_j^\dagger b_j b_l$ with $j \neq l$ is given.

the circuit for other block-encoding operators. The logic of the circuit is as follows. The left-most Toffoli gate picks up the occupancy of the j^{th} and l^{th} modes. If mode j is unoccipied and mode l is occupied, the control structure leads to the clean ancilla to flip. Otherwise, the clean ancilla stays as $|0\rangle$, and then middle Toffoli gate will flip the block-encoding ancilla qubit $|0\rangle_a$ to $|1\rangle$, thus putting it outside of the encoded subspace. The last Toffoli gate is included in order to reset (clean) the clean ancilla to $|0\rangle$ so that it can be used in another block-encoding operator later on.

Lastly, the controlled $\vec{Z}X$ gates flip the occupancies of the states and apply the phase factor. Again, this is applied to all states, but the 'bad' states that it gets applied to (i.e. the states that it should zero out) will already be outside of the encoded subspace, so this is copacetic.

This block-encoding circuit in Fig. **??**(c) has an optimal rescaling factor ($\lambda = 1$), requires a single block-encoding ancilla ($|0\rangle_a$), and uses 8 T gates. A thorough discussion of using clean ancilla and 'elbows' (logical AND gates) to calculate T gates is done well in Ref. [BGB$^+$18] and adequately in Appendix C. More complicated products of fermionic creation and annihilation operators can be created using the

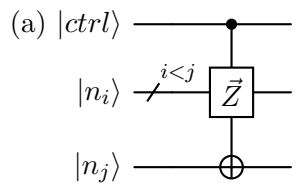

Figure 3.3: **Block-Encoded Sum of Fermionic Operators**: $U_{b_j^\dagger + b_j}$

blueprint of Fig. 3.2(c).

3.1.2.3 Linear Combinations of Fermionic Ladder Operators

In general, block-encoding an operator of the form $b_j^\dagger + b_i$ would constitute an LCO construction, that is, construct $U_{b_j^\dagger}$ and U_{b_i} and use LCU to block-encode their sum.

There are interesting cases, however, that can be more efficiently block-encoded, namely sums of Hermitian pairs, e.g. $O + O^\dagger$. Take, for example $b_j^\dagger + b_j$ and note that this sum of operators acts on the j^{th} mode (disregarding the phase of the preceding modes) as:

$$(b_j^\dagger + b_j)|n_j\rangle \sim \begin{cases} |1\rangle & \text{when } |n_j\rangle = |0\rangle \\ |0\rangle & \text{when } |n_j\rangle = |1\rangle\,, \end{cases} \tag{3.11}$$

which is equivalent to an $X-$gate on the j^{th} qubit. The quantum circuit that implements this operation is shown in Fig. 3.3

It is interesting to note that this construction is identitcal to that which one would arrive at if the operator was transformed via the Wigner transformation. Additionally, this circuit has a rescaling factor of $\lambda = 1$, requires zero clean and block-encoding ancilla, and uses zero non-Clifford operations.

As a more instructive example, consider the operator $b_j b_l + b_l^\dagger b_j^\dagger$ for $j \neq l$. It is useful to order the modes in the operator in the same form, which can be done by obeying the fermionic commutation relation. Therefore $b_j b_l + b_l^\dagger b_j^\dagger = b_j b_l - b_j^\dagger b_l^\dagger$. The action of this operator on a state of the form $|n_j, n_l\rangle$ (again without considering

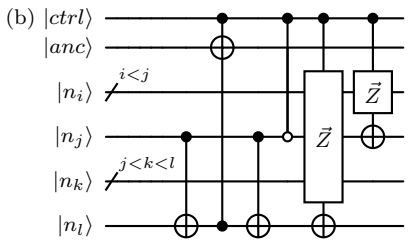

Figure 3.4: **Block-Encoded Sum of Product of Fermionic Operators**: $U_{b_j b_l + b_l^\dagger b_j^\dagger}$

parity) is:

$$(b_j b_l + b_l^\dagger b_j^\dagger)\,|n_j, n_l\rangle \sim \begin{cases} |00\rangle & \text{when } |n_j, n_l\rangle = |11\rangle \\ -|11\rangle & \text{when } |n_j, n_l\rangle = |00\rangle \\ 0 & \text{else.} \end{cases} \tag{3.12}$$

The action of this operator depends on the parity of the occupation of the modes j and l.

Fig. 3.4 shows a circuit that block encodes this operator. The first CNOT gates computes the parity of qubits $|n_j\rangle$ and $|n_l\rangle$. If they are different (i.e. $|n_j n_l\rangle = |01\rangle$ or $|10\rangle$) then the Toffoli gate will flip the block-encoding ancilla to $|1\rangle$, which will put it outside of the encoded subspace. After this, the parity is uncomputed, the controlled-Z-gate picks up the relative sign between $b_j b_l$ and $b_j^\dagger b_l$, and the c-$\vec{Z}X$ gates perform the action on the state and compute the parity of the preceding modes.

The circuit in Fig. 3.4 can be generalized, and is shown in Fig. 3.5. For the generalized case, the rescaling factor is still $\lambda = 1$, a single block-encoding ancilla and $B-1$ clean ancilla are needed and it requires $4(B-1)$ T gates, where B is the number of unique modes being acted on in a given term $+h.c.$.

The CZ gate highlighted in pink in Fig. 3.5 is included *only if* there is a negative sign induced by ordering the operators in the second term in the sum. The addition or lackthereof of this gate can be determined classically.

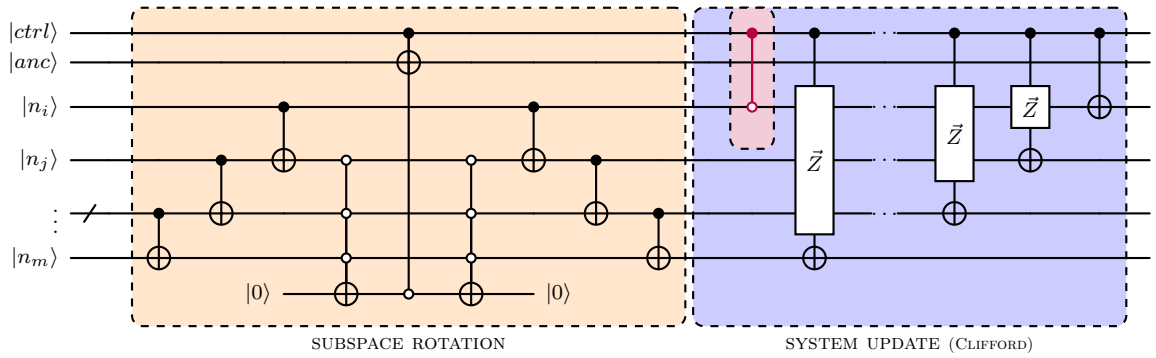

Figure 3.5: **Generalized Block-Encoding for Product of Fermionic Operators Plus Hermitian Conjugate**: $U_{b_i b_j \ldots b_m + b_m^\dagger \ldots b_j^\dagger b_i^\dagger}$.

3.1.2.4 Bosonic Ladder Operators

Here, we define the action of block-encoded bosonic creation and annihilation operators. These block-encodings must satisfy:

$$U_{a_i^\dagger} |\omega_i\rangle |0\rangle_a = \begin{cases} \sqrt{(\omega_i + 1)/\Omega} \, |\omega_i + 1\rangle |0\rangle_a + \beta |\perp\rangle & \text{when } \omega_i < \Omega \\ |\perp\rangle & \text{when } \omega_i \geq \Omega \end{cases} \tag{3.13}$$

$$U_{a_i} |\omega_i\rangle |0\rangle_a = \begin{cases} \sqrt{\omega_i/\Omega} \, |\omega_i - 1\rangle |0\rangle_a + \beta |\perp\rangle & \text{when } \omega_i \leq \Omega \\ |\perp\rangle & \text{when } \omega_i > \Omega. \end{cases} \tag{3.14}$$

In order to implement these unitaries, an *incrementor* must be defined.

The incrementor used in this thesis follows the construction of Gidney in Ref. [Gid15]. The goal of the incrementor is to increase the occupancy of $|n_i\rangle$ by $1 \mod \Omega$. The coefficient $\sim \sqrt{\omega_i/\Omega}$ comes from the fact that $a|n\rangle = \sqrt{n}|n-1\rangle$ and $a^\dagger |n\rangle = \sqrt{n+1}\,|n+1\rangle$, and can be implemented in the circuit by applying uniformly controlled $R_Y(\theta)$-gates to the ancilla qubit, where the angle parameter θ

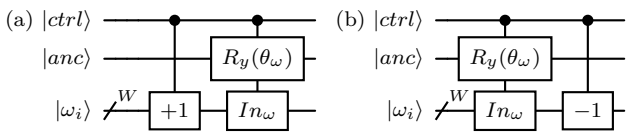

Figure 3.6: **Bosonic Ladder Operator Block Encoding**: (a) $U_{a_i^\dagger}$, (b) U_{a_i}

of the gate corresponds to the coefficient:

$$\theta(\omega_i) = \begin{cases} 2\arccos\left(\sqrt{\omega_i/\Omega}\right), & \text{when } \omega_i < \Omega \\ \pi, & \text{when } \omega_i \geq \Omega, \end{cases} \tag{3.15}$$

which is computed classically. The uniformly controlled rotations follow from [MVBS04]. The circuit that block encodes $a_i^\dagger$ and a_i is shown in Fig. 3.6 (a) and (b) respectively.

The block-encoding $U_{a_i^\dagger}$ in Fig. 3.6(a) applies an incrementor to $|\omega_i\rangle$, followed by a uniformly controlled rotation to pick up the proper coefficient. Alternatively, Fig. 3.6(b) applies the uniformly controlled rotation before the decrementor (-1). The decrementor comes after, because the coefficient depends on ω_i, rather than $\omega_i + 1$, like in Fig. 3.6(a).

Using the incrementor in [Gid15], the construction for these block-encodings uses one block-encoding ancilla, $W = \lceil \log_2(\Omega + 1) \rceil$ clean ancillae, $7W$ $T-$gates, at most $\Omega + 3$ arbitrary rotations and has a rescaling factor of $\lambda = \sqrt{\Omega}$.

3.1.2.5 Products of Bosonic Ladder Operators on the same mode

Since bosonic modes can hold up to Ω bosons (compared to fermions who have an implicit cutoff of 1), operators of the form $(a_i^\dagger)^R$ act non-trivially on bosonic Fock states, and therefore need block-encoding constructions to be defined.

The action of the block-encoded operator $(a_i^\dagger)^R$ must satisfy:

$$U_{(a_i^\dagger)^R} |0\rangle_a |\omega_i\rangle = \begin{cases} \prod_{r=1}^{R} \sqrt{(\omega_i + r)/\Omega} \, |0\rangle_a |\omega_i + R\rangle + \beta |\perp\rangle, & \text{when } \omega_i \leq \Omega - R \\ |\perp\rangle & \text{when } \omega_i > \Omega - R. \end{cases} \tag{3.16}$$

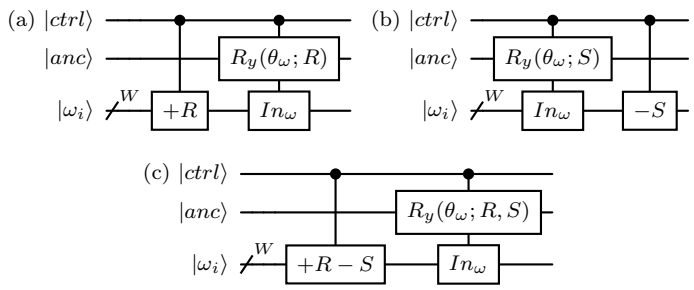

Figure 3.7: **Bosonic Product Ladder Operator Block Encoding on same mode.**

The angles in the R_Y gates are updated by:

$$\theta(\omega_i, R) = \begin{cases} 2\arccos\left(\prod_{r=1}^{R} \sqrt{(\omega_i - r)/\Omega}\right), & \text{when } \omega_i \leq \Omega - R \\ \pi & \text{when } \omega_i > \Omega - R. \end{cases} \tag{3.17}$$

Similarly, the action of $(a_i)^S$ must satisfy:

$$U_{(a_i)^S} |0\rangle_a |\omega_i\rangle = \begin{cases} \prod_{r=1}^{R} \sqrt{(\omega_i - s)/\Omega} |0\rangle_a |\omega_i - S\rangle + \beta |\perp\rangle, & \text{when } \omega_i \leq \Omega + S \\ |\perp\rangle & \text{when } \omega_i > \Omega + S. \end{cases} \tag{3.18}$$

The angles in the R_Y gates are updated by:

$$\theta(\omega_i, S) = \begin{cases} 2\arccos\left(\prod_{s=1}^{S} \sqrt{(\omega_i + s)/\Omega}\right), & \text{when } \omega_i \leq \Omega + S \\ \pi & \text{when } \omega_i > \Omega + S. \end{cases} \tag{3.19}$$

The action of $U_{(a_i^\dagger)^R}, U_{(a_i)^S}$, and $U_{(a_i^\dagger)^R (a_i)^S}$ are shown in Fig. 3.7, where

$$\theta(\omega_i, R, S) = \begin{cases} 2\arccos\left(\prod_{r=1}^{R} \sqrt{(\omega_i - r)/\Omega} \cdot \prod_{s=1}^{S} \sqrt{(\omega_i - R + s)/\Omega}\right), & \text{when } S \leq \omega_i \leq \Omega - R \\ \pi & \text{else.} \end{cases} \tag{3.20}$$

This construction requires at most $7W$ $T-$gates, one block-encoding ancilla, W clean ancillae, $\Omega+3$ arbitrary rotations and has a rescaling factor of $\lambda = \Omega^{(R+S)/2}$.

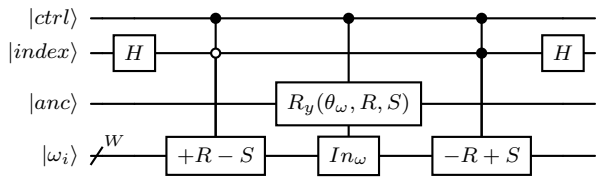

Figure 3.8: Linear Combinations of Bosonic Operators on the same mode: $(a_i^\dagger)^R(a_i)^S + (a_i^\dagger)^S(a_i)^R$.

3.1.2.6 Linear Combinations of Bosonic Ladder Operators

A potential construction for an operator of the form $a_i^\dagger + a_i$ is given in Fig. 3.8(a). The operator should act as:

$$(a_i^\dagger + a_i)\,|\omega_i\rangle = \begin{cases} |0\rangle & \text{when } \omega_i = 1 \\ \sqrt{\omega_i + 1}\,|\omega_i + 1\rangle + \sqrt{\omega_i}\,|\omega_i - 1\rangle & \text{when } 1 < \omega_i < \Omega \\ \sqrt{\Omega}\,|\Omega - 1\rangle & \text{when } \omega_i = \Omega. \end{cases} \tag{3.21}$$

The Hadamard gate on the *index* register creates the superposition $\frac{1}{\sqrt{2}}\Big(\,|0\rangle + |1\rangle\,\Big)\,|\omega_i\rangle$ on the two bottom registers. Conditioned on the *index* qubit being in $|0\rangle$, an incrementor is applied to $|\omega_i\rangle$. After picking up the proper coefficient for $|\omega_i + 1\rangle$ and $|\omega_i\rangle$, the decrementor is applied to the ω_i register, conditioned on the *index* ancilla being in the state $|1\rangle$.

Combining this construction with that of bosonic products discussed previously gives Fig. 3.8(b), which block-encodes operators of the form $(a_i^\dagger)^R(a_i)^S + (a_i^\dagger)^S(a_i)^R$. The extension to the general form: $(a_i^\dagger)^{R_i}(a_i)^{S_i}(a_j^\dagger)^{R_j}(a_j)^{S_j}\ldots(a_l^\dagger)^{R_l}(a_l)^{S_l} + h.c.$ is given in Fig. 3.9.

It is important to note that the constructions for linear combinations of bosonic operators, unlike that of $b_i^\dagger + b_i$, does not lead to a Hermitian block-encoding. This will have an important impact in the next Subsection. For an operator acting on B unique bosonic modes, these constructions require $B+1$ block-encoding ancillae, $\lceil \log_2 \Omega \rceil + 1$ clean ancillae, at most $(12BW - 8B + 4)$ $T-$gates, $B(\Omega + 3)$ arbitrary rotations, and has a rescaling factor of $\lambda = \Omega^{\frac{1}{2}} \sum_i^B (R_i + S_i)$.

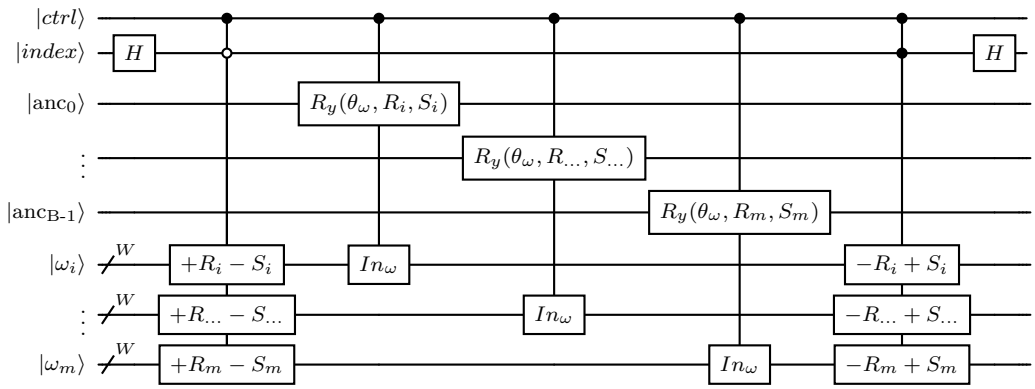

Figure 3.9: **Generalized block-encoding for a product of bosonic ladder operators plus its Hermitian Conjugate**: $U_{(a_i^\dagger)^{R_i}(a_i)^{S_i}...(a_m^\dagger)^{R_m}(a_m)^{S_m}+h.c.}$

3.1.2.7 Linear Combinations of Fermionic *and* Bosonic Operators

Here, we discuss how to block-encode operators which act nontrivially on (anti)fermionic and bosonic operators. Consider the operator $b_i a_j + b_i^\dagger a_j^\dagger$. When the fermionic mode is occupied (unoccupied), only $b_i a_j$ ($b_i^\dagger a_j^\dagger$) will act nontrivially. Therefore, the occupation of the i^{th} fermionic mode can be used as a control of which bosonic operator should be applied to the system. After the appropriate bosonic operator is applied, the fermionic system is updated. This is shown in Fig. 3.10(a). Figs. 3.10(b) and 3.10(c) show block-encodings for operators which are relevant to interacting quantum field theories.

3.1.3 Comparing LOBE to other approaches

In this Subsection, we numerically compute the quantum resource estimates needed to block-encode various operators, and compare the resources to alternative approaches via mappings to Pauli operators. The quantum resources we are interested in are the number of T-gates, non-Clifford rotation gates, block-encoding ancillae, total number of ancillae, and the rescaling factor. While it's true that non-Clifford rotations can be decomposed down to Clifford gates and T-gates via various methods [Cam21], [Gid18], [Kit97], [DN06], we do not choose a specific decomposition. This allows one to choose their preferred decomposition to calculate the add to the total number of $T-$gates, since the decomposition can be algorithmic-dependent, or

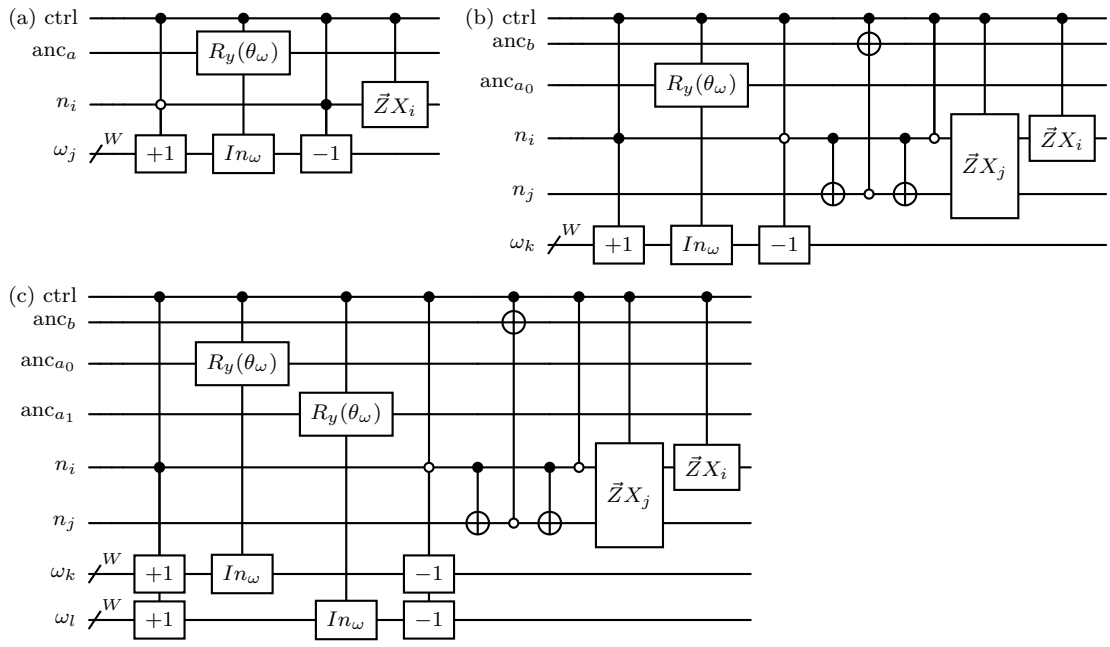

Figure 3.10: **Block-Encoding Terms** In (a), a block-encoding for the operator $b_i^\dagger a_j^\dagger + a_j b_i$ is given. In (b), a block-encoding for the operator $b_i^\dagger b_j^\dagger a_k + a_k^\dagger b_j b_i$ is given. In (c), a block-encoding for the operator $b_i^\dagger b_j^\dagger a_k a_l + a_l^\dagger a_k^\dagger b_j b_i$ is given.

may even be improved in the future.

As a point of comparison, every operator studied will be mapped to Pauli operators and block-encoded with LCU. The fermionic ladder operators are mapped to Paulis via the Jordan-Wigner encoding, while the bosonic ladder operators are mapped via the standard binary encoding. In an attempt to try to improve these standard encodings, we look at two methods for constructing LCU encodings, which we call "Pauli Expansion" and "Piecewise Pauli".

The "Pauli Expansion" method is the 'standard approach' where one fully expands the operator A into Pauli operators. The benefit of this is that there may be cancellations between terms that weren't possible in the ladder operator picture. However, in the worst case the number of operators could scale exponentially with the number of active modes in A. To mitigate this, we also compare with the "Piecewise Pauli" method, each individual ladder operator is block-encoded by expanding it in the Pauli basis and then using LCU and the product of block-encodings in Eq. 3.10.

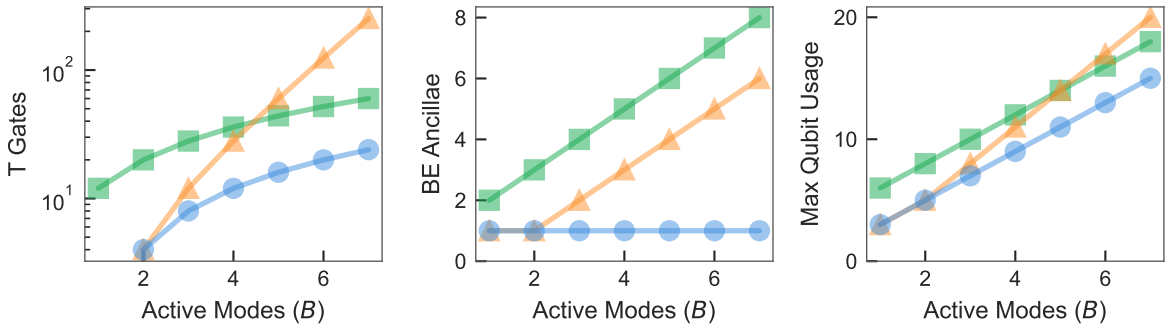

Figure 3.11: **Space-time Cost to Block-Encode** $O = b_0 b_1 \dots b_{B-1} + h.c.$ The number of T gates (left), block-encoding ancillae (middle), and maximum number of qubits used (right) are shown as a function of the number of active modes (B). Results for Pauli Expansion are shown as the orange triangles, results for Piecewise Pauli are shown as the green squares, and results for LOBE are shown as the blue circles. All block-encodings use zero non-Clifford rotations. When $B = 1$ both Pauli Expansion and LOBE require zero T gates. Pauli Expansion and LOBE have rescaling factors of $\lambda = 1$, while Piecewise Pauli has a rescaling factor of $\lambda = 2$.

The first operators we benchmark against do not correspond to a particular physical theory, but are rather the ladder operators that are components to more interesting theories. That is, we look at block-encodings for the operators $b_0 b_1 \dots b_{B-1} + h.c.$, $a_0 a_1 \dots a_{B-1} + h.c.$, and a_0. The results for these operators are given in Figs. 3.11,3.12 and 3.13 respectively.

Now that we can see that LOBE is outperforming Pauli encoding LCU approaches, we extend our analysis to look at how LOBE compares for physical theories of interest.

3.1.3.1 Quartic Harmonic Oscillator

The quartic harmonic oscillator [BW69, GG24, Wó12] is a modification of the standard quantum harmonic oscillator by adding a fourth-order coupling term. The quartic harmonic oscillator Hamiltonian is

$$H = a^\dagger a + g\left(a + a^\dagger\right)^4, \tag{3.22}$$

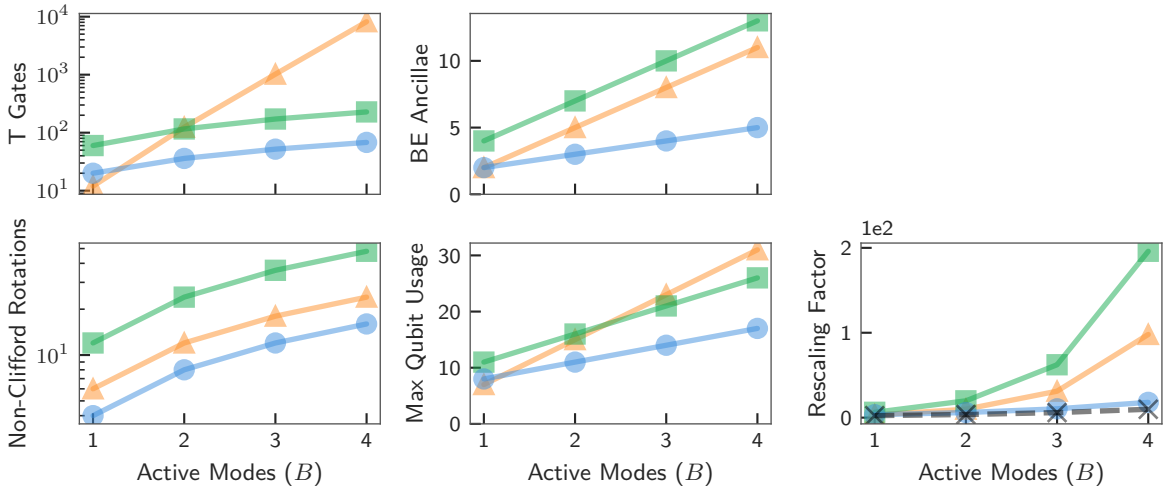

Figure 3.12: **Space-time Cost to Block-Encode** $O = a_0 a_1 \dots a_{B-1} + h.c.$ The number of T gates (upper-left), number of non-Clifford rotations (lower-left), block-encoding ancillae (upper-middle), maximum number of qubits used (lower-middle), and rescaling factor (lower-right) are shown as a function of the number of active modes (B). The bosonic cutoff is fixed to $\Omega = 3$. Results for Pauli Expansion are shown as the orange triangles, results for Piecewise Pauli are shown as the green squares, and results for LOBE are shown as the blue circles. The L2 norm of the matrix representing the operator is shown as the dashed black crosses.

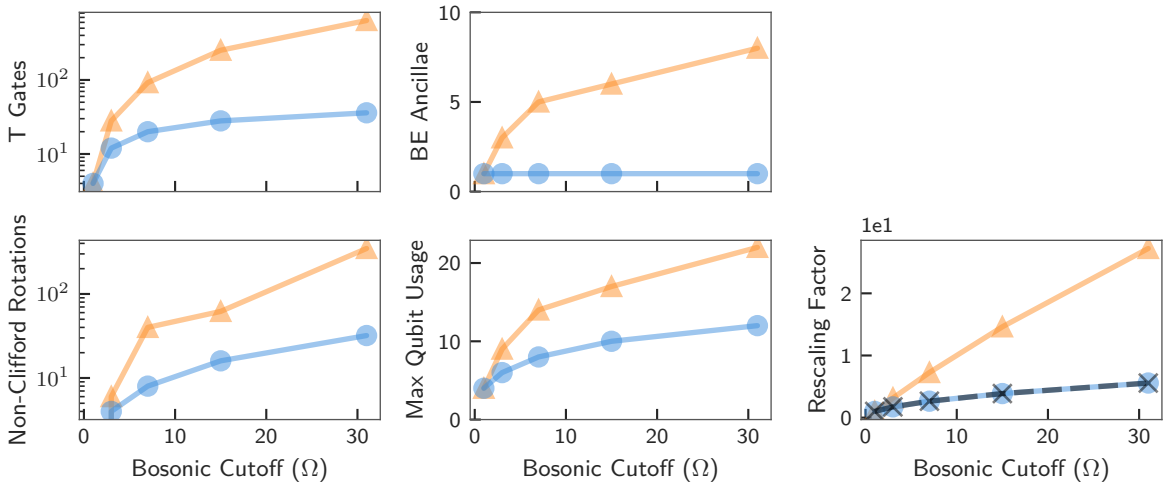

Figure 3.13: **Space-time Cost to Block-Encode Bosonic Annihilation Operator** The number of T gates (upper-left), number of non-Clifford rotations (lower-left), block-encoding ancillae (upper-middle), maximum number of qubits used (lower-middle), and rescaling factor (lower-right) are shown as a function of the bosonic occupation cutoff (Ω). Results for the Pauli method are shown as the orange triangles and results for LOBE are shown as the blue circles. The L2 norm of the matrix representing the operator is shown as the dashed black crosses.

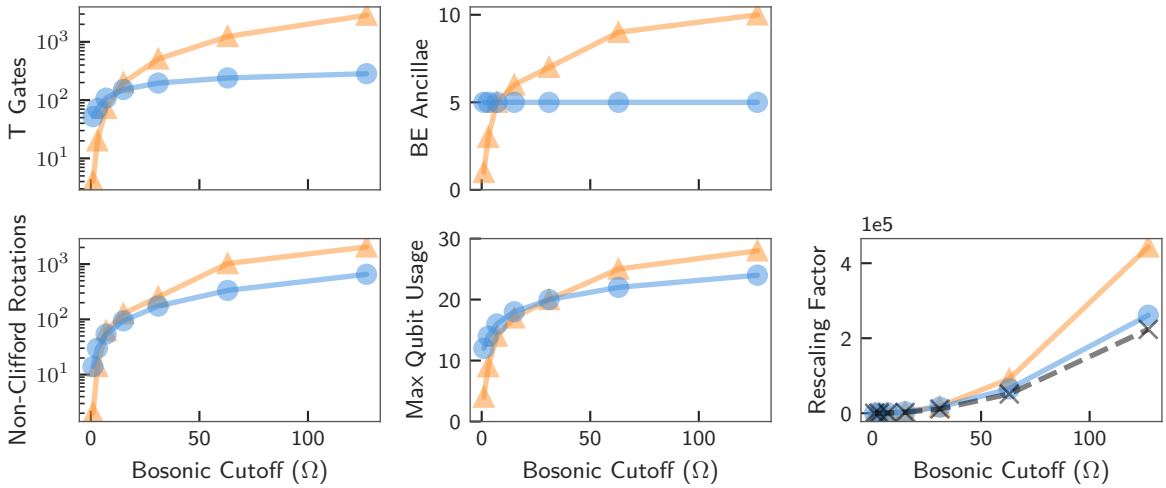

Figure 3.14: **Quartic Harmonic Oscillator** The number of T gates (upper-left), number of non-Clifford rotations (lower-left), block-encoding ancillae (upper-middle), maximum number of qubits used (lower-middle), and rescaling factor (lower-right) are shown as a function of the bosonic occupation cutoff (Ω). The parameter g is set to 1. Results for the Pauli Expansion method are shown as the orange triangles and results for LOBE are shown as the blue circles. The L2 norm of the Hamiltonian is shown as the dashed black crosses.

where g is a dimensionless parameter. After expanding the product and normal ordering all terms, this Hamiltonian can be written in a format that is 'friendly' to LOBE (terms plus their Hermitian conjugate. Note that this isn't necessary, but is the more efficient way of block-encoding this operator):

$$\begin{aligned} H =&(12g+1)a^\dagger a + 6g{a^\dagger}^2 a^2 + 6g\left({a^\dagger}^2 + a^2\right) \\ &+4g\left({a^\dagger}^3 a + a^\dagger a^3\right) + g\left({a^\dagger}^4 + a^4\right) + 3 \end{aligned} \tag{3.23}$$

Since there is only one bosonic mode in this model, we study the resources with increasing Ω, shown in Fig. 3.14. For small values of Ω, the Pauli Expansion method outperforms LOBE, however, as Ω increases above $\Omega \geq 7$, LOBE begins to outperform Pauli Expansion in every metric.

3.1.3.2 Static Yukawa

Another model of interest is a non-relativistic approximation to the Yukawa model, colloquially called the static Yukawa model [Gł21]. This model is the limit of the

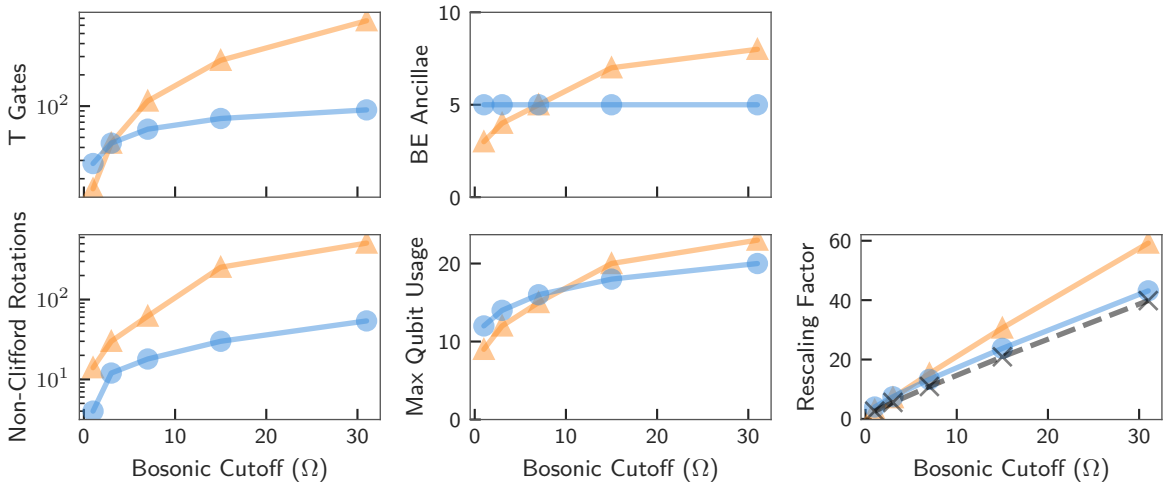

Figure 3.15: **Static Massive Yukawa** The number of T gates (upper-left), number of non-Clifford rotations (lower-left), block-encoding ancillae (upper-middle), maximum number of qubits used (lower-middle), and rescaling factor (lower-right) are shown as a function of the bosonic occupation cutoff (Ω). The parameters C_f, C_b, and g are set to 1. Results for the Pauli Expansion method are shown as the orange triangles and results for LOBE are shown as the blue circles. The L2 norm of the Hamiltonian is shown as the dashed black crosses.

massive Yukawa model with $m_f \to \infty$ (infinite fermion mass). In this limit, the bosons that are emitted or absorbed by these fermions are approximately at rest. This model is of interest because it has an exactly solvable RGPEP solution [Gł21].

The second-quantized Hamiltonian for the static Yukawa model is given by:

$$H = C_f b^\dagger b + C_b a^\dagger a + g b^\dagger b \left(a + a^\dagger\right) \tag{3.24}$$

where C_f and C_b are constants and g represents the strength of the fermion-boson interaction. There is one fermionic mode and one bosonic mode, so the indices on each mode are omitted.

Again, since there is a single mode, we plot results with varying Ω. The results are given in Fig. 3.15. Again, for most metrics, we see a crossover around $\Omega \sim 7$ that the LOBE metrics beat out the Pauli Expansion.

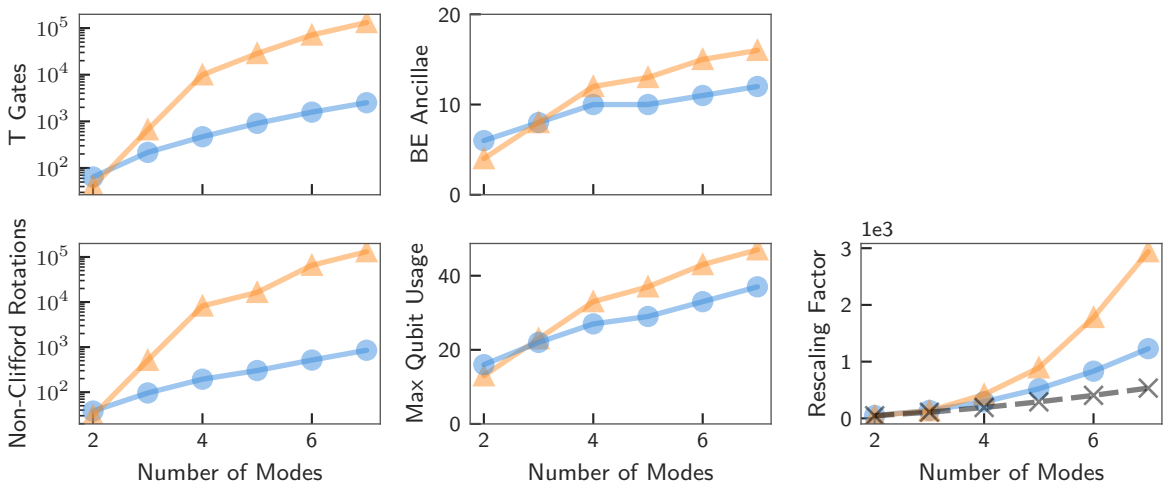

Figure 3.16: ϕ^4 **Theory** The number of T gates (upper-left), number of non-Clifford rotations (lower-left), block-encoding ancillae (upper-middle), maximum number of qubits used (lower-middle), and rescaling factor (lower-right) are shown as a function of the number of momentum modes. The bosonic cutoff is fixed to $\Omega = 3$ and the parameters g and m_b are set to 1. Results for the Pauli Expansion method are shown as the orange triangles and results for LOBE are shown as the blue circles. The L2 norm of the Hamiltonian is shown as the dashed black crosses.

3.1.3.3 ϕ^4 theory

One of the simplest interacting quantum field theories is ϕ^4 theory, which leads to four-point interactions between bosonic fields. Its interacting Lagrangian is given by

$$\mathcal{L}_{\phi^4} = \frac{1}{2}(\partial^\mu \phi)^2 - \frac{1}{2}\mu^2\phi^2 - g\phi^4, \tag{3.25}$$

which can be mapped to a Hamiltonian with terms of the form $a_i^\dagger a^\dagger$, $a_i^\dagger a_j^\dagger a_k a_l + h.c.$, and $a_i^\dagger a_j^\dagger a_k^\dagger a_l + h.c.$, with coefficients which are given explicitly in Ref. [VHJ+22].

Since ϕ^4 theory elicits ladder operators with multiple modes, we plot our results as a funciton of the number of modes at fixed $\Omega = 3$. This is because we know LOBE under performs the Pauli Expansion method at lower Ω. Fig. 3.16 shows the results for this theory. As the number of modes increases, even with fixed low Ω, LOBE out performs the Pauli expansion method in every metric.

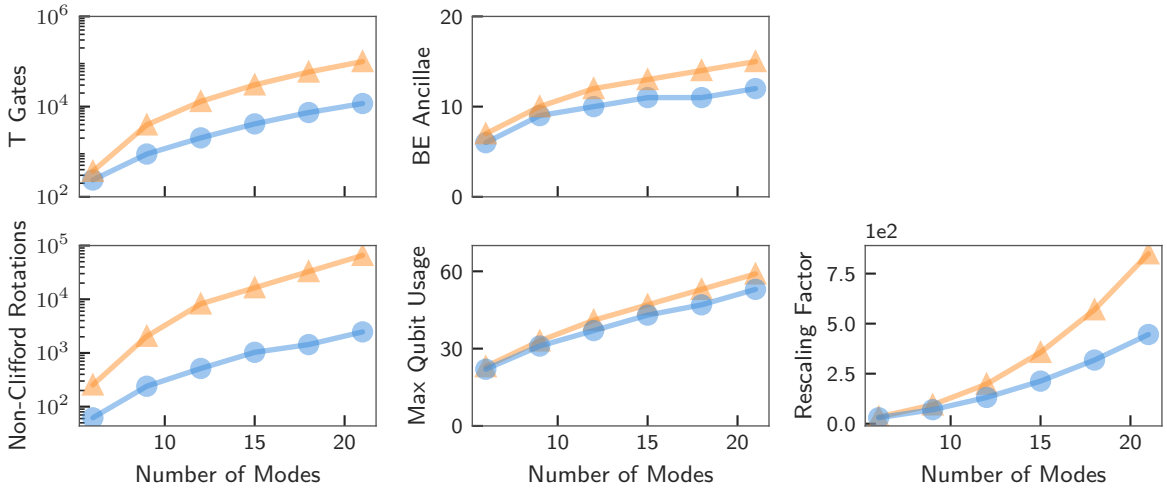

Figure 3.17: **Massive Yukawa** The number of T gates (upper-left), number of non-Clifford rotations (lower-left), block-encoding ancillae (upper-middle), maximum number of qubits used (lower-middle), and rescaling factor (lower-right) are shown as a function of the number of momentum modes. The bosonic cutoff is fixed to $\Omega = 3$ and the parameters m_f, m_b, and g are set to 1. Results for the Pauli Expansion method are shown as the orange triangles and results for LOBE are shown as the blue circles.

3.1.3.4 Yukawa Theory

Lastly, we look at the bare Yukawa model, which is explored in thorough detail in the following Chapter. The Lagrangian of Yukawa theory is

$$\mathcal{L}_Y = i\bar{\psi}\Big(\gamma^\mu \partial_\mu - m_f\Big)\psi + \frac{1}{2}(\partial^\mu \phi)^2 - \frac{1}{2}\mu^2\phi^2 - g\bar{\psi}\psi\phi. \tag{3.26}$$

The explicit forms of the Hamiltonian are given in the following Chapter, so we do not give it here.

In Fig. 3.17, we show results for LOBE vs. Pauli Expansion for varying modes at fixed $\Omega = 3$. Even at a small number of modes, LOBE is out performing the Pauli Expansion in every metric. There are many cancellations that occur in this model when mapping the Hamiltonian to Paulis, which leads to results that are worse, but not by a large margin, in the Pauli Expansion method.

3.1.4 LOBE Summary

LOBE is an efficient framework for constructing unitaries that block encode operators of the form of products of ladder operators acting on (anti)fermionic and bosonic modes. Additionally, we have shown that we can also efficiently construct unitaries where $\bar{O}_l$ is a sum of a term plus it's Hermitian conjugate. After constructing a set of $U_{\bar{O}_l}$'s for every $\bar{O}_l$ in the sum that defines some overall operator $A = \sum_l \alpha_l O_l$, one can use a standard LCU approach to block-encode the overall operator, A, if and only if each $U_{\bar{O}_l}$ shares the same encoded $|0\rangle_{anc.}$ subspace.

As a block-encoding framework, LOBE clearly performs well, and in many cases better, compared to a standard encoding of the operator of interest to Pauli operators and using LCU. However, as we discussed in Chapter 1, a standard block-encoding is not useful to run quantum phase estimation because there is no clear map from the eigenvalues of U_A to the eigenvalues of A. In the next Section, we show how we can extend LOBE to be self-inverse such that the walk operator can be constructed.

3.2 Self-Inverse Ladder Operator Block-Encoding

As discussed in Chapter 1, for the walk operator to be constructed from a block-encoding, the block-encoding must be self-inverse, $U_H^2 = \mathbb{1}$. This condition is satisfied if the SELECT unitary is self-inverse.

Lemma 3.2.1 *The select oracle is self-inverse if the unitaries that it indexes over are self-inverse.*

Proof

$$\begin{aligned} \mathrm{SEL}^2 &= \Big(\sum_l |l\rangle \langle l| \otimes U_l \Big)^2 \\ &= \sum_{l,l'} \delta_{l,l'} |l\rangle \langle l| \otimes U_l U_{l'} \\ &= \sum_l |l\rangle \langle l| \otimes U_l^2 \\ &= \sum_l |l\rangle \langle l| \otimes \mathbb{1} = \mathbb{1}. \end{aligned} \tag{3.27}$$

In this Section, we determine which (if any) of the LOBE U_{O_l}'s defined in the previous Section satisfy $U_{O_l}^2 = \mathbb{1}$. If so, the walk operator can be constructed. If not, we discuss a technique to modify the unitaries $U_{O_l} \to \tilde{U}_{O_l}$ such that $\tilde{U}_{O_l}^2 = \mathbb{1}$.

3.2.1 Self-Inverse Fermionic Ladder Operator Block Encoding

The standard LOBE unitaries for block encodings of fermionic ladder operators are not only unitary by definition, but also are inherently Hermitian. Therefore, the unitary operators obtained from the LOBE construction for products of fermionic creation and annihilation operators satisfy $U_{O_l}^2 = \mathbb{1}$. This implies that the unitaries that block encode products of fermionic creation and annihilation operators plus their Hermitian conjugates can automatically be used to construct the walk operator.

Theorem 3.2.2 *The fermionic LOBE unitary*

$$U_{b_i \ldots b_w + b_w^\dagger \ldots b_i^\dagger} \tag{3.28}$$

is self-inverse.

Proof We define three registers that the unitary $U_{b_i \dots b_w + b_w^\dagger \dots b_i^\dagger}$ acts on: the ancilla register ($|0\rangle_{anc.}$), which is a single qubit, the active system register, and the inactive system register, the last two which combine to compose the entire system register.

The unitary $U_{b_i \dots b_w + b_w^\dagger \dots b_i^\dagger}$ can be broken up into two unitaries:

$$U_{b_i \dots b_w + b_w^\dagger \dots b_i^\dagger} = U_S U_C. \tag{3.29}$$

U_S is a multiqubit Pauli operator that applies $\pm Z$ or $\pm \mathbb{1}$ on each 'inactive' mode and applies $\pm Y$ or $\pm X$ (i.e. flips the occupancy and may add a phase) to each 'active' mode. Therefore, U_S acts only the active and inactive system registers. Explicitly,

$$U_S \left| i, a \right\rangle = p(i) \left| i, \neg a \right\rangle, \tag{3.30}$$

where $|i\rangle$ is a state defined on the inactive register, $|a\rangle$ is a state defined on the active register, and $\neg$ is a negation of all active modes that make up $|a\rangle$. $p(i)$ is a phase factor that takes values $\pm 1, \pm i$

U_C computes the occupancy of the active modes, and flips the ancillary qubit according to whether the active modes are in a 'good' state or not (which will be defined shortly). Therefore, U_C acts only on the ancilla and active registers.

Define the set $\mathcal{M} = \{\text{all possible modes}\}$. The set $\mathcal{A} = \{\text{all active modes}\}$ contains the indices of all active modes in the operator $b_i \dots b_w + b_w^\dagger \dots b_i^\dagger$, while $\mathcal{I} = \mathcal{M} \setminus \mathcal{A}$ is the set of inactive modes.

The "good" states form a set $\mathcal{G}$ which contains states of the form

$$\mathcal{G} = \Big\{ \pm i^n \left|0\right\rangle^{\otimes |\mathcal{A}|}, \pm i^n \left|1\right\rangle^{\otimes |\mathcal{A}|} \Big\}, \tag{3.31}$$

where $i^n = i, -1, -i, 1$ depending on if $n = 1, 2, 3, 4$ respectively. This implies all states of the form $|0 \dots 0\rangle$ and $|1 \dots 1\rangle$ with any phase factor coefficient $\pm 1, \pm i$ are contained in $\mathcal{G}$.

Define the projector onto good states as:

$$P_{\mathcal{G}} = \sum_{g' \in \mathcal{G}} |g'\rangle \langle g'| . \tag{3.32}$$

and the projector onto the bad states is $1 - P_{\mathcal{G}}$. Then,

$$U_C = P_C \otimes \mathbb{1}_{anc.} + (1 - P_C) \otimes X_{anc.}, \tag{3.33}$$

where $\mathbb{1}_{anc.}$ and $X_{anc.}$ act only on the ancilla register $|0\rangle_{anc.}$. If U_C acts on a good state, nothing happens to the block-encoding ancilla; however, for "bad" states ($|b\rangle \notin \mathcal{G}$), X_a acts on the ancilla qubit and flips the state of the ancilla register from $|0\rangle_{anc.} \to |1\rangle_{anc.}$.

In contrast, U_S is the unitary which updates the system register by flipping the active modes, computing the parity of the preceding modes, and applies a controlled-$(-Z)$ gate depending on the sign between $b_i \dots b_w$ and $b_w^\dagger \dots b_i^\dagger$, which can be computed classically. This all happens only on the system register, i.e.

$$U_S = -Z_{a \in \mathcal{A}} \prod_{a' \in \mathcal{A}} \vec{Z}_{i<a'} X_{a'}, \tag{3.34}$$

where $-Z_{a \in \mathcal{A}}$ is the controlled-$(-Z)$ gate on one of (it doesn't matter which) the active modes.

The unitary $U_{b_i \dots b_w + b_w^\dagger \dots b_i^\dagger}$ is self-inverse if

1. $\Big[U_C, U_S\Big] = 0$

2. $U_C^2 = U_S^2 = \mathbb{1}$.

To show (1.), compute

$$\begin{aligned} \Big[U_C, U_S\Big] &= \Big[P_{\mathcal{G}}, U_S \otimes \mathbb{1}_a\Big] + \Big[1 - P_{\mathcal{G}}, U_S \otimes X_a\Big] \\ &= \Big[P_{\mathcal{G}}, U_S\Big] \otimes \Big(\mathbb{1}_a - X_a\Big). \end{aligned} \tag{3.35}$$

Now, if $[P_{\mathcal{G}}, U_S] = 0$, then (1.) is satisfied.

By Eqns. 3.30 and 3.34, $U_S |g\rangle = |g'\rangle$ and $U_S |b\rangle = |b'\rangle$, where $|g\rangle \in \mathcal{G}$ and $|b\rangle \notin \mathcal{G}$. By eq. 3.32, $P_{\mathcal{G}} |g\rangle = |g\rangle$ and $P_{\mathcal{G}} |b\rangle = 0$.

Therefore,

$$\begin{aligned}
\Big[P_{\mathcal{G}}, U_S\Big] |g\rangle &= \Big(P_{\mathcal{G}} U_S - U_S P_{\mathcal{G}}\Big) |g\rangle \\
&= P_{\mathcal{G}} U_S |g\rangle - U_S P_{\mathcal{G}} |g\rangle \\
&= P_{\mathcal{G}} |g'\rangle - U_S |g\rangle \\
&= |g'\rangle - |g'\rangle \\
&= 0. \qquad (3.36)
\end{aligned}$$

and

$$\begin{aligned}
\Big[P_{\mathcal{G}}, U_S\Big] |b\rangle &= \Big(P_{\mathcal{G}} U_S - U_S P_{\mathcal{G}}\Big) |b\rangle \\
&= P_{\mathcal{G}} U_S |b\rangle - U_S P_{\mathcal{G}} |b\rangle \\
&= P_{\mathcal{G}} |b'\rangle - 0 \\
&= 0. \qquad (3.37)
\end{aligned}$$

Therefore, on any arbitrary input state:

$$|n\rangle = \sum_{g \in \mathcal{G}} |g\rangle + \sum_{b \notin \mathcal{G}} |b\rangle ,$$

by linearity, $[P_{\mathcal{G}}, U_S] |n\rangle = 0$ and hence

$$\Big[P_{\mathcal{G}}, U_S\Big] = 0, \qquad (3.38)$$

so (1.) is satisfied.

Now, based on Eq. 3.34, since U_S is only a Pauli string and Pauli strings square to the identity, it is trivial that $U_S^2 = \mathbb{1}$.

The square of U_C can be computed as

$$\begin{aligned} U_C^2 =& P_C^2 \otimes \mathbb{1}_{anc.} + (1-P_C)^2 \otimes X_{anc.}^2 \\ &+ P_C(1-P_C) \otimes X_{anc.} + (1-P_C)P_C \otimes X_{anc.}. \end{aligned} \tag{3.39}$$

Since P_C and $1-P_C$ are defined to be projectors, they are idempotent ($P_C^2 = P_C$, $(1-P_C)^2 = 1-P_C$), orthogonal ($P_C(1-P_C) = (1-P_C)P_C = 0$), and complete ($P_C + (1-P_C) = \mathbb{1}$). Therefore,

$$U_C^2 = \mathbb{1}_{system.} \otimes \mathbb{1}_{anc.}. \tag{3.40}$$

Together, now condition (2.) is satisfied. Therefore,

$$\begin{aligned} U^2_{b_i \ldots b_w + b_w^\dagger \ldots b_i^\dagger} &= U_C U_S U_C U_S \\ &= U_C U_C U_S U_S \\ &= \mathbb{1}. \end{aligned} \tag{3.41}$$

■

3.2.2 Self-Inverse Bosonic Ladder Operator Block Encoding

Unfortunately, the LOBE unitaries constructed in the previous Section for bosonic ladder operators are *not* self-inverse. Luckily, in the original work on qubitization [LC19b], their Lemma 10 proves that $\forall$ SELECT oracles that satisfy the first qubitization condition, $\exists\ \tilde{S}$ requiring one more qubit and controlled calls to SELECT and SELECT†, such that $\tilde{S}$ is self-inverse. Therefore, if one aims to construct the walk operator out of the PREPARE and SELECT unitaries, but SELECT is not self-inverse, the circuit in Fig. 3.18 can be implemented.

Since the LOBE SELECT unitary is not self-inverse (because of the LOBE bosonoic unitaries), it appears as if our only option is to use the circuit in Fig. 3.18; however, there is another option. We know that SELECT is automatically self-

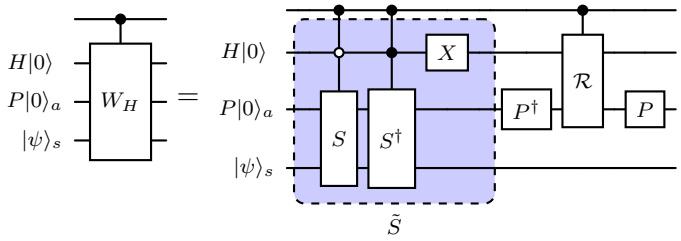

Figure 3.18: A construction for the walk operator built out of SELECT and PREPARE oracles in the case that SELECT is not self-inverse. This is based on Lemma 10 in Ref. [LC19a].

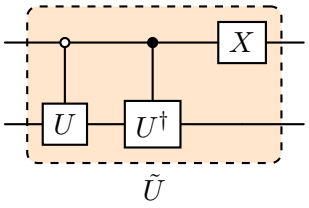

Figure 3.19: **Constructing a self-inverse unitary** from controlled calls to non self-inverse unitaries. $\tilde{U}$ has the property that $(\tilde{U})^2 = \mathbb{1}$.

inverse if the unitaries it indexes over are all self-inverse, therefore, rather than actually constructing the circuit in Fig. 3.18, we can use this idea and generalize it to arbitrary unitaries.

Theorem 3.2.3 *Given arbitrary unitary U such that $U^2 \neq \mathbb{1}$, $\exists \tilde{U}$ such that $(\tilde{U})^2 = \mathbb{1}$. The unitary $\tilde{U}$ can be constructed with a single call to U and a single call to $U^\dagger$ (see Fig. 3.19).*

Proof

$$\begin{aligned}
\tilde{U} &= \Big(|0\rangle\langle 1| \otimes \mathbb{1} + |1\rangle\langle 0| \otimes \mathbb{1} \Big) \Big(|0\rangle\langle 0| \otimes \mathbb{1} + |1\rangle\langle 1| \otimes U^\dagger \Big) \Big(|0\rangle\langle 0| \otimes U + |1\rangle\langle 1| \otimes \mathbb{1} \Big) \\
&= \Big(|0\rangle\langle 1| \otimes \mathbb{1} + |1\rangle\langle 0| \otimes \mathbb{1} \Big) \Big(|0\rangle\langle 0| \otimes U + |1\rangle\langle 1| \otimes U^\dagger \Big) \\
&= |1\rangle\langle 0| \otimes U + |0\rangle\langle 1| \otimes U^\dagger. \qquad (3.42)
\end{aligned}$$

then

$$\begin{aligned}\left(\tilde{U}\right)^2 &= \left(|1\rangle\langle 0| \otimes U + |0\rangle\langle 1| \otimes U^\dagger\right)^2 \\ &= |0\rangle\langle 0| \otimes U^\dagger U + |1\rangle\langle 1| \otimes UU^\dagger \\ &= \mathbb{1} \end{aligned} \tag{3.43}$$

■

Now, we need to modify the unitaries in LOBE with this trick, but this is more effecient than the controlled-SELECT, controlled-SELECT† method because there are gate identities that we can use to cancel gates between U and $U^\dagger$. Before we show the new constructions for $\tilde{U}$ for bosonic ladder operators, we will prove some circuit identities that will help simplify the controlled-U, controlled-$\tilde{U}$ structure in $\tilde{U}$.

Lemma 3.2.4 *Conjugating a $R_y(\theta)$ gate with X is a $R_y(-\theta)$ gate.*

Proof

$$\begin{aligned} XR_y(\theta)X &= \begin{pmatrix} 0 & 1 \\ 1 & 0 \end{pmatrix} \begin{pmatrix} \cos(\theta/2) & -\sin(\theta/2) \\ \sin(\theta/2) & \cos(\theta/2) \end{pmatrix} \begin{pmatrix} 0 & 1 \\ 1 & 0 \end{pmatrix} \\ &= \begin{pmatrix} \cos(\theta/2) & \sin(\theta/2) \\ -\sin(\theta/2) & \cos(\theta/2) \end{pmatrix} \\ &= \begin{pmatrix} \cos(-\theta/2) & -\sin(-\theta/2) \\ \sin(-\theta/2) & \cos(-\theta/2) \end{pmatrix} \\ &= R_y(-\theta) \end{aligned} \tag{3.44}$$

Lemma 3.2.5

$$R_y^\dagger(\theta) = R_y(-\theta) \tag{3.45}$$

Proof

$$R_y^\dagger(\theta) = \begin{pmatrix} \cos(\theta/2) & \sin(\theta/2) \\ -\sin(\theta/2) & \cos(\theta/2) \end{pmatrix}$$
$$= R_y(-\theta) \tag{3.46}$$

Lemma 3.2.6

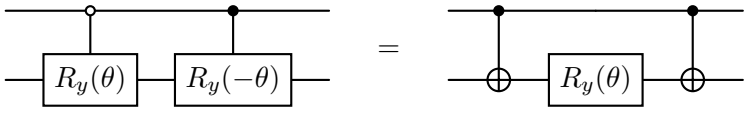

Proof The circuit on the right hand side is

$$\Big(|0\rangle\langle 0| \otimes \mathbb{1} + |1\rangle\langle 1| \otimes X \Big)\Big(\mathbb{1} \otimes R_y(\theta) \Big)\Big(|0\rangle\langle 0| \otimes \mathbb{1} + |1\rangle\langle 1| \otimes X \Big)$$
$$= \Big(|0\rangle\langle 0| \otimes R_y(\theta) + |1\rangle\langle 1| \otimes X R_y(\theta) X \Big)$$
$$= \Big(|0\rangle\langle 0| \otimes R_y(\theta) + |1\rangle\langle 1| \otimes R_y(-\theta) \Big) \tag{3.47}$$

This is the form of the circuit on the left hand side ■

Using Thm 3.2.3 and Lemma 3.2.6 an example new LOBE unitary for the operator $a + a^\dagger$ can be constructed, that is $U_{a+a^\dagger} \rightarrow \tilde{U}_{a+a^\dagger}$, shown in Fig. 3.20. This structure can be extended to arbitrary bosonic operators of the form term plus hermitian conjugate, shown in Fig. 3.21.

In some sense, we could have initially stumbled upon these unitaries, rather than the ones we describe in the LOBE framework earlier since they satisfy qubitization condition 1 which states that they satisfy a block-encoding. However, these unitaries are slightly more expensive, but at the cost of obtaining a self-inverse operator.

3.2.3 Self-Inverse Interaction Ladder Operator Block Encoding

The results from the previous Subsection can be extended to operators that act non-trivially on (anti)fermionic and bosonic modes, the so-called "interaction operators".

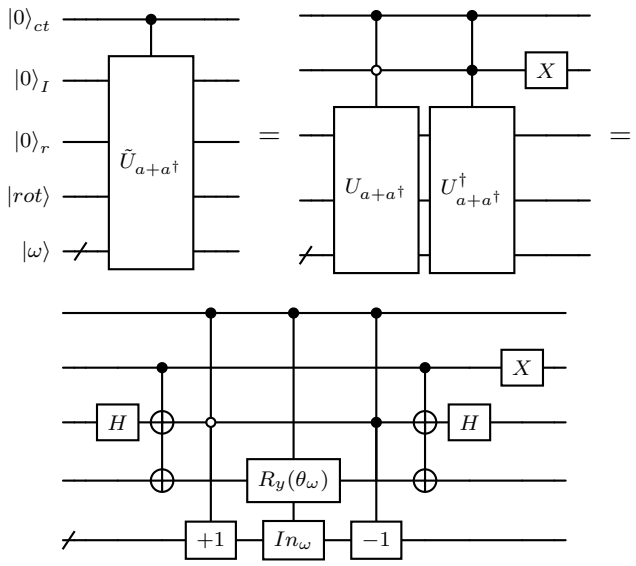

Figure 3.20: **Example Self-Inverse Bosonic LOBE Unitary**. The standard LOBE unitary, $U_{a+a^\dagger}$ is transformed with Thm 3.2.3 and circuit identities. The ancilla qubit $|0\rangle_q$ needed in addition to the ancilla for the non self-inverse $U_{a+a^\dagger}$ gate is to make $\tilde{U}$ self-inverse.

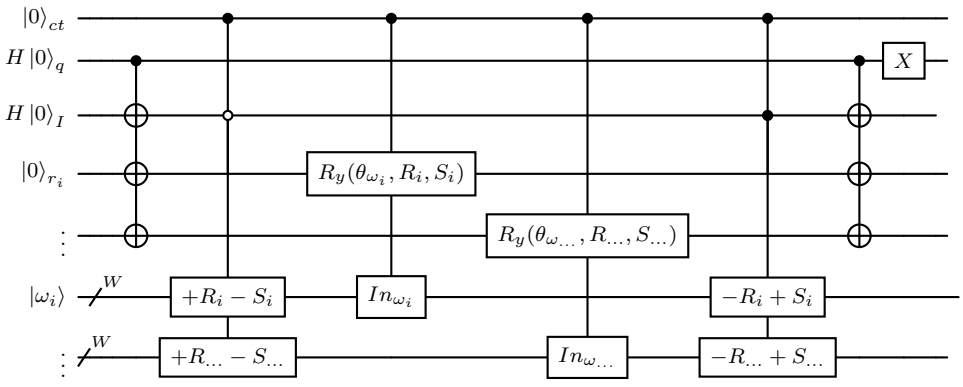

Figure 3.21: **A generalized self-inverse bosonic LOBE unitary** for $O = \prod_i (a_i^\dagger)^{R_i}(a_i)^{S_i} + h.c.$. The top three registers all contain a single qubit each and correspond respectively to the control qubit, the 'qubitization qubit' needed to make the unitary self-inverse, the 'index' qubit which is the same in the non self-inverse block encoding. Then we have a register of the 'rotation' qubits, one for each active mode, followed by the system register.

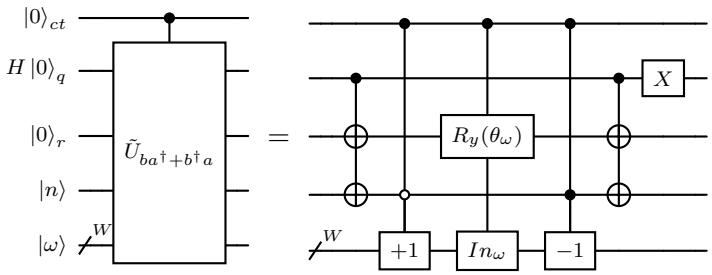

Figure 3.22: **Example Self-Inverse Interaction Walk Operator.** A circuit construction to generate the qubitized walk operator for $O = ba^\dagger + b^\dagger a$, is given.

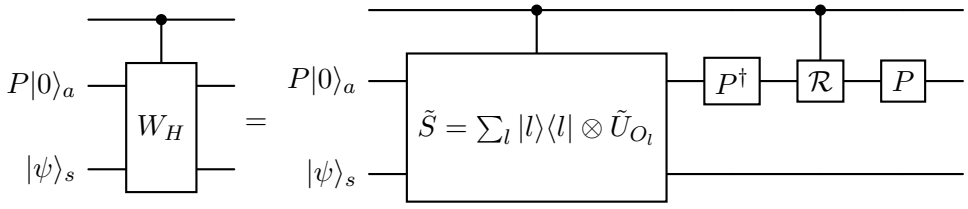

Figure 3.23: **The LOBE Walk Operator**

An example of a self-inverse block-encoding for an interaction operator of the form $b_i a_j^\dagger + b_i^\dagger a_j$ is shown in Fig. 3.22, which can be generalized to arbitrary operators that act on fermionic and bosonic modes.

3.2.4 Self-Inverse LOBE Summary

While the standard LOBE unitaries, defined in the previous Section lead to an efficient block-encoding framework, their drawback is in their inability to satisfy $U_{O_l}^2 = \mathbb{1}$ in general. In this Section, we have shown that at the cost of a single additional ancilla qubit, as well as a few Clifford gates, the LOBE unitaries can be extended to a new set, $\left\{U_{O_l}\right\} \to \left\{\tilde{U}_{O_l}\right\}$ block encode the intended operator and are self-inverse. From here, a new SELECT unitary can be compiled, and the walk operator can be constructed, shown in Fig. 3.23. Overall, the structure of the LOBE framework gives access to both

$$W_H \xleftarrow{\text{SI-LOBE}} H \xrightarrow{\text{LOBE}} U_H. \tag{3.48}$$

3.3 Chapter 3 Summary

In this Chapter, we described Ladder Operator Block-Encoding, an efficient framework for constructing block-encodings of ladder operators acting on (anti)fermionic and bosonic modes. We show various examples of how to compile circuits for these operators, as well as compare our results to standard methods, namely mapping the operators to Paulis. For every example, LOBE out performs the Pauli mapping asymptotically, leading to an advantage for this formalism for problems with this operator structure.

We then extended the LOBE to the Self-Inverse Ladder Operator Block-Encoding (SI-LOBE) framework. SI-LOBE is necessary in the construction of the walk operator. Now, given an operator written as a sum of ladder operators, which is common in both quantum chemistry and quantum field theory, SI-LOBE can efficiently construct a circuit that can be used in quantum phase estimation.

Chapter 4

Quantum Simulation of the Renormalized Yukawa Hamiltonian

In this chapter, the question "Is the cost associated with simulating the effective Hamiltonian, which gives finite results, prohibitively more expensive than that for the bare Hamiltonian?" is addressed for the Yukawa model. To obtain the cost of each Hamiltonian, the continuous version is discretized with discretized lightcone quantization. Mass spectra and structure functions are calculated classically for low-lying two-fermion bound states to verify the renormalization procedure. Finally, the cost associated with a single Ladder Operator Block Encoding is calculated. In this chapter, the Renormalization Group Procedure for Effective Particles (RGPEP) is described in more detail. In Section 4.1, the bare Yukawa Hamiltonian is given. In Section 4.2, order-by-order solutions to the RGPEP equation for Yukawa theory are computed, up to second order in the coupling constant. In Section 4.3, the prescription for choosing proper counterterms is described, which when done properly will remove singularities and yield finite mass spectra. Lastly, Section 4.4 gives results and addresses the question posed above.

This Chapter contains work published in Physical Review D [SGL25, GSS+26].

4.1 The Bare Yukawa Hamiltonian

In this Chapter, we study quantum simullation of 1+1D Yukawa theory in light-front coordinates. While not a gauge theory, or with the full 3+1D spacetime metric, this Chapter still serves as a useful model for understanding RGPEP in an interacting theory with fermions and bosons, and providing some preliminary costs for quantum simulation.

Yukawa theory, proposed in 1935 by Hideki Yukawa [Yuk55], is used as a simple relativistic model for nuclear physics [Mac22]. While not a fundamental theory, the Yukawa model was a historical precursor to QCD. Both Yukawa theory and QCD require strong numerical tools to compute observables, and so Yukawa theory is a useful testbed for new techniques before tackling the many issues arising in gauge theories such as QCD.

The Yukawa Lagrangian is given by

$$\mathcal{L}_{\text{Yukawa}} = \bar{\psi}\left(i\gamma^\mu\partial_\mu - m_0\right)\psi + \frac{1}{2}\partial_\mu\phi\partial^\mu\phi - \frac{1}{2}\mu_0^2\phi^2 - g\bar{\psi}\psi\phi, \tag{4.1}$$

where m_0 is the fermion mass parameter, μ_0 is the boson mass parameter, and g is the coupling strength between the fields. ϕ is a bosonic field mediating interactions between ψ, the fermionic field.

In $1+1D$ momentum space, the bare Yukawa Hamiltonian [SGL25] is:

$$H = H_0 + H_{\bar{\psi}\psi\phi} + H_{\bar{\psi}\phi\phi\psi}, \tag{4.2}$$

where

$$H_0 = \frac{m_0^2}{2}\int\frac{dq^+}{4\pi} : \bar{\psi}(q)\frac{\gamma^+}{q^+}\psi(q) : + \frac{\mu_0^2}{2}\int\frac{dq^+}{4\pi} : \phi(-q)\phi(q) :, \tag{4.3}$$

$$H_{\bar{\psi}\psi\phi} = g\int\frac{dq_1^+dq_2^+dq_3^+}{(4\pi)^3}\,4\pi\delta(q_1^+ + q_2^+ + q_3^+) : \bar{\psi}(-q_1)\psi(q_2)\phi(q_3) :, \tag{4.4}$$

and

$$H_{\bar{\psi}\phi\phi\psi} = g^2 \int \frac{dq_1^+ dq_2^+ dq_3^+ dq_4^+}{(4\pi)^4}\, 4\pi\delta(q_1^+ + q_2^+ + q_3^+ + q_4^+) : \bar{\psi}(-q_1)\phi(q_2)\frac{\gamma^+/2}{q_3^+ + q_4^+}\phi(q_3)\psi(q_4) : . \tag{4.5}$$

The bare Hamiltonian terms can be represented with interaction diagrams:

$H_{\bar{\psi}\psi\phi}$:

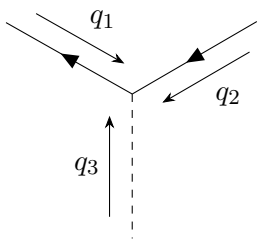

(4.6)

$H_{\bar{\psi}\phi\phi\psi}$:

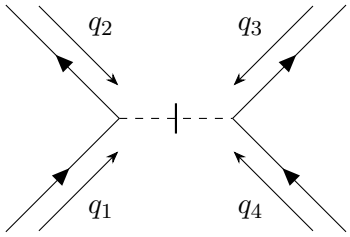

(4.7)

In $1+1D$, the momentum-space fields are

$$\psi(q) = \frac{\theta(q^+)u(q)b(q) + \theta(-q^+)v(-q)d^\dagger(-q)}{|q^+|}, \tag{4.8}$$

and

$$\phi(q) = \frac{\theta(q^+)a(q) + \theta(-q^+)a^\dagger(-q)}{|q^+|}. \tag{4.9}$$

Note that in $1+1D$ Yukawa theory, the creation and annihilation operators do not carry a discrete index. This is because there are no color, flavor, or helicity degrees of freedom.

4.2 The Effective Yukawa Hamiltonian

To compute the effective Hamiltonian of Yukawa theory, the set of differential equations, Eqns. 2.109, must be solved order by order. We begin with a recap of previously established notation, as well as some new useful notation. The dirac delta is condensed such that

$$\delta(q_i + \cdots + q_j) = 2\pi\delta(q_i^+ + \cdots + q_j^+)(2\pi)^2\delta^{(2)}(\vec{q}_i^{\perp} + \cdots + \vec{q}_j^{\perp}), \tag{4.10}$$

while integrals are compacted by

$$\int\limits_{q_i \cdots q_j} = \int_{q_i} \cdots \int_{q_j}, \tag{4.11}$$

where

$$\int_{q_i} = \int_{-\infty}^{\infty}\int_{-\infty}^{\infty}\int_{-\infty}^{\infty} \frac{dq_i^+ d^2\vec{q}_i^{\perp}}{16\pi^3}. \tag{4.12}$$

We define an 'energy function' that takes in n four-momentum vectors and returns a sum of their light-front energy, i.e.

$$\mathcal{Q}^-(q_i, \ldots, q_n) = q_i^- + \cdots + q_n^-. \tag{4.13}$$

This is useful notation because $q_i^- + q_j^- \neq (q_i + q_j)^-$, even though $q_i^+ + q_j^+ = (q_i + q_j)^+$ and $q_i^\perp + q_j^\perp = (q_i + q_j)^\perp$. Lastly, we define an 'energy operator' whose action on individual fields is defined as

$$\hat{\mathcal{Q}}^-\phi(q) = q^-\phi(q), \tag{4.14}$$

$$\hat{\mathcal{Q}}^-\psi(q) = q^-\psi(q), \tag{4.15}$$

$$\hat{\mathcal{Q}}^-\bar{\psi}(-q) = q^-\bar{\psi}(-q), \tag{4.16}$$

and on normal ordered products of fields as

$$\hat{\mathcal{Q}^-}\Big(: \phi(q_1)\phi(q_2) : \Big) = (q_1^- + q_2^-) : \phi(q_1)\phi(q_2) : \tag{4.17}$$

As an illustrative example, we compute the action of this operator on an interacting term in the Hamiltonian

$$\begin{aligned}\hat{\mathcal{Q}}^- H_{\bar{\psi}\psi\phi} &= g \int\limits_{q_1,q_2,q_3} \delta(q_1+q_2+q_3)\hat{\mathcal{Q}^-}\Big(: \bar{\psi}(-q_1)\psi(q_2)\phi(q_3) : \Big) \\ &= g \int\limits_{q_1,q_2,q_3} \delta(q_1+q_2+q_3)(q_1^- + q_2^- + q_3^-) : \bar{\psi}(-q_1)\psi(q_2)\phi(q_3) : . \end{aligned} \tag{4.18}$$

In some sense, we can treat the terms in the Hamiltonian as functionals such that $H_{\bar{\psi}\psi\phi} \equiv \mathbb{H}[: \bar{\psi}(-q_1)\psi(q_2)\phi(q_3) :]$, then

$$\hat{\mathcal{Q}}^- H_{\bar{\psi}\psi\phi} = \hat{\mathcal{Q}^-}\mathbb{H}[: \bar{\psi}(-q_1)\psi(q_2)\phi(q_3) :] = \mathbb{H}[(q_1^- + q_2^- + q_3^-) : \bar{\psi}(-q_1)\psi(q_2)\phi(q_3) :] \tag{4.19}$$

We start by proving a useful theorem which will streamline calculations.

Theorem 4.2.1 *Given a diagram $\mathcal{D}$ that represents an interaction term in the Hamiltonian, $H_{int.}$, with $\mathcal{V} \equiv \{vertices \in \mathcal{D}\}$, the commutator between the free Hamiltonian, H_0, and $H_{int.}$ is the interaction term, modified by the negative sum of q_i^- going into the vertex/vertices, i.e.*

$$\Big[H_0, H_{int.}\Big] = -\sum_{v\in\mathcal{V}} \hat{\mathcal{Q}}_v^- H_{int.}, \tag{4.20}$$

Proof An arbitrary interaction term can be written as

$$H_{int.} = g^n \int_{\{\mathcal{I}\}} C(\mathcal{I})\mathcal{I},$$

where,

$$\mathcal{I} \equiv \mathcal{I}_b\mathcal{I}_d\mathcal{I}_a = \Big(b_{i_1}^\dagger \dots b_{i_I}^\dagger b_{j_1}\dots b_{j_J}\Big)\Big(d_{k_1}^\dagger \dots d_{k_K}^\dagger d_{l_1}\dots d_{l_L}\Big)\Big(a_{m_1}^\dagger \dots a_{m_M}^\dagger a_{n_1}\dots a_{n_N}\Big),$$

$\{\mathcal{I}\} = \{I\} \cup \{\bar{I}\} \cup \{J\} \cup \{\bar{J}\} \cup \{K\} \cup \{\bar{K}\}$, $C(\mathcal{I})$ is a coefficient dependent on the interaction, and the paranthesis separate out $\mathcal{I}_b$, $\mathcal{I}_d$ and $\mathcal{I}_a$. The labels specify a set of quantum numbers, e.g. $i_1 = \{q_1^+, q_1^\perp, \lambda_1, c_1, f_1\}$.

The free part of the Hamiltonian can be written as

$$H_0 = \int_q \frac{m_0^2}{q^+}\Big(b_q^\dagger b_q + d_q^\dagger d_q\Big) + \frac{\mu_0^2}{q^+} a_q^\dagger a_q.$$

Now, it reduces to compute

$$\begin{aligned}
&\Big[b_q^\dagger b_q + d_q^\dagger d_q + a_q^\dagger a_q, \\
&\qquad b_{i_1}^\dagger \dots b_{i_I}^\dagger b_{j_1} \dots b_{j_J} d_{k_1}^\dagger \dots d_{k_K}^\dagger d_{l_1} \dots d_{l_L} a_{m_1}^\dagger \dots a_{m_M}^\dagger a_{n_1} \dots a_{n_N}\Big] = \\
&\Big[b_q^\dagger b_q, b_{i_1}^\dagger \dots b_{i_I}^\dagger b_{j_1} \dots b_{j_J}\Big] d_{k_1}^\dagger \dots d_{k_K}^\dagger d_{l_1} \dots d_{l_L} a_{m_1}^\dagger \dots a_{m_M}^\dagger a_{n_1} \dots a_{n_N} + \\
&b_{i_1}^\dagger \dots b_{i_I}^\dagger b_{j_1} \dots b_{j_J} \Big[d_q^\dagger d_q, d_{k_1}^\dagger \dots d_{k_K}^\dagger d_{l_1} \dots d_{l_L}\Big] a_{m_1}^\dagger \dots a_{m_M}^\dagger a_{n_1} \dots a_{n_N} + \\
&b_{i_I}^\dagger b_{j_1} \dots b_{j_J} d_{k_1}^\dagger \dots d_{k_K}^\dagger d_{l_1} \dots d_{l_L} \Big[a_q^\dagger a_q, a_{m_1}^\dagger \dots a_{m_M}^\dagger a_{n_1} \dots a_{n_N}\Big].
\end{aligned}$$

First, look at

$$\Big[b_q^\dagger b_q, b_{i_1}^\dagger \dots b_{i_I}^\dagger b_{j_1} \dots b_{j_J}\Big] = \Big[b_q^\dagger b_q, b_{i_1}^\dagger \dots b_{i_I}^\dagger\Big] b_{j_1} \dots b_{j_J} - b_{i_1}^\dagger \dots b_{i_I}^\dagger \Big[b_q^\dagger b_q, b_{j_1} \dots b_{j_J}\Big],$$

which reduces to calculating $\Big[b_q^\dagger b_q, b_{i_1}^\dagger \dots b_{i_I}^\dagger\Big]$ and $\Big[b_q^\dagger b_q, b_{j_1} \dots b_{j_J}\Big]$. To simplify these, write out the commutators explicitly and then normal order the output:

$$\Big[b_q^\dagger b_q, b_{i_1}^\dagger \dots b_{i_I}^\dagger\Big] = b_q^\dagger b_q b_{i_1}^\dagger \dots b_{i_I}^\dagger - b_{i_1}^\dagger \dots b_{i_I}^\dagger b_q^\dagger b_q.$$

Only the first time on the right hand side needs to be explicitlyl normal ordered, since the second term already is. Normal ordering $b_q^\dagger b_q b_{i_1}^\dagger \dots b_{i_I}^\dagger$ entails making swaps

between b_q and the creation operator on its right via $\{b_i, b_j^\dagger\} = 4\pi\delta(q_i - q_j)$:

$$\begin{aligned} b_q^\dagger b_q b_{i_1}^\dagger \dots b_{i_I}^\dagger &= b_q^\dagger \Big(4\pi\delta(q^+ - q_{i_1}^+) - b_{i_1}^\dagger b_q\Big) b_{i_2}^\dagger \dots b_{i_I}^\dagger \\ &= 4\pi\delta(q^+ - q_{i_1}^+) b_q^\dagger b_{i_2}^\dagger \dots b_{i_I}^\dagger - b_q^\dagger b_{i_1}^\dagger b_q b_{i_2}^\dagger \dots b_{i_I}^\dagger \\ &= 4\pi\delta(q^+ - q_{i_1}^+) b_q^\dagger b_{i_2}^\dagger \dots b_{i_I}^\dagger + b_{i_1}^\dagger b_q^\dagger b_q b_{i_2}^\dagger \dots b_{i_I}^\dagger, \end{aligned}$$

where $\{b_i^\dagger, b_j^\dagger\} = 0$ lets $b_q^\dagger$ swap with $b_{i_1}^\dagger$ while picking up a minus sign. The first term in this expression is normal ordered, but the second one needs to swap b_q with $b_{i_2}^\dagger$. Doing this will produce a term with a delta and a term with these two swapped, which now causes the need for b_q to be swapped with b_{i_3}. Continuing this pattern, one gets:

$$\begin{aligned} &b_q^\dagger b_q b_{i_1}^\dagger \dots b_{i_I}^\dagger = \\ &\quad 4\pi\delta(q^+ - q_{i_1}^+) b_q^\dagger b_{i_2}^\dagger \dots b_{i_I}^\dagger + 4\pi\delta(q^+ - q_{i_2}^+) b_{i_1}^\dagger b_q^\dagger \dots b_{i_I}^\dagger + \dots 4\pi\delta(q^+ - q_{i_I}^+) b_{i_1}^\dagger \dots b_q^\dagger \\ &\quad + b_{i_1}^\dagger b_{i_2}^\dagger \dots b_{i_I}^\dagger b_q^\dagger b_q. \end{aligned}$$

From this, it is clear that

$$\begin{aligned} \Big[b_q^\dagger b_q, b_{i_1}^\dagger \dots b_{i_I}^\dagger\Big] &= 4\pi\delta(q^+ - q_{i_1}^+) b_q^\dagger b_{i_2}^\dagger \dots b_{i_I}^\dagger + 4\pi\delta(q^+ - q_{i_2}^+) b_{i_1}^\dagger b_q^\dagger \dots b_{i_I}^\dagger + \\ &\qquad \cdots + 4\pi\delta(q^+ - q_{i_I}^+) b_{i_1}^\dagger \dots b_q^\dagger. \end{aligned}$$

Next, compute

$$\Big[b_q^\dagger b_q, b_{j_1} \dots b_{j_J}\Big] = b_q^\dagger b_q b_{j_1} \dots b_{j_J} - b_{j_1} \dots b_{j_J} b_q^\dagger b_q.$$

Here, the second term needs to be normal ordered while the first term already is.

$$\begin{aligned} b_{j_1} \dots b_{j_J} b_q^\dagger b_q &= b_{j_1} \dots \Big(4\pi\delta(q^+ - q_{j_J}^+) - b_q^\dagger b_{j_J}\Big) b_q \\ &= 4\pi\delta(q^+ - q_{j_J}^+) b_{j_1} \dots b_q + b_{j_1} \dots b_q^\dagger b_q b_{j_J} \end{aligned}$$

where $\{b_i, b_j\} = 0$ was invoked. Continuing to move $b_q^\dagger$ to the left on the terms without the deltas gives:

$$b_{j_1} \dots b_{j_J} b_q^\dagger b_q = 4\pi\delta(q^+ - q_{j_J}^+) b_{j_1} \dots b_q + \dots + 4\pi\delta(q^+ - q_{j_1}^+) b_q \dots b_{j_J} + b_q^\dagger b_q b_{j_1} \dots b_{j_J},$$

which leads to the commutator:

$$\left[b_q^\dagger b_q, b_{j_1} \dots b_{j_J}\right] = 4\pi\delta(q^+ - q_{j_J}^+) b_{j_1} \dots b_q + \dots + 4\pi\delta(q^+ - q_{j_1}^+) b_q \dots b_{j_J}$$

Now, these two results can be combined:

$$\begin{aligned}\left[b_q^\dagger b_q, b_{i_1}^\dagger \dots b_{i_I}^\dagger b_{j_1} \dots b_{j_J}\right] = \\ 4\pi\delta(q^+ + q_{i_1}^+) b_q^\dagger \dots b_{i_I}^\dagger b_{j_1} \dots b_{j_J} + \dots + 4\pi\delta(q^+ + q_{i_I}^+) b_{i_1}^\dagger \dots b_q^\dagger b_{j_1} \dots b_{j_J} - \\ 4\pi\delta(q^+ - q_{j_J}^+) b_{i_1}^\dagger \dots b_{i_I}^\dagger b_{j_1} \dots b_q - \dots - 4\pi\delta(q^+ - q_{j_1}^+) b_{i_1}^\dagger \dots b_{i_I}^\dagger b_q \dots b_{j_J},\end{aligned}$$

where due to the momentum prescription, all q_i^+ corresponding to creation operators satisfies $q_i^+ < 0$. Because of this, an index of the form $b_q^\dagger$ should be replaced by $b_{-q}^\dagger$, which leads the deltas above corresponding to $b_q^\dagger$ to acquire the plus sign. Antifermionic operators will lead to the analogous form:

$$\begin{aligned}\left[d_q^\dagger d_q, d_{k_1}^\dagger \dots d_{k_K}^\dagger d_{l_1} \dots d_{l_L}\right] = \\ 4\pi\delta(q^+ + q_{k_1}^+) d_q^\dagger \dots d_{k_K}^\dagger d_{l_1} \dots d_{l_L} + \dots + 4\pi\delta(q^+ + q_{k_K}^+) d_{k_1}^\dagger \dots d_q^\dagger d_{l_1} \dots d_{l_L} - \\ 4\pi\delta(q^+ - q_{l_L}^+) d_{k_1}^\dagger \dots d_{k_K}^\dagger d_{j_1} \dots d_q - \dots - 4\pi\delta(q^+ - q_{j_1}^+) d_{k_1}^\dagger \dots d_{k_K}^\dagger d_q \dots d_{l_L}.\end{aligned}$$

Even though bosonic operators obey different commutation relations, the form of the commutator $\left[a_q^\dagger a_q, a_{m_1}^\dagger \dots a_{m_M}^\dagger a_{n_1} \dots a_{n_N}\right]$ is of the same form to the two fermionic

commutators above because $[a_i, a_j^\dagger] = 4\pi\delta(q_i^+ - q_j^+)$ and $[a_i, a_j] = [a_i^\dagger, a_j^\dagger] = 0$:

$$\Big[a_q^\dagger a_q, a_{m_1}^\dagger \dots a_{m_M}^\dagger a_{n_1} \dots a_{n_N}\Big] =$$
$$4\pi\delta(q^+ + q_{m_1}^+) a_q^\dagger \dots a_{m_M}^\dagger a_{n_1} \dots a_{n_N} + \dots + 4\pi\delta(q^+ + q_{m_M}^\dagger) a_{m_1}^\dagger \dots a_q^\dagger a_{n_1} \dots a_{n_N} -$$
$$4\pi\delta(q^+ - q_{n_N}^+) a_{m_1}^\dagger \dots a_{m_M}^\dagger a_{n_1} \dots a_q - \dots - 4\pi\delta(q^+ - q_{n_1}) a_{m_1}^\dagger \dots a_{m_M}^\dagger a_q \dots a_{n_N}$$

With these commutators worked out:

$$\Big[H_0, H_{int.}\Big] = \left[\int_q \frac{m_0^2}{q^+}\Big(b_q^\dagger b_q + d_q^\dagger d_q\Big) + \frac{\mu_0^2}{q^+} a_q^\dagger a_q, g^n \int_{\{\mathcal{I}\}} C(\mathcal{I})\mathcal{I}\right]$$
$$= g^n \int_{\{\mathcal{I}\}} C(\mathcal{I}) \Bigg(\int_q \frac{m_0^2}{q^+}\Big[b_q^\dagger b_q, \mathcal{I}_b\Big]\mathcal{I}_d\mathcal{I}_a + \int_q \frac{m_0^2}{q^+}\mathcal{I}_b\Big[d_q^\dagger d_q, \mathcal{I}_d\Big]\mathcal{I}_a +$$
$$\int_q \frac{\mu_0^2}{q^+}\mathcal{I}_b\mathcal{I}_d\Big[a_q^\dagger a_q, \mathcal{I}_a\Big]\Bigg),$$

where $\Big[b_q^\dagger b_q, \mathcal{I}_b\Big]$, $\Big[d_q^\dagger d_q, \mathcal{I}_d\Big]$, $\Big[a_q^\dagger a_q, \mathcal{I}_a\Big]$ can be substituted by the results above. When these substitutions are made, the integrals over dq^+ can be done trivially because of the deltas functions. In doing these integrals, both the q^+ in the denominator will change, *and* the subscript q in the operators will change, e.g.:

$$\int_q \frac{m_0^2}{q}\Big[b_q^\dagger b_q, \mathcal{I}_b\Big] = \frac{m_0^2}{-q_{i_1}^+} b_{-q_{i_1}}^\dagger \dots b_{i_I}^\dagger b_{j_1} \dots b_{j_J} + \dots + \frac{m_0^2}{-q_{i_I}} b_{i_1}^\dagger \dots b_{-q_{i_I}}^\dagger b_{j_1} \dots b_{j_J} -$$
$$\frac{m_0^2}{q_{j_J}} b_{i_1}^\dagger \dots b_{i_I}^\dagger b_{j_1} \dots b_{q_{j_J}} - \dots - \frac{m_0^2}{q_{j_1}} b_{i_1}^\dagger \dots b_{i_I}^\dagger b_{q_{j_1}} \dots b_{j_J}$$
$$= -\Big(q_{i_1}^- + \dots + q_{i_I}^- + q_{j_1}^- + \dots + q_{j_J}^-\Big) b_{-q_{i_1}}^\dagger \dots b_{-q_{i_I}}^\dagger b_{q_{j_1}} \dots b_{q_{j_J}}.$$

Similarly,

$$\int_q \frac{m_0^2}{q}\Big[d_q^\dagger d_q, \mathcal{I}_d\Big] = -\Big(q_{k_1}^- + \dots + q_{k_K}^- + q_{l_1}^- + \dots + q_{l_L}^-\Big) d_{-q_{k_1}}^\dagger \dots d_{-q_{k_K}}^\dagger d_{q_{l_1}} \dots d_{q_{l_L}}$$
$$\int_q \frac{\mu_0^2}{q}\Big[a_q^\dagger a_q, \mathcal{I}_a\Big] = -\Big(q_{m_1}^- + \dots + q_{m_M}^- + q_{n_1}^- + \dots + q_{n_N}^-\Big) a_{-q_{n_1}}^\dagger \dots a_{-q_{n_N}}^\dagger a_{q_{m_1}} \dots a_{q_{m_M}}.$$

Combining these:

$$\begin{aligned}\Big[H_0, H_{int.}\Big] &= \left[\int_q \frac{m_0^2}{q^+}\Big(b_q^\dagger b_q + d_q^\dagger d_q\Big) + \frac{\mu_0^2}{q^+}a_q^\dagger a_q, g^n \int_{\{\mathcal{I}\}} C(\mathcal{I})\mathcal{I}\right] \\ &= -g^n \int_{\{\mathcal{I}\}} C(\mathcal{I})\Big(q_{i_1}^- + \cdots + q_{i_I}^- + q_{j_1}^- + \cdots + q_{j_J}^- + q_{k_1}^- + \cdots + q_{k_K}^- \\ &+ q_{l_1}^- + \cdots + q_{l_L}^- + q_{m_1}^- + \cdots + q_{m_M}^- + q_{n_1}^- + \cdots + q_{n_N}^-\Big)\mathcal{I}.\end{aligned}$$

Each vertex $v \in \mathcal{V}$ corresponds to a set of creation and annihilation operators representing q^- flowing into the vertex. The sum of all q^- can be written as $\sum_{v\in\mathcal{V}} \mathcal{Q}_v$, based on the definition of $\mathcal{Q}_v$. Then,

$$\begin{aligned}\Big[H_0, H_{int.}\Big] &= -g^n \int_{\{\mathcal{I}\}} \left(\sum_{v\in\mathcal{V}} \mathcal{Q}_v^-(q_i \in v)\right) C(\mathcal{I})\mathcal{I} \\ &= -\sum_{v\in\mathcal{V}} \hat{\mathcal{Q}}_v^- H_{int.}.\end{aligned}$$

■

4.2.1 $\mathcal{O}(g^0)$ Solution

The RGPEP equation at $\mathcal{O}\Big(g^0\Big)$ is the simplest differential equation to solve in the perturbative expansion 2.109a:

$$\frac{dH_0(s)}{ds} = 0. \tag{4.21}$$

This differential equation is trivial, with the solution

$$H_0(s) = H_0. \tag{4.22}$$

This says that the free terms in the Hamiltonian are the same in the bare and effective Hamiltonians, i.e. they are not affected by the similarity transformation.

4.2.2 $\mathcal{O}(g)$ Solution

The RGPEP equation at $\mathcal{O}(g)$ is:

$$\frac{dH^{(1)}(s)}{ds} = \Big[\Big[H_0, H^{(1)}(s)\Big], H_0\Big]. \tag{4.23}$$

Note that the $\mathcal{O}(g^0)$ solution was substituted into Eq. 4.23.

To solve equation 4.23, first define the generator at $\mathcal{O}(g)$ as

$$\mathcal{G}^{(1)}(s) = \Big[H_0, H^{(1)}(s)\Big]. \tag{4.24}$$

In order to solve Eq. 4.23 an ansatz for $H^{(1)}(s)$ must be chosen. The ansatz chosen assumes the same form as the standard bare $H_{\bar{\psi}\psi\phi}$ vertex, modified by an arbitrary function of the momentum at the vertex, as well as the RGPEP scaling parameter:

$$H^{(1)}(s, s_r) = g \int\limits_{1,2,3} 4\pi\delta(q_1^+ + q_2^+ + q_3^+) f\Big(s; \{q\}\Big) r\Big(s_r; \{q\}\Big) : \bar{\psi}(-q_1)\psi(q_2)\phi(q_3) : . \tag{4.25}$$

The explicit form of the function $f\Big(s; \{q\}\Big)$ will be determined by solving equation 4.23. The regulating function is chosen with a very particular form:

$$r\Big(s_r; \mathcal{Q}^-(q_1, q_2, q_3)\Big) = e^{-s_r\left(q_1^- + q_2^- + q_3^-\right)^2} \tag{4.26}$$

The functional form chosen for the regulating function should be obvious shortly.

The generator, $\mathcal{G}^{(1)}(s)$, given by Eq. 4.24 can be calculated:

$$\begin{aligned}\mathcal{G}^{(1)}(s, s_r) = \Bigg[& \frac{m_0^2}{2} \int \frac{dq^+}{4\pi} : \bar{\psi}(q) \frac{\gamma^+}{q^+} \psi(q) : + \frac{\mu_0^2}{2} \int \frac{dq^+}{4\pi} : \phi(-q)\phi(q) :, \\ & g \int\limits_{1,2,3} 4\pi\delta(q_1^+ + q_2^+ + q_3^+) f\Big(s; \{q\}\Big) r\Big(s_r; \{q\}\Big) : \bar{\psi}(-q_1)\psi(q_2)\phi(q_3) : \Bigg].\end{aligned} \tag{4.27}$$

By Thm 4.2.1, the commutator in equation 4.27 is

$$\mathcal{G}^{(1)}(s,s_r) = -g \int\limits_{1,2,3} 4\pi\delta(q_1^+ + q_2^+ + q_3^+) f\Big(s;\{q\}\Big) r\Big(s_r;\{q\}\Big) \mathcal{Q}^- : \bar{\psi}(-q_1)\psi(q_2)\phi(q_3) : . \tag{4.28}$$

This shows that the generator at $\mathcal{O}(g)$ is the same as $H^{(1)}(s,s_r)$, but with a factor of $\mathcal{Q}^-(q_1,q_2,q_3)$ (sum of q^- into the $H^{(1)}(s,s_r)$ interaction vertices) multiplied in front. To clean up notation, we write the generator as

$$\mathcal{G}^{(1)}(s,s_r) = -\hat{\mathcal{Q}}^- H^{(1)}(s,s_r), \tag{4.29}$$

where the operator $\hat{\mathcal{Q}}^-$ acting on an interaction term multiplies the interaction by the sum of q^- into the vertex, that is

$$\begin{aligned}
\hat{\mathcal{Q}}^- H^{(1)}(s,s_r) &= g \int\limits_{1,2,3} 4\pi\delta(\mathcal{Q}^+) f\Big(s;\{q\}\Big) r\Big(s_r;\{q\}\Big) \\
&\qquad \times (q_1^- + q_2^- + q_3^-) : \bar{\psi}(-q_1)\psi(q_2)\phi(q_3) : \\
&= g \int\limits_{1,2,3} 4\pi\delta(q_1^+ + q_2^+ + q_3^+) f\Big(s;\{q\}\Big) r\Big(s_r;\{q\}\Big) \\
&\qquad \times \mathcal{Q}^-(q_1,q_2,q_3) : \bar{\psi}(-q_1)\psi(q_2)\phi(q_3) :
\end{aligned} \tag{4.30}$$

Now one can work out the outer commutator on the right hand side of equation 4.23, with the new definition of the generator from equation 4.29.

$$\begin{aligned}
\Big[\Big[H_0, H^{(1)}(s,s_r)\Big], H_0\Big] &= \Big[\mathcal{G}^{(1)}(s,s_r), H_0\Big] \\
&= \Big[H_0, \hat{\mathcal{Q}}^- H^{(1)}(s,s_r)\Big] \\
&= -\Big(\hat{\mathcal{Q}}^-\Big)^2 H^{(1)}(s,s_r).
\end{aligned} \tag{4.31}$$

While not immediately obvious that the last line of the above equation is true, if one writes $\hat{\mathcal{Q}}^- H^{(1)}(s,s_r) = \mathbb{H}[(q_1^- + q_2^- + q_3^-) : \bar{\psi}(-q_1)\psi(q_2)\phi(q_3) :]$, then the commutator

$\Big[H_0, \hat{\mathcal{Q}}^- H^{(1)}(s, s_r)\Big]$ is essentially the same as the commutator $\Big[H_0, H^{(1)}(s, s_r)\Big]$ in Eq. 4.27 with an additional factor of $q_1^- + q_2^- + q_3^-$ under the integral. Computing again Eq. 4.27 with this factor will give the same result, but rather with a factor of $-(q_1^- + q_2^- + q_3^-)^2$, which implies that it can be obtained by two actions of the operator $\mathcal{Q}^-$ (with an added minus sign).

This leads to the differential equation

$$\frac{dH^{(1)}(s, s_r)}{ds} = -\left(\hat{\mathcal{Q}}^-\right)^2 H^{(1)}(s, s_r). \tag{4.32}$$

Since only $f(s, \{q\})$ depends on s in $H^{(1)}(s, s_r)$, the differential equation 4.32 reduces to

$$\frac{df(s, \{q\})}{ds} = -\left(\mathcal{Q}^-(q_1, q_2, q_3)\right)^2 f(s, \{q\}), \tag{4.33}$$

with the initial condition $f\Big(0, \{q\}\Big)$ must give the coefficient for this interaction in the bare Hamiltonian.

The solution to this equation is

$$f(s; \mathcal{Q}^-) = e^{-s(\mathcal{Q}^-)^2} = e^{-s\left(q_1^- + q_2^- + q_3^-\right)^2}, \tag{4.34}$$

which is referred to in literature as the *form factor*. Eqtufts. 4.34 should now elucidate why the particular form of the regulator in equation 4.26 was chosen. To be explicit, the form factor and the regulating function can now be combined into one expression:

$$f(s; \mathcal{Q}^-) r(s_r, \mathcal{Q}^-) = e^{-(s+s_r)(q_1^- + q_2^- + q_3^-)^2} \tag{4.35}$$

The full solution to equation 4.23 is now shown to be given as

$$H^{(1)}(s, s_r) = g \int_{1,2,3} 4\pi\delta(q_1^+ + q_2^+ + q_3^+)\; e^{-(s+s_r)(q_1^- + q_2^- + q_3^-)^2} : \bar{\psi}(-q_1)\psi(q_2)\phi(q_3) : . \tag{4.36}$$

Equation 4.36 shows that the form factor (and the regulator) exponentially dampen

the first order interaction vertex. This is the first order effective vertex of Yukawa theory.

4.2.3 $\mathcal{O}(g^2)$ Solution

At $\mathcal{O}(g^2)$, the RGPEP equation is

$$\frac{dH^{(2)}(s,s_r)}{ds} = \Big[\Big[H_0, H^{(2)}(s,s_r)\Big], H_0\Big] + \Big[\Big[H_0, H^{(1)}(s,s_r)\Big], H^{(1)}(s,s_r)\Big]. \tag{4.37}$$

We again assert some parameterized form of $H^{(2)}(s,s_r)$:

$$H^{(2)}(s,s_r) = H^{(2)}_{\bar{\psi}\phi\phi\psi}(s,s_r) + H^{(2)}_c(s,s_r). \tag{4.38}$$

The term $H_{\bar{\psi}\phi\phi\psi}(s,s_r)$ is a parameterized form of the second order term already present in the bare Hamiltonian such that

$$H^{(2)}_{\bar{\psi}\phi\phi\psi}(s,s_r) = g^2 \int\limits_{q_1,q_2,q_3,q_4} 4\pi\delta(q_1^+ + q_2^+ + q_3^+ + q_4^+) F_1\Big(s,\{q\}\Big) r(s_r,\mathcal{Q}^-) \times :\bar{\psi}(-q_1)\phi(q_2)\frac{\gamma^+/2}{q_3^+ + q_4^+}\phi(q_3)\psi(q_4):, \tag{4.39}$$

where F_1 is an arbitrary function that will be determined by solving the $\mathcal{O}(g^2)$ RGPEP equation. The regulating function in $H^{(2)}_{\bar{\psi}\phi\phi\psi}(s,s_r)$ is given explicitly as $r(s_r,\mathcal{Q}^-) = e^{-s_r(q_1^- + q_2^- + q_3^- + q_4^-)^2}$.

Shortly, it will be shown that the second commutator in Eq. 4.37 leads to new second order terms that aren't present in the bare Hamiltonian. To account for these, $H_c(s,s_r)$ is added in equation 4.38. These are called the *contracted* terms. The first nested commutator obtains contributions from both $H^{(2)}_{\bar{\psi}\phi\phi\psi}(s,s_r)$ and $H^{(2)}_c(s,s_r)$, while the second nested commutator will motivate the form of $H^{(2)}_c(s,s_r)$.

The second term on the right hand side of equation 4.37 can be written as

$$\begin{aligned}\Big[\mathcal{G}^{(1)}(s,s_r),H^{(1)}(s,s_r)\Big] &= \Big(-\hat{\mathcal{Q}}^{-}H^{(1)}(s,s_r)\Big)H^{(1)}(s,s_r) \\ &\quad - H^{(1)}(s,s_r)\Big(-\hat{\mathcal{Q}}^{-}H^{(1)}(s,s_r)\Big) \\ &=: C\Big[\Big(-\hat{\mathcal{Q}}^{-}H^{(1)}(s,s_r)\Big)H^{(1)}(s,s_r)\Big]: \\ &\quad -: C\Big[H^{(1)}(s,s_r)\Big(-\hat{\mathcal{Q}}^{-}H^{(1)}(s,s_r)\Big)\Big]:, \end{aligned} \tag{4.40}$$

where $: C[AB] :$ denotes all possible normal ordered contractions between A and B. The final equality comes from the fact

$$[A,B] =: AB: \; + \; : C[AB] : - : BA : - : C[BA] : \tag{4.41}$$

for A and B as products of creation and annihilation operators. Furthermore, it is true for all physical problems of interest because $: AB :=: BA :$, due to an equal number of fermions and antifermions, which leaves only the difference in contractions.

This difference in contractions can be simplified (where we briefly switch to

the compact notation $\mathcal{Q}^+ = q_1^+ + q_2^+ + q_3^+$ and $\mathcal{Q}^- = \mathcal{Q}^-(q_1, q_2, q_3)$):

$$
\begin{aligned}
&: C\Big(\mathcal{G}^{(1)}(s, s_r) H^{(1)}(s, s_r)\Big) : - : C\Big(H^{(1)}(s, s_r)\mathcal{G}^{(1)}(s, s_r)\Big) := \\
&\quad g^2 : C\Bigg(\int_{1,2,3} 4\pi\delta(\mathcal{Q}^+) f(s; \mathcal{Q}^-) r(s_r; \mathcal{Q}^-) \left(-\mathcal{Q}^-\right) \bar{\psi}(-q_1)\psi(q_2)\phi(q_3) \\
&\qquad\qquad \times \int_{1',2',3'} 4\pi\delta(\mathcal{Q}^+) f(s; \mathcal{Q}'^-) r(s_r; \mathcal{Q}'^-) \bar{\psi}(-q_1')\psi(q_2')\phi(q_3') \Bigg) : \\
&\quad - g^2 : C\Bigg(\int_{1,2,3} 4\pi\delta(\mathcal{Q}^+) f(s; \mathcal{Q}^-) r(s_r; \mathcal{Q}^-) \bar{\psi}(-q_1)\psi(q_2)\phi(q_3) \\
&\qquad\qquad \times \int_{1',2',3'} 4\pi\delta(\mathcal{Q}^+) f(s; \mathcal{Q}'^-) r(s_r; \mathcal{Q}'^-) \left(-\mathcal{Q}'^-\right) : \bar{\psi}(-q_1')\psi(q_2')\phi(q_3') \Bigg) : \\
&\quad = -g^2 \int_{\substack{1,2,3 \\ 1',2',3'}} 4\pi\delta(\mathcal{Q}^+) 4\pi\delta(\mathcal{Q}'^+) f(s; \mathcal{Q}^-) f(s; \mathcal{Q}'^-) r(s_r; \mathcal{Q}^-) r(s_r; \mathcal{Q}'^-) \left(\mathcal{Q}^- - \mathcal{Q}'^-\right) \\
&\qquad\qquad \times : C\Big(\bar{\psi}(-q_1)\psi(q_2)\phi(q_3)\bar{\psi}(-q_1')\psi(q_2')\phi(q_3')\Big) : \qquad (4.42)
\end{aligned}
$$

Equation 4.42 now motivates the form of $H_c^{(2)}(s, s_r)$, i.e. we need to include the contracted terms that arise from equation 4.42 into $H^{(2)}(s, s_r)$. To define $H_c^{(2)}(s, s_r)$, we extract the operators and deltas from equation 4.42 only and parameterize by some arbitrary function in s: $F_2(s; \{q\})$, where the subscript 2 differentiates it from the function F_1 in $H^{(2)}_{\bar{\psi}\phi\phi\psi}(s, s_r)$. From this:

$$
\begin{aligned}
H_c^{(2)}(s, s_r) = g^2 \int_{\substack{1,2,3 \\ 1',2',3'}} & 4\pi\delta(q_1^+ + q_2^+ + q_3^+) 4\pi\delta(q_{1'}^+ + q_{2'}^+ + q_{3'}^+) \\
& \times F_2\Big(s; \{q\}\Big) r\Big(s_r, \mathcal{Q}^-(q_1, q_2, q_3)\Big) r\Big(s_r, \mathcal{Q}^-(q_{1'}, q_{2'}, q_{3'})\Big) \\
& \times : C\Big(\bar{\psi}(-q_1)\psi(q_2)\phi(q_3)\bar{\psi}(-q_1')\psi(q_2')\phi(q_3')\Big) : . \qquad (4.43)
\end{aligned}
$$

The relevant non-zero field contractions are

$$\begin{aligned}
\overbrace{\phi(q_1)\phi}(q_2) &= \frac{\theta(q_1)}{|q_1^+|}4\pi\delta(q_1^+ + q_2^+) \\
\overbrace{\bar{\psi}_i(q_1)\psi_j}(q_2) &= -\frac{\theta(-q_1^+)}{q_1^+}4\pi\delta(q_1^+ - q_2^+)\left(\gamma_\mu q_1^\mu + m\right)_{j,i} \\
\overbrace{\psi_i(q_1)\bar{\psi}_j}(q_2) &= \frac{\theta(q_1^+)}{q_1^+}4\pi\delta(q_1^+ - q_2^+)\left(\gamma_\mu q_1^\mu + m\right)_{i,j}\,,
\end{aligned} \tag{4.44}$$

all of which will be needed when simplifying equation 4.40. It is now left to compute the difference in contractions in equation 4.40.

After grouping terms, there Eq. 4.37 has now reduced to two differential equations:

$$\begin{cases}
\frac{dH^{(2)}_{\bar{\psi}\phi\phi\psi}(s,s_r)}{ds} = \Big[\Big[H_0, H^{(2)}_{\bar{\psi}\phi\phi\psi}(s,s_r)\Big], H_0\Big], \\
\frac{dH^{(2)}_c(s,s_r)}{ds} = \Big[\Big[H_0, H^{(2)}_c(s,s_r)\Big], H_0\Big] + \Big[\mathcal{G}^{(1)}(s,s_r), H^{(1)}(s,s_r)\Big].
\end{cases} \tag{4.45}$$

We will start by solving the first equation in 4.45.

In the same way that $\Big[H_0, H^{(1)}(s,s_r)\Big] = -\hat{\mathcal{Q}}^- H^{(1)}(s,s_r)$ was determined in Section 4.2.2, one can show that $\Big[H_0, H^{(2)}_{\bar{\psi}\phi\phi\psi}(s,s_r)\Big] = -\hat{\mathcal{Q}}^- H^{(2)}_{\bar{\psi}\phi\phi\psi}(s,s_r)$. The first equation in equation 4.45 reduces to

$$\frac{dF_1}{dt} = -\left(\hat{\mathcal{Q}}^-\right)^2 F_1, \tag{4.46}$$

with solution

$$F_1(s;\mathcal{Q}^-) = e^{-s\left(q_1^- + q_2^- + q_3^- + q_4^-\right)^2}, \tag{4.47}$$

and revealing the form of $H^{(2)}_{\bar{\psi}\phi\phi\psi}(s,s_r)$:

$$\begin{aligned}
H^{(2)}_{\bar{\psi}\phi\phi\psi}(s,s_r) = g^2 \int_{1,2,3,4} & 4\pi\delta(q_1^+ + q_2^+ + q_3^+ + q_4^+) e^{-(s+s_r)(q_1^- + q_2^- + q_3^- + q_4^-)^2} \\
& \times :\bar{\psi}(-q_1)\phi(q_2)\frac{\gamma^+/2}{q_3^+ + q_4^+}\phi(q_3)\psi(q_4): .
\end{aligned} \tag{4.48}$$

To solve the second equation in equation 4.45, one needs to calculate all possible non-zero contractions,

$$
\begin{aligned}
&: C\Big(\bar{\psi}(-q_1)\psi(q_2)\phi(q_3)\bar{\psi}(-q_1')\psi(q_2')\phi(q_3')\Big) : = \\
&\quad : \bar{\psi}(-q_1)\psi(q_2)\overbrace{\phi(q_3)\bar{\psi}(-q_1')\psi(q_2')}\phi(q_3') : + : \overbrace{\bar{\psi}(-q_1)\psi(q_2)\phi(q_3)\bar{\psi}(-q_1')}\psi(q_2')\phi(q_3') : \\
&+ : \bar{\psi}(-q_1)\overbrace{\psi(q_2)\phi(q_3)\bar{\psi}(-q_1')}\psi(q_2')\phi(q_3') : + : \overbrace{\bar{\psi}(-q_1)\psi(q_2)\overbrace{\phi(q_3)\bar{\psi}(-q_1')}\psi(q_2')}\phi(q_3') : \\
&+ : \bar{\psi}(-q_1)\overbrace{\psi(q_2)\overbrace{\phi(q_3)\bar{\psi}(-q_1')}\psi(q_2')}\phi(q_3') : + : \overbrace{\bar{\psi}(-q_1)\overbrace{\psi(q_2)\phi(q_3)}\bar{\psi}(-q_1')\psi(q_2')}\phi(q_3') :,
\end{aligned}
\tag{4.49}
$$

and then calculate the commutator of this sum with H_0.

Corollary 4.2.2

$$
\Big[H_0, H_c^{(2)}(s, s_r)\Big] = -\Big(\hat{\mathcal{Q}}^- - \hat{\mathcal{Q}}'^-\Big) H_c^{(2)}(s, s_r) \tag{4.50}
$$

Proof See Thm. 4.2.1

$H_c^{(2)}(s, s_r)$ comes from the contractions of two first order diagrams, each of which have their own distinct $\mathcal{Q}^-$, the sum of q^- going into a first order vertex. Since there are two first order vertices, one is labeled with a prime and one without.

From this, it is straightforward to obtain

$$
\Big[\Big[H_0, H_c^{(2)}(s, s_r)\Big], H_0\Big] = -\Big(\hat{\mathcal{Q}}^- + \hat{\mathcal{Q}}'^-\Big)^2 H_c^{(2)}(s, s_r). \tag{4.51}
$$

Now the second equation in equation 4.45 can be reduced to an equation for F_2 (where we again briefly use compact notation $\mathcal{Q}^- = \mathcal{Q}^-(q_1, q_2, q_3, q_4)$ and $\mathcal{Q}'^- = \mathcal{Q}^-(q_{1'}, q_{2'}, q_{3'}, q_{4'})$:

$$
\frac{dF_2}{ds} = -\Big(\mathcal{Q}^- + \mathcal{Q}'^-\Big)^2 F_2 - \Big(\mathcal{Q}^- - \mathcal{Q}'^-\Big) f(s; \mathcal{Q}^-) f(s; \mathcal{Q}'^-). \tag{4.52}
$$

This gives the solution[1]:

$$F_2(s) = \frac{1}{2}\Big(\frac{1}{\mathcal{Q}^-} - \frac{1}{\mathcal{Q}'^-}\Big)\Bigg(f(s;\mathcal{Q}^-)f(s;\mathcal{Q}'^-) - f(s;\mathcal{Q}^- + \mathcal{Q}'^-)\Bigg). \tag{4.53}$$

This gives the full form of the contracted second order terms:

$$\begin{aligned} H_c^{(2)}(s,s_r) = g^2 \int\limits_{\substack{1,2,3\\1',2',3'}} & 4\pi\delta(q_1^+ + q_2^+ + q_3^+)4\pi\delta(q_{1'}^+ + q_{2'}^+ + q_{3'}^+) \\ & \times \frac{1}{2}\Big(\frac{1}{\mathcal{Q}^-(q_1,q_2,q_3)} - \frac{1}{\mathcal{Q}'^-(q_{1'},q_{2'},q_{3'})}\Big) \\ & \times \Big(f(s;\mathcal{Q}^-(q_1,q_2,q_3))f(s;\mathcal{Q}'^-(q_{1'},q_{2'},q_{3'}) \\ & \qquad - f(s;\mathcal{Q}^-(q_1,q_2,q_3+\mathcal{Q}'^-(q_{1'},q_{2'},q_{3'}))\Big) \\ & \times r(s_r,\mathcal{Q}^-(q_1,q_2,q_3)r(s_r,\mathcal{Q}'^-(q_{1'},q_{2'},q_{3'}) \\ & \times :C\Big[\bar\psi(-q_1)\psi(q_2)\phi(q_3)\bar\psi(-q_1')\psi(q_2')\phi(q_3')\Big]: . \end{aligned} \tag{4.54}$$

There are six nonzero contractions in equation 4.54:

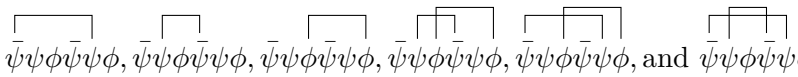

The single contractions lead to exchange diagrams, the so-called fermion exchange term:

$H_{\text{fe}}^{(2)}(s,s_r)$:

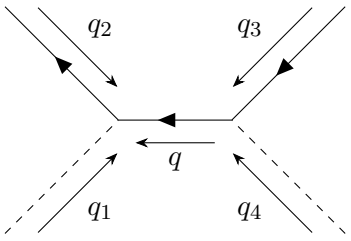

(4.55)

[1] A differential equation of the form

$$\frac{dy}{dt} = -p(t)y(t) + q(t)$$

has the general solution

$$y(t) = e^{-h(t)}\int dt e^{h(t)}q(t) + Ce^{-h(t)},$$

where

$$h(t) = \int dt p(t)$$

and the gluon exchange term

$H^{(2)}_{\rm fe}(s,s_r)$:

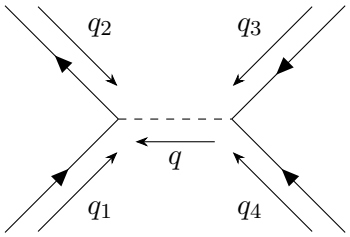

(4.56)

while the double contractions lead to loop diagrams:

$H^{(2)}_{\delta\mu^2}$:

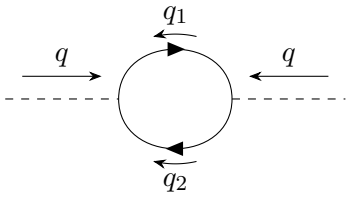

(4.57)

$H^{(2)}_{\delta m^2}$:

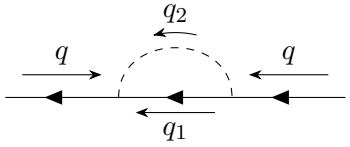

(4.58)

By using the fact that $:\overbrace{ABCD}: = \overbrace{AD}:BC:$, both exchange terms can be simplified and are given as:

$$
\begin{aligned}
H^{(2)}_{\rm fe}(s,s_r) = \int\limits_{\substack{1,2,3\\ 1',2',3'}} & 4\pi\delta(q_1^+ + q_2^+ + q_3^+)4\pi\delta(q_{1'}^+ + q_{2'}^+ + q_{3'}^+) \\
& \times 4\pi\delta(q_2^+ + q_{1'}^+)\frac{\mathcal{R}\Big(s,s_r;\mathcal{Q}(q_1,q_2,q_3),\mathcal{Q}'(q_{1'},q_{2'},q_{3'})\Big)}{q_2^+} \\
& \times :\bar{\psi}(-q_1)\phi(q_3)\Big(\gamma_\mu q_2^\mu + m_0\Big)\phi(q_{3'})\psi(q_{2'}):, \qquad (4.59)
\end{aligned}
$$

and

$$H^{(2)}_{\rm be}(s,s_r) = \int\limits_{\substack{1,2,3\\1',2',3'}} 4\pi\delta(q_1^+ + q_2^+ + q_3^+)4\pi\delta(q_{1'}^+ + q_{2'}^+ + q_3^+) \\ \times 4\pi\delta(q_3^+ + q_{3'}^+)\frac{\theta(q_3^+)\mathcal{R}\Big(s,s_r;\mathcal{Q}(q_1,q_2,q_3),\mathcal{Q}(q_{1'},q_{2'},q_{3'})\Big)}{q_3^+} \\ \times :\bar\psi(-q_1)\psi(q_2)\bar\psi(-q_{1'})\psi(q_{2'}):. \tag{4.60}$$

The function $\mathcal{R}(s,s_r;a,b)$ is an extension of F_2 and is given explicitly as:

$$\mathcal{R}(s,s_r;a,b) = \frac{1}{2}\left(\frac{1}{a}-\frac{1}{b}\right)\Big(f(s;a)\cdot f(s,;b) - f(s;a+b)\Big)r(s_r;a)r(s_r;b) \tag{4.61}$$

4.3 Renormalization and Counterterms

Counterterms are additional terms added to the Hamiltonian to remove divergences and renormalize the theory to yield physical results. In this section, the loop integrals are computed to show the form of the divergence, which gives insight into the choice of counterterms. Throughtout this Section, the notation $o(1)$ stands for terms that go to zero as $s_r \to 0$.

4.3.1 Regularization

The first step of renormalization is always regularization. Two common regularization techniques used in standard field theory calculations in a Lagrangian approach are Pauli-Villars [PV49] and dimensional regularization [BG72]. The goal of regularization is to regulate parameters that cause divergent observables. For example, many higher order scattering matrix element calculations contain integrals of the form $1/k$ which diverges at small k [Sch14].

The simplest regularization technique (although not Lorentz invariant) is to regulate the upper bound of the integral by some cutoff Λ. This leads to a convergent integral $\sim \log(1/\Lambda^2)$, but the result is highly sensative to the choice of the cutoff. Renormalization, through the choice of appropriate counterterms,

removes the dependence on a regulator, Λ.

4.3.2 Loop Integrals

The loop interaction diagrams, $H^{(2)}_{\delta\mu^2}(s, s_r)$ and $H^{(2)}_{\delta m^2}(s, s_r)$ are finite for finite $s_r > 0$, but since observables now depend on this regulating parameter s_r, ideally, it should be removed by taking the limit $s_r \to 0$. Unfortunatley, in doing so, we recover divergent observables. The goal of renormalization is to add appropriate counterterms, which is equivalent to changing the parameters of the theory, such that observables come out finite. In order to determine which counterterms should be added to the Lagrangian, the divergences in $H^{(2)}_{\delta\mu^2}(s, s_r)$ and $H^{(2)}_{\delta m^2}(s, s_r)$ must be extracted.

4.3.2.1 Boson Loop

Using the facts that $\mathrm{Tr}[AB] = A_{ij}B_{ji}$ and that

$$\mathrm{Tr}\Big[(\gamma_\mu q_1^\mu - m_0)(\gamma_\nu q_2^\nu + m_0)\Big], \tag{4.62}$$

the boson loop term can be reduced to:

$$\begin{aligned} H^{(2)}_{\delta\mu^2}(s, s_r) = g^2 \int_{1,2,3} 4\pi\delta(q_1^+ + q_2^+ + q_3^+) \frac{m_0^2(q_1^+ - q_2^+)^2}{q_1^+ q_2^+ (q_1^+ + q_2^+ + q_3^+)} \frac{\theta(q_1^+)\theta(q_2^+)}{|q_1^+||q_2^+|} \\ \times \Big(f^2(s, \mathcal{Q}^-(q_1, q_2, q_3) - 1\Big) r\Big(s_r; \mathcal{Q}^-(q_1, q_2, q_3)\Big) \\ \times : \phi(q_3)\phi(-q_3) :, \end{aligned} \tag{4.63}$$

While not immediately obvious, the divergence in $H^{(2)}_{\delta\mu^2}(s, s_r)$ comes from the '-1' factor. A counterterm must be chosen to cancel this -1.

$H_{\delta\mu^2}(s, s_r)$ can be written in a form that mirrors the free boson Hamiltonian by changing $q_3^+ \to q^+$, which shows that the bare boson mass is shifted when

including the loop contribution, i.e. $\mu_0^2 \to \mu_0^2 + \delta\mu^2$.

$$H^{(2)}_{\delta\mu^2}(s, s_r) = \frac{1}{2}\int_q \delta\mu^2(q^+) : \phi(q)\phi(-q) :, \tag{4.64}$$

where

$$\delta\mu^2(q^+) = 2\int_{-\infty}^{\infty}\int_{-\infty}^{\infty} dq_1^+ dq_2^+ \delta(q_1^+ + q_2^+ - q^+)\frac{1}{q_1^- + q_2^- - q^-}\frac{\theta(q_1^+)\theta(q_2^+)}{|q_1^+||q_2^+|}\frac{m_0^2(q_1^+ - q_2^+)^2}{q_1^+ q_2^+}$$
$$\times \left(e^{-2(s+s_r)(q_1^- + q_2^- - q^-)^2} - e^{-2s_r(q_1^- + q_2^- - q^-)^2}\right).$$

Note that q has changed signs. This is because the combination of $\delta(q_1^+ + q_2^+ + q^+)\theta(q_1^+)\theta(q_2^+)$ implies $q^+ < 0$.

From here, a change of variables from q_1^+, q_2^+ to a new set x, y, can be made to trivially compute one of the integrals: $x \equiv q_1^+/q^+$, and $y \equiv q_1^+ + q_2^+$. x can be interpreted as the fraction of momentum carried by the fermion '1'. The $\delta(q_1^+ + q_2^+ - q^+)$ implies $y = q^+$, which shows that $q_2^+ = q^+(1-x)$, or that the antifermion '2' carries $1-x$ fraction of the momentum of q^+. The Jacobian, $\mathbf{J}$, of this change of variables is

$$\mathbf{J} = \det\begin{pmatrix} \partial q_1^+/\partial x & \partial q_1^+/\partial y \\ \partial q_2^+/\partial x & \partial q_2^+/\partial y \end{pmatrix} = \det\begin{pmatrix} q^+ & x \\ -q^+ & 1-x \end{pmatrix} = q^+. \tag{4.65}$$

The integration bounds now change:

$$\int_0^{\infty}\int_0^{\infty} dq_1^+ dq_2^+ \to \int_0^{\infty}\int_0^1 q^+ dx dy.$$

Now, after canceling factors of q^+ and trivially computing the dy integral,

$$\delta\mu^2(q^+) = 2\int_0^1 \frac{dx}{x(1-x)}\frac{m_0^2(2x-1)^2}{x(1-x)}\frac{1}{\mathcal{M}^2_{f\bar{f}}(x) - \mu_0^2}$$
$$\times \left(e^{-\frac{2(s+s_r)}{(q^+)^2}\left(\mathcal{M}^2_{f\bar{f}}(x) - \mu_0^2\right)^2} - e^{-\frac{2s_r}{(q^+)^2}\left(\mathcal{M}^2_{f\bar{f}}(x) - \mu_0^2\right)^2}\right),$$

where the invariant mass of the fermion-antifermion pair is

$$\mathcal{M}^2_{f\bar{f}}(x) = \frac{m_0^2}{x} + \frac{m_0^2}{1-x}. \tag{4.66}$$

Now $\delta\mu^2(q^+)$ can be written as $\delta\mu^2(q^+) = I_B(s+s_r) - I_B(s_r)$, such that

$$I_B(s) = 2\int_0^1 \frac{dx}{x(1-x)} \frac{m_0^2(2x-1)^2}{x(1-x)} \frac{1}{\mathcal{M}^2_{f\bar{f}}(x) - \mu_0^2} e^{-\tilde{s}\left(\mathcal{M}^2_{f\bar{f}}(x) - \mu_0^2\right)^2}, \tag{4.67}$$

where $\tilde{s}$ is shorthand for $\tilde{s} = 2s/(q^+)^2$.

Changing the integration measure from dx to $d\mathcal{M}^2_{f\bar{f}}$ is useful; however, $\mathcal{M}^2_{f\bar{f}}(x) = \frac{m_0^2}{x} + \frac{m_0^2}{1-x}$ is not a valid substitution on $[0,1]$ because this function is not injective. It is injective, however, from $x = 0$ to the minimum of $\mathcal{M}^2_{ff}$ at $x = \frac{1}{2}$ and on $(1/2, 1)$, so the integral can be split over these two ranges. Under substitution, the integration measure changes:

$$\frac{d\mathcal{M}^2_{f\bar{f}}}{dx} = \frac{m_0^2(2x-1)}{x^2(1-x)^2},$$

which, with the bounds changing by $\mathcal{M}^2_{f\bar{f}}(0) = \mathcal{M}^2_{f\bar{f}}(1) = \infty$, $\mathcal{M}^2_{f\bar{f}}(1/2) = 4m_0^2$:

$$\begin{aligned} I_B(s) = 2\int_{\infty}^{4m_0^2} d\mathcal{M}^2_{f\bar{f}} \frac{2x-1}{\mathcal{M}^2_{f\bar{f}} - \mu_0^2} e^{-\tilde{s}\left(\mathcal{M}^2_{f\bar{f}} - \mu_0^2\right)^2} \\ + 2\int_{4m_0^2}^{\infty} d\mathcal{M}^2_{f\bar{f}} \frac{2x-1}{\mathcal{M}^2_{f\bar{f}} - \mu_0^2} e^{-\tilde{s}\left(\mathcal{M}^2_{f\bar{f}} - \mu_0^2\right)^2}. \end{aligned}$$

This integral still depends on x, which can be written in terms of $\mathcal{M}^2_{f\bar{f}}$ by solving for x in terms of $\mathcal{M}^2_{f\bar{f}}$:

$$\begin{aligned} & x^2 - x + \frac{m_0^2}{\mathcal{M}^2_{f\bar{f}}} = 0 \\ & \implies 2x - 1 = \pm \frac{1}{\mathcal{M}_{f\bar{f}}} \sqrt{\mathcal{M}^2_{f\bar{f}} - 4m_0^2}, \end{aligned}$$

where the negative root is taken on $x \in (0, 1/2)$, since $2x - 1 < 0$ on this range, and

the positive root is taken on $x \in (1/2, 1)$, since $2x - 1 > 0$ on this range. $I_B(s)$ can now be simplified:

$$I_B(s) = 4g^2 \int_{4m_0^2}^{\infty} d\mathcal{M}^2_{f\bar{f}} \frac{\sqrt{1 - 4m_0^2/\mathcal{M}^2_{f\bar{f}}}}{\mathcal{M}^2_{f\bar{f}} - \mu_0^2} e^{-\tilde{s}\left(\mathcal{M}^2_{f\bar{f}} - \mu_0^2\right)^2}, \tag{4.68}$$

Because of the singularity at resonance, i.e. when $4m_0^2 = \mu_0^2$, it is necessary to take $m_0 > \mu_0^2/2$.

Lemma 4.3.1

$$\lim_{\Lambda\to\infty} \int_{4m_0^2}^{\infty} d\mathcal{M}^2 \left(\sqrt{1 - 4m_0^2/\mathcal{M}^2_{f\bar{f}}} - 1\right) = \int_{4m_0^2}^{\infty} \lim_{\Lambda\to\infty} d\mathcal{M}^2 \left(\sqrt{1 - 4m_0^2/\mathcal{M}^2_{f\bar{f}}} - 1\right)$$

Proof A limit can be taken under the integral if and only if the integrand passes the dominated convergence theorem, given in the appendices. The function this must be shown for is

$$f_s(x) = \frac{\sqrt{1 - 4m_0^2/x} - 1}{x - \mu_0^2} e^{-\tilde{s}(x - \mu_0^2)^2},$$

where $x = \mathcal{M}^2_{f\bar{f}}$, and n becomes $1/s$.

$$\lim_{1/s\to\infty} f_{1/s}(x) = \frac{\sqrt{1 - 4m_0^2/x} - 1}{x - \mu_0^2},$$

i.e. $f_{1/s}(x)$ converges pointwise to a function f. Now, take $g(x) = \frac{1}{x - \mu_0^2}$:

$$\begin{aligned}
|f_{1/s}(x)| &= \left| \frac{\sqrt{1 - 4m_0^2/x} - 1}{x - \mu_0^2} e^{-\tilde{s}(x - \mu_0^2)^2} \right| \\
&\leq \left| \frac{\sqrt{1 - 4m_0^2/x} - 1}{x - \mu_0^2} \right| \\
&= \frac{4m_0^2}{x(x - \mu_0^2)\left(\sqrt{1 - 4m_0^2/x} + 1\right)} \\
&\leq \frac{4m_0^2}{x(x - \mu_0^2)} = g(x).
\end{aligned}$$

Furthermore,

$$\int_{4m_0^2}^{\infty} dx \frac{4m_0^2}{x(x-\mu_0^2)} = -\frac{4m_0^2}{\mu_0} \log\left(1 - \frac{\mu_0^2}{4m_0^2}\right)$$

shows that the dominating function, $g(x)$ converges on $[4m_0^2, \infty)$. Thus, the dominated convergence theorem is satisfied, and the limit can be properly taken under the integral. ■

We can extract the form of the divergence in the boson loop by the following Theorem.

Theorem 4.3.2

$$\begin{aligned} 4\int_{4m_0^2}^{\infty} d\mathcal{M}_{f\bar{f}}^2 \frac{\sqrt{1-4m_0^2/\mathcal{M}_{f\bar{f}}^2}}{\mathcal{M}_{f\bar{f}}^2 - \mu_0^2} e^{-\tilde{s}\left(\mathcal{M}_{f\bar{f}}^2 - \mu_0^2\right)^2} = \\ 2\Bigg(-\gamma - \ln\left(2s(4m_0^2-\mu_0^2)^2/(q_3^+)^2\right)\Bigg) \\ + 4\Bigg(-\frac{2}{\mu_0}\sqrt{4m_0^2-\mu_0^2}\arctan\frac{\mu_0}{\sqrt{4m_0^2-\mu_0^2}} + \ln\left((4m_0^2-\mu_0^2)m_0^2\right)\Bigg) \\ + o(1) \end{aligned} \tag{4.69}$$

Proof

$$\begin{aligned} \int_{4m_0^2}^{\infty} d\mathcal{M}_{f\bar{f}}^2 \frac{\sqrt{1-4m_0^2/\mathcal{M}_{f\bar{f}}^2}}{\mathcal{M}_{f\bar{f}}^2 - \mu_0^2} e^{-\tilde{s}\left(\mathcal{M}_{f\bar{f}}^2 - \mu_0^2\right)^2} &= \int_{4m_0^2}^{\infty} d\mathcal{M}_{f\bar{f}}^2 \frac{1}{\mathcal{M}^2 - \mu_0^2} e^{-\tilde{s}\left(\mathcal{M}_{f\bar{f}}^2 - \mu_0^2\right)^2} \\ &+ \int_{4m_0^2}^{\infty} d\mathcal{M}_{f\bar{f}}^2 \frac{\left(\sqrt{1-4m_0^2/\mathcal{M}_{f\bar{f}}^2} - 1\right)}{\mathcal{M}_{f\bar{f}}^2 - \mu_0^2} e^{-\tilde{s}\left(\mathcal{M}_{f\bar{f}}^2 - \mu_0^2\right)^2} \end{aligned} \tag{4.70}$$

As $s \to 0$, the first integral on the right hand side diverges while the second integral

is finite. The finiteness of the second integral can be shown by

$$\begin{aligned}
&\lim_{1/s\to\infty}\int_{4m_0^2}^{\infty} d\mathcal{M}^2_{f\bar{f}}\frac{\left(\sqrt{1-4m_0^2/\mathcal{M}^2_{f\bar{f}}}-1\right)}{\mathcal{M}^2_{f\bar{f}}-\mu_0^2}e^{-\tilde{s}\left(\mathcal{M}^2_{f\bar{f}}-\mu_0^2\right)^2}\\
&\quad=\int_{4m_0^2}^{\infty} d\mathcal{M}^2_{f\bar{f}}\lim_{1/s\to\infty}\frac{\left(\sqrt{1-4m_0^2/\mathcal{M}^2_{f\bar{f}}}-1\right)}{\mathcal{M}^2_{f\bar{f}}-\mu_0^2}e^{-\tilde{s}\left(\mathcal{M}^2_{f\bar{f}}-\mu_0^2\right)^2}\\
&\quad=\int_{4m_0^2}^{\infty} d\mathcal{M}^2_{f\bar{f}}\frac{\left(\sqrt{1-4m_0^2/\mathcal{M}^2_{f\bar{f}}}-1\right)}{\mathcal{M}^2_{f\bar{f}}-\mu_0^2}\\
&\quad=-\frac{2}{\mu_0}\sqrt{4m_0^2-\mu_0^2}\arctan\frac{\mu_0}{\sqrt{4m_0^2-\mu_0^2}}+\ln\left((4m_0^2-\mu_0^2)m_0^2\right)
\end{aligned}\tag{4.71}$$

where lemma 4.3.1 was invoked.

For the first divergent integral, define the substitution, $t=\tilde{s}\left(\mathcal{M}^2_{f\bar{f}}-\mu_0^2\right)^2$. Then

$$\begin{aligned}
&\int_{4m_0^2}^{\infty} d\mathcal{M}^2_{f\bar{f}}\frac{1}{\mathcal{M}^2_{f\bar{f}}-\mu_0^2}e^{-\tilde{s}\left(\mathcal{M}^2_{f\bar{f}}-\mu_0^2\right)^2}\\
&\quad=\frac{1}{2}\int_{\tilde{s}(4m_0^2-\mu_0^2)^2}^{\infty}\frac{dt}{\tilde{s}\left(\mathcal{M}^2_{f\bar{f}}-\mu_0^2\right)}\frac{1}{\mathcal{M}^2_{f\bar{f}}-\mu_0^2}e^{-t}\\
&\quad=\frac{1}{2}\int_{\tilde{s}(4m_0^2-\mu_0^2)^2}^{\infty}\frac{dt}{t}e^{-t}\\
&\quad=\frac{1}{2}\Gamma\left(0,\tilde{s}(4m_0^2-\mu_0^2)^2\right)\\
&\quad=\frac{1}{2}\left(-\gamma-\ln\left(2s(4m_0^2-\mu_0^2)^2/(q_3^+)^2\right)\right)+o(1),
\end{aligned}$$

where

$$\Gamma(a,z)=\int_z^{\infty}t^{a-1}e^{-t}dt,\tag{4.72}$$

is the incomplete gamma function.

Combining these integrals,

$$I_B(s) = 2\bigg(-\gamma - \ln\Big(2s(4m_0^2-\mu_0^2)^2/(q_3^+)^2\Big)\bigg) + 4\bigg(-\frac{2}{\mu_0}\sqrt{4m_0^2-\mu_0^2}\arctan\frac{\mu_0}{\sqrt{4m_0^2-\mu_0^2}} + \ln\Big((4m_0^2-\mu_0^2)m_0^2\Big)\bigg) + o(1)$$

■

Here, we have a new constant, the Euler-Mascheroni constant, γ, whose formal definiton is

$$\gamma = \lim_{n\to\infty}\left(\sum_{k=1}^{n}\frac{1}{k} - \log n\right). \tag{4.73}$$

This result shows that the boson loop is logarithmically divergent.

4.3.2.2 Fermion Loop

The fermion and antifermion mass loop come from the double contractions:

$$:\Big(\bar{\psi}(-q_1)\overbrace{\psi(q_2)\phi(q_3)\bar{\psi}(-q_1')}\psi(q_2')\phi(q_3')\Big): \text{ and } :\Big(\overbrace{\bar{\psi}(-q_1)\psi(q_2)\phi(q_3)\bar{\psi}(-q_1')\psi(q_2')\phi(q_3')}\Big):.$$

Along with the following identity

$$:\bar{\psi}(q_1)(\gamma_\mu q_2^\mu + m_0)\psi(q_1): = \Big(q_2^- q_1^+ + q_2^+ q_1^- + 2m_0^2\Big):\bar{\psi}(q_1)\frac{\gamma^+}{2q_1^+}\psi(q_1):, \tag{4.74}$$

the fermion loop term can be written as:

$$H^{(2)}_{\delta m^2}(s,s_r) = \frac{1}{2}\int_q \delta m^2 :\bar{\psi}(q)\frac{\gamma^+}{q^+}\psi(q), \tag{4.75}$$

where

$$\delta m^2(q^+) = g^2 \int_{2,3} 4\pi\delta(q_2^+ + q_3^+ - q^+)\frac{\theta(q_3^+)}{q_2^+ q_3^+}\left(\frac{q_2^- q^+ + q_2^+ q^- + 2m_0^2}{q_2^- + q_3^- - q^-}\right) \times \left(e^{-2(s+s_r)(q_2^+ + q_3^+ - q^+)^2} - e^{-2s_r(q_2^+ + q_3^+ - q^+)^2}\right) \tag{4.76}$$

Under the change of variables, $x \equiv q_3^+/q^+$ and $y \equiv q_2^+ + q_3^+$, with the Jacobian $\mathbf{J} = q^+$, δm^2 can be written in the new variables as $\delta m^2(q^+) = I_F(s+s_r) - I_F(s_r)$, where

$$I_F(s) = \int_0^1 \frac{dx}{x(1-x)}\frac{1}{\mathcal{M}_{fb}^2(x) - m_0^2}\frac{m_0^2(1+x)^2}{x}e^{-\tilde{s}\left(\mathcal{M}_{fb}^2(x) - m_0^2\right)^2}, \tag{4.77}$$

again, where $\tilde{s} \equiv 2s/(q^+)^2$.

Taking $x_{min} = m_0/(m_0 + \mu_0)$, the minimum of the curve $\mathcal{M}_{fb}^2(x)$, the following two Lemmas help prove the Thm. 4.3.5 which gives the form of the divergence in I_F.

Lemma 4.3.3

$$\lim_{1/s\to\infty} \int_{x_{min}}^1 \frac{dx}{x(1-x)}\frac{1}{\mathcal{M}_{fb}^2(x) - m_0^2}\frac{m_0^2(1+x)^2}{x}e^{-\tilde{s}\left(\mathcal{M}_{fb}^2(x) - m_0^2\right)^2} \tag{4.78}$$

$$= \int_{x_{min}}^1 \lim_{1/s\to\infty} \frac{dx}{x(1-x)}\frac{1}{\mathcal{M}_{fb}^2(x) - m_0^2}\frac{m_0^2(1+x)^2}{x}e^{-\tilde{s}\left(\mathcal{M}_{fb}^2(x) - m_0^2\right)^2} \tag{4.79}$$

Proof Lebesgue's dominated convergence theorem must be satisfied, where

$$f_{1/s}(x) = \frac{1}{x(1-x)}\frac{1}{\mathcal{M}_{fb}^2(x) - m_0^2}\frac{m_0^2(1+x)^2}{x}e^{-\tilde{s}\left(\mathcal{M}_{fb}^2(x) - m_0^2\right)^2}.$$

Choose

$$g(x) = \frac{1}{x(1-x)}\frac{1}{\mathcal{M}_{fb}^2(x) - m_0^2}\frac{4m_0^2(1+x)^2}{x}.$$

Then

$$|f_\Lambda(x)| \leq \frac{1}{x(1-x)} \frac{1}{\mathcal{M}_{fb}^2(x) - m_0^2} \frac{m_0^2(1+x)^2}{x} < 4 \frac{1}{x(1-x)} \frac{1}{\mathcal{M}_{fb}^2(x) - m_0^2} \frac{m_0^2(1+x)^2}{x}.$$

Now it suffices to show the integral of $g(x)$ converges on $[x_{min}, 1]$:

$$\begin{aligned}
&\int_{x_{min}}^1 dx \frac{1}{x(1-x)} \frac{1}{\mathcal{M}_{fb}^2(x) - m_0^2} \frac{4m_0^2(1+x)^2}{x} \\
&\quad = \frac{8\sqrt{4m_0^2 - \mu_0^2}}{\mu_0} \left(- \operatorname{arccot} \left(\frac{(m_0 + \mu_0)\sqrt{4m_0^2 - \mu_0^2}}{-2m_0^2 + m_0\mu_0 + \mu_0^2} \right) + \arctan \left(\frac{\mu_0}{\sqrt{4m_0^2 - \mu_0^2}} \right) \right) \\
&\qquad - 2\log(m_0) + 2\log(m_0 + \mu_0) < \infty.
\end{aligned}$$

■

Lemma 4.3.4

$$\begin{aligned}
&\lim_{1/s \to \infty} \int_0^{x_{min}} \frac{dx}{x(1-x)} \frac{e^{-\tilde{s}\left(\mathcal{M}_{fb}^2(x) - m_0^2\right)^2}}{\left(\mathcal{M}_{fb}^2(x) - m_0^2\right)^2} \left(\frac{m_0^2(1+x)^2}{x} + \frac{\mu_0^2 x^2 - m_0^2(1-x)^2}{x^2(1-x)^2} x(1-x) \right) \\
&\quad = g^2 \int_0^{x_{min}} \lim_{1/s \to \infty} \frac{dx}{x(1-x)} \frac{e^{-\tilde{s}\left(\mathcal{M}_{fb}^2(x) - m_0^2\right)^2}}{\left(\mathcal{M}_{fb}^2(x) - m_0^2\right)^2} \left(\frac{m_0^2(1+x)^2}{x} + \frac{\mu_0^2 x^2 - m_0^2(1-x)^2}{x^2(1-x)^2} x(1-x) \right)
\end{aligned}$$

Proof Lebesgue's dominated convergence theorem must be satisfied, where

$$f_{1/s}(x) = \frac{1}{x(1-x)} \frac{e^{-\tilde{s}\left(\mathcal{M}_{fb}^2(x) - m_0^2\right)^2}}{\left(\mathcal{M}_{fb}^2(x) - m_0^2\right)} \left(\frac{m_0^2(1+x)^2}{x} + \frac{\mu_0^2 x^2 - m_0^2(1-x)^2}{x^2(1-x)^2} x(1-x) \right).$$

Choose

$$g(x) = 2 \cdot \frac{1}{x(1-x)} \frac{1}{\left(\mathcal{M}_{fb}^2(x) - m_0^2\right)} \left(\frac{m_0^2(1+x)^2}{x} + \frac{\mu_0^2 x^2 - m_0^2(1-x)^2}{x^2(1-x)^2} x(1-x) \right).$$

Then,

$$\left|f_\Lambda(x)\right| \le \frac{1}{x(1-x)}\frac{1}{\left(\mathcal{M}_{fb}^2(x)-m_0^2\right)}\left(\frac{m_0^2(1+x)^2}{x}+\frac{\mu_0^2x^2-m_0^2(1-x)^2}{x^2(1-x)^2}x(1-x)\right) < g(x).$$

Now it suffices to show the integral of $g(x)$ converges on $[0, x_{min}]$:

$$\begin{aligned}
&2\int_0^{x_{min}} dx \frac{1}{x(1-x)}\frac{1}{\left(\mathcal{M}_{fb}^2(x)-m_0^2\right)}\left(\frac{m_0^2(1+x)^2}{x}+\frac{\mu_0^2x^2-m_0^2(1-x)^2}{x^2(1-x)^2}x(1-x)\right)\\
&\quad= \frac{4\sqrt{4m_0^2-\mu_0^2}\left(\operatorname{arccot}\left(\frac{\mu_0\sqrt{4m_0^2-\mu_0^2}}{2m_0^2-\mu_0^2}\right)+\operatorname{arccot}\left(\frac{(m_0+\mu_0)\sqrt{4m_0^2-\mu_0^2}}{-2m_0^2+m_0\mu_0+\mu_0^2}\right)\right)}{\mu_0}\\
&\qquad+2\log(\mu_0)-2\log(m_0(m_0+\mu_0))+2\log(2m_0+\mu_0)<\infty
\end{aligned}$$

■

Theorem 4.3.5

$$\begin{aligned}
I_F(s) &= \frac{2\sqrt{4m_0^2-\mu_0^2}\left(-\operatorname{arccot}\left(\frac{(m_0+\mu_0)\sqrt{4m_0^2-\mu_0^2}}{-2m_0^2+m_0\mu_0+\mu_0^2}\right)+\arctan\left(\frac{\mu_0}{\sqrt{4m_0^2-\mu_0^2}}\right)\right)}{\mu_0}\\
&\quad+\frac{2\sqrt{4m_0^2-\mu_0^2}\left(\operatorname{arccot}\left(\frac{\mu_0\sqrt{4m_0^2-\mu_0^2}}{2m_0^2-\mu_0^2}\right)+\operatorname{arccot}\left(\frac{(m_0+\mu_0)\sqrt{4m_0^2-\mu_0^2}}{-2m_0^2+m_0\mu_0+\mu_0^2}\right)\right)}{\mu_0}\\
&\quad-\log(m_0)+\log(m_0+\mu_0)+\log(\mu_0)-\log(m_0(m_0+\mu_0))+\log(2m_0+\mu_0)\\
&\quad+\frac{1}{2}\left(-\gamma-\ln\left(2s(\mu_0^2+2\mu_0m_0)^2/(q^+)^2\right)\right)+o(1)
\end{aligned}$$

Proof

$$\begin{aligned}
I_F(s) &= \int_0^1 \frac{dx}{x(1-x)}\frac{1}{\mathcal{M}_{fb}^2(x)-m_0^2}\frac{m_0^2(1+x)^2}{x}e^{-\tilde{s}\left(\mathcal{M}_{fb}^2(x)-m_0^2\right)^2}\\
&= \int_0^{x_{min}} \frac{dx}{x(1-x)}\frac{1}{\mathcal{M}_{fb}^2(x)-m_0^2}\frac{m_0^2(1+x)^2}{x}e^{-\tilde{s}\left(\mathcal{M}_{fb}^2(x)-m_0^2\right)^2}\\
&\qquad+\int_{x_{min}}^1 \frac{dx}{x(1-x)}\frac{1}{\mathcal{M}_{fb}^2(x)-m_0^2}\frac{m_0^2(1+x)^2}{x}e^{-\tilde{s}\left(\mathcal{M}_{fb}^2(x)-m_0^2\right)^2}
\end{aligned}$$

The second integral on the range $[x_{min}, 1]$ can be computed by using lemma 4.3.3:

$$\begin{aligned}
&\lim_{1/s\to\infty} g^2 \int_{x_{min}}^{1} \frac{dx}{x(1-x)} \frac{1}{\mathcal{M}_{fb}^2(x) - m_0^2} \frac{m_0^2(1+x)^2}{x} e^{-\tilde{s}\left(\mathcal{M}_{fb}^2(x) - m_0^2\right)^2} \\
&\quad = g^2 \int_{x_{min}}^{1} \lim_{1/s\to\infty} \frac{dx}{x(1-x)} \frac{1}{\mathcal{M}_{fb}^2(x) - m_0^2} \frac{m_0^2(1+x)^2}{x} e^{-\tilde{s}\left(\mathcal{M}_{fb}^2(x) - m_0^2\right)^2} \\
&\quad = g^2 \int_{x_{min}}^{1} \frac{dx}{x(1-x)} \frac{1}{\mathcal{M}_{fb}^2(x) - m_0^2} \frac{m_0^2(1+x)^2}{x} \\
&\quad = \frac{2\sqrt{4m_0^2 - \mu_0^2}}{\mu_0} \left(- \operatorname{arccot}\left(\frac{(m_0+\mu_0)\sqrt{4m_0^2 - \mu_0^2}}{-2m_0^2 + m_0\mu_0 + \mu_0^2} \right) + \arctan\left(\frac{\mu_0}{\sqrt{4m_0^2 - \mu_0^2}} \right) \right) \\
&\qquad - \log(m_0) + \log(m_0 + \mu_0)
\end{aligned}$$

The first integral on the range $[0, x_{min}]$ must be split into a divergent piece plus a finite part.

$$\begin{aligned}
&\int_0^{x_{min}} \frac{dx}{x(1-x)} \frac{1}{\left(\mathcal{M}_{fb}^2(x) - m_0^2\right)^2} \frac{m_0^2(1+x)^2}{x} e^{-\tilde{s}\left(\mathcal{M}_{fb}^2(x) - m_0^2\right)^2} \\
&= \int_0^{x_{min}} dx \left| \frac{d\mathcal{M}_{fb}^2}{dx} \right| \frac{e^{-\tilde{s}\left(\mathcal{M}_{fb}^2(x) - m_0^2\right)^2}}{\left(\mathcal{M}_{fb}^2(x) - m_0^2\right)^2} \\
&\quad + \int_0^{x_{min}} \frac{dx}{x(1-x)} \frac{1}{\left(\mathcal{M}_{fb}^2(x) - m_0^2\right)^2} e^{-\tilde{s}\left(\mathcal{M}_{fb}^2(x) - m_0^2\right)^2} \left(\frac{m_0^2(1+x)^2}{x} - \left| \frac{d\mathcal{M}_{fb}^2}{dx} \right| x(1-x) \right).
\end{aligned}$$

On the region $[0, x_{min}]$, $\left|d\mathcal{M}_{fb}^2/dx\right| < 0$, so $\left|d\mathcal{M}_{fb}^2/dx\right| = -d\mathcal{M}_{fb}^2/dx$. In the first integral, a change of variables from $x \to \mathcal{M}_{fb}^2$ is done, but in the second integral, it

is kept in terms of x. From this, the first integral in the split version of I_F is:

$$\int_0^{x_{min}} \frac{dx}{x(1-x)} \frac{1}{\left(\mathcal{M}_{fb}^2(x) - m_0^2\right)^2} \frac{m_0^2(1+x)^2}{x} e^{-\tilde{s}\left(\mathcal{M}_{fb}^2(x)-m_0^2\right)^2}$$

$$= \int_{(m_0+\mu_0)^2}^{\infty} d\mathcal{M}_{fb}^2 \frac{1}{\left(\mathcal{M}_{fb}^2(x) - m_0^2\right)^2} e^{-\tilde{s}\left(\mathcal{M}_{fb}^2(x)-m_0^2\right)^2}$$

$$+ \int_0^1 \frac{dx}{x(1-x)} \frac{e^{-\tilde{s}\left(\mathcal{M}_{fb}^2(x)-m_0^2\right)^2}}{s(x)} \left(\frac{m_0^2(1+x)^2}{x} + \frac{\mu_0^2 x^2 - m_0^2(1-x)^2}{x^2(1-x)^2} x(1-x) \right),$$

where $d\mathcal{M}_{fb}^2/dx$ was explicitly computed based on the definition of $\mathcal{M}_{fb}^2$. The second integral here is convergent. To verify this, lemma 4.3.4 is used, and the following integral is calculated:

$$\int_0^1 \frac{dx}{x(1-x)} \frac{1}{\left(\mathcal{M}_{fb}^2(x) - m_0^2\right)^2} \left(\frac{m_0^2(1+x)^2}{x} + \frac{\mu_0^2 x^2 - m_0^2(1-x)^2}{x^2(1-x)^2} x(1-x) \right)$$

$$= \frac{2\sqrt{4m_0^2 - \mu_0^2} \left(\operatorname{arccot}\left(\frac{\mu_0 \sqrt{4m_0^2-\mu_0^2}}{2m_0^2-\mu_0^2} \right) + \operatorname{arccot}\left(\frac{(m_0+\mu_0)\sqrt{4m_0^2-\mu_0^2}}{-2m_0^2+m_0\mu_0+\mu_0^2} \right) \right)}{\mu_0}$$

$$+ \log(\mu_0) - \log(m_0(m_0+\mu_0)) + \log(2m_0+\mu_0)$$

Finally, with the divergent part of I_F fully extracted:

$$\int_{(m_0+\mu_0)^2}^{\infty} d\mathcal{M}_{fb}^2 \frac{1}{\left(\mathcal{M}_{fb}^2(x) - m_0^2\right)^2} e^{-\tilde{\Lambda}\left(\mathcal{M}_{fb}^2(x)-m_0^2\right)^2}$$

$$= \frac{1}{2} g^2 \left(-\gamma - \ln\left(2s(\mu_0^2 + 2\mu_0 m_0)^2/(q^+)^2 \right) \right) + o(1)$$

■

From this, $\delta m^2(q^+) = I_F(s+s_r) - I_F(s_r)$ can be computed explicitly.

4.3.3 Perturbative Mass Renormalization

The counterterm is fixed with perturbation theory. The perturbative correction of the n^{th} eigenvalue is

$$E_n = E_n^{(0)} + \langle n^{(0)}|V|n^{(0)}\rangle + \sum_{k\neq n} \frac{|\langle k^{(0)}|V|n^{(0)}\rangle|^2}{E_n^{(0)} - E_k^{(0)}} + \mathcal{O}\left(\lambda^3\right), \tag{4.80}$$

written explicitly up to $\mathcal{O}\left(\lambda^3\right)$, where λ is a parameter dictating the strength of the interacting part of the Hamiltonian.

The *physical fermion mass* m^2 is defined as:

$$m^2 \equiv M_0^2\Big|_{Q=1}, \tag{4.81}$$

i.e. the lowest eigenvalue corresponding to the state in the $Q = 1$ sector that is dominated by a single fermion (this will be the ground state of this sector. The ground state in this sector is actually $\left(M_0^2 + (\vec{P}^{\perp})^2\right)/P^+$, but in this Chapter, we use the standard frame with $P^+ = 1, \vec{P}^{\perp} = 0$).

In order to properly renormalize a parameter in the theory, a *renormalization condition* must be set. The condition for the mass term is

$$m^2 = m_0^2, \tag{4.82}$$

i.e. the renormalized mass of a single fermion is the same as the mass in the Lagrangian (bare fermion mass).

With this definition, the perturbative corrections, up to $\mathcal{O}\left(g^2\right)$, to this eigenvalue is[2]:

$$\frac{m^2}{P^+} = \left(\frac{m^2}{P^+}\right)^{(0)} + \left(\frac{m^2}{P^+}\right)^{(1)} + \left(\frac{m^2}{P^+}\right)^{(2)} \tag{4.83}$$

$\left(\frac{m^2}{P^+}\right)^{(0)}$ is the unperturbed eigenvalue, i.e the eigenvalue when there is no interaction. This is simply m_0^2/P^+, the parameter in the Lagrangian. The first order correction is zero since $H^{(1)}|f\rangle \sim |fb\rangle$.

There are two nonzero contributions to the second order correction. The first

[2]Recall, the eigenvalues of $\hat{P}^-$ (in $1+1D$) are $\left(\frac{m^2}{P^+}\right)$. Additionally, while it is true that $P^+ = 1$ is set throughout this thesis, in this derivation, it is computed for arbitrary P^+.

comes from the standard second order correction in equation 4.80, and the second is a correction that arises from the loop diagram $H^{(2)}_{\delta m^2}(s, s_r)$ that comes from solving the RGPEP equation.

$$(m^2)^{(2)} = \langle f|H^{(2)}_{\delta m^2}(s, s_r)|f\rangle + \langle f|H^{(1)}(s, s_r)\frac{1}{m_0^2/P^+ - H_0}H^{(1)}(s, s_r)|f\rangle.$$

The first term in this is

$$\begin{aligned}\langle f|H^{(2)}\delta m^2(s, s_r)|f\rangle &= \delta m^2 \\ &= I_F(s + s_r) - I_F(s_r),\end{aligned}$$

while the second term requires some simplification. The resolvent of the free Hamiltonian [BPP98], $(m_0^2 - H_0)^{-1}$, can be written in its spectral decomposition as:

$$\frac{1}{m_0^2/P^+ - H_0} = \sum_n \int \frac{dq_1^+ \dots dq_n^+}{4\pi q_1^+ \dots 4\pi q_n^+}|n\rangle\frac{1}{m_0^2/P^+ - \sum_{i\in n} q_n^-}\langle n|, \tag{4.84}$$

where n refers to all intermediate states. In the context of the fermion loop, $|n\rangle = |fb\rangle$, and $q_n^- = m_0^2/q_f^+ + \mu_0^2/q_b^+$. The second term in $m^{2(2)}$ can now be simplified:

$$\begin{aligned}&\langle f|H^{(1)}(s, s_r)\frac{1}{m_0^2/P^+ - H_0}H^{(1)}(s, s_r)|f\rangle \\ &\qquad = \int \frac{dq_f^+ dq_b^+}{4\pi q_f^+ 4\pi q_b^+}\frac{\langle f|\, H^{(1)}\,|fb\rangle\,\langle fb|\, H^{(1)}\,|f\rangle}{m_0^2/P^+ - q_f^- - q_b^-}.\end{aligned}$$

Writing $|fb\rangle = b^\dagger_{q_f} a^\dagger_{q_b}|0\rangle$ and $|f\rangle = b^\dagger_{-q}|0\rangle$, and keeping consistency with notation $\langle fb| = \langle 0|\, b_{q_f} a_{q_b}$ and $\langle f| = \langle 0|\, b_{q'}$, the numerator can be written as

$$\langle f|\, H^{(1)}\,|fb\rangle\,\langle fb|\, H^{(1)}\,|f\rangle = \delta(q_f^+ + q_b^+ - q'^+)\delta(q^+ + q'^+)e^{-2s(q_f^- + q_b^- - q^-)^2}\bar{u}(q')u(q_f)\bar{u}(q_f)u(-q) \tag{4.85}$$

Inserting this above, and changing the indices from $f \to 2, b \to 3$:

$$\begin{aligned}\langle f|H^{(1)}(s,s_r)\frac{1}{m_0^2-H_0}H^{(1)}(s,s_r)|f\rangle = \\ -\int \frac{dq_2^+ dq_3^+}{4\pi q_2^+ 4\pi q_3^+}\delta(q_2^+ + q_3^+ - q^+)e^{-2(s+s_r)(q^- - q_2^- - q_3^-)^2} \\ \times \delta(q^+ + q'^+)\frac{\bar{u}(q')(\gamma_\mu q_2^\mu + m_0)u(q')}{q_2^- + q_3^- - m_0^2/P^+},\end{aligned}$$

where

$$u_\sigma(q)\bar{u}_\sigma(q) = \sum_\sigma(\gamma^\mu q_\mu + m_0) \tag{4.86}$$

was used. Furthermore,

$$\begin{aligned}\bar{u}(q)(\gamma_\mu q_2^\mu + m_0)u(q) &= (q_2^- q^+ + q_2^+ q^- + 2m_0^2)\frac{\bar{u}(q)\gamma^+ u(q)}{2q^+} \\ &= (q_2^- q^+ + q_2^+ q^- + 2m_0^2).\end{aligned}$$

Lastly, $P^+ = q^+$. This is true because the momentum of the single fermion state, q^+ *must* be P^+, the total momentum, since there is a single fermion and nothing else. From this, $m_0^2/P^+ = q^-$. All together:

$$\begin{aligned}\langle f|H^{(1)}(s,s_r)\frac{1}{m_0^2-H_0}H^{(1)}(s,s_r)|f\rangle = \\ -\delta(q^+ + q'^+)\int \frac{dq_2^+ dq_3^+}{4\pi q_2^+ 4\pi q_3^+}\delta(q_2^+ + q_3^+ - q^+) \\ \times e^{-2(s+s_r)(q^- - q_2^- - q_3^-)^2}\frac{(q_2^- q^+ + q_2^+ q^- + 2m_0^2)}{q_2^- + q_3^- - q^-}.\end{aligned}$$

From this, it is clear that

$$\langle f|H^{(1)}(s,s_r)\frac{1}{m_0^2-H_0}H^{(1)}(s,s_r)|f\rangle = -\delta(q^+ + q'^+)I_F(s+s_r), \tag{4.87}$$

where $\delta(q^+ + q'^+)$ is a normalization factor, which can be disregarded.

The full second order perturbative correction to m^2 (where P^+ is now again

taken to be 1) can now be simplified:

$$\begin{aligned}(m^2)^{(2)} &= I_F(s+s_r) - I_F(s_r) - I_F(s+s_r) \\ &= -I_F(s_r),\end{aligned}$$

which gives the form of the perturbative correction to m^2:

$$m^2 = m_0^2 - I_F(s_r). \tag{4.88}$$

Equation 4.88 explicitly gives the proper form of the fermion mass counterterm that needs to be added to $H(s)$ to remove the divergence:

$$X_{\delta m^2} = I_F\left(s_r\right). \tag{4.89}$$

The combination of both $H^{(2)}_{\delta m^2}$ and $X_{\delta m^2}$ in $H(s)$ leads to a term $\sim I_F\left(s, s_r\right) b^\dagger b$. The regulator can now be removed $s_r \to 0$ with results remaining finite.

The boson renormalization is slightly different. We define

$$\mu^2 \equiv M_0^2\Big|_{Q=0}, \tag{4.90}$$

with renormalization condition

$$\mu^2 = \mu_0^2. \tag{4.91}$$

One can work out the same steps to get the boson mass counterterm:

$$X_{\delta\mu^2} = I_B(s_r), \tag{4.92}$$

After adding the appropriate counterterms, the effective Hamiltonian now obtains effective mass terms:

$$H_0 \to H_{0,eff}(s) = \int_q \frac{m^2(s;q)}{q^+} : \bar{\psi}(q)\frac{\gamma^+}{q^+}\psi(q) : + \int_q \mu^2(s;q) : \phi(-q)\phi(q) :, \tag{4.93}$$

where

$$m^2(s;q) = m_0^2 + g^2 \int_{2,3} \frac{\theta(q_2^+)\theta(q_3^+)}{|q_2^+||q_3^+|} \frac{m_0^2(q_2^+ - q_3^+)^2}{q_2^+ q_3^+ (q_2^+ + q_3^+ - q^+)} e^{-2s(q_2^+ + q_3^+ - q^+)^2}, \quad (4.94)$$

and

$$\mu^2(s;q) = \mu_0^2 + g^2 \int_{1,2} \frac{\theta(q_1^+)\theta(q_2^+)}{|q_1^+||q_2^+|} \frac{\mathrm{Tr}\Big[(\gamma_\mu q_1^\mu - m_0)(\gamma_\nu q_2^\nu + m_0)\Big]}{q_1^+ q_2^+ (q_1^+ + q_2^+ - q^+)} e^{-2s(q_1^+ + q_2^+ - q^+)^2}, \quad (4.95)$$

4.3.4 Summary of the Effective Yukawa Hamiltonian

The effective Yukawa Hamiltonian is given as

$$\mathcal{H}(s) = H_{0,\mathrm{eff}}(s) + gH^{(1)}(s) + g^2 \left(H^{(2)}_{\bar{\psi}\phi\phi\psi}(s) + H^{(2)}_{\mathrm{fe}}(s) + H^{(2)}_{\mathrm{be}}(s) \right). \quad (4.96)$$

In what follows, this Hamiltonian will be discretized and used as input for numerics.

4.4 Renormalized Yukawa Hamiltonian Numerics

In the rest of this chapter, the question "Is the cost associated with simulating the effective Hamiltonian, which gives finite results, exponentially more expensive than that of the bare Hamiltonian?" is addressed for the Yukawa model. To obtain the cost of each Hamiltonian, the continuous version is discretized with discretized light-cone quantization. Mass spectra and structure functions are calculated classically for low-lying two-fermion bound states to verify the renormalization procedure. Finally, the cost associated with a single Ladder Operator Block Encoding is calculated.

4.4.1 Discretized Lightcone Quantization

Following [KKG+22], given the total bound state two-momentum P^μ, the invariant momentum squared in $1+1D$ is $P^-P^+ = M^2$. When this is quantized, so that P^+ and P^- become operators, this relation can be interpreted as an eigenvalue

equation:

$$\left(\hat{P}^{-}\hat{P}^{+}\right)|\psi\rangle = M^{2}|\psi\rangle\,. \tag{4.97}$$

Since $\hat{P}^{+}$ and $\hat{P}^{-}$ commute, they can be simultaneously diagonalized.

We take $|\psi\rangle$ to be an eigenstate of $\hat{P}^{+}$ with the eigenvalue of the total bound state longitudinal momentum, P^{+}. That is, we diagonalize $\hat{P}^{-}$ in a basis of fixed P^{+}. Eq. 4.97 then simplifies to

$$\hat{P}^{-}|\psi\rangle = \left(\frac{M^{2}}{P^{+}}\right)|\psi\rangle\,. \tag{4.98}$$

While $\hat{P}^{-}$ is frame-dependent (it is simply a component of a four-vector), $\hat{P}^{-}\hat{P}^{+}$ is a Lorentz scalar. Consequently, we can choose any value of $P^{+} > 0$ for the total bound state longitudinal momentum of $|\psi\rangle$, diagonalize $\hat{P}^{-}$, and expect the same M^{2} value for any choice of P^{+}. The light-front energy operator $\hat{P}^{-}$ will be denoted as the Hamiltonian, H, for the remainder of this paper.

We solve Eq. 4.98 by restricting $x^{-} \in [-L, L]$, i.e. placing the fields in a box. The integrals in each Hamiltonian term over continuous q_{i}^{+} become sums over discrete longitudinal momentum, defined as $q^{+}(k_{i})$, where k_{i} is a momentum quantum number. k will be referred to as momentum throughout, even though $q^{+}(k)$ is the actual momentum and k is the momentum quantum number.

The continuous longitudinal momentum takes on any value from 0 to P^{+} in a block of fixed P^{+}, while $q^{+}(k)$ is discretized such that

$$q^{+}(k) = \frac{2\pi}{L}k. \tag{4.99}$$

The momentum quantum number, k in $q^{+}(k)$ takes on values $\frac{1}{2}, \frac{3}{2}, \frac{5}{2}, \ldots$ for (anti-)fermions, and values $1, 2, 3, \ldots$ for bosons to satisfy boundary conditions of the fields imposed at $x^{-} = \pm L$. This follows by the conditions that a bosonic field satisfies periodic boundary conditions, i.e. $\phi(L) = \phi(-L)$, while a fermionic field satisfies antiperiodic boundary conditions i.e. $\psi(L) = -\psi(-L)$.

The continuum limit is recovered by taking $L \to \infty$. In a bound state

calculation, by choosing a finite value of L, it necessarily restricts the space of allowed states, due to the positivity of P^+, and the fact that the k_i's are discrete. Increasing L leads to a better approximation to the continuum limit. In practice, L is taken to be integer multiples of 2π, such that $L = 2\pi K L_0$, where K is referred to as the *harmonic resolution*, and L_0 is some arbitrary reference length (which in this work is taken to be $L_0 = 1$). The harmonic resolution can be taken as any value $\frac{1}{2}, 1, \frac{3}{2}, \ldots$.

The continuum limit ($L \to \infty$) can now be traded for the limit $K \to \infty$. The constraint that all constituent longitudinal momenta q_i^+ must sum to the total longitudinal momentum P^+ when discretized becomes

$$P^+ = \frac{1}{K} \sum_i k_i, \tag{4.100}$$

which implies that the bound state constituent momenta quantum numbers k_i in a given Fock state must all sum to $P^+ K$.

The DLCQ procedure can be summarized as follows:

1. Fix P^+
2. Choose a *resolution* K.
3. Enumerate a finite set of Fock states whose individual partonic momentum each sum to $P^+ K$.
4. Obtain a finite matrix of $\hat{P}^-$ in the basis of the discrete Fock states.
5. Diagonalize to obtain $M^2(K)$ spectrum at a given resolution.
6. Increase K, repeat steps 2-5 and extrapolate to $K \to \infty$ to recover the continuum M^2 value.

In the following section, the Hamiltonian is discretized so that DLCQ results can be calculated.

T_n	$\theta(k_1,k_2,k_3)$	Spinors	Operator
T_1	$-++$	$\bar{u}(-k_1)u(k_2)$	$b^\dagger_{-k_1}b_{k_2}a_{k_3}$
T_2	$-+-$	$\bar{u}(-k_1)u(k_2)$	$b^\dagger_{-k_1}b_{k_2}a^\dagger_{-k_3}$
T_3	$+-+$	$\bar{v}(k_1)v(-k_2)$	$d_{k_1}d^\dagger_{-k_2}a_{k_3}$
T_4	$+--$	$\bar{v}(k_1)v(-k_2)$	$d_{k_1}d^\dagger_{-k_2}a^\dagger_{-k_3}$
T_5	$--+$	$\bar{u}(-k_1)v(-k_2)$	$b^\dagger_{-k_1}d^\dagger_{-k_2}a_{k_3}$
T_6	$++-$	$\bar{v}(k_1)u(k_2)$	$d_{k_1}b_{k_2}a^\dagger_{-k_3}$

Table 4.1: **Discrete 3-point Yukawa interaction** : The standard three-point Yukawa term is a sum of the above 6 rows, where $k_1, k_2 \in \mathbb{Z}+1/2$, $k_3 \in \mathbb{Z}\backslash\{0\}$, and $\theta(k_1,k_2,k_3) \equiv \theta(k_1)\theta(k_2)\theta(k_3)$. The spinors are implicitly assumed to mean $u(k) = u(q^+(k))$.

4.4.2 Discrete Yukawa Hamiltonian

Using the definition of the discretized energy:

$$q^-(k_i) = \frac{m_i^2}{q^+(k_i)} = \Big(\frac{L}{2\pi}\Big)\frac{m_i^2}{k_i} = \frac{L}{2\pi}k_i^-, \tag{4.101}$$

what follows are the explicit forms of the discretized effective Yukawa Hamiltonian.

The $\mathcal{O}(g)$ term is given as

$$H^{(1)}(s) = \frac{2L}{(4\pi)^{3/2}}\sum_n \sum_{k_1,k_2,k_3} \frac{\delta_{k_1+k_2+k_3,0}}{\sqrt{|k_1k_2k_3|}} e^{-sL^2(k_1^-+k_2^-+k_3^-)^2/4\pi^2} : T_n^{(\mathrm{I})}(k_1,k_2,k_3) :, \tag{4.102}$$

where k_1 and k_2 are the fermion momenta and k_3 is the boson momentum.

The instantaneous exchange term $H^{(2)}_{\bar{\psi}\phi\phi\psi}(s)$ given as:

$$H^{(2)}_{\bar{\psi}\phi\phi\psi}(s) = \frac{2L}{(4\pi)^2}\sum_n \sum_{\substack{k_1,k_2\\k_3,k_4}} \frac{\delta_{k_1+k_2+k_3+k_4,0}}{\sqrt{|k_1k_2k_3k_4|}} e^{-sL^2(k_1^-+k_2^-+k_3^-+k_4^-)^2/4\pi^2} : T_n^{(\mathrm{II})}(k_1,k_2,k_3,k_4) :, \tag{4.103}$$

where k_1 and k_4 are the fermion momenta while k_2 and k_3 are the boson momenta.

T_n	$\theta(k_1,k_2,k_3,k_4)$	Spinors	Operator
T_1	$-+++$	$\bar{u}(-k_1)\gamma^+u(k_4)$	$b^\dagger_{-k_1}b_{k_4}a_{k_2}a_{k_3}$
T_2	$--++$	$\bar{u}(-k_1)\gamma^+u(k_4)$	$b^\dagger_{-k_1}b_{k_4}a^\dagger_{-k_2}a_{k_3}$
T_3	$-+-+$	$\bar{u}(-k_1)\gamma^+u(k_4)$	$b^\dagger_{-k_1}b_{k_4}a_{k_2}a^\dagger_{-k_3}$
T_4	$---+$	$\bar{u}(-k_1)\gamma^+u(k_4)$	$b^\dagger_{-k_1}b_{k_4}a^\dagger_{-k_2}a^\dagger_{-k_3}$
T_5	$+++-$	$\bar{v}(k_1)\gamma^+v(-k_4)$	$d_{k_1}d^\dagger_{-k_4}a_{k_2}a_{k_3}$
T_6	$+-+-$	$\bar{v}(k_1)\gamma^+v(-k_4)$	$d_{k_1}d^\dagger_{-k_4}a^\dagger_{-k_2}a_{k_3}$
T_7	$++--$	$\bar{v}(k_1)\gamma^+v(-k_4)$	$d_{k_1}d^\dagger_{-k_4}a_{k_2}a^\dagger_{-k_3}$
T_8	$+---$	$\bar{v}(k_1)\gamma^+v(-k_4)$	$d_{k_1}d^\dagger_{-k_4}a^\dagger_{-k_2}a^\dagger_{-k_3}$
T_9	$-++-$	$\bar{u}(-k_1)\gamma^+v(-k_4)$	$b^\dagger_{-k_1}d^\dagger_{-k_4}a_{k_2}a_{k_3}$
T_{10}	$--+-$	$\bar{u}(-k_1)\gamma^+v(-k_4)$	$b^\dagger_{-k_1}d^\dagger_{-k_4}a^\dagger_{-k_2}a_{k_3}$
T_{11}	$-+--$	$\bar{u}(-k_1)\gamma^+v(-k_4)$	$b^\dagger_{-k_1}d^\dagger_{-k_4}a_{k_2}a^\dagger_{-k_3}$
T_{12}	$+-++$	$\bar{v}(k_1)\gamma^+u(k_4)$	$d_{k_1}b_{k_4}a^\dagger_{-k_2}a_{k_3}$
T_{13}	$++-+$	$\bar{v}(k_1)\gamma^+u(k_4)$	$d_{k_1}b_{k_4}a_{k_2}a^\dagger_{-k_3}$
T_{14}	$+--+$	$\bar{v}(k_1)\gamma^+u(k_4)$	$d_{k_1}b_{k_4}a^\dagger_{-k_2}a^\dagger_{-k_3}$

Table 4.2: **Discrete Instantaneous Yukawa Interaction** The instantaneous Yukawa Hamiltonian is a sum of the terms in the above 14 rows, where $k_1, k_4 \in \mathbb{Z}+1/2$, $k_2, k_3 \in \mathbb{Z}\backslash\{0\}$, and $\theta(k_1,k_2,k_3,k_4) \equiv \theta(k_1)\theta(k_2)\theta(k_3)\theta(k_4)$. The spinors are implicitly assumed to mean $u(k) = u(q^+(k))$.

The discretized boson exchange term, $H_{\rm be}(\lambda)$, is given as

$$H^{(2)}_{\rm be}(s) = \frac{1}{2L(4\pi)^4}\sum_n \sum_{\substack{k_1,k_2,k_3\\ k_{1'},k_{2'}}} \frac{\theta(k_3)\delta_{k_1,-k_2-k_3}\delta_{k_3,k_{1'}+k_{2'}}}{\sqrt{|k_1k_2k_{1'}k_{2'}|}}\mathcal{R}(s;\mathcal{Q},\mathcal{Q}') : T^{(\rm III)}_n(k_1,k_2,k_{1'},k_{2'}) :, \tag{4.104}$$

where $k_1, k_2, k_{1'}, k_{2'}$ correspond to the fermion momenta while k_3 corresponds to the exchanged boson momentum. $T^{(\rm III)}_n$ corresponds to a term in a row in Table 4.3. $\mathcal{Q}$ and $\mathcal{Q}'$ both correspond to their discrete counterparts, e.g. $\mathcal{Q}^- = q^-(k_1)+q^-(k_2)+q^-(k_3)$.

The discretized fermion exchange term $H^{(2)}_{\rm fe}(s)$ is given as

$$H^{(2)}_{\rm fe}(s) = \frac{1}{2L(4\pi)^4}\sum_n \sum_{\substack{k_1,k_2,k_3\\ k_{1'},k_{2'}}} \frac{\delta_{k_1,-k_2-k_3}\delta_{k_2,k_{2'}+k_{3'}}}{\sqrt{|k_1k_{2'}k_3k_{3'}|}}\mathcal{R}(s;\mathcal{Q},\mathcal{Q}') : T^{(\rm IV)}_n(k_1,k_{2'},k_3,k_{3'}) :, \tag{4.105}$$

where $k_1, k_2, k_{2'}$ correspond to the fermion momenta, while k_3 and $k_{3'}$ correspond

T_n	θ	Spinors	Operator
T_1	$-+-+$	$\bar{u}(-k_1)u(k_2)\bar{u}(-k_{1'})u(k_{2'})$	$b^\dagger_{-k_1} b_{k_2} b^\dagger_{-k_{1'}} b_{k_{2'}}$
T_2	$-+--$	$\bar{u}(-k_1)u(k_2)\bar{u}(-k_{1'})v(-k_{2'})$	$b^\dagger_{-k_1} b_{k_2} b^\dagger_{-k_{1'}} d^\dagger_{-k_{2'}}$
T_3	$-++-$	$\bar{u}(-k_1)u(k_2)\bar{v}(k_{1'})u(k_{2'})$	$b^\dagger_{-k_1} b_{k_2} d_{k_{1'}} b_{k_{2'}}$
T_4	$-++-$	$\bar{u}(-k_1)u(k_2)\bar{v}(k_{1'})v(-k_{2'})$	$b^\dagger_{-k_1} b_{k_2} d_{k_{1'}} d^\dagger_{-k_{2'}}$
T_5	$+--+$	$\bar{v}(k_1)v(-k_2)\bar{u}(-k_{1'})u(k_{2'})$	$d_{k_1} d^\dagger_{-k_2} b^\dagger_{-k_{1'}} b_{k_{2'}}$
T_6	$+---$	$\bar{v}(k_1)v(-k_2)\bar{u}(-k_{1'})v(-k_{2'})$	$d_{k_1} d^\dagger_{-k_2} b^\dagger_{-k_{1'}} d^\dagger_{-k_{2'}}$
T_7	$+-+-$	$\bar{v}(k_1)v(-k_2)\bar{v}(k_{1'})u(k_{2'})$	$d_{k_1} d^\dagger_{-k_2} d_{k_{1'}} b_{k_{2'}}$
T_8	$+-+-$	$\bar{v}(k_1)v(-k_2)\bar{v}(k_{1'})v(-k_{2'})$	$d_{k_1} d^\dagger_{-k_2} d_{k_{1'}} d^\dagger_{-k_{2'}}$
T_9	$---+$	$\bar{u}(-k_1)v(-k_2)\bar{u}(-k_{1'})u(k_{2'})$	$b^\dagger_{-k_1} d^\dagger_{-k_2} b^\dagger_{-k_{1'}} b_{k_{2'}}$
T_{10}	$--+-$	$\bar{u}(-k_1)v(-k_2)\bar{v}(k_{1'})u(k_{2'})$	$b^\dagger_{-k_1} d^\dagger_{-k_2} d_{k_{1'}} b_{k_{2'}}$
T_{11}	$--+-$	$\bar{u}(-k_1)v(-k_2)\bar{v}(k_{1'})v(-k_{2'})$	$b^\dagger_{-k_1} d^\dagger_{-k_2} d_{k_{1'}} d^\dagger_{-k_{2'}}$
T_{12}	$++-+$	$\bar{v}(k_1)u(k_2)\bar{u}(-k_{1'})u(k_{2'})$	$d_{k_1} b_{k_2} b^\dagger_{-k_{1'}} b_{k_{2'}}$
T_{13}	$+++-$	$\bar{v}(k_1)u(k_2)\bar{v}(k_{1'})v(-k_{2'})$	$d_{k_1} b_{k_2} d_{k_{1'}} d^\dagger_{-k_{2'}}$
T_{14}	$++--$	$\bar{v}(k_1)u(k_2)\bar{u}(-k_{1'})v(-k_{2'})$	$d_{k_1} b_{k_2} b^\dagger_{-k_{1'}} d^\dagger_{-k_{2'}}$

Table 4.3: **Discrete Fermion Exchange Interaction** : $k_i \in \mathbb{Z} + 1/2 \ \forall i$. The column θ is simplified as $\theta \equiv \theta(k_1, k_2, k_{1'}, k_{2'})$ for brevity. The spinors are implicitly assumed to mean $u(k) = u(q^+(k))$.

T_n	θ	Spinors	Operator
T_1	$-+++$	$\bar{u}(-k_1)(\gamma_\mu {q_2}^\mu + m)u(k_{2'})$	$b^\dagger_{-k_1} b_{k_{2'}} a_{k_3} a_{k_{3'}}$
T_2	$-+-+$	$\bar{u}(-k_1)(\gamma_\mu {q_2}^\mu + m)u(k_{2'})$	$b^\dagger_{-k_1} b_{k_{2'}} a^\dagger_{-k_3} a_{k_{3'}}$
T_3	$-++-$	$\bar{u}(-k_1)(\gamma_\mu {q_2}^\mu + m)u(k_{2'})$	$b^\dagger_{-k_1} b_{k_{2'}} a_{k_3} a^\dagger_{-k_{3'}}$
T_4	$-+--$	$\bar{u}(-k_1)(\gamma_\mu {q_2}^\mu + m)u(k_{2'})$	$b^\dagger_{-k_1} b_{k_{2'}} a^\dagger_{-k_3} a^\dagger_{k_{3'}}$
T_5	$+-++$	$\bar{v}(k_1)(\gamma_\mu {q_2}^\mu + m)v(-k_{2'})$	$d_{k_1} d^\dagger_{-k_{2'}} a_{k_3} a_{k_{3'}}$
T_6	$+--+$	$\bar{v}(k_1)(\gamma_\mu {q_2}^\mu + m)v(-k_{2'})$	$d_{k_1} d^\dagger_{-k_{2'}} a^\dagger_{-k_3} a_{k_{3'}}$
T_7	$+-+-$	$\bar{v}(k_1)(\gamma_\mu {q_2}^\mu + m)v(-k_{2'})$	$d_{k_1} d^\dagger_{-k_{2'}} a_{k_3} a^\dagger_{-k_{3'}}$
T_8	$+---$	$\bar{v}(k_1)(\gamma_\mu {q_2}^\mu + m)v(-k_{2'})$	$d_{k_1} d^\dagger_{-k_{2'}} a^\dagger_{-k_3} a^\dagger_{-k_{3'}}$
T_9	$-+-+$	$\bar{u}(-k_1)(\gamma_\mu {q_2}^\mu + m)v(-k_{2'})$	$b^\dagger_{-k_1} d^\dagger_{-k_{2'}} a_{k_3} a_{k_{3'}}$
T_{10}	$--+-$	$\bar{u}(-k_1)(\gamma_\mu {q_2}^\mu + m)v(-k_{2'})$	$b^\dagger_{-k_1} d^\dagger_{-k_{2'}} a^\dagger_{-k_{3'}} a_{k_3}$
T_{11}	$-+--$	$\bar{u}(-k_1)(\gamma_\mu {q_2}^\mu + m)v(-k_{2'})$	$b^\dagger_{-k_1} d^\dagger_{-k_{2'}} a_{k_3} a^\dagger_{-k_{3'}}$
T_{12}	$+-++$	$\bar{v}(k_1)(\gamma_\mu {q_2}^\mu + m)u(k_{2'})$	$d_{k_1} b_{k_{2'}} a^\dagger_{-k_3} a_{k_{3'}}$
T_{13}	$++-+$	$\bar{v}(k_1)(\gamma_\mu {q_2}^\mu + m)u(k_{2'})$	$d_{k_1} b_{k_{2'}} a_{k_3} a^\dagger_{-k_{3'}}$
T_{14}	$+--+$	$\bar{v}(k_1)(\gamma_\mu {q_2}^\mu + m)u(k_{2'})$	$d_{k_1} b_{k_{2'}} a^\dagger_{-k_2} a^\dagger_{-k_{3'}}$

Table 4.4: **Discrete Boson Exchange Interaction**: $k_1, k_{2'} \in \mathbb{Z} + 1/2, \ k_3, k_{3'} \in \mathbb{Z}\backslash\{0\}$. The column θ is simplified as $\theta \equiv \theta(k_1, k_{2'}, k_3, k_{3'})$ for brevity. The spinors are implicitly assumed to mean $u(k) = u(q^+(k))$.

to the boson momenta. $T_n^{(\mathrm{IV})}$ corresponds to a term in a row in Table 4.4.

The effective mass terms are discretized as:

$$H_0 = \frac{L}{2\pi} \sum_{k \in \mathbb{Z}^+ - 1/2} \left(\frac{m^2(s;k)}{k} \right) \left(b_k^\dagger b_k + d_k^\dagger d_k \right) + \frac{L}{2\pi} \sum_{k \in \mathbb{Z}^+} \left(\frac{\mu^2(s;k)}{k} \right) a_k^\dagger a_k. \tag{4.106}$$

where

$$m^2(s;k) = m_0^2 + \int_0^1 \frac{dx}{x(1-x)} \frac{1}{\mathcal{M}_{fb}^2(x) - m_0^2} \frac{m_0^2(1+x)^2}{x} e^{-2sL^2 \left(\mathcal{M}_{fb}^2(x) - m_0^2 \right)^2 / (4\pi k^2)}, \tag{4.107}$$

and

$$\mu^2(s;k) = \mu_0^2 + 2\int_0^1 \frac{dx}{x(1-x)} \frac{1}{\mathcal{M}_{f\bar{f}}^2(x) - \mu_0^2} \frac{m_0^2(2x-1)^2}{x(1-x)} e^{-2sL^2 \left(\mathcal{M}_{f\bar{f}}^2(x) - \mu_0^2 \right)^2 / (4\pi k^2)}. \tag{4.108}$$

The loop integrals are finite since s is finite, and they don't depend on s_0. While it may be possible to find closed forms of these integrals, they can be computed numerically.

This Hamiltonian serves as the input to all numerical calculations performed in this paper (apart from the bare Hamiltonian spectrum in Fig. 4.1).

With these discrete Hamiltonians, mass spectra and structure functions are computed classicaly and results are given in the next two sections.

4.5 Results

In this Section, we give numerical results for the mass spectrum, parton distribution function, and quantum resource estimates for a single 'Ladder Operator Block-Encoding'. Our results are given in terms of the more physical RGPEP parameter, λ.

4.5.1 Numerical calculations of the M^2 spectrum

Calculating the eigenvalues of Eq. 4.98 gives the spectrum of the corresponding bound eigenstates. After choosing a harmonic resolution, K, a combinatorics problem arises, where one must construct all states whose discrete momentum quantum numbers k sum to K. This collection of Fock states can now be partitioned into sectors by their constitution, i.e.

$$|\psi\rangle \in \Big\{|f\rangle, |\bar{f}\rangle, |b\rangle, |fb\rangle, |f\bar{f}b\rangle, \dots\Big\},$$

where $|f\rangle$ corresponds to all Fock states of a single fermion, $|fb\rangle$ corresponds to all Fock states of a fermion + a boson, etc. such that their momenta sum to K. The *charge* $Q \equiv N_f - N_{\bar{f}}$ is a conserved quantity that is defined as the number of fermions minus the number of antifermions.

Fig. 4.1 shows that the lowest eigenvalues in the charge $Q = 0, 1$, and 2 sectors of the bare Hamiltonian tend towards negative M^2 values. This arises because the canonical Hamiltonian is ill-defined. This problem should be solved by a proper renormalization procedure.

All of the plots for the numerical effective mass spectrum contain red lines which represent the non-relativistic approximation of Yukawa theory. The non-relativistic limit can be studied by taking $(p-p')^2 = -|\mathbf{p}-\mathbf{p'}|^2 + \mathcal{O}(\mathbf{p})^4$ in the scattering matrix element [PS95]. For the t-channel interaction, the (spin-less) scattering matrix element is

$$\begin{aligned} i\mathcal{M} &= \bar{u}(p')u(p)\frac{-ig^2}{(p-p')^2-\mu^2}\bar{u}(k')u(k) \\ &= \frac{(2m)^2 ig^2}{|\mathbf{p}-\mathbf{p'}|^2+\mu^2}. \end{aligned} \tag{4.109}$$

The Born approximation to the scattering amplitude in non-relativistic quantum mechanics is given as $\langle p'|iT|p\rangle = -i\tilde{V}(\mathbf{q})(2\pi)\delta(E_p - E_{p'})$. Defining $\mathbf{q} \equiv \mathbf{p}-\mathbf{p'}$,

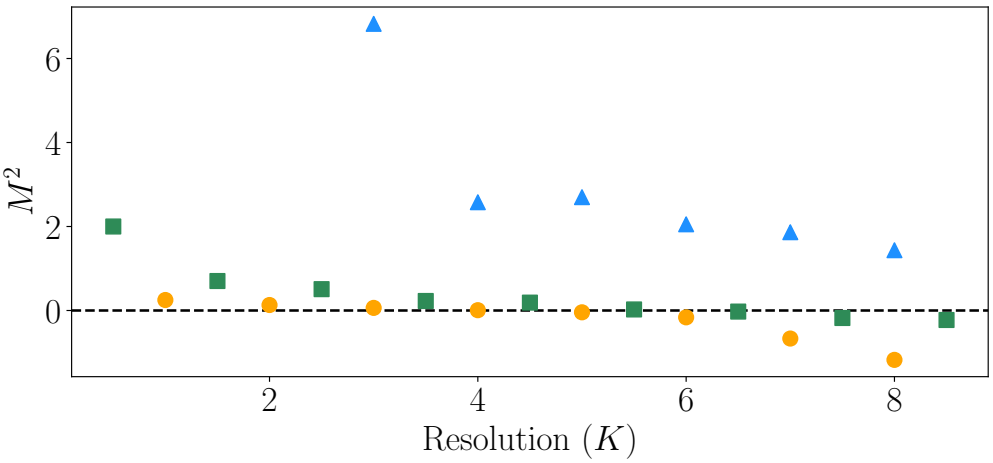

Figure 4.1: **Bare spectrum** Canonical Yukawa Hamiltonian spectrum with increasing harmonic resolution. Yellow circles correspond to the $Q = 0$ sector, green squares correspond to the $Q = 1$ sector, and blue triangles correspond to the $Q = 2$ sector. A cutoff on the maximum number of particles, n_p in a Fock state is made ($n_p = 4$). The relevant parameters are $m = 1$, $\mu = 0.5$, $g = 1$.

one can compare this expression with Eq. 4.109 to get

$$\tilde{V}(\mathbf{q}) = \frac{-g^2}{|\mathbf{q}|^2 + \mu^2}, \tag{4.110}$$

the 1D Yukawa potential in momentum space. Note that the relativistic normalization that gives the two factors of $2m$ must be removed in the non-relativistic limit, as non-relativistic normalization must be imposed. Additionally, the delta disappears when integrating over the momentum of the target [PS95].

Taking a Fourier transform to position space (and un-bolding q since it is a 1D vector),

$$\begin{aligned} V(z) &= \int_{-\infty}^{\infty} \frac{dq}{2\pi} \tilde{V}(q) e^{iqz} \\ &= \frac{-g^2}{2\pi} \int_{-\infty}^{\infty} dq \frac{e^{iqz}}{q^2 + \mu^2} \\ &= \frac{-g^2}{2\pi} \int_{-\infty}^{\infty} dq \frac{e^{iqz}}{(q + i\mu)(q - i\mu)} \end{aligned} \tag{4.111}$$

This integral must be handled separately for $z \geq 0$ and $z < 0$. For $z \geq 0$, a counterclockwise contour is taken to enclose the pole at $q = i\mu$:

$$\begin{aligned} V(z) &= \frac{-g^2}{2\pi} 2\pi i \frac{e^{i(i\mu)z}}{i\mu + i\mu} \\ &= \frac{-g^2}{2\mu} e^{-\mu z} \end{aligned}$$

For $z < 0$, a clockwise contour is taken to enclose the pole at $q = -i\mu$:

$$\begin{aligned} V(z) &= (-1)\frac{-g^2}{2\pi} 2\pi i \frac{e^{i(-i\mu)z}}{-i\mu - i\mu} \\ &= \frac{-g^2}{2\mu} e^{\mu z} \end{aligned}$$

Both solutions can be taken together to give

$$V(z) = \frac{-g^2}{2\mu} e^{-\mu|z|} \tag{4.112}$$

Fig. 4.2 shows the eigenvalues at fixed g while varying μ. For larger g, one expects the number of bound states to increase. The limit $\mu \to 0$ doesn't recover the 1D Coulomb potential, as one gets in 3D. Fig. 4.2 shows that for the plots in figure 4.3, one would expect 1 (2) bound state(s) for $g = 0.3$ ($g = 1$) given the choice of $\mu = 0.5$.

Fig. 4.3 shows the extrapolated fermion-fermion (top dots) effective bound state M^2 extrapolated to infinite harmonic resolution for two different couplings: (a) $g = 1$ and (b) $g = 0.3$.

The bottom (green) dots in both subplots in Fig. 4.3, come from diagonalizing the Hamiltonian matrix in the Fock basis

$$\Big\{ |f\rangle, |fb\rangle \Big\},$$

which are in the $Q = 1$ charge sector. These points are included, not to show

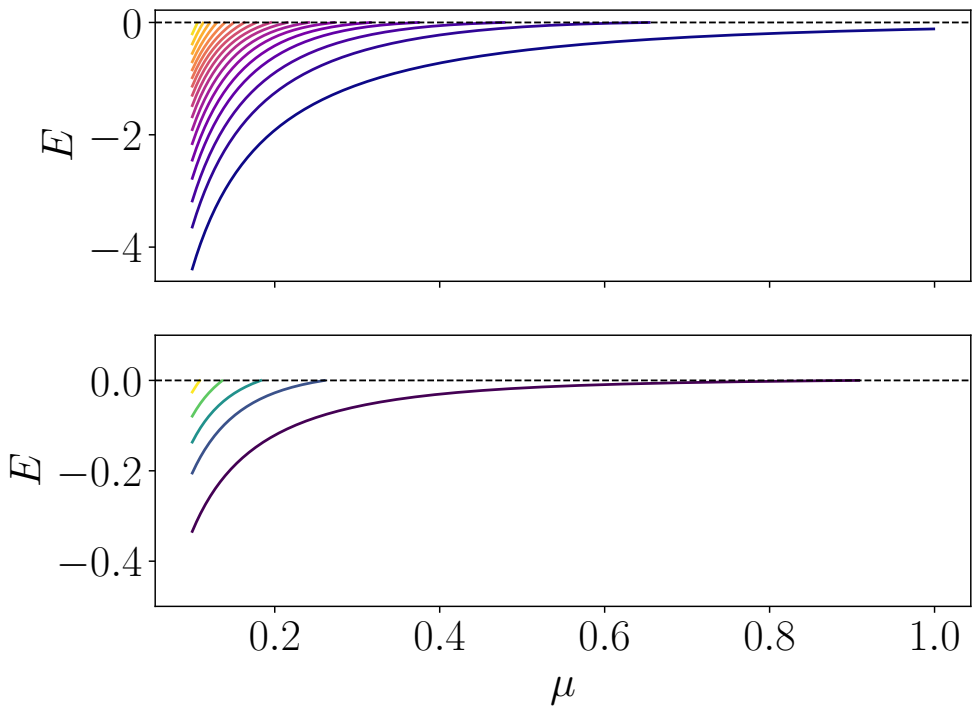

Figure 4.2: **Eigenvalues of the non-relativistic 1D Yukawa Potential** with changing boson mass μ. (Top) $g = 1$. (Bottom) $g = 0.3$.

a bound state (as a single fermion bound state is not a well-defined object), but rather to show how well the renormalization condition has been satisfied.

The top (blue) dots in both subplots in Fig. 4.3 come from diagonalizing the Hamiltonian matrix in the Fock basis

$$\left\{ |ff\rangle, |ffb\rangle \right\},$$

which are in the $Q = 2$ sector.

The 'flow' of the Hamiltonian under the RGPEP equations is shown in Figures 4.4, 4.5. Fig. 4.4 shows the extrapolated ($K \to \infty$) lowest M^2 eigenvalues flowing with λ for the same sectors in Fig. 4.3. Fig. 4.5 shows the flow of the entire spectrum with λ for fixed $K = 22$, and in a larger Fock basis:

$$\left\{ |ff\rangle, |ffb\rangle, |ffbb\rangle, \left|fff\bar{f}\right\rangle \right\},$$

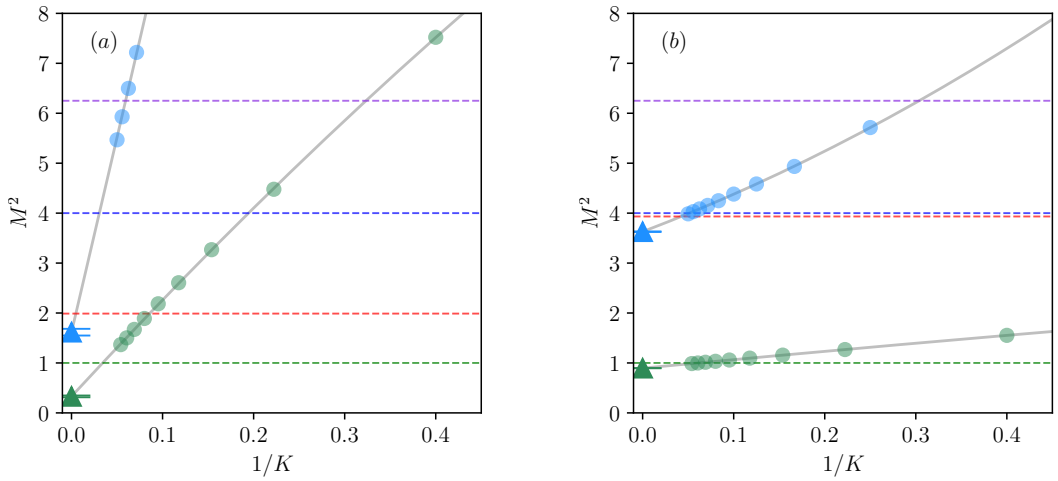

Figure 4.3: **Extrapolations** Convergent M^2 eigenvalues of the renormalized Hamiltonian. Relevant parameters in both plots are $m = 1$, $\mu = 0.5$, and $\lambda = 10^6$. The horizontal dashed lines represent, respectively from bottom to top, m^2, non-relativistic approximation, $(2m)^2$, and $(2m+\mu)^2$. The top set of dots corresponds to the lowest eigenvalue of the ff, ffb sectors, while the bottom set of dots corresponds to the lowest eigenvalue of the f, fb sectors. The fits are of the form $a + b/K + c/K^2$. (a) $(g = 1)$ $1/K \to 0$ extrapolations, yielding the values $M_f^2 = 0.33m^2$, $M_{ff}^2 = 1.616m^2$ (compared to the non-relativistic value of $M_{ff}^2 = 1.998m^2$). (b) $(g = 0.3)$ $1/K \to 0$ extrapolations, yielding the values $M_f^2 = 0.896m^2$, $M_{ff}^2 = 3.628m^2$ (compared to the non-relativistic value of $M_{ff}^2 = 3.933m^2$). In both plots, there are error bars included on the triangles which correspond to the uncertainty in the fit.

also in the $Q = 2$ sector.

The boost-invariance of the eigenvalues M^2 is only approximate due to our choice of generator in Eq. 2.81. The form factors that arise from this generator, which modify the vertices, give explicit dependence on longitudinal momentum in the Hamiltonian matrix element. While a loss of exact boost-invariance appears to remove a major benefit of the light-front approach, there are two important comments to make regarding this. The longitudinal boost invariance has become connected to the RGPEP scale invariance through the form factors, and since the RGPEP equation is solved perturbatively, one can recover boost invariance to a desired accuracy through higher order perturbative solutions. Second, while there are generators that preserve boost invariance [Gla12], we choose a generator that does not preserve this invariance due to the benefits one will receive when studying QCD. Light-front QCD contains infrared divergences in the matrix elements of the bare and effective Hamiltonians. With the choice of generator in this work, the infrared divergences are canceled in the color-singlet subspace of the Fock space [SGRMG24]. Since the cancellation of divergences is the main priority when trying to compute finite observables, we sacrifice exact boost invariance to achieve this goal, while still maintaining an approximate boost invariance.

The scaling of the lowest M^2 eigenvalue in the $Q = 1$ and $Q = 2$ sectors (in the same basis in Fig. 4.3) vs. the coupling constant g is shown in Fig. 4.7. The combined behavior of $M^2(g, \lambda)$ is shown in Fig. 4.8.

An important metric that describes the renormalized Hamiltonian is the number of terms. The number of terms in the renormalized Hamiltonian, denoted by $||H(\lambda)||_0$, is greater than the number of terms in the bare Hamiltonian, denoted $||H||_0$. Fig. 4.6 shows the relative scaling in the number of terms in the bare vs. effective Hamiltonians.

Asymptotically (at $K \to \infty$), the scaling for the bare Hamiltonian is:

$$||H||_0 = \frac{5}{3}K^3 + \mathcal{O}(K^2), \tag{4.113}$$

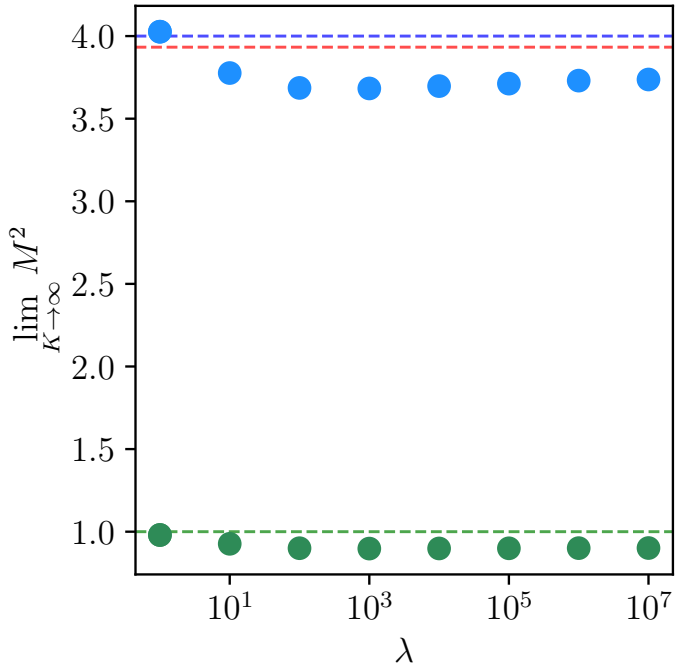

Figure 4.4: **Eigenstate scaling with λ** Extrapolated lowest M^2 values in $\{|f\rangle, |fb\rangle\}$ sector (bottom) and $\{|ff\rangle, |ffb\rangle\}$ sector (top) as a function of λ at $g = 0.3$, $m = 1$, $\mu = 0.5$, and $K_{\max} = 20$. As λ is decreased to $\lambda \sim 1$, the interactions have been dampened so much that the approximation becomes the free theory.

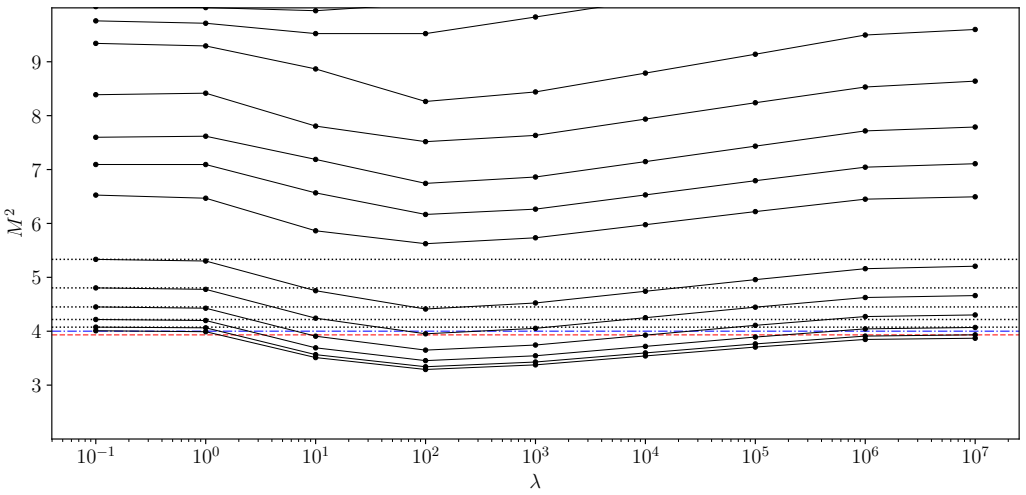

Figure 4.5: **Flow of Renormalized Hamiltonian Eigenvalues:** The Yukawa model parameters for this plot are $m = 1$, $\mu = 0.5$, $g = 0.5$, and $K = 22$. The Hamiltonian was diagonalized in the Fock basis: $\left\{ |ff\rangle, |ffb\rangle, |ffbb\rangle, \left|ffff\bar{f}\right\rangle \right\}$. The blue (dashed and dotted) horizontal line corresponds to the mass of two free fermions, while the red (dashed) line is the non-relativistic approximation. The grey (dotted) horizontal lines correspond to the first few eigenvalues of the free ($g = 0$) Hamiltonian (above the $4m^2$ free Hamiltonian eigenvalue). At $\lambda \sim 1$, the calculated eigenvalues line up with the free theory, which is an incorrect approximation to the interacting theory. In this limit, the calculated eigenvalues match the free theory eigenvalues because of the form factors, which strongly dampen the interactions in this regime. Note that the higher spectrum is cutoff in order to show the behavior of the low-lying eigenstates more clearly.

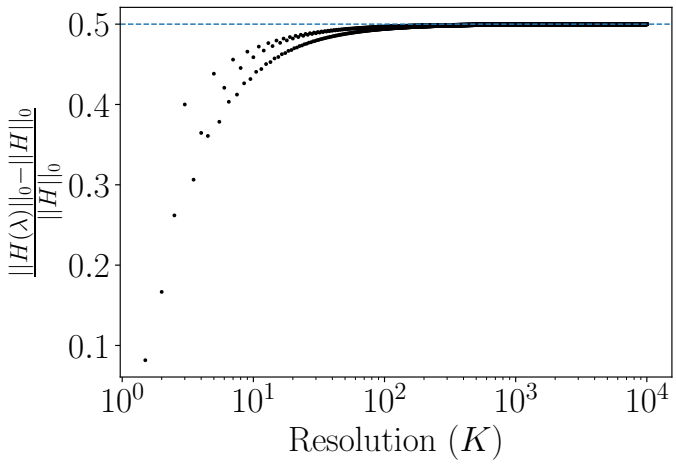

Figure 4.6: **Hamiltonian scalings** Relative scaling of the number of terms in the effective Hamiltonian $||H(\lambda)||_0$ vs. the number of terms in the bare Hamiltonian $||H||_0$. The scaling behaves as $\sim 0.5 + o(1)$, where $o(1) \to 0$ as $K \to \infty$.

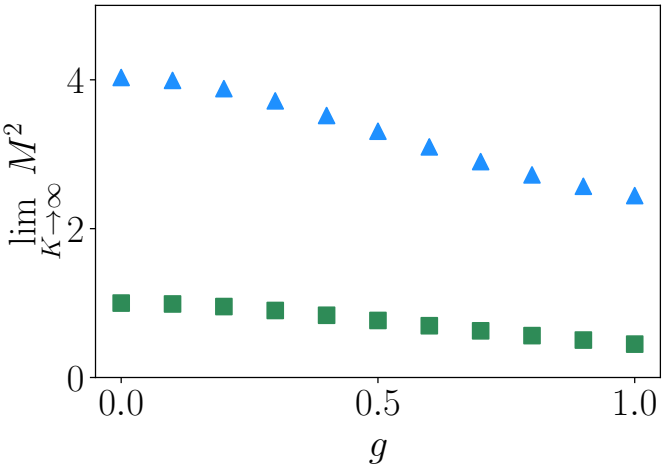

Figure 4.7: **Extrapolated M^2 vs. g:** As g is increased, the extrapolated M^2 eigenvalue begins to decrease. This shows the perturbative solution to the RGPEP equation breaking down at higher g. In this plot, $K_{\max} = 20$, $m = 1, \mu = 0.5$. The squares and triangles describe the same sectors as Fig. 4.1.

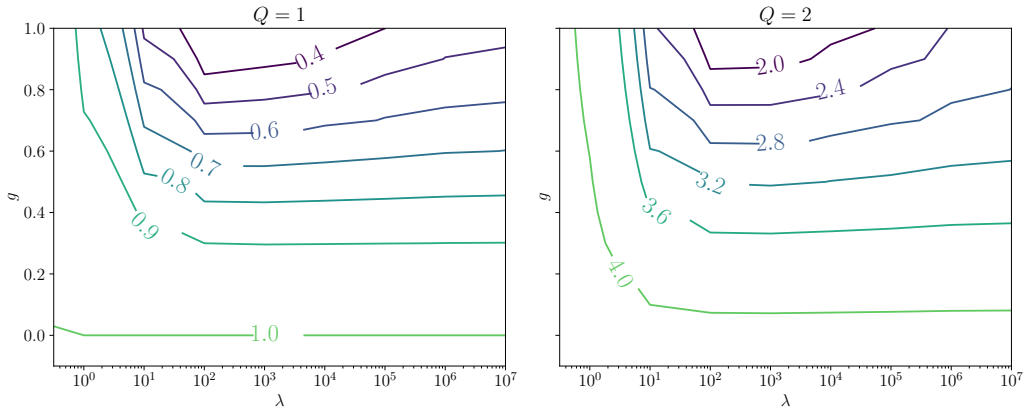

Figure 4.8: **Eigenvalue scaling with both g and λ:** Contour plots displaying extrapolated $M^2(\lambda, g)$ eigenvalues at $K_{\max} = 20$, $m = 1, \mu = 0.5$. The Fock basis used is the same as that in Fig. 4.3. At small g, it is clear that the similarity transformation maintains the same spectrum, whereas as g increases, this begins to break down.

while the scaling for the renormalized Hamiltonian is:

$$||H(\lambda)||_0 = \frac{5}{2}K^3 + \mathcal{O}(K^2). \tag{4.114}$$

Calculating the relative increase in the number of terms in the effective Hamiltonian compared to the bare Hamiltonian, we compute

$$\frac{||H(\lambda)||_0 - ||H||_0}{||H||_0},$$

which tends to a constant factor of $1/2$ as $K \to \infty$, shown in Fig. 4.6. This implies there are roughly 50% more terms asymptotically in the effective Hamiltonian compared to the bare Hamiltonian.

For weak coupling, we expect the two fermion bound state mass to be less than the invariant mass of two free fermions $4m^2$. In both cases of coupling tested in this paper, this is true. Additionally, the ground state masses we obtain (for small coupling) qualitatively agree with comparable results from 3+1D calculations [Qia20, GHP$^+$93], in that they elicit stronger binding than those produced by the non-relativistic results.

4.5.2 Parton Distribution Functions

A *parton* is a constituent of a bound state of any quantum field theory. Parton distribution functions [Col11, Sop97] for fermionic fields are given by:

$$f_i(x) = \int \frac{dy^-}{4\pi} e^{ixP^+y^-} \langle P| \bar{\psi}_i(y^-)\gamma^+\psi_i(0) |P\rangle . \tag{4.115}$$

These functions contain information about the distribution of longitudinal momentum carried by the constituents that make up a particular bound state, described by $|P\rangle$.

Given a bound state $|\psi\rangle$, its parton distribution function can be determined by calculating

$$f_p(x) \equiv \langle\psi|\hat{N}_p(x)|\psi\rangle\,, \tag{4.116}$$

where $\hat{N}_p(x)$ is given as the number operator of a particle of type p (i.e. $p =$ fermion, antifermion, boson) with momentum fraction $x = k/K$ [HBP90]. Increasing K increases the number of points along the x-axis in a plot of a parton distribution function, hence why it is referred to as the harmonic resolution.

For example, the fermionic parton distribution function requires computing expectation values of a bound state $|\psi\rangle$ with the operator

$$\hat{N}_f(x) = b_k^\dagger b_k. \tag{4.117}$$

Fig. 4.9 gives the parton distribution function calculated for the state with the lowest M^2 eigenvalue in the

$$\left\{|ff\rangle\,, |ffb\rangle\right\}$$

sectors.

The main features of this plot are that the fermionic parton distribution function peaks at around $x = 0.5$, implying that each fermion shares roughly half of the total momentum. Additionally, there is a small bosonic contribution from the $|ffb\rangle$ states that arises at small x values.

4.5.3 Block-Encoding Metrics

Renormalization introduces additional terms into the Hamiltonian, and may change its norm, which can affect the cost of quantum simulation algorithms. In this Section, we evaluate the relative cost of simulating the renormalized Hamiltonian, as compared to the bare Hamiltonian, to evaluate the effect of renormalization on the cost of quantum simulation.

Quantum computers can only perform unitary operations, as it is these operations that do not change the norm of the qubit states. Many interesting operators, such as the Hamiltonian in general is not unitary. Block encoding is a technique to

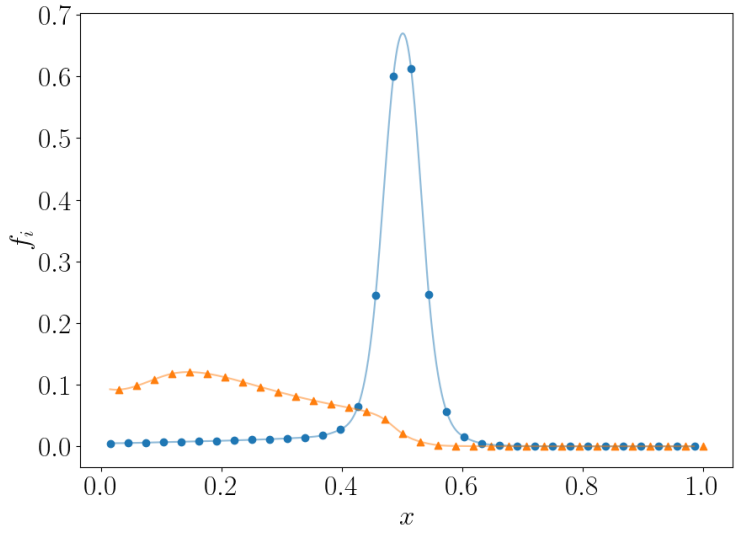

Figure 4.9: **Parton Distribution Functions** (PDF) for the lowest M^2 bound state in the $\{|ff\rangle, |ffb\rangle\}$ sectors, with $f_i = f_f, 10f_b$. The blue dots represent the fermionic PDF. The orange triangles represent the bosonic PDF, which is scaled up by a factor of 10 to show its behavior in the low-x region. The solid lines are numerical fits to the data. The relevant parameters are $m = 1$, $\mu = 0.5$, $g = 1$, $\lambda = 10^6$, $K = 34$.

encode the Hamiltonian in a block of a larger unitary. This necessitates the addition of ancillary qubits which increases the overall size of the Hilbert space. The cost associated with these block encodings is used as a metric for how expensive quantum simulation would be with a given Hamiltonian.

It is important to note that these costs do not give the total resource estimates for a full end-to-end simulation of Yukawa theory; however, the resources needed to apply the block encoding shows how the cost associated with storing the Hamiltonian on a quantum device scales with the problem size. The cost of a block encoding can also be used as a starting point to estimate the cost of state preparation and quantum simulation algorithms. We leave more detailed estimates to future work.

Many Hamiltonian simulation algorithms are built upon block-encodings of the Hamiltonian, therefore we quantify the cost of quantum simulation by calculating the quantum resource estimates for implementing a single block-encoding of the Yukawa Hamiltonian. The block-encodings for each Hamiltonian are constructed

using the Ladder Operator Block-Encoding (LOBE) framework [SGS+25].

Block-encoding [Chi09c, CGJ19, Lin22] is a subroutine that provides access to information regarding non-unitary operators, such as the Hamiltonian, within quantum algorithms. Block-encodings can be used for various methods including estimating the eigenvalues of the block-encoded operator, generating the time-evolution operator, or producing arbitrary polynomial functions of the time-evolution operator [PKS+18, GSLW19, MRTC21b, BGB+18, LC19a, LC17b, CW12b].

Quantum resource estimates for a block-encoding can be quantified in terms of the number of qubits (space) and the number of operations (time) needed to implement the block-encoding. Block-encodings require ancillae qubits, some of which are only temporarily allocated. Therefore, we quantify the number of qubits needed in terms of both the number of block-encoding ancillae and the maximum number of qubits used. The most costly operations to perform in fault-tolerant architectures are typically non-transversal operations. Under the surface code [**?**], the T gate and non-Clifford rotations about the z-axis are non-transversal, therefore we count these two operations to quantify the time complexity. Finally, the overall rescaling factor associated with each block-encoding often proportionally increases the cost of implementing simulation algorithms constructed using block-encodings. To account for this, we directly compare the rescaling factors associated with each Hamiltonian.

The resource estimates are computed numerically, using the software package *LOBE* [**?**]. The software takes as input sums of products of ladder operators, H, and constructs a unitary operator, U_H, which block encodes H, and returns the exact cost in terms of number of quantum resources to construct this unitary. For those interested in further details in how U_H is constructed, the original reference for this framework [SGS+25] gives explicit examples.

The quantum resource estimates are shown as a function of the harmonic resolution (K) in Fig. 4.10 and as a function of the number of terms in the Hamiltonian in Fig. 4.11. The costs for the bare Hamiltonians are shown in orange and the costs for the renormalized Hamiltonians are shown in blue.

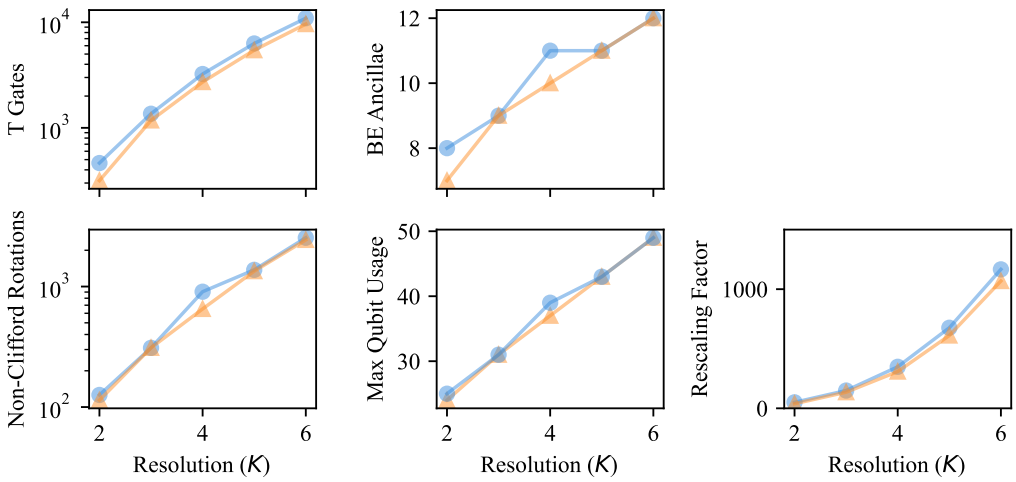

Figure 4.10: **Block-Encoding Metrics** The number of T gates (upper-left), number of non-Clifford rotations (lower-left), block-encoding ancillae (upper-middle), maximum number of qubits used (lower-middle), and rescaling factor (lower-right) are shown as a function of the harmonic resolution (K). The renormalization parameter is set to $\lambda = 10^{7/2}$, the bosonic cutoff is fixed to $\Omega = 3$, and the coefficients m, μ, and g are set to 1 for all data points. Metrics for the bare Hamiltonians are shown in orange and the metrics associated with the renormalized Hamiltonian are shown in blue.

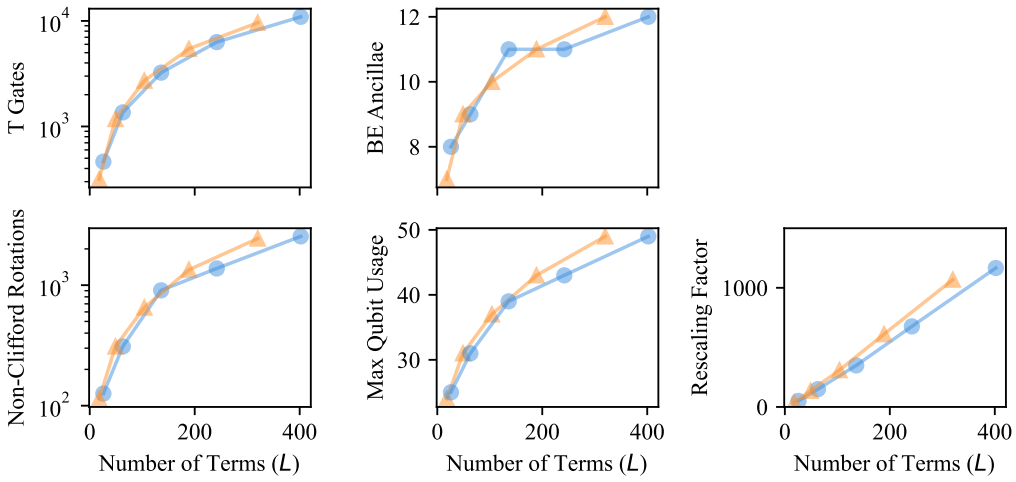

Figure 4.11: **Block-Encoding Metrics** The number of T gates (upper-left), number of non-Clifford rotations (lower-left), block-encoding ancillae (upper-middle), maximum number of qubits used (lower-middle), and rescaling factor (lower-right) are shown as a function of the number of terms in a given Hamiltonian. The renormalization parameter is set to $\lambda = 10^{7/2}$, the bosonic cutoff is fixed to $\Omega = 3$, and the coefficients m, μ, and g are set to 1 for all data points. Metrics for the bare Hamiltonians are shown in orange and the metrics associated with the renormalized Hamiltonian are shown in blue.

At each resolution, the quantum resource estimates for block-encoding the renormalized Hamiltonians are larger for all metrics that we consider. However, the increase in quantum resources is a small portion of the overall cost. As shown in Fig. 4.11, the renormalized Hamiltonians require fewer quantum resources per term. This implies that the increase in quantum resources is due to renormalization introducing more terms, but it does not introduce terms that are more expensive to block-encode on average. These numerical quantum resource estimates, along with the results of Fig. 4.6, suggest that renormalization up to second order increases the cost of quantum simulation algorithms that use block-encodings of the Yukawa Hamiltonian, in the worst case, by roughly 50% asymptotically.

4.6 Summary

In this Chapter, we outlined explicit steps for constructing the effective light-front Yukawa Hamiltonian in the RGPEP framework. With the discrete effective Hamiltonian, we numerically computed mass spectra, and show that the counterterms added in the effective Hamiltonian lead to finite observables.

Additionally, we have calculated the first estimates of quantum resources necessary for quantum simulation of a renormalized Quantum Field Theory, the Yukawa model in particular, in the front form. As a metric for the number of quantum resources necessary for quantum simulation, we calculated the cost associated with a single block encoding of the Hamiltonian using the Ladder Operator Block Encoding framework [SGS$^+$25]. To contextualize our results, we comment that the resources required to solve this theory in Euclidean space using Monte Carlo techniques require a lattice size on the order $\mathcal{O}(6000^3)$ [dSAd12].

The results presented in Section 4.5.3 provide motivation that leads us to believe that quantum simulation of renormalized quantum field theories in the front-form approach is not an intractable framework.

Chapter 5

Quantum Chromodynamics

The interactions between quarks and gluons, assumed to be the smallest indivisible particles, possess *color symmetry*, described by the non-Abelian symmetry group $SU(3)$. The Lagrangian of the theory is given by:

$$\mathcal{L}_{\rm QCD} = \bar{\psi}_c\Big(i\gamma^\mu D_\mu - m\Big)\psi_c - \frac{1}{4}G_a^{\mu\nu}G^a_{\mu\nu}, \tag{5.1}$$

where D^μ is the covariant derivative:

$$D_\mu = \partial_\mu - igT_aA^a_\mu. \tag{5.2}$$

The gluon field strength tensor $G_a^{\mu\nu}$ is

$$G_a^{\mu\nu} = \partial^\mu A_a^\nu - \partial^\nu A_a^\mu - f_{abc}A_b^\mu A_c^\nu. \tag{5.3}$$

The quarkk fields, $\psi_{c,\lambda}$ carry a color index, c that runs from 1 to $N_c = 3$, with colors "red, green, and blue", and a helicity index $\lambda = \pm 1$. The gluon vector field is a four-vector, i.e. $A^\mu_{a,\sigma} = (A^0_{a,\sigma}, A^1_{a,\sigma}, A^2_{a,\sigma}, A^3_{a,\sigma})$, where a is the gluon color index that runs from 1 to $N_c^2 - 1 = 8$. The gluon polarization $\sigma = \pm 1$.

The generators of the $SU(3)$ group are T^a, $N_c^2 - 1 = 8$ 3×3 matrices satisfying the Lie Algebra of $\mathfrak{so}(3)$,

$$\Big[T^a, T^b\Big] = if^{abc}T^c, \tag{5.4}$$

where f^{abc} are the structure constants of the group. Conventionally, the T^a's are taken to be $\lambda^a/2$, where the λ^a's are the Gell-Mann matrices, which are the analog of the Pauli matrices for $\mathfrak{so}(2)$. There are three QCD color factors, C_F, C_A, T_F, where in the fundamental representation of the $SU(3)$ algebra (with $N_c = 3$), [Mic00]:

$$C_F = \frac{1}{3}\mathrm{Tr}\Big(\lambda^a\lambda^a\Big) = \frac{4}{3} \tag{5.5}$$

$$C_A\delta^{cd} = f^{abc}f^{abd} = 3\delta^{cd} \tag{5.6}$$

$$T_F\delta^{ab} = \mathrm{Tr}\Big(\lambda^a\lambda^b\Big) = \frac{1}{2}\delta^{ab} \tag{5.7}$$

QCD elicits several unique types of interaction diagrams due to its group structure. Many interaction vertices are analogous to those in $U(1)$ QED; however, the non-zero structure constants of $SU(3)$ (coming from the fact that this group is non-Abelian) lead to 3 and 4-gluon vertices.

In this Chapter, we compute the effective theory of QCD from solving the RGPEP equations up to second order in the coupling constant. Since QCD elicits asymptotic freedom, there is an energy scale in which $g \ll 1$, which implies this perturbative expansion should be very effective. We describe how to counterterms for loop diagrams, as well as small q^+ divergences that arise in the exchange momentum in some second order diagrams. Lastly, we provide preliminary results for the cost of a (self-inverse) block-encoding of the renormalized QCD Hamiltonian and approximate costs for quantum phase estimation.

5.1 Bare QCD Hamiltonian

The QCD Lagrangian in Equation 5.1 elicits the equations of motion:

$$(i\gamma^\mu D_\mu - m_q)\psi = 0, \tag{5.8}$$

for the quark field, and

$$D_\mu G_a^{\mu\nu} = J_a^\nu, \tag{5.9}$$

for the gluon field, where the color current J_a^μ is

$$J_a^\mu(x) = g\bar{\psi}(x)\gamma^\mu T_a\psi(x) - igf^{abc}A_b^\nu(x)i\partial^\mu A_{\nu c}(x). \tag{5.10}$$

The choice of gauge used in this thesis is the "light-cone gauge", $A^+ = 0$, which is commonly used in literature. The quark field ψ has a dynamical and constrained component, just like in the free theory. In the light-cone gauge, the $\vec{A}^\perp$ component of A^μ is dynamical, while A^- is constrained.

The front-form canonical QCD Hamiltonian [BPP98] breaks up into eight distinct terms:

$$H_{\rm QCD} = H_0 + H_{\bar{\psi}\psi A} + H_{A^3} + H_{A^4} + H_{\widetilde{\psi}^4} + H_{\widetilde{\bar{\psi}AA\psi}} + H_{\widetilde{\psi^2 A^2}} + H_{\widetilde{A}^4}. \tag{5.11}$$

From right to left, these terms correspond to the free quark and gluon Hamiltonian (H_0), the quark-gluon vertex ($H_{\bar{\psi}\psi A}$), the three-point gluon (H_{A^3}) and four-point gluon (H_{A^4}) vertices (these are all standard QCD-like diagrams). The last four terms with tildes above the fields in the subscript are the so-called 'instantaneous' interaction terms. These arise from the choice of gauge and eliminating the dependent degrees of freedom. These instantaneous terms do not arise in equal-time coordinates, but nonetheless are necessary for computation.

The fermionic fields now carry color and flavor degrees of freedom, in addition

to spin. In momentum space, they are given as

$$\psi_{c,f,\lambda}(q) = \frac{\theta(q^+)u_\lambda(q)b_{c,f,\lambda}(q) + \theta(-q^+)v_\lambda(-q)d_{c,f,\lambda}(-q)}{|q^+|}\chi_c, \tag{5.12}$$

where χ_c is a 3×1 vector in color space defined as $\chi_c = (\delta_{c,r}, \delta_{c,g}, \delta_{c,b})^T$. In general, we will drop the flavor degree of freedom. The gluon fields carry color and polarization degrees of freedom, where in momentum space they are

$$A^\mu_{a,\sigma}(q) = \frac{\theta(q^+)\epsilon^\mu_\sigma(q)a_{a,\sigma}(q) + \theta(-q^+)\epsilon^{\star\mu}_\sigma(-q)a^\dagger_{a,\lambda}(-q)}{|q^+|}. \tag{5.13}$$

The full fields are then given by

$$\psi(q) = \sum_{c,f,\lambda} \psi_{c,f,\lambda}(q) \tag{5.14}$$

$$A^\mu_a(q) = \sum_\sigma A^\mu_{a,\sigma}(q). \tag{5.15}$$

The gluon propagator is

$$\begin{aligned} d^{\mu\nu}(q) &= \sum_\sigma \epsilon^\mu_\sigma(q)\epsilon^{\star\nu}_\sigma(q) \\ &= -g^{\mu\nu} + \frac{\eta^\mu q^\nu + \eta^\nu q^\mu}{q^+} - \eta^\mu\eta^\nu\frac{m_g^2}{(q^+)^2}, \end{aligned} \tag{5.16}$$

where η^μ is the lightcone null vector, and is given as

$$\eta^\nu = (0, 2, \vec{0}^\perp), \tag{5.17}$$

such that $\eta^\mu q_\mu = q^+$. Even though m_g appears in the definition of $d^{\mu\nu}(q)$, it is actually independent of the gluon mass. This can be made obvious by looking at

$d^{\mu\nu}$ component-wise:

$$d^{--}(q) = \frac{4(\vec{q}^{\perp})^2}{(q^+)^2} \tag{5.18}$$

$$d^{-i}(q) = d^{i-}(q) = \frac{2\vec{q}^{\perp}}{q^+} \tag{5.19}$$

$$d^{ij}(q) = \delta^{ij}. \tag{5.20}$$

Even though we have imposed a nonzero gluon mass, it is vanishingly small and satisfies $m_q \gg m_g$.

In momentum space each of the eight terms can be shown explicitly. The free quark and gluon kinetic energy is:

$$H_0 = \int_q q^- : \bar{\psi}(q)\frac{\gamma^+}{2}\psi(q) : + \int_q \frac{1}{2} : A^\mu(-q)\Big(m_g^2 + (\vec{q}^{\perp})^2\Big)A_\mu(q) : . \tag{5.21}$$

Here, H_0 is a slightly modified version of the standard H_0 part because we've added a term of the form $\sim m_g^2(A^\perp)^2$ to remove the issue of zero modes. There are two three-point interaction vertices, the quark-gluon 3-point diagram and the 3-point gluon vertex, both given as:

$$H_{\bar{\psi}\psi A} = g \int\limits_{q_1,q_2,q_3} \delta(q_1 + q_2 + q_3)\bar{\psi}(-q_1)T_a\gamma^\mu\psi(q_2)A^a_{\mu,\sigma}(q_3), \tag{5.22}$$

and

$$H_{A^3} = -\frac{1}{3!}igf^{abc} \int\limits_{q_1,q_2,q_3} \delta(q_1 + q_2 + q_3)F_{\alpha\beta\gamma}(q_1, q_2, q_3) : A^\alpha_a(q_1)A^\beta_b(q_2)A^\gamma_c(q_3) : \tag{5.23}$$

where

$$F_{\alpha\beta\gamma}(q_1, q_2, q_3) = (q_{2\gamma} - q_{1\gamma})g_{\alpha\beta} + (q_{3\alpha} - q_{2\alpha})g_{\beta\gamma} + (q_{1\beta} - q_{3\beta})g_{\gamma\alpha}. \tag{5.24}$$

The four-point gluon vertex is

$$H_{A^4} = \frac{1}{24} g^2 \int\limits_{\substack{q_1,q_2,\\ q_3,q_4}} \delta(q_1+q_2+q_3+q_4) \Gamma^{abcd}_{\alpha\beta\gamma\delta} : A^\alpha_a(q_1) A^\beta_b(q_2) A^\gamma_c(q_3) A^\delta_d(q_4) : \quad (5.25)$$

where

$$\Gamma^{abcd}_{\alpha\beta\gamma\delta} = f^{abe} f^{cde} (g_{\alpha\gamma} g_{\beta\delta} - g_{\alpha\delta} g_{\beta\gamma}) + f^{ace} f^{bde} (g_{\alpha\beta} g_{\gamma\delta} - g_{\alpha\delta} g_{\beta\gamma}) + f^{ade} f^{bce} (g_{\alpha\beta} g_{\gamma\delta} - g_{\alpha\gamma} g_{\beta\delta}), \quad (5.26)$$

which notably does not depend on the individual constituent's momenta.

The instantaneous fermion interaction is given as:

$$H_{\widetilde{\bar\psi A A \psi}} = \frac{1}{2} g^2 \int\limits_{\substack{q_1,q_2,\\ q_3,q_4}} \delta(q_1+q_2+q_3+q_4) : \bar\psi(-q_1) T_a \gamma^\mu A^a_\mu(q_2) \frac{\gamma^+}{q_3^+ + q_4^+} T_b \gamma^\nu A^b_\nu(q_3) \psi(q_4) : . \quad (5.27)$$

There are three types of instantaneous gluon interaction diagrams:

$$H_{\widetilde{\psi^4}} = g^2 \int\limits_{\substack{q_1,q_2,\\ q_3,q_4}} \delta(q_1+q_2+q_3+q_4) : \bar\psi(-q_1) T^a \gamma^+ \psi(q_2) \frac{1}{2(q^+)^2} \bar\psi(-q_3) T^a \gamma^+ \psi(q_4) :, \quad (5.28)$$

$$H_{\widetilde{A^4}} = (ig)^2 \int\limits_{\substack{q_1,q_2,\\ q_3,q_4}} \delta(q_1+q_2+q_3+q_4) f^{abe} \frac{q_2^+ - q_1^+}{2} \frac{1}{2(q^+)} f^{cde} \frac{q_4^+ - q_3^+}{2} g_{\alpha\beta} g_{\gamma\delta} \times : A^\alpha_a(q_1) A^\beta_b(q_2) A^\gamma_c(q_3) A^\delta_d(q_4) :, \quad (5.29)$$

and

$$H_{\widetilde{\psi^2 A^2}} = ig^2 \int\limits_{\substack{q_1,q_2,\\ q_3,q_4}} \delta(q_1+q_2+q_3+q_4)\Bigg(: \bar{\psi}(-q_1)T^a\gamma^+\psi(q_2)\frac{1}{2(q^+)^2}f^{abc}\frac{q_4^+ - q_3^+}{2}g_{\beta\gamma}A_b^\beta(q_3)A_c^\gamma(q_4) :$$

$$+ : A_b^\beta(q_1)A_c^\gamma(q_2)\frac{1}{2(q^+)^2}f^{abc}\frac{q_2^+ - q_1^+}{2}g_{\beta\gamma}\bar{\psi}(q_3)T^a\gamma^+\psi(q_4) :\Bigg) \tag{5.30}$$

What follows are diagramatic forms of the bare QCD Hamiltonian interaction vertices in the $A^+ = 0$ gauge.

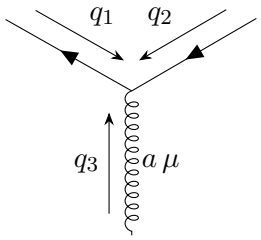

$$= T^a\gamma^\mu \tag{5.31}$$

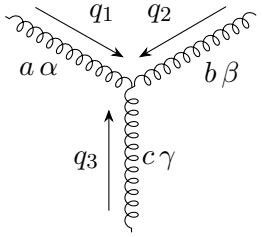

$$= \frac{1}{3!}f^{abc}F_{\alpha\beta\mu}(q_1,q_2,q_3) \tag{5.32}$$

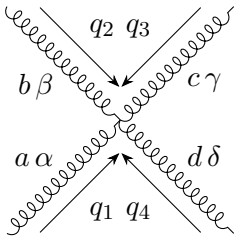

$$= \frac{1}{4!}F^{abcd}_{\alpha\beta\gamma\delta}, \tag{5.33}$$

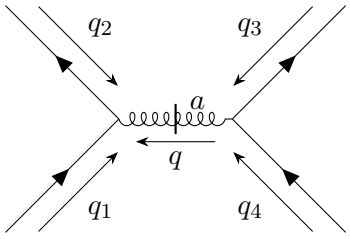

$$= \gamma^+T^a\frac{1}{2(q^+)^2}T^a\gamma^+ \tag{5.34}$$

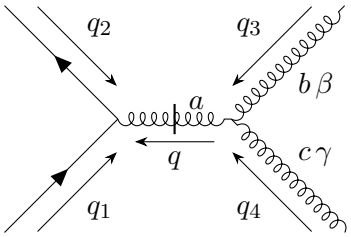

$$= \gamma^+ T^a \frac{1}{2(q^+)^2} f^{abc} \frac{q_4^+ - q_3^+}{2} g_{\beta\gamma} \tag{5.35}$$

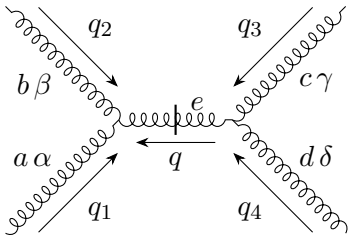

$$= f^{eab} \frac{q_2^+ - q_1^+}{2} \frac{1}{2(q^+)^2} f^{ecd} \frac{q_4^+ - q_3^+}{2} g_{\alpha\beta} g_{\gamma\delta} \tag{5.36}$$

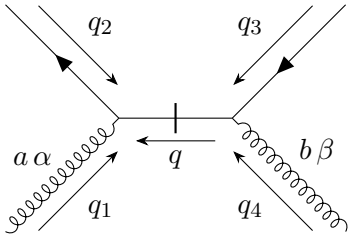

$$= \gamma^+ T^a \frac{1}{2q^+} T^b \gamma^+ g_{\alpha\beta} \tag{5.37}$$

5.1.1 Extensions to QCD: The quark-diquark model of baryons

Baryons can pose a challenge as their valence structure is a 3-body problem. Interesting phenomenological models study baryons by introducing a diquark field [GHL11, LG95], leading to baryons described by coupled quarks to diquarks. This can be described by extending the QCD Lagrangian

$$\mathcal{L} = \mathcal{L}_{QCD} + (D^\mu \Phi)^\dagger (D_\mu \Phi) - m_D \Phi^\dagger \Phi, \tag{5.38}$$

which couples a diquark field Φ to the gluon field through D^μ. This leads to an additional interaction diagram:

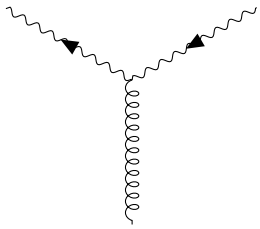

(5.39)

, where the top two legs correspond to a diquark particle.

5.2 The Effective QCD Hamiltonian

In this Section, the RGPEP Equation is solved for QCD. Then appropriate counterterms are computed. Lastly, the effective QCD Hamiltonian is given.

5.2.1 Solution to the RGPEP Equation for QCD

The unitary-transformed QCD Hamiltonian is

$$H_{\rm QCD}(s,s_r) = \underbrace{H_0(s,s_r)}_{H^{(0)}(s,s_r)} + g\Big(\underbrace{H_{\bar\psi\psi A}(s,s_r) + H_{A^3}(s,s_r)}_{H^{(1)}(s,s_r)}\Big) + g^2\Big(\underbrace{H_{\psi^4}(s,s_r) + H_{A^4}(s,s_r) + H_{\psi^2A^2}(s,s_r) + H_{\bar\psi AA\psi}(s,s_r)}_{H^{(2)}(s,s_r)}\Big). \tag{5.40}$$

where $H_0(s,s_r) = H_0$, i.e. the effective zeroth order solution is the same as the bare free Hamiltonian in Eq. 5.21 by the zeroth order RGPEP Eq. The $\mathcal{O}(g)$ and $\mathcal{O}(g^2)$ terms will be computed in this Section. Note that the form of the regulating funciton is the same that was used in Yukawa theory

$$r\Big(s_r;\mathcal{Q}^-(q_1,q_2,q_3)\Big) = e^{-s_r\left(q_1^-+q_2^-+q_3^-\right)^2}. \tag{5.41}$$

Contractions between the fields will be relevant shortly, so we define them

explicitly here:

$$\overbrace{A_a^\mu(q_1)A_b^\nu}(q_2) = \frac{\theta(q_1^+)}{|q_1^+|}\delta(q_1+q_2)\delta_{a,b}\; d^{\mu\nu}(q_1) \tag{5.42}$$

$$\overbrace{\bar{\psi}_{c_1}(q_1)\psi}_{c_1}(q_2) = \frac{\theta(q_1^+)}{|q_1^+|}\delta(q_1+q_2)\delta_{c_1,c_2}\;\Big(\gamma_\alpha q_1^\alpha - m_q\Big) \tag{5.43}$$

$$\overbrace{\psi_{c_1}(q_1)\bar{\psi}}_{c_1}(q_2) = \frac{\theta(q_1^+)}{|q_1^+|}\delta(q_1+q_2)\delta_{c_1,c_2}\;\Big(\gamma_\alpha q_1^\alpha + m_q\Big). \tag{5.44}$$

The solution the RGPEP Equation at first order is the same for QCD as it was for Yukawa theory; that is, each bare QCD 3-point vertex gets modified by a form factor

$$f\Big(s;\mathcal{Q}^-(q_1,q_2,q_3)\Big) = e^{-s(q_1^-+q_2^-+q_3^-)^2} \tag{5.45}$$

Therefore, the quark gluon vertex goes from its bare form to its effective form by:

$$H_{\bar{\psi}\psi A} \to H_{\bar{\psi}\psi A}(s,s_r) = g\int\limits_{q_1,q_2,q_3}\delta(q_1+q_2+q_3)e^{-(s+s_r)\Big(q_1^-+q_2^-+q_3^-\Big)^2} \times :\bar{\psi}_{c_1}(-q_1)\gamma_\mu A_a^\mu(q_3)T^a\psi_{c_2}(q_2): . \tag{5.46}$$

Similarly, the 3-point gluon vertex A^3 becomes:

$$H_{A^3} \to H_{A^3}(s,s_r) = -\frac{1}{3!}igf^{abc}\int\limits_{q_1,q_2,q_3}\delta(q_1+q_2+q_3)e^{-(s+s_r)\Big(q_1^-+q_2^-+q_3^-\Big)^2} \times F_{\alpha\beta\gamma}(q_1,q_2,q_3):A_a^\alpha(q_1)A_b^\beta(q_2)A_c^\gamma(q_3): \tag{5.47}$$

Matrix elements of $H_{\bar{\psi}\psi A}(s,s_r)$ and $H_{A^3}(s,s_r)$ are regular in the limit $s_r \to 0$ since s is nonzero and the form factor acts as a regulator. Therefore, the limit $s_r \to 0$ can be taken for these terms.

There are two classes of terms of $\mathcal{O}(g^2)$ in the effective Hamiltonian. The first are terms that are native to the bare Hamiltonian, the instantaneous interaction terms: $H_{\widetilde{A^4}}, H_{\widetilde{\psi^4}}, H_{\widetilde{\bar{\psi}AA\psi}}$, and $H_{\widetilde{\psi^2A^2}}$, all of which are $\mathcal{O}(g^2)$. These terms, similarly

to the bare 3-point vertices, obtain a form factor of the form

$$f\Big(s;\mathcal{Q}^-(q_1,q_2,q_3,q_4)\Big)=e^{-s(q_1^-+q_2^-+q_3^-+q_4^-)^2}. \tag{5.48}$$

The more interesting class of terms is those arising from the contractions of two first order effective terms. The three categories of these contractions are type 1: contractions between $H_{\bar{\psi}\psi A}(s)$ with $H_{\bar{\psi}\psi A}(s)$, type 2: contractions between $H_{A^3}(s)$ with $H_{A^3}(s)$, and mixed type (type 3): contractions between $H_{\bar{\psi}\psi A}(s)$ with $H_{A^3}(s)$. In Yukawa theory, there were only type 1 contractions since 3-point boson vertices didn't exist; however, here more contractions must be computed. The explicit calculations of the contractions are omitted because they are essentially the same computations that were done in Chapter 4. Here, we simply group terms and summarize the results.

We group terms based on their external legs. The terms with four external gluon legs are

$$H_{A^4}(s,s_r)=\int\limits_{\substack{q_1,q_2,q\\q_3,q_4}}\delta(q_1+q_2+q)\delta(q_3+q_4-q)\Gamma^{abcd}_{\alpha\beta\gamma\delta}\Big(s,s_r;q_1,q_2,q,q_3,q_4\Big):A^\alpha_a(q_1)A^\beta_b(q_2)A^\gamma_c(q_3)A^\delta_d(q_4):, \tag{5.49}$$

where

$$\begin{aligned}\Gamma^{abcd}_{\alpha\beta\gamma\delta}\Big(s,s_r;&q_1,q_2,q_3,q_4\Big)=\frac{1}{24}e^{-(s+s_r)\left(q_1^-+q_2^-+q_3^-+q_4^-\right)^2}\Big(F^{abcd}_{\alpha\beta\gamma\delta}+f^{abe}\frac{q_2^+-q_1^+}{2}\frac{1}{2(q^+)}f^{cde}\frac{q_4^+-q_3^+}{2}g_{\alpha\beta}g_{\gamma\delta}\Big)\\&+\frac{1}{36}f^{abe}f^{cde}\frac{d^{\mu\nu}(q)}{q^+}F_{\alpha\beta\mu}(q_1,q_2,q)F_{\delta\gamma\nu}(q_3,q_4,-q)\\&\times\mathcal{R}\Big(s;\mathcal{Q}^-(q_1,q_2,q),\mathcal{Q}^-(q_3,q_4,-q)\Big)r\Big(s_r;\mathcal{Q}^-(q_1,q_2,q)\Big)r\Big(s_r;\mathcal{Q}^-(q_3,q_4,-q)\Big).\end{aligned} \tag{5.50}$$

The terms that compose H_{A^4} are the effective 4-point gluon term, the instantaneous gluon exchange term with gluon legs, and the effective gluon exchange with gluon

legs. The last term has the interaction diagram:

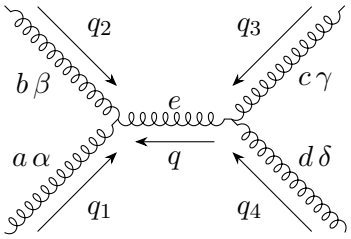

$$= \frac{1}{36} f^{abe} f^{dce} \frac{d^{\mu\nu}(q)}{q^+} F_{\alpha\beta\mu}(q_1, q_2, q) F_{\delta\gamma\nu}(q_3, q_4, -q) \times \mathcal{R}\Big(s; \mathcal{Q}^-(q_1, q_2, q), \mathcal{Q}^-(q_3, q_4, -q)\Big) \times r\Big(s_r; \mathcal{Q}^-(q_1, q_2, q)\Big) r\Big(s_r; \mathcal{Q}^-(q_3, q_4, -q)\Big)$$

The effective gluon exchange term with quark legs is the only term that contributes to $H_{\psi^4}(s)$:

$$H_{\psi^4}(s) = \frac{1}{2} \int\limits_{\substack{q_1,q_2,q \\ q_3,q_4}} \delta(q_1+q_2+q)\delta(q_3+q_4-q) \Lambda_{\mu\nu}(q_1, q_2, q, q_3, q_4) : \bar{\psi}(-q_1)\gamma^\mu T^a \psi(q_2) \bar{\psi}(-q_3)\gamma^\nu T_a \psi(q_4) :, \tag{5.51}$$

where

$$\Lambda_{\mu\nu}(q_1, q_2, q, q_3, q_4) = 4 g_{-\mu} g_{-\nu} e^{-s(q_1^- + q_2^- + q_3^- + q_4^-)^2} + \frac{\theta(q^+)}{q^+} d_{\mu\nu}(q) \mathcal{R}\Big(s; \mathcal{Q}^-(q_1, q_2, q), \mathcal{Q}^-(q_3, q_4, -q)\Big) r\Big(s_r; \mathcal{Q}^-(q_1, q_2, q)\Big) r\Big(s_r; \mathcal{Q}^-(q_3, q_4, -q)\Big). \tag{5.52}$$

The corresponding interaction diagram is:

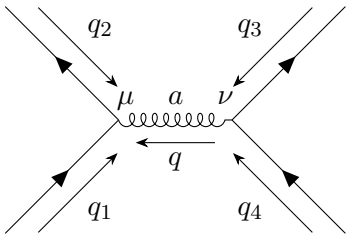

$$= T^a \frac{d^{\mu\nu}(q)}{q^+} T^a \mathcal{R}\Big(s; \mathcal{Q}^-(q_1, q_2, q), \mathcal{Q}^-(q_3, q_4, -q)\Big). \tag{5.53}$$

Finally, there are the terms with mixed legs: the effective gluon exchange with mixed legs, and the effective quark exchange with mixed legs. They are given

as

$$H_{\psi^2A^2}(s,s_r) = \int\limits_{\substack{q_1,q_2,q\\q_3,q_4}} \delta(q_1+q_2+q)\delta(q_3+q_4-q)\Omega^{abc}_{\mu\alpha\beta}(s,s_r;q_1,q_2,q,q_3,q_4)$$
$$\times :\bar{\psi}(-q_1)\gamma^\mu T^c\psi(q_2)A^\alpha_a(q_3)A^\beta_b(q_4):, \qquad (5.54)$$

where

$$\Omega^{abc}_{\mu\alpha\beta}(s,s_r;q_1,q_2,q,q_3,q_4) = -if^{abc}\Big(\frac{q_4^+-q_3^+}{2}\Big)g_{-\mu}g_{i\alpha}g_{i\beta}e^{-(s+s_r)\Big(q_1^-+q_2^-+q_3^-+q_4^-\Big)^2}$$
$$+\frac{\theta(q^+)}{q^+}g_{\mu\omega}d^{\omega\nu(q)}\frac{1}{2}F^{abc}_{\alpha\beta\nu}(q_3,q_4,-q)\mathcal{R}\Big(s;\mathcal{Q}^-(q_1,q_2,q),\mathcal{Q}^-(q_3,q_4,-q)\Big)$$
$$\times r\Big(s_r;\mathcal{Q}^-(q_1,q_2,q)\Big)r\Big(s_r;\mathcal{Q}^-(q_3,q_4,-q)\Big), \qquad (5.55)$$

and

$$H_{\bar{\psi}AA\psi}(s,s_r) = \int\limits_{\substack{q_1,q_2,q\\q_3,q_4}} \delta(q_1+q_2+q)\delta(q_3+q_4-q)r\Big(s_r;\mathcal{Q}^-(q_1,q_2,q)\Big)r\Big(s_r;\mathcal{Q}^-(q_3,q_4,-q)\Big)$$
$$\times :\bar{\psi}(-q_1)\gamma_\mu T^aA^\mu(q_2)\Pi_{\mu\nu}\Big(s;q_1,q_2,q,q_3,q_4\Big)\gamma_\nu T^bA^\nu_b(q_3)\psi(q_4):, \qquad (5.56)$$

where

$$\Pi_{\mu\nu}\Big(s;q_1,q_2,q,q_3,q_4\Big) = \frac{\gamma^+}{q^+}e^{-s\Big(q_1^-+q_2^-+q_3^-+q_4^-\Big)^2}$$
$$+\frac{\theta(q^+)}{q^+}\Big(\gamma^\alpha q_\alpha+m_q\Big)\mathcal{R}\Big(s;\mathcal{Q}^-(q_1,q_2,q),\mathcal{Q}^-(q_3,q_4,-q)\Big) \qquad (5.57)$$

Two example interaction diagrams are given by:

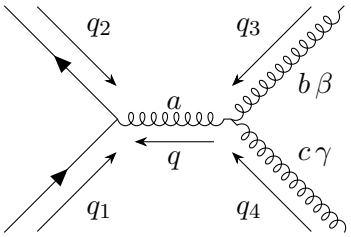

$$= \frac{\theta(q^+)}{q^+} g_{\mu\omega} d^{\omega\nu(q)} \frac{1}{2} F^{abc}_{\alpha\beta\nu}(q_3, q_4, -q)$$
$$\times \mathcal{R}\Big(s; \mathcal{Q}^-(q_1, q_2, q), \mathcal{Q}^-(q_3, q_4, -q)\Big)$$
$$\times r\Big(s_r; \mathcal{Q}^-(q_1, q_2, q)\Big) r\Big(s_r; \mathcal{Q}^-(q_3, q_4, -q)\Big),$$

and

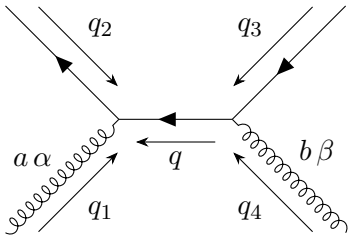

$$= T^a \gamma^\alpha \frac{\gamma^\mu q_\mu + m_q}{q^+} T^b \gamma^\beta \mathcal{R}\Big(s; \mathcal{Q}^-(q_1, q_2, q), \mathcal{Q}^-(q_3, q_4, -q)\Big)$$
$$\times r\Big(s_r; \mathcal{Q}^-(q_1, q_2, q)\Big) r\Big(s_r; \mathcal{Q}^-(q_3, q_4, -q)\Big)$$

The double contractions lead to loop diagrams. There are *three* distinct loop diagrams, rather than the two that arose in Yukawa theory. Out of the three loop diagrams, two contribute to $H_{\delta m_g^2}(s, s_r)$, and one contributes to $H_{\delta m_q^2}(s, s_r)$. All three of these terms diverge as $s_r \to 0$, and thus must be renormalized.

The quark mass loop is given as

$$H_{\delta m_q^2}(s, s_r) = C_F \int\limits_{q_1, q_2, q_3} \frac{\theta(q_2^+)\theta(q_3^+)}{q_2^+ q_3^+} \frac{1}{q_1^- + q_2^- + q_3^-} \delta(q_1 - q_2 - q_3)$$
$$\times : \bar{\psi}(q_1) \gamma^\mu d_{\mu\nu}(q_3) \Big(\gamma^\rho q_{2\rho} + m_0\Big) \gamma^\nu \psi(q_1) :$$
$$\times \Big(e^{-2(s+s_r)(q_1^- + q_2^- + q_3^-)^2} - e^{-2s_r(q_1^- + q_2^- + q_3^-)^2}\Big), \qquad (5.58)$$

and has the interaction diagram

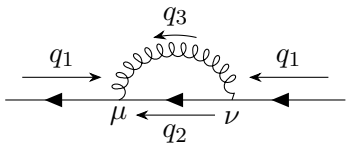

(5.59)

The gluon mass loops are given as

$$H_{\delta m_g^2}(s,s_r) = \int\limits_{q_1,q_2,q_3} \frac{\theta(q_1^+)\theta(q_2^+)}{q_1^+ q_2^+} \frac{1}{q_1^- + q_2^- + q_3^-}\delta(q_1+q_2-q_3)$$
$$\times \left(\delta m_g^2\right)_{\mu\nu} : A^{\mu a}(q_3)A^{\nu b}(-q_3) :$$
$$\times \left(e^{-2(s+s_r)(q_1^- + q_2^- + q_3^-)^2} - e^{-2s_r(q_1^- + q_2^- + q_3^-)^2}\right), \tag{5.60}$$

where

$$\left(\delta m_g^2\right)_{\mu\nu} = T_F\ \delta^{ab}\mathrm{Tr}\Big[(\gamma_\rho q_q^\rho - m_q)\gamma_\mu(\gamma_\alpha q_2^\alpha + m_q)\gamma_\nu\Big]$$
$$+ C_A d^{\alpha\rho}(q_1)F_{\alpha\beta\mu}(q_1,q_2,q_3)F_{\rho\kappa\nu}(-q_1,-q_2,-q_3)d^{\beta\kappa}(q_2). \tag{5.61}$$

The interaction diagrams are:

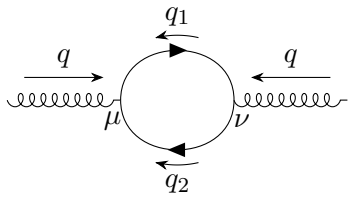

(5.62)

and

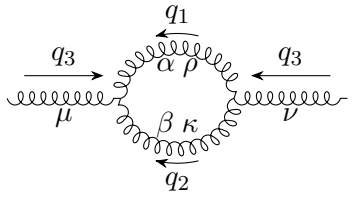

(5.63)

5.3 Renormalization and Counterterms

All of the loop diagrams above, as well as the effective and instantaneous gluon exchange terms require counterterms since they diverge in the limit $s_r \to 0$. In this section, we provide explicit calculations of the counterterms in the limit $s_r \to 0$.

Some relevant integrals are given here (where the notation $o(1)$ stands for

terms which go to zero as $s_r \to 0$):

$$\int_{z_0}^{\infty} dz\ e^{-s_r z^2} = \frac{\sqrt{\pi}}{2}\mathrm{erfc}(z_0\sqrt{s_r}) = \frac{\sqrt{\pi}}{2\sqrt{s_r}} - z_0 + o(1) \tag{5.64}$$

$$\int_{z_0}^{\infty} dz \frac{1}{z} e^{-s_r z^2} = \frac{1}{2}\Gamma\Big(0, s z_0^2\Big) = \frac{1}{2}\bigg(-\gamma + \log\Big(\frac{1}{s_r z_0^2}\Big)\bigg) + o(1) \tag{5.65}$$

$$\int_{z_0}^{\infty} dz\ z e^{-s_r z^2} = \frac{e^{-s_r z_0^2}}{2s} = \frac{1 - s z_0^2}{2s} + o(1) \tag{5.66}$$

$$\int_{z_0}^{\infty} dz \log\Big(z/m\Big) \exp\Big(-s_r z^2\Big) = \frac{\sqrt{\pi}}{4\sqrt{s_r}}\bigg(-\gamma + \log\Big(\frac{1}{4m^2 s_r}\Big)\bigg) + z_0\Big(1 + \log(m/z_0)\Big) + o(1) \tag{5.67}$$

$$\int_{z_0}^{\infty} dz \frac{1}{z} \log\Big(z/m\Big) \exp\Big(-s_r z^2\Big) = \frac{\pi^2}{48} + \frac{1}{8}\Big(\gamma + \log(s_r)\Big)^2 + \frac{1}{2}\log(m)\Big(\gamma + \log\Big(s_r z_0^2\Big)\Big) - \frac{1}{2}\log^2(z_0) + o(1) \tag{5.68}$$

The general steps to solve the loop integrals in this Section are as follows:

1. Replace all particle momentum, q_i in the integrand with relative momentum of the two particles in the loop, x and $\kappa^{\perp}$ by a change of variables, while computing the Jacobian.

2. The integration variables should now be dx and $d^2\kappa^{\perp}$. A single integral can be done trivially by changing to polar coordinates: $d^2\kappa^{\perp} = \kappa d\kappa d\phi$, where the

integral over ϕ simply gives 2π.

3. Now change variables from $d\kappa \to d\mathcal{M}^2$ by writing down the invariant masses of the particles in the loop in terms of x and κ^2. This will remove a factor of $x(1-x)$ in the denominator.

4. It is now almost always easier to integrate when the order of integration is reversed, that is integrating with respect to $d\mathcal{M}^2 dx$, rather than $dx d\mathcal{M}^2$. This is shown in Fig. 5.1. To do this, rather than integrating from $x = 0$ to $x = 1$ and then integrating along $\mathcal{M}^2$ from the fixed value of x in the outer integral to infinity, $\mathcal{M}^2$ can be solved in terms of x (which will give two solutions, denoted x_1 and x_2). Now, one can integrate from $\mathcal{M}^2_{min.}$ to infinity while integrating along x from x_1 to x_2, both which depend on the outer value of $\mathcal{M}^2$. Lastly, note that $\mathcal{M}^2_{min.} \equiv \mathcal{M}^2(x_{min.}, 0)$, where $x_{min.}$ is the minimum of the curve $\mathcal{M}^2$.

5. Lastly, when you obtain an integral of the form

$$I = \int d\eta \; \iota(\eta) f(s_r, \eta), \tag{5.69}$$

and if this integral diverges as $s_r \to 0$, split up the integral in the following manner:

$$I = \int d\eta \, \iota(\eta) f(s_r, \eta) = \int d\eta \Big(\iota(\eta) - \mathrm{div}\Big(\iota(\eta)\Big) \Big) f(s_r, \eta) + \int d\eta \, \mathrm{div}\Big(\iota(\eta)\Big) f(s_r, \eta). \tag{5.70}$$

Here, $\mathrm{div}(\iota)$ stands for the divergent part of the integrand, $\iota(\eta)$. This can in general be determined by looking at the Taylor series of $\iota(\eta)$ at $\eta \to \infty$. The first integral in the split has the integrand $\Big(\iota - \mathrm{div}(\iota)\Big) f(s_r, \eta)$, which is finite when $s_r = 0$ if and only if it passes Lebesque's dominated convergence theorem A.0.1. In this case, one can freely take $s_r \to 0$ and likely find a closed form of the integral. The second integral with integrand $\mathrm{div}(\iota) f(s_r, \eta)$ diverges when $s_r \to 0$. In general, a closed form solution to this integral cannot be found;

rather, a solution with explicit s_r dependence can be given with additional terms that tend to zero as $s_r \to 0$.

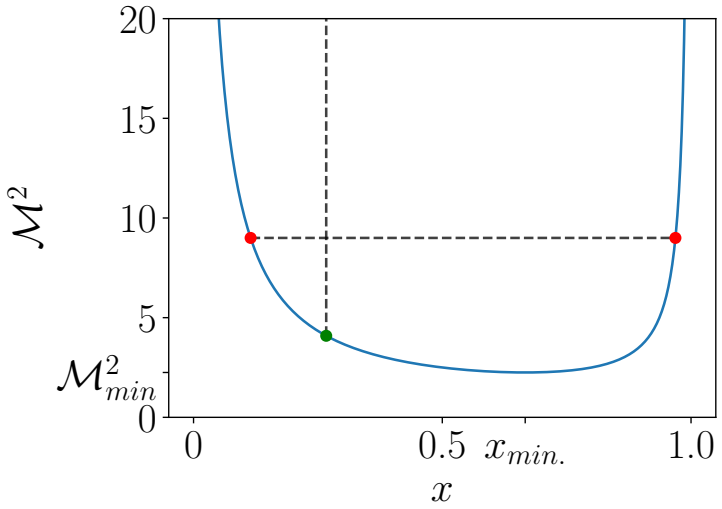

Figure 5.1: **Example of integration region**: Integration of a function over the region defined in gray can be made easier in many cases by switching the order of integration from $dx\ d\mathcal{M}^2 \to d\mathcal{M}^2\ dx$.

5.3.1 Gluon Mass Loops

There are two contributions to the gluon mass loop, the quark loop 5.62, and the gluon loop 5.63.

5.3.1.1 Gluon Mass Loop: Quark Loop

The contraction $\bar{\psi}\gamma^\mu T^a \psi A^a_\mu \bar{\psi}\gamma^\nu T^b \psi A^b_\nu$ leads to the quark loop 5.62, given by

$$H_{(\delta m_g^2)_1} = \int_{q_3} \int_{q_1,q_2} \frac{\theta(q_1^+)\theta(q_2^+)}{q_1^+ q_2^+ (q_1^- + q_2^- - q_3^-)} \delta(q_1 + q_2 - q_3) T_F \delta^{ab} \times \mathrm{Tr}\Big[(\gamma_\rho q_1^\rho - m_q)\gamma^\mu(\gamma_\alpha q_2^\alpha + m_q)\gamma^\nu\Big] : A^a_\mu(q_3) A^b_\nu(-q_3) : \quad (5.71)$$

The trace can be simplified:

$$\mathrm{Tr}\Big[(\gamma_\rho q_1^\rho - m_q)\gamma^\mu(\gamma_\alpha q_2^\alpha + m_q)\gamma^\nu\Big] = 4\Big(q_1^\mu q_2^\nu + q_1^\nu q_2^\mu - g^{\mu\nu}(q_1 \cdot q_2 + m_q^2)\Big) \quad (5.72)$$

therefore,

$$H_{(\delta m_g^2)_1} = \int_{q_3}\int_{q_1,q_2} \frac{\theta(q_1^+)\theta(q_2^+)}{q_1^+ q_2^+(q_1^- + q_2^- - q_3^-)}\frac{1}{2}\delta_{ab}\delta(q_1+q_2-q_3) \\ \times 4\Big(q_1^\mu q_2^\nu + q_1^\nu q_2^\mu - g^{\mu\nu}(q_1\cdot q_2 + m_q^2)\Big)A_\mu^a(q_3)A_\nu^b(-q_3). \quad (5.73)$$

The factor $\frac{\theta(q_1^+)\theta(q_2^+)}{q_1^+ q_2^+}\delta(q_1+q_2-q_3)$ implies $q_3^+ > 0$ which allows the fields to be written in terms of the polarization vectors and ladder operators:

$$H_{(\delta m_g^2)_1} = T_F\int_{q_3}\int_{q_1,q_2} \frac{\theta(q_1^+)\theta(q_2^+)}{q_1^+ q_2^+(q_1^- + q_2^- - q_3^-)}\delta(q_1+q_2-q_3) \\ \times 4\Big(q_1^\mu q_2^\nu + q_1^\nu q_2^\mu - g^{\mu\nu}(q_1\cdot q_2 + m_q^2)\Big)\frac{\epsilon_\mu^\sigma(q_3)\epsilon_\nu^{\sigma'\star}(q_3)}{(q_3^+)^2}a^\dagger_{a,\sigma'}(q_3)a_{a,\sigma}(q_3), \quad (5.74)$$

where the bosonic creation and annihilation operators were normal ordered.

The following can be simplified:

$$\Big(q_1^\mu q_2^\nu + q_1^\nu q_2^\mu - g^{\mu\nu}(q_1\cdot q_2 + m_q^2)\Big)\epsilon_\mu^\sigma(q_3)\epsilon_\nu^{\sigma'\star}(q_3) \\ = \Bigg(\Big(q_1\cdot\epsilon_\mu^\sigma(q_3)\Big)\Big(q_2\cdot\epsilon_\nu^{\sigma'\star}(q_3)\Big) + \Big(q_1\cdot\epsilon_\mu^\sigma(q_3)\Big)\Big(q_2\cdot\epsilon_\nu^{\sigma'\star}(q_3)\Big) \\ - (q_1\cdot q_2 + m_q^2)\epsilon_\mu^\sigma(q_3)\cdot\epsilon^{\mu\sigma'\star}(q_3)\Bigg). \quad (5.75)$$

Next, note that

$$\epsilon_\mu^\sigma(q_3)\cdot\epsilon^{\mu\sigma'\star}(q_3) = -\delta_{\sigma,\sigma'} \quad (5.76)$$

and

$$q_3\cdot\epsilon_\sigma(q_3) = 0. \quad (5.77)$$

Since q_2 is contracted with ϵ, q_2^- will not appear in this expression since $\epsilon^+ = 0$.

Therefore, q_2 can be written as $q_1 - q_3$, which simplifies the expression to:

$$\begin{aligned} &2\Big(q_1 \cdot \epsilon_\sigma(q_3)\Big)\Big(q_1 \cdot \epsilon^\star_{\sigma'}(q_3)\Big) + (q_1 \cdot q_2 + m_q^2)\delta_{\sigma,\sigma'} \\ &= 2\Big(-\kappa \cdot \varepsilon^\perp_\sigma\Big)\Big(-\kappa \cdot \varepsilon^{\perp\star}_{\sigma'}\Big) + (q_1 \cdot q_2 + m_q^2)\delta_{\sigma,\sigma'} \end{aligned} \tag{5.78}$$

where the following identity was used:

$$\begin{aligned} q_1 \cdot \epsilon_\sigma(q_3) &= \frac{1}{2} q_1^+ \epsilon^-_\sigma(q_3) - q_1^\perp \epsilon^\perp_\sigma(q_3) \\ &= \frac{1}{2} x q_3^+ \Big(\frac{2 q_3^\perp \varepsilon^\perp_\sigma}{q_3^+}\Big) - q_1^\perp \varepsilon^\perp_\sigma \\ &= x q_3^+ \varepsilon^\perp_\sigma - q_1^\perp \varepsilon^\perp_\sigma \\ &= -\kappa \cdot \varepsilon^\perp_\sigma \end{aligned} \tag{5.79}$$

By the identity

$$\int d^2\kappa f(\kappa)\kappa^i\kappa^j = \frac{1}{2}\delta_{ij}\int d^2\kappa f(\kappa)\kappa^2, \tag{5.80}$$

we get (with $q_3 \to q$ and the fields reinserted)

$$\begin{aligned} H_{(\delta m_g^2)_1} &= \int_q \int_{q_1,q_2} \frac{\theta(q_1^+)\theta(q_2^+)}{q_1^+ q_2^+ (q_1^- + q_2^- - q_3^-)} \delta(q_1 + q_2 - q) \\ &\qquad \times \Big(2(q_1 \cdot q_2 + m_q^2) - 2\kappa^2\Big) A^a_\mu(q) A^\mu_a(-q) \\ &= \int_q \Big(\delta m_g^2(q)\Big)_1 A^a_\mu(q) A^\mu_a(-q), \end{aligned} \tag{5.81}$$

where

$$\begin{aligned} \Big(\delta m_g^2(q)\Big)_1 &= \int_{q_1,q_2} \frac{\theta(q_1^+)\theta(q_2^+)}{q_1^+ q_2^+} \delta(q_1 + q_2 - q) \frac{\mathcal{M}^2_{q\bar{q}}(x,\kappa) - 2\kappa^2}{q_1^- + q_2^- - q^-} \\ &\qquad \times f^2\Big(s + s_r;\ q_1^- + q_2^- - q^-\Big) - f^2\Big(s_r;\ q_1^- + q_2^- - q^-\Big) \\ &= I_{G,1}(s + s_r) - I_{G,1}(s_r) \end{aligned} \tag{5.82}$$

since $2q_1 \cdot q_2 + 2m_q^2 = (q_1 + q_2)^2$, which is the invaraint mass of the quark-antiquark pair, $\mathcal{M}^2_{q\bar{q}}(x,\kappa)$.

Now,

$$I_{G,1}(s_r) = \frac{T_F}{16\pi^2}\int_0^1 dx \int\limits_{\frac{m_q^2}{x(1-x)}}^{\infty} d\mathcal{M}^2 \frac{\mathcal{M}^2(2x^2-2x+1)+2m_q^2}{\mathcal{M}^2-m_g^2}\exp\left(\frac{-2s_r}{(q^+)^2}\Big(\mathcal{M}^2-m_g^2\Big)^2\right)$$
$$= \frac{T_F}{16\pi^2}\int\limits_{4m_q^2}^{\infty} d\mathcal{M}^2 \int_{x_1}^{x_2} dx \frac{\mathcal{M}^2(2x^2-2x+1)+2m_q^2}{\mathcal{M}^2-m_g^2}\exp\left(\frac{-2s_r}{(q^+)^2}\Big(\mathcal{M}^2-m_g^2\Big)^2\right), \tag{5.83}$$

where $\mathcal{M}^2_{q\bar{q}}$ can be solved in terms of x and the roots are x_1 and x_2 such that

$$(x_1, x_2) \to \left(-\frac{1}{2} - \frac{1}{2\mathcal{M}}\sqrt{\mathcal{M}^2-4m_q^2}, -\frac{1}{2}+\frac{1}{2\mathcal{M}}\sqrt{\mathcal{M}^2-4m_q^2}\right) \tag{5.84}$$

After integrating over x and making the substitution $z = \mathcal{M}^2 - m_q^2$ and defining $\tilde{s}_r = 2s_r/(q^+)^2$:

$$I_{g,1}(s_r) = \frac{T_F}{16\pi^2}\int_{3m_g^2}^{\infty} dz \frac{1}{z}\left(\frac{2}{3}\sqrt{(z+m_g^2)(z-3m_g^2)} + \frac{4}{3}m_q^2\sqrt{1-\frac{4m_q^2}{z+m_q^2}}\right)e^{-\tilde{s}_r z^2}. \tag{5.85}$$

Using the series expansion about $z \to \infty$,

$$\frac{2}{3z}\sqrt{(z+m_g^2)(z-3m_g^2)} = z - m_g^2 - \frac{2m_g^4}{z} + \mathcal{O}(z^{-2}), \tag{5.86}$$

and

$$\frac{4m_g^2}{3z}\sqrt{1-\frac{4m_q^2}{z+m_g^2}} = \frac{4m_g^2}{3z} + \mathcal{O}(z^{-2}), \tag{5.87}$$

then

$$I_{G,1}(s_r) = \frac{T_F}{16\pi^2}\Bigg\{ \int_{3m_q^2}^{\infty} dz \left(\frac{2}{3z}\sqrt{(z+m_g^2)(z-3m_g^2)} - \frac{2}{3} + \frac{2m_g^2}{3z} \right) e^{-\tilde{s}_r z^2} + \int_{3m_q^2}^{\infty} dz \left(\frac{2}{3} - \frac{2m_g^2}{3z} \right) e^{-\tilde{s}_r z^2} + \int_{3m_q^2}^{\infty} dz \frac{4m_g^2}{3z} \left(\sqrt{1 - \frac{4m_q^2}{z+m_q^2}} - 1 \right) e^{-\tilde{s}_r z^2} + \int_{3m_q^2}^{\infty} dz \frac{4m_g^2}{3z} e^{-\tilde{s}_r z^2} \Bigg\}. \tag{5.88}$$

The first and third integrals are convergent in the limit $s_r \to 0$ by Lebeque's dominated convergence theorem (see Chapter 4) with the dominating functions

$$\frac{2}{3z}\left(\sqrt{(z+m_g^2)(z-3m_g^2)} - z + m_g^2 \right) \tag{5.89}$$

and

$$\frac{4m_g^2}{3z}\left(\sqrt{1 - \frac{4m_q^2}{z+m_q^2}} - 1 \right) \tag{5.90}$$

respectively. The second and fourth integrals diverge in the limit $s_r \to 0$, and therefore must be computed explicitly in terms of s_r.

Altogether, the total integral is

$$I_{G,1}(s_r) = \frac{T_F}{16\pi^2}\Bigg\{ \frac{2m_g^2}{9}\Big(6 + 3\sqrt{3}\pi - \log 27\Big) - 3m_q^2 + \frac{q^+\sqrt{\pi}}{3\sqrt{2s_r}} \frac{m_g^2}{3} \left(-\gamma + \log\Big(\frac{(q^+)^2}{6m_q^2 s_r}\Big) \right) \Bigg\} + o(1) \tag{5.91}$$

5.3.1.2 Gluon Mass Loop: Gluon Loop

The contraction $A_a^\mu \overbrace{A_f^\sigma A_c^\gamma A_d^\delta} A_e^\omega A_b^\nu$ leads to the gluon loop 5.63, given by

$$\begin{aligned} H_{(\delta m_g^2)_2} = \int_{q_3} \int_{q_1,q_2} & \frac{\theta(q_1^+)\theta(q_2^+)}{q_1^+ q_2^+ (q_1^- + q_2^- - q_3^-)} \delta(q_1+q_2-q_3) C_A \delta^{ab} \\ & \times d^{\alpha\rho}(q_1) F_{\alpha\beta\mu}(q_1,q_2,q_3) F_{\rho\kappa\nu}(-q_1,-q_2,-q_3) d^{\beta\kappa}(q_2) \\ & \times : A_a^\mu(q_3) A_b^\nu(-q_3) : . \end{aligned} \tag{5.92}$$

The factor $d^{\alpha\rho}(q_1)F_{\alpha\beta\mu}(q_1,q_2,q_3)F_{\rho\kappa\nu}(-q_1,-q_2,-q_3)d^{\beta\kappa}(q_2)$ must be simplified first:

$$\begin{aligned} & -d^{\alpha\rho}(q_1)F_{\alpha\beta\mu}(q_1,q_2,q_3)d^{\beta\kappa}(q_2)F_{\rho\kappa\nu}(-q_1,-q_2,-q_3) \\ & \quad = d^{\alpha\rho}(q_1)F_{\alpha\beta\mu}(q_1,q_2,q_3)d^{\beta\kappa}(q_2)F_{\rho\kappa\nu}(q_1,q_2,q_3) \\ & \quad = 2(q_2-q_1)_\mu(q_2-q_1)_\nu + 2\Big(q_1^\beta q_1^\kappa d_{\beta\kappa}(q_2)d_{\mu\nu}(q_1) + q_2^\beta q_2^\kappa d_{\beta\kappa}(q_1)d_{\mu\nu}(q_2)\Big) \\ & \qquad + 4\Big(q_1^\kappa d_{\kappa\mu}(q_2) q_2^\alpha d_{\alpha\nu}(q_1) - q_2^\kappa d_{\kappa\mu}(q_1) q_1^\alpha d_{\alpha\nu}(q_2)\Big) \\ & \qquad + 2(q_2-q_1)_\mu\Big(q_{1\rho} d^{\rho\beta}(q_2) d_{\beta\nu}(q_1) - q_{2\rho} d^{\rho\beta}(q_1) d_{\beta\nu}(q_2)\Big) \\ & \qquad + 2(q_2-q_1)_\nu\Big(q_{1\beta} d^{\beta\rho}(q_2) d_{\rho\mu}(q_1) - q_{2\beta} d^{\beta\rho}(q_1) d_{\rho\mu}(q_2)\Big) \end{aligned} \tag{5.93}$$

This can be simplified by the following relations:

1. $q_\mu d^{\mu\nu}(p) = \frac{1}{2} q^+ d^{-\nu}(p) - q^\perp \cdot d^{\perp\nu}(p)$
2. $q_\mu q_\nu d^{\mu\nu}(p) = \left(\frac{q^+ p^\perp - q^\perp p^+}{p^+}\right)^2$
3. $q_\mu d^{\mu\alpha}(p) d_{\alpha\nu}(q) = \frac{q^+ p^\perp - q^\perp p^+}{p^+} \cdot d_{\perp\nu}(q)$

From these, we can simplify above with

$$16(q_2-q_1)_\mu(q_2-q_1)_\nu A^\mu(q_3)A^\nu(-q_3) = 64\ \kappa^2 A^\mu(q_3)A_\mu(-q_3), \tag{5.94}$$

$$
\begin{aligned}
&4\Big(q_1^\beta q_1^\kappa d_{\beta\kappa}(q_2)d_{\mu\nu}(q_1)+q_2^\beta q_2^\kappa d_{\beta\kappa}(q_1)d_{\mu\nu}(q_2)\Big)A^\mu(q_3)A^\nu(-q_3)\\
&\quad=4\left(\frac{(q_1^+q_2^\perp-q_2^+q_1^\perp)^2}{(q_2^+)^2}+\frac{(q_2^+q_1^\perp-q_1^+q_2^\perp)^2}{(q_1^+)^2}\right)A^\mu(q_3)A_\mu(-q_3)\\
&\quad=4\kappa^2\left(\frac{1}{x^2}+\frac{1}{(1-x)^2}\right),
\end{aligned}
\tag{5.95}
$$

$$
\begin{aligned}
&-4\Big(q_1^\kappa d_{\kappa\mu}(q_2)q_2^\alpha d_{\alpha\nu}(q_1)+q_2^\kappa d_{\kappa\mu}(q_1)q_1^\alpha d_{\alpha\nu}(q_2)\Big)A^\mu(q_3)A^\nu(-q_3)\\
&\quad=-4\Bigg((q_1^+\times-1\frac{q_2^\perp}{q_2^+}+q_1^\perp)(q_2^+\times-1\frac{q_1^\perp}{q_1^+}+q_2^\perp)\\
&\qquad\quad+(q_2^+\times-1\frac{q_1^\perp}{q_1^+}+q_2^\perp)(q_1^+\times-1\frac{q_2^\perp}{q_2^+}+q_1^\perp)\Bigg)A^\mu(q_3)A_\mu(-q_3)\\
&\quad=\frac{-8\kappa^2}{x(1-x)}A^\mu(q_3)A_\mu(-q_3),
\end{aligned}
\tag{5.96}
$$

and

$$
\begin{aligned}
&2(q_2-q_1)_\mu\Big(q_{1\rho}d^{\rho\beta}(q_2)d_{\beta\nu}(q_1)-q_{2\rho}d^{\rho\beta}(q_1)d_{\beta\nu}(q_2)\Big)\\
&+2(q_2-q_1)_\nu\Big(q_{1\beta}d^{\beta\rho}(q_2)d_{\rho\mu}(q_1)-q_{2\beta}d^{\beta\rho}(q_1)d_{\rho\mu}(q_2)\Big)A^\mu(q_3)A^\nu(-q_3)\\
&=2(q_2-q_1)^\perp\epsilon_\sigma^\perp(q_3)\Big(\frac{q_1^+q_2^\perp-q_2^+q_1^\perp}{q_2^+}-\frac{q_2^+q_1^\perp-q_1^+q_2^\perp}{q_1^+}\Big)\\
&\qquad+2(q_2-q_1)^\perp\epsilon_\sigma^\perp(-q_3)\Big(\frac{q_1^+q_2^\perp-q_2^+q_1^\perp}{q_2^+}-\frac{q_2^+q_1^\perp-q_1^+q_2^\perp}{q_1^+}\Big)A^\mu(q_3)A_\mu(-q_3)\\
&=\frac{8\kappa^2}{x(1-x)}A^\mu(q_3)A_\mu(-q_3)
\end{aligned}
\tag{5.97}
$$

Under the integral, $2(q_2-q_1)_\mu(q_2-q_1)_\nu\epsilon_\sigma^\mu(q)\epsilon_{\sigma'}^\nu(q)=4\kappa^2\ \delta_{\sigma\sigma'}$ such that

$$
\begin{aligned}
&\int d^2\kappa\ d^{\alpha\rho}(q_1)F_{\alpha\beta\mu}(q_1,q_2,q)d^{\beta\kappa}(q_2)F_{\rho\kappa\nu}(-q_1,-q_2,-q)A^\mu(q)A^\nu(-q)\\
&\qquad\qquad=-4\int d^2\kappa\ \kappa^2\left(1+\frac{1}{x^2}+\frac{1}{(1-x)^2}\right)A^\mu(q)A_\mu(-q)
\end{aligned}
\tag{5.98}
$$

Therefore,

$$H_{(\delta m_g^2)_2} = \int_q (\delta m_g^2)_2 A_\mu^a(q) A_a^\mu(-q), \tag{5.99}$$

where

$$\begin{aligned}
I_{g,2}(s_r) &= -4C_A \int \frac{dx d^2\kappa}{16\pi^3\ x(1-x)} \frac{\kappa^2}{\mathcal{M}_{gg}^2(x,\kappa) - m_g^2} \frac{P_{gg}(x)}{2x(1-x)} \exp\left[\frac{-2s_r}{(q^+)^2}\Big(\mathcal{M}_{gg}^2(x,\kappa) - m_g^2\Big)^2\right] \\
&= -\frac{C_A}{4\pi^2} \int_0^1 dx \int\limits_{\frac{m_g^2}{x(1-x)}}^{\infty} d\mathcal{M}^2 \frac{\mathcal{M}^2 x(1-x) - m_g^2}{\mathcal{M}^2 - m_g^2} \frac{P_{gg}(x)}{2x(1-x)} \exp\left[\frac{-2s_r}{(q^+)^2}\Big(\mathcal{M}^2 - m_g^2\Big)^2\right] \\
&= -\frac{C_A}{4\pi^2} \int_{4m_g^2}^{\infty} d\mathcal{M}^2 \frac{1}{\mathcal{M}^2 - m_g^2} \exp\left[\frac{-2s_r}{(q^+)^2}\Big(\mathcal{M}^2 - m_g^2\Big)^2\right] \\
&\quad \times \int_{x_1}^{x_2} dx \left(\frac{\mathcal{M}^2 x(1-x) - m_g^2}{x(1-x)}\right)\left(1 + \frac{1}{x^2} + \frac{1}{(1-x)^2}\right)
\end{aligned} \tag{5.100}$$

where $P_{gg}(x)$ is the Altarelli-Parisi [AP77, GRG15, GVGR23] gluon splitting function, given as

$$P_{gg}(z) = 2N_c\left(\frac{1-z}{z} + \frac{z}{1-z} + z(1-z)\right), \tag{5.101}$$

where the roots are

$$(x_1, x_2) = \left(\frac{\mathcal{M}^2 - \sqrt{\mathcal{M}^4 - 4m_g^2\mathcal{M}^2}}{\mathcal{M}^2}, \frac{\mathcal{M}^2 + \sqrt{\mathcal{M}^4 - 4m_g^2\mathcal{M}^2}}{\mathcal{M}^2}\right).$$

After the dx integration we get two integrals, where the variable substitution $z = \mathcal{M}^2 - m_g^2$ was used:

$$\begin{aligned}
I_{g,2}(s_r) = -\frac{N_c}{4\pi^2}\Bigg\{ &- \int_{3m_g^2}^{\infty} dz \sqrt{(z+m_g^2)(z-3m_g^2)} e^{-s_r' z^2} \\
&- 12m_g^2 \int_{3m_g^2}^{\infty} dz \frac{1}{z} \text{arctanh}\left(\sqrt{1 - \frac{4m_g^2}{z+m_g^2}}\right) e^{-s_r' z^2}\Bigg\}.
\end{aligned} \tag{5.102}$$

The same procedure can be used to compute both of these integrals. That is,

extract the divergent part by expanding the integrand (with $s_r = 0$) about $z \to \infty$.

$$\begin{aligned}
&\int_{3m_g^2}^{\infty} dz \sqrt{(z+m_g^2)(z-3m_g^2)} \exp\left[\frac{-2s_r}{(q^+)^2} z^2\right] \\
&= \int_{3m_g^2}^{\infty} dz \left[\sqrt{(z+m_g^2)(z-3m_g^2)} - \Big(z - m_g^2 - \frac{2m_g^4}{z}\Big)\right] \\
&+ \int_{3m_g^2}^{\infty} dz \Big(z - m_g^2 - \frac{2m_g^4}{z}\Big) \exp\left[\frac{-2s_r}{(q^+)^2} z^2\right] \\
&= m_g^4(1 - \log 9) + \frac{1}{2s_r} - m_g^2 \frac{\sqrt{\pi}}{2\sqrt{s_r}} + m_g^4 \left(\gamma + \log\Big(9m_g^4 s_r\Big) - \frac{3}{2}\right) + o(1) \qquad (5.103)
\end{aligned}$$

In the first integral after the equal sign, the limit can be taken inside the integral by the dominated convergence theorem A.0.1 with the dominating function $\sqrt{(z+m_g^2)(z-3m_g^2)} - \Big(z - m_g^2 - \frac{2m_g^4}{z}\Big)$ which converges to $m_g^4(1 - \log 9)$.

To extract the divergent part of $\operatorname{arctanh}(x)$, it is easier to write this in terms of log since the function we're interested in expanding is a composite function and $\operatorname{arctanh}(x)$ is not defined $\forall x \in \mathbb{R}$. Therefore,

$$\frac{1}{z}\operatorname{arctanh}\left(\sqrt{1 - \frac{4m_g^2}{z+m_g^2}}\right) = \frac{1}{z}\log\Big(\frac{z}{m_g^2}\Big) + \mathcal{O}(z^{-2}) \qquad (5.104)$$

Then,

$$\begin{aligned}
&\int_{3m_g^2}^{\infty} dz \frac{1}{z} \operatorname{arctanh}\left(\sqrt{1 - \frac{4m_g^2}{z+m_g^2}}\right) \exp\left[\frac{-2s_r}{(q^+)^2} z^2\right] \\
&\quad = \underbrace{\int_{3m_g^2}^{\infty} dz \frac{1}{z}\left(\operatorname{arctanh}\left(\sqrt{1 - \frac{4m_g^2}{z+m_g^2}}\right) - \frac{1}{2}\log\Big(\frac{z}{m_g^2}\Big)\right)}_{\frac{1}{36}\left(9\log^2(3) - 2\pi^2\right)} \\
&\quad + \frac{1}{2}\int_{3m_g^2}^{\infty} dz \frac{1}{z} \log\Big(z/m_g^2\Big) \exp\left[\frac{-2s_r}{(q^+)^2} z^2\right] \\
&\quad - \frac{1}{2}\log^2(z_0)^2 + \frac{1}{4}\log^2(3) - \frac{5\pi^2}{144} \qquad (5.105)
\end{aligned}$$

The limit is implicitly brough into the integral in the first integral after the equal

sign by the dominated convergence theorem A.0.1 with the dominating function, $\frac{1}{z}\left(\operatorname{arctanh}\left(\sqrt{1-\frac{4m_g^2}{z+m_g^2}}\right)-\frac{1}{2}\log\left(\frac{z}{m_g^2}\right)\right)$ which converges to the value under the brace. The second integral is computed in the limit that $s_r \to 0$, and evaluates to

$$\begin{aligned}
&\int_{3m_g^2}^{\infty} dz \frac{\ln z/m_g^2}{2z} e^{-s_r' z^2} \\
&\quad = \frac{1}{2}\Bigg\{\frac{1}{8}\left(\gamma - \log\Big(\frac{(q^+)^2}{2s_r}\Big)\right)^2 + \frac{1}{2}\log\Big(m_g^2\Big)\left(\gamma - \log\Big(\frac{(q^+)^2 m_g^2}{2s_r}\Big)\right) \\
&\qquad + \frac{\pi^2}{48} - \frac{1}{2}\log^2(3m_g^2)\Bigg\} + o(1)
\end{aligned} \tag{5.106}$$

All together,

$$\begin{aligned}
I_{g,2}(s_r) = -\frac{C_A}{4\pi^2}\Bigg\{ & m_g^4(\log 9 - 1) - \frac{1}{2s_r} + m_g^2\frac{\sqrt{\pi}}{2\sqrt{s_r}} - m_g^4\left(\gamma + \log\Big(9m_g^4 s_r\Big) - \frac{3}{2}\right) \\
& - 12m_g^2\left(\frac{1}{4}\log^2(3) + \frac{1}{16}\left(\gamma - \log\Big(\frac{(q^+)^2}{2s_r}\Big)\right)^2 + \frac{1}{4}\log\Big(m_g^2\Big)\left(\gamma - \log\Big(\frac{(q^+)^2 m_g^2}{2s_r}\Big)\right)\right. \\
& \left. - \frac{13\pi^2}{288} - \frac{1}{2}\log^2(3m_g^2)\right)\Bigg\}
\end{aligned} \tag{5.107}$$

Again motivated by the calculation in Chapter 4, we take the counterterm to be $X_{\delta m_g^2}(s_r) = I_{g,1}(s_r) + I_{g,2}(s_r)$. Therefore, the gluon mass term in the Hamiltonian is given in terms of λ as

$$H_{\delta m_g^2}(s) = \frac{1}{2}\int_q : A^\mu(-q)\Big(m_g^2(s) + (\vec{q}^{\perp})^2\Big)A_\mu(q) :, \tag{5.108}$$

where

$$
\begin{aligned}
m_g^2(s,q) &= I_{g,1}(s,q) + I_{g,2}(s,q) \\
&= \int \frac{dx d^2\kappa}{16\pi^3 x(1-x)} \Bigg(\frac{\mathcal{M}^2_{q\bar{q}}(x,\kappa^2) - 2\kappa^2}{\mathcal{M}^2_{q\bar{q}}(x,\kappa^2) - m_g^2} \exp\Big[\frac{-2s}{(q^+)^2}\Big(\mathcal{M}^2_{q\bar{q}}(x,\kappa^2) - m_g^2\Big)\Big] \\
&\quad - 4\kappa^2 \frac{1 + x^{-1} + x^{-2}}{\mathcal{M}^2_{gg}(x,\kappa^2) - m_g^2} \exp\Big[\frac{-2s}{(q^+)^2}\Big(\mathcal{M}^2_{gg}(x,\kappa^2) - m_g^2\Big)\Big] \Bigg)
\end{aligned}
\tag{5.109}
$$

5.3.2 Quark Mass Loop

The quark mass loop in Fig. 5.58 is given by:

$$
\begin{aligned}
H_{\delta m_q^2}(s,s_r) = C_F \int\limits_{q_1,q_2,q_3} & \frac{\theta(q_2^+)\theta(q_3^+)}{q_2^+ q_3^+} \frac{1}{q_1^- + q_2^- + q_3^-} \delta(q_1 - q_2 - q_3) \\
& \times : \bar{\psi}(q_1)\gamma^\mu d_{\mu\nu}(q_3)\Big(\gamma^\rho q_{2\rho} + m_0\Big)\gamma^\nu \psi(q_1) : \\
& \times \Big(f^2(s; q_1 - q_2 - q_3) - 1\Big) r^2(s_r; q_1 - q_2 - q_3).
\end{aligned}
\tag{5.110}
$$

The Gamma matrices can be simplified by the identities:

$$
1.\ \gamma^\mu \gamma^\nu d_{\mu\nu}(q) = -2\mathbb{1} \tag{5.111}
$$

$$
2.\ \gamma^\mu \gamma^\rho \gamma^\nu d_{\mu\nu}(q) = \frac{2}{q^+}\Big(\gamma^+ q^\rho + g^{+\rho}\gamma\cdot q\Big) - \frac{2m_g^2}{(q^+)^2}\gamma^+ g^{+\rho} \tag{5.112}
$$

Relative momentum coordinates are useful. That is,

$$
x = \frac{q_2^+}{q_2^+ + q_3^+} \tag{5.113}
$$

$$
\kappa^\perp = (1-x)q_2^\perp - x q_3^\perp \tag{5.114}
$$

$$
= q_2^\perp - x q_1^\perp \tag{5.115}
$$

Under the $\delta(q_1 - q_2 - q_3)$, $q_2^+ + q_3^+$ can be replaced with q_1^+, and the same with $q_2^\perp + q_3^\perp$ with $q_1^\perp$.

Then

$$\begin{aligned}
&\bar{u}(q_1)\gamma^\mu d_{\mu\nu}(q_3)\Big(\gamma^\rho q_{2\rho} + m_q\Big)\gamma^\nu u(q_1) \\
&\quad = \bar{u}(q_1)\gamma^\mu\gamma^\rho\gamma^\nu d_{\mu\nu}(q_3) q_{2\rho} u(q_1) + m_q \bar{u}(q)\gamma^\mu\gamma^\nu d_{\mu\nu}(q_3) u(q) \\
&\quad = \frac{2q_2^+}{q_3^+}\bar{u}(q)\gamma^\mu u(q) q_{3\mu} + \left(\frac{2q_3\cdot q_2}{q_3^+} - \frac{2m_g^2 q_2^+}{(q_3^+)^2}\right)\bar{u}(q)\gamma^+ u(q) - 2m_q\bar{u}(q)u(q).
\end{aligned} \tag{5.116}$$

Now, the following relations can be invoked:

$$\begin{aligned}
2\ q_2\cdot q_3 &= \mathcal{M}_{qg}^2(x,\kappa^2) - m_q^2 - m_g^2 \\
2\ q\cdot q_3 &= x\Big(\mathcal{M}_{qg}^2(x,\kappa^2) - m_q^2\Big) + m_g^2
\end{aligned} \tag{5.117}$$

to obtain

$$\begin{aligned}
&\bar{u}(q_1)\gamma^\mu d_{\mu\nu}(q_3)\Big(\gamma^\rho q_{2\rho} + m_q\Big)\gamma^\nu u(q_1) \\
&\quad = 2\left(\frac{x}{1-x}\Big(x(\mathcal{M}^2 - m_q^2) + m_g^2\Big) + \frac{1}{1-x}\Big(\mathcal{M}^2 - m_q^2 - m_g^2 - \frac{2m_g^2 x}{1-x}\Big)\right) - 4m_q^2 \\
&\quad = 2\left(\Big(\frac{2}{1-x} - 1 - x\Big)\Big(\mathcal{M}^2 - m_q^2 - \frac{m_g^2}{1-x}\Big)\right) - 4m_q^2
\end{aligned} \tag{5.118}$$

Therefore, the quark mass loop can be written:

$$H_{\delta m_q^2}(s,s_r) = \int_{q_1}\frac{\delta m_q^2(s,s_r;q_1)}{q_1^+}\frac{\bar{\psi}(q_1)\gamma^+\psi(q_1)}{2}, \tag{5.119}$$

where

$$\begin{aligned}
\delta m_q^2(s,s_r;q_1) &= C_F\int_{q_2,q_3}\delta(q_1-q_2-q_3)\frac{\theta(q_2^+)\theta(q_3^+)}{q_2^+ q_3^+}\frac{1}{q_1^- + q_2^- + q_3^-} \\
&\quad\times 2\left(\Big(\frac{2}{1-x} - 1 - x\Big)\Big(\mathcal{M}^2 - m_q^2 - \frac{m_g^2}{1-x}\Big)\right) - 4m_q^2 \\
&\quad\times\Big(f^2(s;q_1-q_2-q_3) - 1\Big)r^2(s_r;q_1-q_2-q_3) \\
&\quad\equiv I_Q(s+s_r) - I_Q(s_r).
\end{aligned} \tag{5.120}$$

We now must simplify $I_Q(s_r)$:

$$I_Q(s_r) = \int_{q_2,q_3} \delta(q_2+q_3-q_1)\frac{\theta(q_2^+)\theta(q_3^+)}{q_2^+ q_3^+}\frac{1}{q_2^- + q_3^- - q_1^-} \times \Big(\frac{\kappa^2 + m_q^2(1-x)^2}{x}\Big)\exp\Big[-2s_r(q_2^- + q_3^- - q_1^-)^2\Big]. \tag{5.121}$$

Define the change of variables: $y = q_2^+ + q_3^+, x = q_2^+/y, \kappa^\perp = (1-x)q_2^\perp - xq_3^\perp$, and $y^\perp = q_2^\perp + q_3^\perp$, where x and $\kappa^\perp$ are the relative momentum variables for two particles (relative to the 'parent' quark with momentum q_1). The Jacobian of this change of variables is $\mathbf{J} = y$.

$$I_Q(s_r) = \int \frac{y\ dy\ dx\ dy^\perp\ d\kappa^\perp}{16\pi^3}\ 16\pi^3\delta(y-q_1^+)\delta^2(y^\perp - q_1^\perp) \times \frac{1}{xq_1^+(1-x)q_1^+}\Big(\frac{\kappa^2+m_q^2(1-x)^2}{x}\Big) \times \frac{q_1^+}{(q_2+q_3)^2 - q_1^2}\exp\left[\frac{-2s_r}{(q_1^+)^2}\Big((q_2+q_3)^2 - q_1^2\Big)^2\right], \tag{5.122}$$

where $q_2^- + q_3^- - q_1^- = ((q_2+q_3)^2 - q_1^2)/q_1^+$. The integrals over dy and $dy^\perp$ are trivial because of the deltas:

$$I_Q(s_r) = \int \frac{dx\ d^2\kappa}{x(1-x)}\frac{1}{\mathcal{M}_{23}^2(x,\kappa) - m_q^2}\Big(\frac{\kappa^2+m_q^2(1-x)^2}{x}\Big)\exp\left[\frac{-2s_r}{(q_1^+)^2}\Big(\mathcal{M}_{23}^2(x,\kappa) - m_q^2\Big)^2\right], \tag{5.123}$$

where

$$\mathcal{M}_{23}^2(x,\kappa) = \frac{m_q^2+\kappa^2}{x} + \frac{m_g^2+\kappa^2}{1-x}.$$

After writing κ^2 in terms of $\mathcal{M}_{23}^2$, and changing the $d^2\kappa$ integral to polar

coordinates of $\kappa d\kappa d\phi$, the integral becomes:

$$
\begin{aligned}
I_Q(s_r) &= \int_0^1 dx \int_{\mathcal{M}_{23}^2(x,0)}^{\infty} d\mathcal{M}^2 \frac{(\mathcal{M}^2 - m_q^2)(1-x) - m_g^2}{\mathcal{M}^2 - m_q^2} \exp\left[\frac{-2s_r}{(q_1^+)^2}\Big(\mathcal{M}^2 - m_q^2\Big)^2\right] \\
&= \underbrace{\int_0^1 dx \int_{\mathcal{M}_{23}^2(x,0)}^{\infty} d\mathcal{M}^2 \ (1-x) \exp\left[\frac{-2s_r}{(q_1^+)^2}\Big(\mathcal{M}^2 - m_q^2\Big)^2\right]}_{I_1} \\
&\quad - m_g^2 \underbrace{\int_0^1 dx \int_{\mathcal{M}_{23}^2(x,0)}^{\infty} d\mathcal{M}^2 \frac{1}{\mathcal{M}^2 - m_q^2} \exp\left[\frac{-2s_r}{(q_1^+)^2}\Big(\mathcal{M}^2 - m_q^2\Big)^2\right]}_{I_2}. \qquad (5.124)
\end{aligned}
$$

The integration region for I_Q is the shaded region in Fig. 5.1. As it is currently written, the integration orders show that as you integrate along x from 0 to 1, you integrate along $\mathcal{M}^2$ from $\mathcal{M}^2(x,0)$ to ∞, shown as the vertical dashed line. Alternatively, the bounds can be changed if the integration region is also changed, that is, if you integrate along $\mathcal{M}^2$ from $\mathcal{M}^2_{min}$ to ∞ and for each $\mathcal{M}^2$ value, you integrate in x along the horizontal dashed line. $\mathcal{M}^2_{min.}$ is defined to be the value of $\mathcal{M}^2$ evaluated at $x_{min.} = m_q/(m_q+m_g)$, which happens to be $\mathcal{M}^2_{min} = (m_q+m_g)^2$.

After switching the order of integration and defining $\tilde{s} = 2s_r/(q_1^+)^2$,

$$
\begin{aligned}
I_2 &= \int_{m_g(m_g+2m_q)}^{\infty} d\mathcal{M}^2 \int_{x_1}^{x_2} dx \frac{1}{\mathcal{M}^2 - m_q^2} e^{-\tilde{s}\left(\mathcal{M}^2 - m_q^2\right)^2} \\
&= \int_{m_g(m_g+2m_q)}^{\infty} d\mathcal{M}^2 \frac{1}{\mathcal{M}^2 - m_q^2} e^{-\tilde{s}\left(\mathcal{M}^2 - m_q^2\right)^2} \cdot (x_2 - x_1) \\
&= \int_{m_g(m_g+2m_q)}^{\infty} d\mathcal{M}^2 \frac{\sqrt{(\mathcal{M}^2 + m_q^2 - m_g^2)^2 - 4\mathcal{M}^2 m_q^2}}{\mathcal{M}^2(\mathcal{M}^2 - m_q^2)} e^{-\tilde{s}\left(\mathcal{M}^2 - m_q^2\right)^2} \qquad (5.125)
\end{aligned}
$$

where

$$
\begin{aligned}
x_1 &= \frac{\mathcal{M}^2 - m_q^2 - m_g^2 - \sqrt{(\mathcal{M}^2 - m_q^2 - m_g^2)^2 - 4\mathcal{M}^2 m^2}}{2\mathcal{M}^2} \\
x_2 &= \frac{\mathcal{M}^2 - m_q^2 - m_g^2 + \sqrt{(\mathcal{M}^2 - m_q^2 - m_g^2)^2 - 4\mathcal{M}^2 m^2}}{2\mathcal{M}^2}
\end{aligned}
$$

Lebesque's dominated convergence theorem A.0.1 allows the limit $\tilde{s} \to 0$ to be taken inside the integral by the dominating function $\frac{\sqrt{(y+m_q^2-m_g^2)^2 - 4m_q^2 y}}{y(y-m_q^2)}$, leading

to an integral of a rational function (with $y = \mathcal{M}^2$). Using Euler's first substitution,

$$I_2 = \frac{1}{2m_q^2} \log\left(1 + \frac{2m_q^3(m_q - 2m_g)}{m_g^2(1 + 4m_q m_g + m_g^2) + m_q^2(4m_g^2 - 1)}\right) \tag{5.126}$$

The order of integration in I_1 can also be changed:

$$\begin{aligned} I_1 &= \int\limits_{m_g(m_g+2m_q)}^{\infty} d\mathcal{M}^2 \exp\left[\frac{-2s_r}{(q_1^+)^2}\Big(\mathcal{M}^2 - m_q^2\Big)^2\right] \int_{x_1}^{x_2} dx(1-x) \\ &= \int\limits_{m_g(m_g+2m_q)}^{\infty} d\mathcal{M}^2 \frac{(\mathcal{M}^2 - m_q^2 + m_g^2)\sqrt{(\mathcal{M}^2 + m_q^2 - m_g^2)^2 - 4m_q^2\,\mathcal{M}^2}}{2(\mathcal{M}^2)^2} \\ &\qquad \times \exp\left[\frac{-2s_r}{(q_1^+)^2}\Big(\mathcal{M}^2 - m_q^2\Big)^2\right] \\ &= \frac{1}{2}\int\limits_{m_g(m_g+2m_q)}^{\infty} d\mathcal{M}^2\Big(1 - \frac{m_q^2 - m_g^2}{\mathcal{M}^2}\Big)\sqrt{\left(1 - \frac{2(m_q^2 + m_g^2)}{\mathcal{M}^2} + \frac{(m_q^2 - m_g^2)^2}{\mathcal{M}^4}\right)} \\ &\qquad \times \exp\left[\frac{-2s_r}{(q_1^+)^2}\Big(\mathcal{M}^2 - m_q^2\Big)^2\right] \end{aligned} \tag{5.127}$$

We can Taylor expand the integrand by

$$\begin{aligned} &\frac{1}{2}\Big(1 - \frac{m_q^2 - m_g^2}{\mathcal{M}^2}\Big)\sqrt{\left(1 - \frac{2(m_q^2 + m_g^2)}{\mathcal{M}^2} + \frac{(m_q^2 - m_g^2)^2}{\mathcal{M}^4}\right)} \\ &\qquad = \frac{1}{2} - \frac{m_q^2}{\mathcal{M}^2} + \frac{1}{2}\frac{\Big(m_q^4 - m_g^4 - 2m_q^2 m_g^2\Big)}{\mathcal{M}^4} + \mathcal{O}\Big(\frac{1}{\mathcal{M}^6}\Big) \end{aligned} \tag{5.128}$$

The first two terms in this expansion cause a divergence when $s_r \to 0$ since they fail the p-test for convergence. The third term (and all higher orders) will pass the

p-test for convergence when the regulator is removed. Therefore,

$$\begin{aligned}
&\frac{1}{2}\int\limits_{m_g(m_g+2m_q)}^{\infty} d\mathcal{M}^2 \frac{(\mathcal{M}^2 - m_q^2 + m_g^2)\sqrt{(\mathcal{M}^2 + m_q^2 - m_g^2)^2 - 4m_q^2\ \mathcal{M}^2}}{\mathcal{M}^4} \\
&\qquad\qquad \times \exp\left[\frac{-2s_r}{(q_1^+)^2}\Big(\mathcal{M}^2 - m_q^2\Big)^2\right] \\
&= \int\limits_{m_g(m_g+2m_q)}^{\infty} d\mathcal{M}^2\Big(\frac{1}{2} - \frac{m_q^2}{\mathcal{M}^2}\Big)\exp\left[\frac{-2s_r}{(q_1^+)^2}\Big(\mathcal{M}^2 - m_q^2\Big)^2\right] \\
&+ \frac{1}{2}\int\limits_{m_g(m_g+2m_q)}^{\infty} d\mathcal{M}^2\left(\frac{(\mathcal{M}^2 - m_q^2 + m_g^2)\sqrt{(\mathcal{M}^2 + m_q^2 - m_g^2)^2 - 4m_q^2\ \mathcal{M}^2}}{\mathcal{M}^4} - 1 + 2\frac{m_q^2}{\mathcal{M}^2}\right) \\
&\qquad\qquad \times \exp\left[\frac{-2s_r}{(q_1^+)^2}\Big(\mathcal{M}^2 - m_q^2\Big)^2\right]. \qquad (5.129)
\end{aligned}$$

The first integral above diverges with $s_r \to 0$, while the second integral is finite at $s_r = 0$ because the divergence determined by expanding the integrand is subtracted out (and it passes the dominated convergence theorem A.0.1).

Therefore,

$$\begin{aligned}
&\frac{1}{2}\int\limits_{m_g(m_g+2m_q)}^{\infty} d\mathcal{M}^2\left(\frac{(\mathcal{M}^2 - m_q^2 + m_g^2)\sqrt{(\mathcal{M}^2 + m_q^2 - m_g^2)^2 - 4m_q^2\ \mathcal{M}^2}}{\mathcal{M}^4} - 1 + 2\frac{m_q^2}{\mathcal{M}^2}\right) \\
&= 4m_q^2\log\Big(m_q^2\Big) - 2m_g^2 + m_q^2\log(4) \\
&\quad + \frac{m_q^2\Big(m_q\sqrt{m_q^2 - 4m_q m_g} - 4m_g^2\Big) + 2m_q m_g\Big(m_q\sqrt{m_q^2 - 4m_q m_g} - 2m_g^2\Big) - m_g^4}{m_g(m_g + 2m_q)} \\
&\quad + 2m_q^2\log\left[m_g(m_q + 2m_g)\Big(m_q^2 - 2m_q m_g + m_q\sqrt{m_q^2 - 4m_q m_g}\Big)\right] \\
&\quad + 2m_q^2\ \mathrm{arctanh}\left(\frac{m_g^2 + 2m_g m_q - m_q\sqrt{m_q^2 - 4m_q m_g}}{m_q^2 - m_g^2}\right) \qquad (5.130)
\end{aligned}$$

$$\int\limits_{m_g(m_g+2m_q)}^{\infty} d\mathcal{M}^2\Big(\frac{1}{2}-\frac{m_q^2}{\mathcal{M}^2}\Big)\exp\left[\frac{-2s_r}{(q_1^+)^2}\Big(\mathcal{M}^2-m_q^2\Big)^2\right]$$
$$=\frac{1}{2}\int\limits_{m_g(m_g+2m_q)}^{\infty} d\mathcal{M}^2\exp\left[\frac{-2s_r}{(q_1^+)^2}\Big(\mathcal{M}^2-m_q^2\Big)^2\right]$$
$$-m_q^2\int\limits_{m_g(m_g+2m_q)}^{\infty}\frac{d\mathcal{M}^2}{\mathcal{M}^2}\exp\left[\frac{-2s_r}{(q_1^+)^2}\Big(\mathcal{M}^2-m_q^2\Big)^2\right] \tag{5.131}$$

$$\frac{1}{2}\int\limits_{m_g(m_g+2m_q)}^{\infty} d\mathcal{M}^2\exp\left[\frac{-2s_r}{(q_1^+)^2}\Big(\mathcal{M}^2-m_q^2\Big)^2\right]$$
$$=\frac{q_1^+\sqrt{\pi}}{2\sqrt{2s_r}}\Big(1+\mathrm{erf}\Big[\frac{2s_r}{(q_1^+)^2}(m_q^2-m_g^2-2m_gm_q)\Big]\Big)$$
$$=\frac{q_1^+\sqrt{\pi}}{2\sqrt{2s_r}}+o(1) \tag{5.132}$$

Let $u=\sqrt{\frac{2s_r}{(q_1^+)^2}}\Big(\mathcal{M}^2-m_q^2\Big)$. Then $du=z\ d\mathcal{M}^2$ where $z=\sqrt{\frac{2s_r}{(q^+)^2}}$

$$\int\limits_{m_g(m_g+2m_q)}^{\infty}\frac{d\mathcal{M}^2}{\mathcal{M}^2}\exp\left[z^2\Big(\mathcal{M}^2-m_q^2\Big)^2\right]$$
$$=\int\limits_{z(m_g^2-m_q^2+2m_qm_g)}^{\infty} du\frac{1}{u+z\ m_q^2}e^{-u^2}$$
$$=\int\limits_{z(m_g^2-m_q^2+2m_qm_g)}^{\infty} du\ \Big(\frac{1}{u}e^{-u^2}+o(1)\Big)$$
$$=\frac{1}{2}\Gamma\Big(0,z^2(m_g^2-m_q^2+2m_qm_g)^2\Big)$$
$$=\frac{1}{2}\Big(-\gamma-\ln\Big(\frac{2s_r}{(q_1^+)^2}(m_g^2-m_q^2+2m_qm_g)^2\Big)+o(1)\Big) \tag{5.133}$$

All together,

$$
\begin{aligned}
I_Q(s_r) = &\frac{1}{2m_q^2}\log\left(1+\frac{2m_q^3(m_q-2m_g)}{m_g^2(1+4m_qm_g+m_g^2)+m_q^2(4m_g^2-1)}\right)\\
&+4m_q^2\log\Big(m_q^2\Big)-2m_g^2+m_q^2\log(4)+2m_q^2\log(m_g(m_g+2m))\\
&+\frac{-m_g^4+m_q^2\Big(m_q\sqrt{m_q^2-4m_qm_g}-4m_g^2\Big)+2m_qm_g\Big(m_q\sqrt{m_q^2-4m_qm_g}-2m_g^2\Big)}{m_g(m_g+2m_q)}\\
&+2m_q^2\log\left[m_g(m_q+2m_g)\Big(m_q^2-2m_qm_g+m_q\sqrt{m_q^2-4m_qm_g}\Big)\right]\\
&+2m_q^2\ \mathrm{arctanh}\left(\frac{m_g^2+2m_gm_q-m_q\sqrt{m_q^2-4m_qm_g}}{m_q^2-m_g^2}\right)\\
&+\frac{q_1^+\sqrt{\pi}}{2\sqrt{2s_r}}+\frac{1}{2}\Big(-\gamma-\ln\Big(\frac{2s_r}{(q_1^+)^2}(m_g^2-m_q^2+2m_qm_g)^2\Big)+o(1). \qquad (5.134)
\end{aligned}
$$

Motivated by the calculation in Chapter 4, we take the counterterm to be $X_{\delta m_q^2}(s_r) = I_q(s_r)$. Therefore, the quark mass term in the Hamiltonian is given in terms of s as

$$H_{\delta m_q^2}(s) = \int_q \frac{m_q^2(s)+(q^\perp)^2}{q^+} : \bar\psi(q)\frac{\gamma^+}{2}\psi(q) :, \qquad (5.135)$$

where

$$m_q^2(s) = m_q^2 + \int \frac{dxd^2\kappa}{x(1-x)}\frac{\kappa^2+m_q^2(1-x)^2}{x(\mathcal{M}_{qg}^2(x,\kappa)-m_q^2)}e^{-2s(\mathcal{M}_{qg}^2(x,\kappa)-m_q^2)^2/(q^+)^2} \qquad (5.136)$$

5.3.3 Small q^+ Singularities

The instantaneous and effective exchange terms all contain factors of $1/q^+$ or $1/(q^+)^2$, which have the ability to diverge as the limit $s_r \to 0$ is taken. The factors of q_i^+ which come from the field operators will not cause divergences because all $q_i^+ > 0$.

As an example of a term that diverges with $s_r \to 0$, consider the effective

gluon exchange with quark legs:

$$H_{\psi^4,\text{eff}}(s,s_r) = \int\limits_{\substack{q_1,q_2,q\\ q_3,q_4}} \delta(q_1+q_2+q)\delta(q_3+q_4-q)\frac{\theta(q^+)d_{\mu\nu}(q)}{q^+}$$
$$\times : \bar{\psi}(-q_1)\gamma^\mu T^a \psi(q_2)\bar{\psi}(-q_3)\gamma^\nu T_a \psi(q_4) :$$
$$\times \mathcal{R}\Big(s; \mathcal{Q}^-(q_1,q_2,q), \mathcal{Q}^-(q_3,q_4,-q)\Big)$$
$$\times r\Big(s_r; \mathcal{Q}^-(q_1,q,q)\Big) r\Big(s_r; \mathcal{Q}^-(q_3,q_4,-q)\Big) \qquad (5.137)$$

At first glance, it appears that the $1/q^+$ factor will cause problems, but it turns out this is actually not the source of the divergence. This can be seen by looking at

$$\begin{aligned}\frac{\mathcal{R}\Big(s; \mathcal{Q}^-(q_1,q_2,q), \mathcal{Q}^-(q_3,q_4,-q)\Big)}{q^+} &= \frac{1}{2q^+}\left(\frac{1}{q_1^- + q_2^- + q^-} - \frac{1}{q_3^- + q_4^- - q^-}\right)\\ &\quad\cdot\Big(f(s;\mathcal{Q}^-(q_1,q_2,q))\cdot f(s;\mathcal{Q}^-(q_3,q_4,-q))\\ &\quad - f^2(s;\mathcal{Q}^-(q_1,q_2,q_3,q_4))\Big)\\ &= \frac{1}{2}\left(\frac{1}{q^2-(q_1+q_2)^2} + \frac{1}{q^2-(q_3+q_4)^2}\right)\\ &\quad\cdot\Big(f(s;\mathcal{Q}^-(q_1,q_2,q))\cdot f(s;\mathcal{Q}^-(q_3,q_4,-q))\\ &\quad - f^2(s;\mathcal{Q}^-(q_1,q_2,q_3,q_4))\Big).\end{aligned} \qquad (5.138)$$

q is the momentum four-vector for the exchange gluon so $q^2 = m_g^2$. The denominators above will not vanish, even in the limit as $q^+ \to 0$. This is because $(q_1+q_2)^2 \geq 4m_q^2 \gg m_g^2$ or $(q_1+q_2)^2 \leq 0$ (see Chapter 2). Also, as $q^+ \to 0$, $q^- \to \infty$, which will send the two form factors that have explicit dependence on q^- to zero. Therefore, this is not the source of the divergence because it is finite in the limit $q^+ \to 0$.

To determine the divergence, define the quark part of the color current as

$J_q^{\mu a}(q_1,q_2,q) = \delta(q_1+q_2+q) : \bar{\psi}(-q_1)\gamma^\mu T^a \psi(q_2) :$, consider the expression

$$d_{\mu\nu}(q) J_q^{\mu a}(q_1,q_2,q) J_q^{\nu a}(q_3,q_4,-q).$$

This splits up into two pieces:

$$-g_{\mu\nu} J_q^{\mu a}(q_1,q_2,q) J_q^{\nu a}(q_3,q_4,-q) + \frac{\eta_\mu q_\nu + \eta_\nu q_\mu}{q^+} J_q^{\mu a}(q_1,q_2,q) J_q^{\nu a}(q_3,q_4,-q). \tag{5.139}$$

The first term has no factors of $1/q^+$, unlike the second term. We need to compute $\eta_\mu q_\nu J_q^{\mu a}(q_1,q_2,q) J_q^{\nu a}(q_3,q_4,-q)$ and $\eta_\nu q_\mu J_q^{\mu}(q_1,q_2,q) J_q^{\nu}(q_3,q_4,-q)$. First consider

$$\delta(q_1+q_2+q) \implies q_\mu = -q_{1\mu} - q_{2\mu} + \frac{1}{2}\eta_\mu (q_1^- + q_2^- + q^-) \tag{5.140}$$

and similarly for $\delta(q_3+q_4-q)$. Now

$$\begin{aligned} q_\mu J_q^{\mu a}(q_1,q_2,q) &= \Big(- q_{1\mu} - q_{2\mu} + \frac{1}{2}\eta_\mu (q_1^- + q_2^- + q^-)\Big) \delta(q_1+q_2+q) : \bar{\psi}(-q_1)\gamma^\mu T^a \psi(q_2) : \\ &= - : \bar{\psi}(-q_1)\gamma^\mu q_{1\mu} T^a \psi(q_2) : - : \bar{\psi}(-q_1)\gamma^\mu q_{2\mu} T^a \psi(q_2) : \\ &\qquad + \frac{q_1^- + q_2^- + q^-}{2} J_q^+(q_1,q_2,q) \\ &= \frac{q_1^- + q_2^- + q^-}{2} J_q^{+a}(q_1,q_2,q), \end{aligned} \tag{5.141}$$

where to obtain the last line, the Dirac equation (and its conjugate) are used to cancel the first two terms. Therefore,

$$\begin{aligned} &\frac{\eta_\mu q_\nu + \eta_\nu q_\mu}{q^+} J_q^{\mu a}(q_1,q_2,q) J_q^{\nu a}(q_3,q_4,-q) \\ &\qquad = \frac{1}{q^+}\Big(J_q^{+a}(q_1,q_2,q) q_\nu J_q^{\nu a}(q_3,q_4,-q) + q_\mu J_q^{\mu a}(q_1,q_2,q) J_q^{+a}(q_3,q_4,-q)\Big) \\ &\qquad = \frac{1}{q^+}\left(\frac{q^- - q_3^- - q_4^-}{2} + \frac{q_1^- + q_2^- + q^-}{2}\right) J_q^{+a}(q_1,q_2,q) J_q^{+a}(q_3,q_4,-q) \\ &\qquad = -\frac{(q_1+q_2)^2 + (q_3+q_4)^2}{2(q^+)^2} J_q^{+a}(q_1,q_2,q) J_q^{+a}(q_3,q_4,-q). \end{aligned} \tag{5.142}$$

Now, the combination

$$\frac{\mathcal{R}\Big(s;\mathcal{Q}^-(q_1,q_2,q),\mathcal{Q}^-(q_3,q_4,-q)\Big)}{q^+}d_{\mu\nu}J_q^{\mu a}(q_1,q_2,q)J_q^{\nu a}(q_3,q_4,-q) \tag{5.143}$$

splits into four pieces (all multiplied by the regular factor $\frac{1}{2}\Big((q^2-(q_1+q_2)^2)^{-1}+(q^2-(q_3+q_4)^2)^{-1}\Big)$):

1.

$$f\Big(s;\mathcal{Q}^-(q_1,q_2,q)\Big)f\Big(s;\mathcal{Q}^-(q_3,q_4,-q)\Big)g_{\mu\nu}J_q^{\mu a}(q_1,q_2,q)J_q^{\nu a}(q_3,q_4,-q)$$

2.

$$-f\Big(s;\mathcal{Q}^-(q_1,q_2,q)\Big)f\Big(s;\mathcal{Q}^-(q_3,q_4,-q)\Big)\frac{(q_1+q_2)^2+(q_3+q_4)^2}{2(q^+)^2}J_q^{+a}(q_1,q_2,q)J_q^{+a}(q_3,q_4,-q)$$

3.

$$f\Big(s;\mathcal{Q}^-(q_1,q_2,q_3,q_4)\Big)g_{\mu\nu}J_q^{\mu a}(q_1,q_2,q)J_q^{\nu a}(q_3,q_4,-q)$$

4.

$$f\Big(s;\mathcal{Q}^-(q_1,q_2,q_3,q_4)\Big)\frac{(q_1+q_2)^2+(q_3+q_4)^2}{2(q^+)^2}J_q^{+a}(q_1,q_2,q)J_q^{+a}(q_3,q_4,-q)$$

The first and third expressions do not contain any factors of powers of $1/q^+$ and consequently are finite at small q^+. At first glance, it appears that the second expression may lead to a problem because it is proportional to $1/(q^+)^2$; however, the form factors mitigate this divergence. To see this explicitly:

$$\lim_{q^+\to 0}\frac{e^{-s(q_1^-+q_2^-+q^-)^2}}{q^+}=\lim_{q^+\to 0}\frac{e^{-s\Big(q^2-(q_1+q_2)^2\Big)^2/(q^+)^2}}{q^+}=0. \tag{5.144}$$

Therefore, the second expression is not only finite as $q^+\to 0$, but approaches 0.

We now look at the fourth term and discover that this is the source of the

divergence. First, we evaluate $(q_1+q_2)^2$ and $(q_3+q_4)^2$ in the limit $q^+=0$:

$$\frac{1}{2}\left(\frac{1}{q^2-(q_1+q_2)^2}+\frac{1}{q^2-(q_3+q_4)^2}\right)\frac{(q_1+q_2)^2+(q_3+q_4)^2}{2}\bigg|_{q^+=0}. \tag{5.145}$$

This can be simplified by considering

$$(q_1+q_2)^2\big|_{q^+=0}=(q_1^+ + q_2^+)(q_1+q_2)^- - (q_1^\perp+q_2^\perp)^2=-(q^\perp)^2, \tag{5.146}$$

where the delta function in momentum was imposed. A similar result shows $(q_3+q_4)\big|_{q^+=0}=-(q^\perp)^2$.

One may think that the form factor in the fourth expression could regulate this divergence since the other four momenta depend on q_3 through the Dirac deltas $(\delta(q_1+q_2+q)\delta(q_3+q_4-q))$, but we can quickly show why this is incorrect:

$$\begin{aligned}\exp\Big(-s(q_1^-+q_2^-+q_3^-+q_4^-)^2\Big)&=\exp\Big(-s(q_1^-+q_2^-+q^-+q_3^-+q_4^--q^-)^2\Big)\\&=\exp\left[-s\left(\frac{q^2-(q_1+q_2)^2}{q^+}+\frac{(q_3+q_4)^2-q^2}{q^+}\right)^2\right].\end{aligned} \tag{5.147}$$

In the limit that $q^+\to 0$:

$$\begin{aligned}\lim_{q^+\to 0}\exp\left[-s\left(\frac{q^2-(q_1+q_2)^2}{q^+}+\frac{(q_3+q_4)^2-q^2}{q^+}\right)^2\right]&\\=\exp\left[\frac{-s}{(q^+)^2}\Big((q^\perp)^2-(q^\perp)^2\Big)^2\right]&\\=1&\end{aligned}$$

Therefore, the form factor will not regulate the factor of $1/(q^+)^2$. This term is the source of the small q^+ divergence as $s_r\to 0$. We want to include a counterterm that acts only at $q^+=0$, but otherwise is absent. Therefore excluding the form factor,

the fourth term has the following form in the limit of small q^+:

$$\frac{1}{2}\left(\frac{1}{q^2-(q_1+q_2)^2}+\frac{1}{q^2-(q_3+q_4)^2}\right)\frac{(q_1+q_2)^2+(q_3+q_4)^2}{2}\bigg|_{q^+=0}=\frac{-(q^\perp)^2}{m_g^2+(q^\perp)^2}. \tag{5.148}$$

To determine the counterterm, we consider the combination of the effective gluon exchange and the instantaneous gluon exchange, i.e. $H_{\psi^4}(s,s_r)$

$$\begin{aligned}\lim_{q^+\to 0} H_{\psi^4}(s,s_r) = \int_q \frac{1}{(q^+)^2}\Big(1-\frac{(q^\perp)^2}{m_g^2+(q^\perp)^2}\Big)e^{-2s_r\left(m_g^2+(q^\perp)^2\right)^2/(q^+)^2} \\ \cdot \int\limits_{q_1,q_2,q_3,q_4} \delta(q_1+q_2+q)\delta(q_3+q_4-q)J_q^+(q_1,q_2,q)J_q^+(q_3,q_4,-q) \\ \times f\Big(s;\mathcal{Q}^-(q_1,q_2,q_3,q_4)\Big)\end{aligned} \tag{5.149}$$

The integral over q^+ is

$$\left(1-\frac{(q^\perp)^2}{m_g^2+(q^\perp)^2}\right)\int_{-\infty}^{\infty}\frac{dq^+}{(q^+)^2}\exp\left[\frac{-2s_r}{(q^+)^2}\left(m_g^2+(q^\perp)^2\right)^2\right]=\frac{m_g^2}{\left(m_g^2+(q^\perp)^2\right)^2}\sqrt{\frac{\pi}{2s_r}}. \tag{5.150}$$

Therefore, we want to choose a counterterm which acts only at $q^+=0$ and will cancel out the term on the right hand side of the above equation. This leads us to the following counterterm:

$$\begin{aligned}X_{\psi^4}(s,s_r) = -\int\limits_{\substack{q_1,q_2,q\\ q_3,q_4}} \delta(q_1+q_2+q)\delta(q_3+q_4-q)f\Big(s;\mathcal{Q}^-(q_1,q_2,q_3,q_4)\Big) \\ \times\delta(q^+)\frac{m_g^2}{\left(m_g^2+(q^\perp)^2\right)^2}\sqrt{\frac{\pi}{2s_r}}J_q^+(q_1,q_2,q)J_q^+(q_3,q_4,-q)\end{aligned} \tag{5.151}$$

The same procedure can be applied to all gluon exchange vertices (effective + instantaneous) to determine a similar counterterm.

Next, we must determine if counterterms are necessary for the fermion exchange terms. Combining the effective and instantaneous quark exchange terms,

recall:

$$H_{\bar{\psi}AA\psi}(s,s_r) = \int\limits_{\substack{q_1,q_2,q\\ q_3,q_4}} \delta(q_1+q_2+q)\delta(q_3+q_4-q) r\Big(s_r;\mathcal{Q}^-(q_1,q_2,q)\Big) r\Big(s_r;\mathcal{Q}^-(q_3,q_4,-q)\Big) \\ \times :\bar{\psi}(-q_1)\gamma_\mu T^a A^\mu(q_2)\Pi_{\mu\nu}\Big(s;q_1,q_2,q,q_3,q_4\Big)\gamma_\nu T^b A^\nu_b(q_3)\psi(q_4):, \tag{5.152}$$

where

$$\Pi_{\mu\nu}\Big(s;q_1,q_2,q,q_3,q_4\Big) = \frac{\gamma^+}{2q^+} e^{-s\Big(q_1^-+q_2^-+q_3^-+q_4^-\Big)^2} \\ + \frac{\mathcal{R}\Big(s;\mathcal{Q}^-(q_1,q_2,q),\mathcal{Q}^-(q_3,q_4,-q)\Big)}{q^+}\Big(\gamma^\alpha q_\alpha + m_q\Big). \tag{5.153}$$

We need to determine the divergence (or lack thereof) in $\Pi_{\mu\nu}$ as $s_r \to 0$. We know that without the effective exchange term (the second term in $\Pi_{\mu\nu}$), this term will diverge because the form factor in the first term of $\Pi_{\mu\nu}$ cannot dampen the $1/q^+$. The only hope that this converges if if the addition of the second term makes all of $\Pi_{\mu\nu}$ finite.

We can split $\Pi_{\mu\nu}$ into two parts:

$$\frac{\mathcal{R}\Big(s;\mathcal{Q}^-(q_1,q_2,q),\mathcal{Q}^-(q_3,q_4,-q)\Big)}{q^+}\Big(\frac{1}{2}q^+\gamma^- - q^\perp\ \cdot\gamma^\perp + m_q\Big). \tag{5.154}$$

which we know from the previous calculations that the numerator will regulate the $1/q^+$ factor, rendering this term finite. The other term is

$$f\Big(s;\mathcal{Q}^-(q_1,q_2,q_3,q_4)\Big)\frac{\gamma^+}{2}\Bigg[\frac{1}{q^+} + \frac{q^-}{2q^+}\Bigg(\frac{1}{\mathcal{Q}^-(q_1,q_2,q)} - \frac{1}{\mathcal{Q}^-(q_3,q_4,-q)}\Bigg) \\ \cdot\Bigg(\frac{f\Big(s;\mathcal{Q}^-(q_1,q_2,q)\Big)f\Big(s;\mathcal{Q}^-(q_3,q_4,-q)\Big)}{f\Big(s;\mathcal{Q}^-(q_1,q_2,q_3,q_4)} - 1\Bigg)\Bigg] \tag{5.155}$$

which further splits into two terms, one of which is clearly finite because of the form factors:

$$\frac{q^-}{2q^+}\left(\frac{1}{\mathcal{Q}^-(q_1,q_2,q)}-\frac{1}{\mathcal{Q}^-(q_3,q_4,-q)}\right)\frac{f\Big(s;\mathcal{Q}^-(q_1,q_2,q)\Big)f\Big(s;\mathcal{Q}^-(q_3,q_4,-q)\Big)}{f\Big(s;\mathcal{Q}^-(q_1,q_2,q_3,q_4)\Big)}. \tag{5.156}$$

The other term (disregarding the factor of $f\Big(s;\mathcal{Q}^-(q_1,q_2,q_3,q_4)\Big)\gamma^+/2$ which is finite) is

$$\frac{1}{q^+}-\frac{q^-}{2q^+}\left(\frac{1}{\mathcal{Q}^-(q_1,q_2,q)}-\frac{1}{\mathcal{Q}^-(q_3,q_4,-q)}\right), \tag{5.157}$$

which does not have form factors to regulate it. Nevertheless, we simplify it:

$$\begin{aligned}
&\frac{1}{q^+}-\frac{q^-}{2q^+}\left(\frac{1}{q_1^-+q_2^-+q^-}-\frac{1}{q_3^-+q_4^--q^-}\right)\\
&\quad=\frac{1}{2q^+}\left(2-\frac{q^-}{q_1^-+q_2^-+q^-}-\frac{q^-}{q_3^-+q_4^--q^-}\right)\\
&\quad=\frac{1}{2q^+}\left(\frac{q_1^-+q_2^-+q^--q^-}{q_1^-+q_2^-+q^-}+\frac{q_1^-+q_2^-+q^--q^-}{q_3^-+q_4^--q^-}\right)\\
&\quad=\frac{1}{2}\left(\frac{q_1^-+q_2^-}{q^2-(q_1+q_2)^2}-\frac{q_3^-+q_4^-}{q^2-(q_3+q_4)^2}\right),
\end{aligned} \tag{5.158}$$

which now is obviously finite as $q^+\to 0$. Therefore

$$\lim_{q^+\to 0}\Pi_{\mu\nu}\Big(s;q_1,q_2,q,q_3,q_4\Big)<\infty. \tag{5.159}$$

Remarkably, the $1/q^+$ singularities that arise in the instantaneous quark exchange are regulated by the addition of the effective quark exchange, i.e. the sum of the two diagrams are finite. Therefore, the limit $s_r\to 0$ can be taken for all quark exchange diagrams

$$H_{\bar\psi AA\psi}(s,s_r)\to H_{\bar\psi AA\psi}(s). \tag{5.160}$$

In summary, we have determined the quark exchange diagrams that compose $H_{\bar\psi AA\psi}(s)$ are finite and s_r can be sent to zero. We also discovered for the gluon

exchange terms, even the combination of the instantaneous and effective gluon exchange terms will lead to small q^+ divergences. These gluon exchange terms each now require a counterterm

$$\propto -\int_q \delta(q^+)\frac{m_g^2}{\Big(m_g^2+(q^\perp)^2\Big)}\sqrt{\frac{\pi}{2s_r}}. \tag{5.161}$$

Lastly, the loop diagrams $H_{\delta m_q^2}(s,s_r)$ and $H_{\delta m_g^2}(s,s_r)$, which diverge in the $s_r\to 0$ limit because of large q^+ were renormalized by adding counterterms to give the effective mass terms.

The full expression for the effective QCD Hamiltonian is

$$\begin{aligned}\mathcal{H}_{\rm QCD}(s) = \mathcal{H}_0(s) &+ g\Big(\mathcal{H}_{\bar\psi\psi A}(s)+\mathcal{H}_{A^3}(s)\Big)\\ &+ g^2\Big(\mathcal{H}_{\bar\psi AA\psi}(s)+\mathcal{H}_{\psi^2A^2}(s)+\mathcal{H}_{A^4}(s)+\mathcal{H}_{\psi^4}(s)\Big),\end{aligned} \tag{5.162}$$

where $\mathcal{H}_{\bar\psi\psi A}(s)=H_{\bar\psi\psi A}(s)$, $\mathcal{H}_{A^3}(s)=H_{A^3}(s)$, and , $\mathcal{H}_{\bar\psi AA\psi}(s)=H_{\bar\psi AA\psi}(s)$(i.e. their effective forms and unitarily transformed forms are the same since they do not require counterterms). The remaining three terms are effective in the sense that they are a sum of their unitarily transformed term plus a counterterm, e.g.

$$\mathcal{H}_0(s)=H_0(s,s_r)+X_0(s_r) \tag{5.163}$$

The addition of counterterms amounts to defining effective vertices:

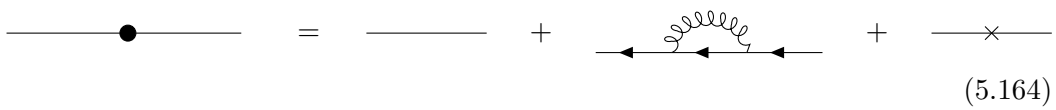

(5.164)

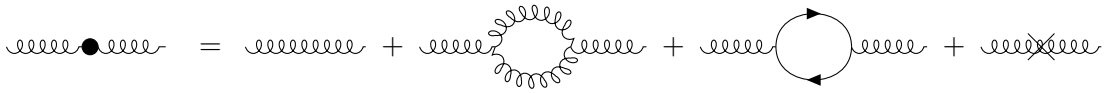

(5.165)

5.4 Preliminary Resource Estimates for Quantum Simulation of Renormalized QCD

In this Section, we provide preliminary results for resource estimates needed to compute the hadronic mass spectrum via quantum simulation. We are interested in costs for full quantum phase estimation on the walk operator encoding $\mathcal{H}_{\mathrm{QCD}}(s)$. We give costs as number of T-gates, number of arbitrary (non-Clifford) rotations, block-encoding ancillae, total number of qubits, and rescaling factor.

The cost associated with a particular unitary, U, is given as C_U, where C refers to the number of T-gates needed to implement U. For n phase qubits, the number of calls to the walk operator is given by[1]

$$\sum_{j=0}^{n-1} 2^j = 2^n - 1. \tag{5.166}$$

Therefore, the cost of QPE is

$$C_{\mathrm{QPE}} = (C_{\text{State Prep.}} + C_{\mathrm{PREPARE}}) + (2^n - 1)C_{W_H} + C_{\mathrm{QFT}_n^\dagger}, \tag{5.167}$$

where

$$C_{W_H} = 2 \cdot C_{\mathrm{PREPARE}} + C_{\mathrm{SELECT}} + C_{\mathrm{Refl}_{|0\rangle_a}}. \tag{5.168}$$

The cost of PREPARE is

$$C_{\mathrm{PREPARE}} \leq L - 1 \text{ Arb. rots.} \approx r\ (L-1) \text{ T gates}, \tag{5.169}$$

where r stands for the ratio of number of T-gates needed to decompose an arbitrary single rotation gate. As a rough estimate, we take $r = 50$ [RS16]. An additional C_{PREPARE} is included after the cost of state preparation because the initial state

[1] Here we use the geometric series

$$\sum_{k=0}^{n} r^k = \frac{1 - r^{n-1}}{1 - r}$$

must be of the form $|0\rangle_{anc.} \otimes \text{ PREP } |\psi\rangle_s$ [PKS+18].

The cost of SELECT is

$$C_{\text{SEL}} = 4 \cdot N_{\text{Elbows}} + r \cdot N_{\text{Arb. rots.}}, \tag{5.170}$$

and the cost of $\text{Refl}_{|0\rangle_{anc}}$ is

$$C_{\text{Refl}_{|0\rangle_a}} = C_{\text{Toff}_{n_a+1}} = 4(n_a + 1) \text{ T gates}, \tag{5.171}$$

where n_a is the number of block-encoding ancillae [CSS18]. Recall that the number of block-encoding ancillae is one more than would be needed in a standard LOBE block-encoding because we add an additional ancillae qubit to make the bosonic unitaries self-inverse. The +1 corresponds to the control on the phase register.

Lastly, the cost of $\text{QFT}^\dagger$ on n-qubits, is

$$C_{\text{QFT}_n^\dagger} = r \cdot n(n+1). \tag{5.172}$$

This number comes from the fact that $\text{QFT}^\dagger$ on n-qubits requires $n(n+1)/2$ arbitrary controlled rotations, which can be implemented with $n(n+1)$ arbitrary rotations. There are approximate QFT circuits which require $\mathcal{O}(n \log n)$ T-gates [NSM20]; however, since this is not the dominating cost of QPE in our construction, we stick to the standard QFT implementation.

Figures 5.2 and 5.3 show resource estimate scalings as a function of K and $K^\perp$ respectively. The first plot fixes $K^\perp = 1$, while the second plot fixes $K = 1$. Given these results, as well as an additional data point at $(K, K^\perp) = (2, 2)$ which requires $76,901,308$ T-gates, $42,965,478$ arbitrary rotations, 27 block-encoding ancillae, a rescaling factor of $1,063,175,421.09$, and 2202 system qubits, we can extrapolate to arbitrary $(K, K^\perp)$.

Using the cost of QPE in Eq. 5.167, we provide approximations to the cost of QPE for a $10 \times 10 \times 10$ lattice in momentum space[2] for varying number of phase

[2]Corresponding to $(K, K^\perp) = (10, 5)$

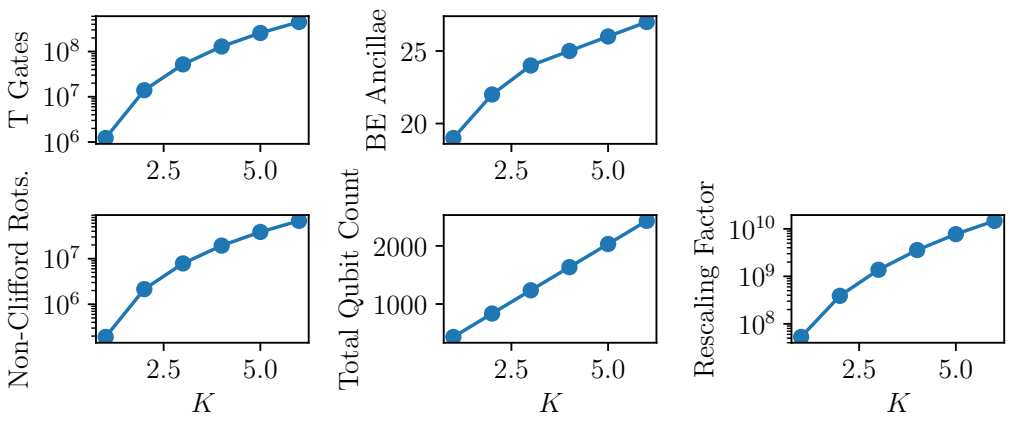

Figure 5.2: **Renormalized QCD Resource Estimates** for a single LOBE block-encoding at fixed $K^{\perp} = 1$. In this plot, $m_q = 1.0$, $m_g = 10^{-2}$, $s = 0.1$, $g = 0.1$.

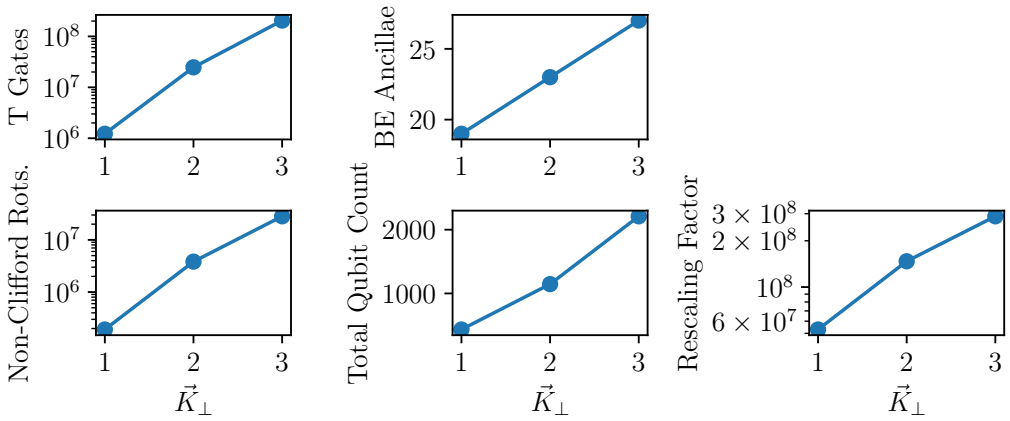

Figure 5.3: **Renormalized QCD Resource Estimates** for a single LOBE block-encoding at fixed $K = 1$. In this plot, $m_q = 1.0$, $m_g = 10^{-2}$, $s = 0.1$, $g = 0.1$.

qubits. Assuming state preparation of a "simple state", i.e. a quark-antiquark state with zero transverse momentum, and each parton sharing $K/2$ longitudinal momentum (which corresponds to a single Fock state), the cost of QPE is shown in Table 5.1

5.5 Chapter 5 Summary

In this Chapter, we provided the renormalized front-form QCD Hamiltonian, devoid of divergent observables stemming from large q^+ and small exchange q^+. This

Table 5.1: An approximate number of T-gates to estimate mass eigenvalues from the renormalized QCD Hamiltonian with QPE with $\epsilon = 10^{-3}$ set as the precision. Note that these are preliminary and quite optimistic, as they do not take the $\mathcal{O}(10^{11})$ rescaling factor into account. A more pesimistic estimate for number of $T-$gates is roughly $10^{14} \times 10^{11} = 10^{25}$ (number of calls $*$ the rescaling factor). Further work needs to be done to properly nail down this number.

# phase qubits	# T-gates
1	$3.99 \cdot 10^{11}$
2	$1.197 \cdot 10^{12}$
4	$5.983 \cdot 10^{12}$
8	$1.017 \cdot 10^{14}$
10	$4.080 \cdot 10^{14}$
11	$8.166 \cdot 10^{14}$

Hamiltonian contains a nonzero gluon mass which gives rise to a term $\sim m_g^2 (A^\perp)^2$, which is absent in a massless gluon Hamiltonian. More tests need to be performed on this Hamiltonian via classical methods to confirm the spectrum matches experimental data, and to study the limit as $m_g \to 0$.

Additionally, we gave preliminary resource estimations for how expensive quantum phase estimation would be to measure the mass spectrum of hadrons from the renormalized QCD Hamiltonian. We give extrapolations for this cost for a $10 \times 10 \times 10$ lattice in momemtum space. Without classical verification of the utility of this Hamiltonian, it is unreasonable to comment on how this compares to lattice gauge theory-based quantum simulation techniques; however, comparable calculations can be found in the following references: [RKP24, KN22]. Further tests of how well this Hamiltonian recovers elementary observables such as the proton and pion mass, chiral condensate, and quark-gluon string breaking serve as future work.

Chapter 6

Conclusion

This thesis proposes an end-to-end framework, starting from a quantum field theory Lagrangian, and ending with physical observables computed via quantum computers. This is an increasingly important problem to study, specifically in the early fault tolerant quantum computing era, in which searches for quantum advantage are vital. We base this framework on top of two pillars: the Renormalization Group Procedure for Effective Particles (RGPEP), and Ladder Operator Block-Encodings (LOBE).

RGPEP defines an effective Hamiltonian, which (excluding counterterms) is unitarily equivalent to the corresponding model, or canonical, Hamiltonian describing a particular quantum field theory. The unitary which defines the effective Hamiltonian is determined perturbatively, as it is in general too difficult to do otherwise. In this thesis, we computed solutions to the RGPEP equation up to second order in the coupling strength only, and determined necessary counterterms to render observables finite. Higher order solutions are of interest and are left for future work.

To use these Hamiltonians for quantum simulation, we developed a new block-encoding framework called Ladder Operator Block-Encoding (LOBE), which takes as input a second-quantized operator, and returns a unitary which efficiently block-encodes the operator. We have shown that given a second-quantized Hamiltonian, it is generally advantageous to use the LOBE framework, rather than mapping

these operators to Pauli operators based on the results in Chapter 3. We argue that you should exploit the natural language that the Hamiltonian is written in, that is if you have a system described by a linear combination of unitaries, then that framework makes sense to use. Alternatively, if you are interested in a theory that is naturally described in second-quantization, mapping this operator to Paulis almost always leads to unecessary overhead. We then extend the LOBE framework to the self-inverse LOBE framework, which guarantees that all of the LOBE unitaries are self-inverse. This is crucial in the construction of the walk operator. This step leads to a simple map from the eigenvalues of the walk operator to the eigenvalues of the operator it block-encodes, a necessary condition for quantum phase estimation.

In summary, this thesis defines the following pipeline:

$$\mathcal{L} \xrightarrow[\text{FF transf.}]{\text{Legendre}} H \xrightarrow{\text{Regulate}} H(s_r) \xrightarrow{U(s)} H(s, s_r) \xrightarrow{+X(s_r)} \mathcal{H}(s) \xrightarrow{\text{SI-LOBE}} \tilde{U}_{\mathcal{H}(s)} \xrightarrow{\text{Qubitization}} W_{\mathcal{H}(s)} \xrightarrow{\text{QPE}} M^2. \tag{6.1}$$

This largely obfuscates the important details – much work needs to go into the pipeline by calculating solutions to the RGPEP equation order-by-order; however, in theory, we have defined an end-to-end approach that given an arbitrary quantum field theory, described by a Lagrangian, one can output the corresponding mass spectrum with quantum phase estimation. This can be extended to computing any observable of interest, such as a PDF or GPD.

A significant result of this thesis, while highly preliminary, is the first calculation for the resource estimates needed for quantum simulation of renormalized QCD in the front-form. It is useful to put these results in context with quantum chemistry. The so-called 'white whale' of quantum chemistry is FeMoCo, which is a molecule microbes in soil use to efficiently convert nitrogen into ammonia. This is a significantly cleaner way to produce ammonia in comparison to the primary man-made procedure via the Haber-Bosch process, which amounts to roughly 3% of global carbon emissions [Ali25]. Efficient quantum algorithms aim to compute properties of FeMoCo, which may lead to a better understanding of how it is produced,

and ultimately could reduce global emissions.

The first estimates for FeMoCo from 2017 suggested 5.0×10^{13} Toffolis and 111 logical qubits [RWS+17]. As of the writing of this thesis, the state-of-the-art estimates require 3.42×10^8 Toffolis and 1132 logical qubits [LKB+25]. In comparison, the original estimates for quantum simulation of QCD require $> 10^{50}$ T-gates and $> 10^6$ qubits [KN22], while current published costs are roughly 1.2×10^{28} T-gates and 6×10^{10} qubits [RKP24]. Even given the preliminary results we've presented in Chapter 5, if quantum simulation of QCD is our 'white whale', then we still have a long way to go. A pessimistic reading of this conclusion may be that quantum simulation of QCD *in any framework* is unfeasible.

Nevertheless, many outstanding problems still require consideration. First of all, the effective QCD Hamiltonian defined in Chapter 5 is untested even on a classical level; that is, we aren't sure if its spectrum will match experiment. A thorough study of the effective QCD Hamiltonian on classical computers, likely with symmetry-adapted basis functions, is necessary to justify its use in quantum simulation. Also, we must study the limit of $m_g \to 0$, to determine the significance of vacuum effects.

At the algorithms level, Trotter-based methods should be considered and cost out for a fair comparison to the LOBE approach. We are largely interested in developing quantum algorithms around the similarity renormalization group flow, and in particular applying the principles of RGPEP to other branches of fundamental physics, such as quantum chemistry and low-energy nuclear physics.

Largely, we hope this thesis acts as proof that quantum simulation of quantum field theories in the front-form using RGPEP and LOBE is a viable framework when compared to alternative approaches. To some extent it is an issue of resources – as a back of the envelope calculation, we can use Google Scholar to find within the last year, $\sim 8,670$ results for 'lattice QCD', $\sim 8,910$ results for 'quantum simulation QCD', ~ 731 results for 'lightfront QCD', and ~ 603 results for 'lightfront quantum simulation of QCD' (although it appears many of these results are not in fact quantum simulation papers). As an additional data point, the search for 'quan-

tum chemistry' yields $\sim 19,800$ results. We argue that the best way to improve the framework described in this thesis is by increasing the number of scientists working on this problem.

Bibliography

[ABC+26] Y. Aoki, T. Blum, S. Collins, L. Del Debbio, M. Della Morte, P. Dimopoulos, X. Feng, M. Golterman, Steven Gottlieb, R. Gupta, G. Herdoíza, P. Hernandez, A. Jüttner, T. Kaneko, E. Lunghi, S. Meinel, C. Monahan, A. Nicholson, T. Onogi, P. Petreczky, A. Portelli, A. Ramos, S. R. Sharpe, J. N. Simone, S. Sint, R. Sommer, N. Tantalo, R. Van de Water, A. Vaquero, U. Wenger, and H. Wittig. Flag review 2024. *Physical Review D*, 113(1), January 2026.

[ACM24] Paul M. Alsing, Carlo Cafaro, and Stefano Mancini. Feynman's "simulating physics with computers", 2024.

[AEWHR24] Amnon Aharony, Ora Entin-Wohlman, David A Huse, and Leo Radzihovsky. *50 Years of the Renormalization Group*. WORLD SCIENTIFIC, 2024.

[Ali25] Oct 2025.

[AP77] Guido Altarelli and G. Parisi. Asymptotic Freedom in Parton Language. *Nucl. Phys. B*, 126:298–318, 1977.

[AZL+21] Yasar Y Atas, Jinglei Zhang, Randy Lewis, Amin Jahanpour, Jan F Haase, and Christine A Muschik. Su (2) hadrons on a quantum computer via a variational approach. *Nature communications*, 12(1):6499, 2021.

[BC09] Dominic W Berry and Andrew M Childs. Black-box hamiltonian simulation and unitary implementation. *arXiv preprint arXiv:0910.4157*, 2009.

[BCC+15] Dominic W. Berry, Andrew M. Childs, Richard Cleve, Robin Kothari, and Rolando D. Somma. Simulating hamiltonian dynamics with a truncated taylor series. *Phys. Rev. Lett.*, 114:090502, Mar 2015.

[BDM+20] M. Benali, C. Desnault, M. Mazouz, Z. Ahmed, H. Albataineh, K. Allada, K. A. Aniol, V. Bellini, W. Boeglin, P. Bertin, M. Brossard, A. Camsonne, M. Canan, S. Chandavar, C. Chen, J. P. Chen, M. Defurne, C. W. de Jager, R. de Leo, A. Deur, L. El Fassi, R. Ent, D. Flay, M. Friend, E. Fuchey, S. Frullani, F. Garibaldi, D. Gaskell, A. Giusa, O. Glamazdin, S. Golge, J. Gomez, O. Hansen, D. Higinbotham, T. Holmstrom, T. Horn, J. Huang, M. Huang, G. M. Huber, C. E. Hyde, S. Iqbal, F. Itard, Ho. Kang, Hy. Kang, A. Kelleher, C. Keppel, S. Koirala, I. Korover, J. J. LeRose, R. Lindgren, E. Long, M. Magne, J. Mammei, D. J. Margaziotis, P. Markowitz, A. MartíJiménez-Argüello, F. Meddi, D. Meekins, R. Michaels, M. Mihovilovic, N. Muangma, C. Muñoz Camacho, P. Nadel-Turonski, N. Nuruzzaman, R. Paremuzyan, R. Pomatsalyuk, A. Puckett, V. Punjabi, Y. Qiang, A. Rakhman, M. N. H. Rashad, S. Riordan, J. Roche, G. Russo, F. Sabatié, K. Saenboonruang, A. Saha, B. Sawatzky, L. Selvy, A. Shahinyan, S. Sirca, P. Solvignon, M. L. Sperduto, R. Subedi, V. Sulkosky, C. Sutera, W. A. Tobias, G. M. Urciuoli, D. Wang, B. Wojtsekhowski, H. Yao, Z. Ye, L. Zana, X. Zhan, J. Zhang, B. Zhao, Z. Zhao, X. Zheng, and P. Zhu. Deeply virtual compton scattering off the neutron. *Nature Physics*, 16(2):191–198, 2020.

[Ben79] Paul Benioff. THE COMPUTER AS A PHYSICAL SYSTEM: A MICROSCOPIC QUANTUM MECHANICAL HAMILTONIAN

MODEL OF COMPUTERS AS REPRESENTED BY TURING MACHINES. 2 1979.

[Bet47] Hans Albrecht Bethe. The electromagnetic shift of energy levels. *Physical Review*, 72(4):339, 1947.

[BG72] C. G. Bollini and J. J. Giambiagi. Dimensional Renormalization: The Number of Dimensions as a Regularizing Parameter. *Nuovo Cim. B*, 12:20–26, 1972.

[BGB+18] Ryan Babbush, Craig Gidney, Dominic W. Berry, Nathan Wiebe, Jarrod McClean, Alexandru Paler, Austin Fowler, and Hartmut Neven. Encoding electronic spectra in quantum circuits with linear t complexity. *Phys. Rev. X*, 8:041015, Oct 2018.

[BPP98] Stanley J Brodsky, Hans-Christian Pauli, and Stephen S Pinsky. Quantum chromodynamics and other field theories on the light cone. *Physics Reports*, 301(4-6):299–486, 1998.

[BW69] Carl M. Bender and Tai Tsun Wu. Anharmonic oscillator. *Phys. Rev.*, 184:1231–1260, Aug 1969.

[BY06] Tim Byrnes and Yoshihisa Yamamoto. Simulating lattice gauge theories on a quantum computer. *Physical Review A—Atomic, Molecular, and Optical Physics*, 73(2):022328, 2006.

[Cal70] Curtis G. Callan. Broken scale invariance in scalar field theory. *Phys. Rev. D*, 2:1541–1547, Oct 1970.

[Cam21] Earl T Campbell. Early fault-tolerant simulations of the hubbard model. *Quantum Science and Technology*, 7(1):015007, nov 2021.

[CGJ19] Shantanav Chakraborty, András Gilyén, and Stacey Jeffery. The power of block-encoded matrix powers: Improved regression techniques via faster hamiltonian simulation. In *46th International Col-*

loquium on Automata, Languages, and Programming (ICALP 2019), pages 33–1. Schloss Dagstuhl–Leibniz-Zentrum für Informatik, 2019.

[Chi09a] Andrew M. Childs. On the relationship between continuous- and discrete-time quantum walk. *Communications in Mathematical Physics*, 294(2):581–603, October 2009.

[Chi09b] Andrew M. Childs. Universal computation by quantum walk. *Phys. Rev. Lett.*, 102:180501, May 2009.

[Chi09c] Andrew M Childs. Universal computation by quantum walk. *Physical review letters*, 102(18):180501, 2009.

[CKS17] Andrew M. Childs, Robin Kothari, and Rolando D. Somma. Quantum algorithm for systems of linear equations with exponentially improved dependence on precision. *SIAM Journal on Computing*, 46(6):1920–1950, January 2017.

[CMN+18] Andrew M Childs, Dmitri Maslov, Yunseong Nam, Neil J Ross, and Yuan Su. Toward the first quantum simulation with quantum speedup. *Proceedings of the National Academy of Sciences*, 115(38):9456–9461, 2018.

[Col11] John Collins. *Foundations of Perturbative QCD*. Cambridge Monographs on Particle Physics, Nuclear Physics and Cosmology. Cambridge University Press, 2011.

[Cop02] Don Coppersmith. An approximate fourier transform useful in quantum factoring. *arXiv preprint quant-ph/0201067*, 2002.

[CSS04] John C. Collins, Davison E. Soper, and George Sterman. Factorization of hard processes in qcd, 2004.

[CSS18] Anirban Narayan Chowdhury, Yigit Subasi, and Rolando D. Somma. Improved implementation of reflection operators, 2018.

[CW12a] Andrew M Childs and Nathan Wiebe. Hamiltonian simulation using linear combinations of unitary operations. *arXiv preprint arXiv:1202.5822*, 2012.

[CW12b] Andrew M. Childs and Nathan Wiebe. Hamiltonian simulation using linear combinations of unitary operations. *Quantum Info. Comput.*, 12(11–12):901–924, November 2012.

[DBK+22] Andrew J Daley, Immanuel Bloch, Christian Kokail, Stuart Flannigan, Natalie Pearson, Matthias Troyer, and Peter Zoller. Practical quantum advantage in quantum simulation. *Nature*, 607(7920):667–676, 2022.

[Die03] Markus Diehl. Generalized parton distributions. *Physics Reports*, 388(2-4):41–277, 2003.

[Dir49] P. A. M. Dirac. Forms of relativistic dynamics. *Rev. Mod. Phys.*, 21:392–399, Jul 1949.

[DiV00] David P. DiVincenzo. The physical implementation of quantum computation. *Fortschritte der Physik*, 48(9–11):771–783, September 2000.

[DN06] Christopher M. Dawson and Michael A. Nielsen. The Solovay-Kitaev algorithm. *Quant. Inf. Comput.*, 6:081–095, 2006.

[DNB+22] Zohreh Davoudi, Ethan T. Neil, Christian W. Bauer, Tanmoy Bhattacharya, Thomas Blum, Peter Boyle, Richard C. Brower, Simon Catterall, Norman H. Christ, Vincenzo Cirigliano, Gilberto Colangelo, Carleton DeTar, William Detmold, Robert G. Edwards, Aida X. El-Khadra, Steven Gottlieb, Rajan Gupta, Daniel C. Hackett, Anna Hasenfratz, Taku Izubuchi, William I. Jay, Luchang Jin, Christopher Kelly, Andreas S. Kronfeld, Christoph Lehner, Huey-Wen Lin, Meifeng Lin, Andrew T. Lytle, Stefan Meinel, Yannick Meurice, Swagato Mukherjee, Amy Nicholson, Sasa Prelovsek, Martin J. Savage,

Phiala E. Shanahan, Ruth S. Van De Water, Michael L. Wagman, and Oliver Witzel. Report of the snowmass 2021 topical group on lattice gauge theory, 2022.

[Dok77] Yuri L. Dokshitzer. Calculation of the Structure Functions for Deep Inelastic Scattering and e+ e- Annihilation by Perturbation Theory in Quantum Chromodynamics. *Sov. Phys. JETP*, 46:641–653, 1977.

[dSAd12] Feliciano de Soto and Jean-Christian Anglès d'Auriac. Yukawa model on a lattice in the quenched approximation. *Phys. Rev. E*, 85:041121, Apr 2012.

[Dys49] Freeman J Dyson. The s matrix in quantum electrodynamics. *Physical Review*, 75(11):1736, 1949.

[EERS21] MG Echevarria, IL Egusquiza, E Rico, and G Schnell. Quantum simulation of light-front parton correlators. *Physical Review D*, 104(1):014512, 2021.

[EK09] Bryan Eastin and Emanuel Knill. Restrictions on transversal encoded quantum gate sets. *Phys. Rev. Lett.*, 102:110502, Mar 2009.

[Fey50] Richard Phillips Feynman. Mathematical formulation of the quantum theory of electromagnetic interaction. *Physical Review*, 80(3):440, 1950.

[Fey18a] Richard P Feynman. Simulating physics with computers. In *Feynman and computation*, pages 133–153. cRc Press, 2018.

[Fey18b] Richard P Feynman. The theory of positrons. In *Quantum Electrodynamics*, pages 167–177. CRC Press, 2018.

[FF65] S. Fubini and G. Furlan. Renormalization effects for partially conserved currents. *Physics Physique Fizika*, 1:229–247, Jan 1965.

[FK72] Jerome I Friedman and Henry W Kendall. Deep inelastic electron scattering. *Annual Review of Nuclear Science*, 22(1):203–254, 1972.

[FMMC12] Austin G Fowler, Matteo Mariantoni, John M Martinis, and Andrew N Cleland. Surface codes: Towards practical large-scale quantum computation. *Physical Review A—Atomic, Molecular, and Optical Physics*, 86(3):032324, 2012.

[Fri12] Harald Fritzsch. The history of qcd. *CERN Courier, Sept*, 27:21–24, 2012.

[GBM98] K. J. Golec-Biernat and A. D. Martin. Off-diagonal parton distributions and their evolution. *Physical Review D*, 59(1), December 1998.

[Geo82] H. Georgi. *LIE ALGEBRAS IN PARTICLE PHYSICS. FROM ISOSPIN TO UNIFIED THEORIES*, volume 54. 1982.

[Geo18] Frédéric Georges. *Deeply virtual Compton scattering at Jefferson Lab.* PhD thesis, Orsay, IPN, 2018.

[GG24] M. Girguś and S. D. Głazek. Spiral flow of quantum quartic oscillator with energy cutoff, 2024.

[GHL11] Gary R. Goldstein, J. Osvaldo Gonzalez Hernandez, and Simonetta Liuti. Flexible parametrization of generalized parton distributions from deeply virtual compton scattering observables. *Phys. Rev. D*, 84:034007, Aug 2011.

[GHP+93] Stanisław Głazek, Avaroth Harindranath, Stephen Pinsky, Junko Shigemitsu, and Kenneth Wilson. Relativistic bound-state problem in the light-front yukawa model. *Phys. Rev. D*, 47:1599–1619, Feb 1993.

[Gid15] Craig Gidney. Constructing large increment gates, Jun 2015.

[Gid18] Craig Gidney. Halving the cost of quantum addition. *Quantum*, 2:74, June 2018.

[GL72] V. N. Gribov and L. N. Lipatov. Deep inelastic e p scattering in perturbation theory. *Sov. J. Nucl. Phys.*, 15:438–450, 1972.

[Gł21] Stanisław D. Głazek. Elementary example of exact effective-hamiltonian computation. *Phys. Rev. D*, 103:014021, Jan 2021.

[Gla12] Stanislaw D. Glazek. Perturbative formulae for relativistic interactions of effective particles, 2012.

[GML54] M. Gell-Mann and F. E. Low. Quantum electrodynamics at small distances. *Phys. Rev.*, 95:1300–1312, Sep 1954.

[Got97] Daniel Gottesman. *Stabilizer codes and quantum error correction*. California Institute of Technology, 1997.

[GR02] Lov Grover and Terry Rudolph. Creating superpositions that correspond to efficiently integrable probability distributions, 2002.

[GRG15] María Gómez-Rocha and Stanisław D. Głazek. Asymptotic freedom in the front-form hamiltonian for quantum chromodynamics of gluons. *Phys. Rev. D*, 92:065005, Sep 2015.

[Gro] Particle Data Group. Structure functions.

[Gro96] Lov K Grover. A fast quantum mechanical algorithm for database search. In *Proceedings of the twenty-eighth annual ACM symposium on Theory of computing*, pages 212–219, 1996.

[GSLW19] András Gilyén, Yuan Su, Guang Hao Low, and Nathan Wiebe. Quantum singular value transformation and beyond: exponential improvements for quantum matrix arithmetics. In *Proceedings of the 51st Annual ACM SIGACT Symposium on Theory of Computing*, pages 193–204, 2019.

[GSS+25] Carter Gustin, William Simon, Kamil Serafin, Alexis Ralli, and Ella Guo. OpenParticle, June 2025.

[GSS+26] Carter M. Gustin, Kamil Serafin, William A. Simon, Alexis Ralli, Gary R. Goldstein, and Peter J. Love. Renormalized yukawa hamiltonian: Spectrum, parton distribution functions, and resource estimates for quantum simulation. *Phys. Rev. D*, 113:016018, Jan 2026.

[GVGR23] Juan José Gálvez-Viruet and María Gómez-Rocha. Cancellation of small-x divergences in the three-gluon-vertex hamiltonian with canonical gluon mass. *Phys. Rev. D*, 108:096001, Nov 2023.

[GW73] David J. Gross and Frank Wilczek. Ultraviolet behavior of non-abelian gauge theories. *Phys. Rev. Lett.*, 30:1343–1346, Jun 1973.

[GW93] Stanisław D. Głazek and Kenneth G. Wilson. Renormalization of hamiltonians. *Phys. Rev. D*, 48:5863–5872, Dec 1993.

[HBP90] Kent Hornbostel, Stanley J. Brodsky, and Hans-Christian Pauli. Light-cone-quantized qcd in 1+1 dimensions. *Phys. Rev. D*, 41:3814–3821, Jun 1990.

[Hil16] J.R. Hiller. Nonperturbative light-front hamiltonian methods. *Progress in Particle and Nuclear Physics*, 90:75–124, September 2016.

[HM84] F. Halzen and Alan D. Martin. *QUARKS AND LEPTONS: AN INTRODUCTORY COURSE IN MODERN PARTICLE PHYSICS*. 1984.

[HS05] Naomichi Hatano and Masuo Suzuki. Finding exponential product formulas of higher orders. In *Quantum annealing and other optimization methods*, pages 37–68. Springer, 2005.

[IY88] K. Igeta and Y. Yamamoto. Quantum mechanical computers with single atom and photon fields. In *International Conference on Quantum Electronics*, page TuI4. Optica Publishing Group, 1988.

[Ji97] Xiangdong Ji. Deeply virtual compton scattering. *Physical Review D*, 55(11):7114, 1997.

[JLP12] Stephen P. Jordan, Keith S. M. Lee, and John Preskill. Quantum algorithms for quantum field theories. *Science*, 336(6085):1130–1133, 2012.

[JLP+25] David Jennings, Matteo Lostaglio, Sam Pallister, Andrew T Sornborger, and Yiğit Subaşı. Randomized adiabatic quantum linear solver algorithm with optimal complexity scaling and detailed running costs, 2025.

[KBB+22] Andreas S. Kronfeld, Tanmoy Bhattacharya, Thomas Blum, Norman H. Christ, Carleton DeTar, William Detmold, Robert Edwards, Anna Hasenfratz, Huey-Wen Lin, Swagato Mukherjee, Konstantinos Orginos, Richard Brower, Vincenzo Cirigliano, Zohreh Davoudi, Bálint Jóo, Chulwoo Jung, Christoph Lehner, Stefan Meinel, Ethan T. Neil, Peter Petreczky, David G. Richards, Alexei Bazavov, Simon Catterall, Jozef J. Dudek, Aida X. El-Khadra, Michael Engelhardt, George T. Fleming, Joel Giedt, Rajan Gupta, Maxwell T. Hansen, Taku Izubuchi, Frithjof Karsch, Jack Laiho, Keh-Fei Liu, Aaron S. Meyer, Enrico Rinaldi, Martin Savage, David Schaich, Phiala E. Shanahan, Stephen R. Sharpe, Raza Sufian, Sergey Syritsyn, Ruth S. Van de Water, Michael L. Wagman, Evan Weinberg, Oliver Witzel, Christopher Aubin, Peter Boyle, Shailesh Chandrasekharan, Ian C. Clöet, Martha Constantinou, Kimmy Cushman, Thomas DeGrand, Zoltan Fodor, Sam Foreman, Steven Gottlieb, Daniel Hoying, Yong-Chull Jang, William I. Jay, Xiao-Yong Jin, Christopher Kelly, Julius Kuti, Henry Lamm, Meifeng Lin, Yin Lin, Andrew T. Lytle, Paul Mackenzie, Jeffrey Mandula, Yannick Meurice, Christopher Monahan, Colin Morningstar, James C. Osborn, Sungwoo Park, James N. Simone, Alexei Strelchenko, Masaaki Tomii, Ale-

jandro Vaquero, Pavlos Vranas, Bigeng Wang, Walter Wilcox, Boram Yoon, and Yong Zhao. Lattice qcd and particle physics, 2022.

[Kir23] William M. Kirby. *Contextuality and Sparsity in Quantum Algorithms*. PhD thesis, 2023. Copyright - Database copyright ProQuest LLC; ProQuest does not claim copyright in the individual underlying works; Last updated - 2023-03-10.

[Kit95] A Yu Kitaev. Quantum measurements and the abelian stabilizer problem. *arXiv preprint quant-ph/9511026*, 1995.

[Kit97] A. Yu. Kitaev. Quantum computations: algorithms and error correction. *Russian Math Surveys*, 52:1191–1249, 1997.

[KJK+21a] Michael Kreshchuk, Shaoyang Jia, William M. Kirby, Gary Goldstein, James P. Vary, and Peter J. Love. Light-Front Field Theory on Current Quantum Computers. *Entropy*, 23(5):597, 2021.

[KJK+21b] Michael Kreshchuk, Shaoyang Jia, William M. Kirby, Gary Goldstein, James P. Vary, and Peter J. Love. Simulating Hadronic Physics on NISQ devices using Basis Light-Front Quantization. *Phys. Rev. A*, 103(6):062601, 2021.

[KKG+22] Michael Kreshchuk, William M. Kirby, Gary Goldstein, Hugo Beauchemin, and Peter J. Love. Quantum simulation of quantum field theory in the light-front formulation. *Phys. Rev. A*, 105:032418, Mar 2022.

[KN22] Angus Kan and Yunseong Nam. Lattice quantum chromodynamics and electrodynamics on a universal quantum computer, 2022.

[KS70] John B. Kogut and Davison E. Soper. Quantum electrodynamics in the infinite-momentum frame. *Phys. Rev. D*, 1:2901–2914, May 1970.

[KS75] John Kogut and Leonard Susskind. Hamiltonian formulation of wilson's lattice gauge theories. *Phys. Rev. D*, 11:395–408, Jan 1975.

[LBH+25] N. Lacroix, A. Bourassa, F. J. H. Heras, L. M. Zhang, J. Bausch, A. W. Senior, T. Edlich, N. Shutty, V. Sivak, A. Bengtsson, M. McEwen, O. Higgott, D. Kafri, J. Claes, A. Morvan, Z. Chen, A. Zalcman, S. Madhuk, R. Acharya, L. Aghababaie Beni, G. Aigeldinger, R. Alcaraz, T. I. Andersen, M. Ansmann, F. Arute, K. Arya, A. Asfaw, J. Atalaya, R. Babbush, B. Ballard, J. C. Bardin, A. Bilmes, S. Blackwell, J. Bovaird, D. Bowers, L. Brill, M. Broughton, D. A. Browne, B. Buchea, B. B. Buckley, T. Burger, B. Burkett, N. Bushnell, A. Cabrera, J. Campero, H. S. Chang, B. Chiaro, L. Y. Chih, A. Y. Cleland, J. Cogan, R. Collins, P. Conner, W. Courtney, A. L. Crook, B. Curtin, S. Das, S. Demura, L. De Lorenzo, A. Di Paolo, P. Donohoe, I. Drozdov, A. Dunsworth, A. Eickbusch, A. Moshe Elbag, M. Elzouka, C. Erickson, V. S. Ferreira, L. Flores Burgos, E. Forati, A. G. Fowler, B. Foxen, S. Ganjam, G. Garcia, R. Gasca, É. Genois, W. Giang, D. Gilboa, R. Gosula, A. Grajales Dau, D. Graumann, A. Greene, J. A. Gross, T. Ha, S. Habegger, M. Hansen, M. P. Harrigan, S. D. Harrington, S. Heslin, P. Heu, R. Hiltermann, J. Hilton, S. Hong, H. Y. Huang, A. Huff, W. J. Huggins, E. Jeffrey, Z. Jiang, X. Jin, C. Joshi, P. Juhas, A. Kabel, H. Kang, A. H. Karamlou, K. Kechedzhi, T. Khaire, T. Khattar, M. Khezri, S. Kim, P. V. Klimov, B. Kobrin, A. N. Korotkov, F. Kostritsa, J. Mark Kreikebaum, V. D. Kurilovich, D. Landhuis, T. Lange-Dei, B. W. Langley, P. Laptev, K. M. Lau, J. Ledford, K. Lee, B. J. Lester, L. Le Guevel, W. Yan Li, Y. Li, A. T. Lill, W. P. Livingston, A. Locharla, E. Lucero, D. Lundahl, A. Lunt, A. Maloney, S. Mandrà, L. S. Martin, O. Martin, C. Maxfield, J. R. McClean, S. Meeks, A. Megrant, K. C. Miao, R. Molavi, S. Molina, S. Montazeri, R. Movassagh, C. Neill, M. Newman, A. Nguyen, M. Nguyen, C. H. Ni, M. Y. Niu, L. Oas, W. D. Oliver, R. Orosco, K. Ottosson, A. Pizzuto, R. Potter, O. Pritchard, C. Quintana, G. Ramachandran,

M. J. Reagor, R. Resnick, D. M. Rhodes, G. Roberts, E. Rosenberg, E. Rosenfeld, E. Rossi, P. Roushan, K. Sankaragomathi, H. F. Schurkus, M. J. Shearn, A. Shorter, V. Shvarts, S. Small, W. Clarke Smith, S. Springer, G. Sterling, J. Suchard, A. Szasz, A. Sztein, D. Thor, E. Tomita, A. Torres, M. Mert Torunbalci, A. Vaishnav, J. Vargas, S. Vdovichev, G. Vidal, C. Vollgraff Heidweiller, S. Waltman, J. Waltz, S. X. Wang, B. Ware, T. Weidel, T. White, K. Wong, B. W. K. Woo, M. Woodson, C. Xing, Z. Jamie Yao, P. Yeh, B. Ying, J. Yoo, N. Yosri, G. Young, Y. Zhang, N. Zhu, N. Zobrist, H. Neven, P. Kohli, A. Davies, S. Boixo, J. Kelly, C. Jones, C. Gidney, and K. J. Satzinger. Scaling and logic in the colour code on a superconducting quantum processor. *Nature*, 645(8081):614–619, 2025.

[LC17a] Guang Hao Low and Isaac L Chuang. Optimal hamiltonian simulation by quantum signal processing. *Physical review letters*, 118(1):010501, 2017.

[LC17b] Guang Hao Low and Isaac L. Chuang. Optimal hamiltonian simulation by quantum signal processing. *Phys. Rev. Lett.*, 118:010501, Jan 2017.

[LC19a] Guang Hao Low and Isaac L. Chuang. Hamiltonian Simulation by Qubitization. *Quantum*, 3:163, July 2019.

[LC19b] Guang Hao Low and Isaac L Chuang. Hamiltonian simulation by qubitization. *Quantum*, 3:163, 2019.

[LG95] H. Liebl and Gary R. Goldstein. Electromagnetic polarizabilities and charge radii of the nucleons in the diquark-model. *Physics Letters B*, 343(1–4):363–368, January 1995.

[Lin22] Lin Lin. Lecture notes on quantum algorithms for scientific computation. *arXiv preprint arXiv:2201.08309*, 2022.

[Lin23] Huey-Wen Lin. Overview of lattice results for hadron structure. *Few-Body Systems*, 64(3):58, 2023.

[LKB+25] Guang Hao Low, Robbie King, Dominic W. Berry, Qiushi Han, A. Eugene DePrince, Alec F. White, Ryan Babbush, Rolando D. Somma, and Nicholas C. Rubin. Fast quantum simulation of electronic structure by spectral amplification. *Phys. Rev. X*, 15:041016, Oct 2025.

[LKS70] H. Leutwyler, J. R. Klauder, and L. Streit. Quantum field theory on lightlike slabs. *Il Nuovo Cimento A (1965-1970)*, 66(3):536–554, 1970.

[LL93] A. K. (Arjen K.) Lenstra and H. W. Lenstra. *The development of the number field sieve*. Lecture notes in mathematics, 1554. Springer-Verlag, Berlin ;, 1993.

[Llo96] Seth Lloyd. Universal quantum simulators. *Science*, 273(5278):1073–1078, 1996.

[LS78] H. Leutwyler and J. Stern. Relativistic dynamics on a null plane. *Annals of Physics*, 112(1):94–164, 1978.

[Mac22] R. Machleidt. *Phenomenology and Meson Theory of Nuclear Forces*, pages 1–53. 2022.

[Man80] Vychislimoe i nevychislimoe (computable and noncomputable). 1980.

[Mez22] Cédric Mezrag. An introductory lecture on generalised parton distributions. *Few-Body Systems*, 63(3), August 2022.

[Mic00] Michelangelo L. Mangano . Introduction to QCD, August 2000.

[Mie98] A. Mielke. Flow equations for band-matrices. *The European Physical Journal B*, 5(3):605–611, October 1998.

[MMK+95] C. Monroe, D. M. Meekhof, B. E. King, W. M. Itano, and D. J. Wineland. Demonstration of a fundamental quantum logic gate. *Phys. Rev. Lett.*, 75:4714–4717, Dec 1995.

[MRTC21a] John M Martyn, Zane M Rossi, Andrew K Tan, and Isaac L Chuang. Grand unification of quantum algorithms. *PRX quantum*, 2(4):040203, 2021.

[MRTC21b] John M. Martyn, Zane M. Rossi, Andrew K. Tan, and Isaac L. Chuang. Grand unification of quantum algorithms. *PRX Quantum*, 2:040203, Dec 2021.

[MTK+23] J Morgner, B Tu, CM König, T Sailer, F Heiße, H Bekker, B Sikora, C Lyu, VA Yerokhin, Z Harman, et al. Stringent test of qed with hydrogen-like tin. *Nature*, 622(7981):53–57, 2023.

[MTV20] Niklas Mueller, Andrey Tarasov, and Raju Venugopalan. Deeply inelastic scattering structure functions on a hybrid quantum computer. *Physical Review D*, 102(1):016007, 2020.

[MVBS04] Mikko Mottonen, Juha J. Vartiainen, Ville Bergholm, and Martti M. Salomaa. Transformation of quantum states using uniformly controlled rotations, 2004.

[NC10] Michael A. Nielsen and Isaac L. Chuang. *Quantum Computation and Quantum Information: 10th Anniversary Edition*. Cambridge University Press, 2010.

[NIS] NIST. Fundamental physical constants: proton mass.

[NSM20] Yunseong Nam, Yuan Su, and Dmitri Maslov. Approximate quantum fourier transform with o(n log(n)) t gates. *npj Quantum Information*, 6(1):26, 2020.

[PKS+18] David Poulin, Alexei Kitaev, Damian S Steiger, Matthew B Hastings, and Matthias Troyer. Quantum algorithm for spectral measurement with a lower gate count. *Physical review letters*, 121(1):010501, 2018.

[Pol73] H. David Politzer. Reliable perturbative results for strong interactions? *Phys. Rev. Lett.*, 30:1346–1349, Jun 1973.

[Pre18] John Preskill. Quantum computing in the nisq era and beyond. *Quantum*, 2:79, August 2018.

[Pre25] John Preskill. Beyond nisq: The megaquop machine. *ACM Transactions on Quantum Computing*, 6(3):1–7, April 2025.

[PS95] Michael E. Peskin and Daniel V. Schroeder. *An Introduction to quantum field theory*. Addison-Wesley, Reading, USA, 1995.

[PSCMAC21] Adrián Pérez-Salinas, Juan Cruz-Martinez, Abdulla A Alhajri, and Stefano Carrazza. Determining the proton content with a quantum computer. *Physical Review D*, 103(3):034027, 2021.

[PV49] W. Pauli and F. Villars. On the invariant regularization in relativistic quantum theory. *Rev. Mod. Phys.*, 21:434–444, Jul 1949.

[Qia20] Wenyang Qian. *Relativistic bound states within Basis Light-Front Quantization*. PhD thesis, Iowa State U. (main), Iowa State U. (main), 2020.

[RGR+25] Emma Rosenfeld, Craig Gidney, Gabrielle Roberts, Alexis Morvan, Nathan Lacroix, Dvir Kafri, Jeffrey Marshall, Ming Li, Volodymyr Sivak, Dmitry Abanin, Amira Abbas, Rajeev Acharya, Laleh Aghababaie Beni, Georg Aigeldinger, Ross Alcaraz, Sayra Alcaraz, Trond I. Andersen, Markus Ansmann, Frank Arute, Kunal Arya, Walt Askew, Nikita Astrakhantsev, Juan Atalaya, Ryan Babbush, Brian Ballard, Joseph C. Bardin, Hector Bates, Andreas Bengtsson, Majid Bigdeli Karimi, Alexander Bilmes, Simon Bilodeau,

Felix Borjans, Jenna Bovaird, Dylan Bowers, Leon Brill, Peter Brooks, Michael Broughton, David A. Browne, Brett Buchea, Bob B. Buckley, Tim Burger, Brian Burkett, Nicholas Bushnell, Jamal Busnaina, Anthony Cabrera, Juan Campero, Hung-Shen Chang, Silas Chen, Zijun Chen, Ben Chiaro, Liang-Ying Chih, Agnetta Y. Cleland, Bryan Cochrane, Matt Cockrell, Josh Cogan, Paul Conner, Harold Cook, Rodrigo G. Cortiñas, William Courtney, Alexander L. Crook, Ben Curtin, Martin Damyanov, Sayan Das, Dripto M. Debroy, Sean Demura, Paul Donohoe, Ilya Drozdov, Andrew Dunsworth, Valerie Ehimhen, Alec Eickbusch, Aviv Moshe Elbag, Lior Ella, Mahmoud Elzouka, David Enriquez, Catherine Erickson, Lara Faoro, Vinicius S. Ferreira, Marcos Flores, Leslie Flores Burgos, Sam Fontes, Ebrahim Forati, Jeremiah Ford, Brooks Foxen, Masaya Fukami, Alan Wing Lun Fung, Lenny Fuste, Suhas Ganjam, Gonzalo Garcia, Christopher Garrick, Robert Gasca, Helge Gehring, Robert Geiger, Élie Genois, William Giang, Dar Gilboa, James E. Goeders, Edward C. Gonzales, Raja Gosula, Stijn J. de Graaf, Alejandro Grajales Dau, Dietrich Graumann, Joel Grebel, Alex Greene, Jonathan A. Gross, Jose Guerrero, Loïck Le Guevel, Tan Ha, Steve Habegger, Tanner Hadick, Ali Hadjikhani, Michael C. Hamilton, Monica Hansen, Matthew P. Harrigan, Sean D. Harrington, Jeanne Hartshorn, Stephen Heslin, Paula Heu, Oscar Higgott, Reno Hiltermann, Jeremy Hilton, Hsin-Yuan Huang, Mike Hucka, Christopher Hudspeth, Ashley Huff, William J. Huggins, Lev B. Ioffe, Evan Jeffrey, Shaun Jevons, Zhang Jiang, Xiaoxuan Jin, Chaitali Joshi, Pavol Juhas, Andreas Kabel, Hui Kang, Kiseo Kang, Amir H. Karamlou, Ryan Kaufman, Kostyantyn Kechedzhi, Tanuj Khattar, Mostafa Khezri, Seon Kim, Paul V. Klimov, Can M. Knaut, Bryce Kobrin, Alexander N. Korotkov, Fedor Kostritsa, John Mark Kreikebaum, Ryuho Kudo, Ben Kueffler, Arun Kumar, Vladislav D. Kurilovich,

Vitali Kutsko, Tiano Lange-Dei, Brandon W. Langley, Pavel Laptev, Kim-Ming Lau, Emma Leavell, Justin Ledford, Joy Lee, Kenny Lee, Brian J. Lester, Wendy Leung, Lily Li, Wing Yan Li, Alexander T. Lill, William P. Livingston, Matthew T. Lloyd, Aditya Locharla, Laura De Lorenzo, Erik Lucero, Daniel Lundahl, Aaron Lunt, Sid Madhuk, Aniket Maiti, Ashley Maloney, Salvatore Mandrà, Leigh S. Martin, Orion Martin, Eric Mascot, Paul Masih Das, Dmitri Maslov, Melvin Mathews, Cameron Maxfield, Jarrod R. McClean, Matt McEwen, Seneca Meeks, Anthony Megrant, Kevin C. Miao, Zlatko K. Minev, Reza Molavi, Sebastian Molina, Shirin Montazeri, Charles Neill, Michael Newman, Anthony Nguyen, Murray Nguyen, Chia-Hung Ni, Murphy Yuezhen Niu, Nicholas Noll, Logan Oas, William D. Oliver, Raymond Orosco, Kristoffer Ottosson, Alice Pagano, Agustin Di Paolo, Sherman Peek, David Peterson, Alex Pizzuto, Elias Portoles, Rebecca Potter, Orion Pritchard, Michael Qian, Chris Quintana, Ganesh Ramachandran, Arpit Ranadive, Matthew J. Reagor, Rachel Resnick, David M. Rhodes, Daniel Riley, Roberto Rodriguez, Emma Ropes, Lucia B. De Rose, Eliott Rosenberg, Dario Rosenstock, Elizabeth Rossi, Pedram Roushan, David A. Rower, Robert Salazar, Kannan Sankaragomathi, Murat Can Sarihan, Max Schaefer, Sebastian Schroeder, Henry F. Schurkus, Aria Shahingohar, Michael J. Shearn, Aaron Shorter, Noah Shutty, Vladimir Shvarts, Spencer Small, W. Clarke Smith, David A. Sobel, Barrett Spells, Sofia Springer, George Sterling, Jordan Suchard, Aaron Szasz, Alexander Sztein, Madeline Taylor, Jothi Priyanka Thiruraman, Douglas Thor, Dogan Timucin, Eifu Tomita, Alfredo Torres, M. Mert Torunbalci, Hao Tran, Abeer Vaishnav, Justin Vargas, Sergey Vdovichev, Guifre Vidal, Benjamin Villalonga, Catherine Vollgraff Heidweiller, Meghan Voorhees, Steven Waltman, Jonathan Waltz, Shannon X. Wang, Danni Wang, Brayden Ware, James D. Watson, Yonghua

Wei, Travis Weidel, Theodore White, Kristi Wong, Bryan W. K. Woo, Christopher J. Wood, Maddy Woodson, Cheng Xing, Z. Jamie Yao, Ping Yeh, Bicheng Ying, Juhwan Yoo, Noureldin Yosri, Elliot Young, Grayson Young, Adam Zalcman, Ran Zhang, Yaxing Zhang, Ningfeng Zhu, Nicholas Zobrist, Zhenjie Zou, Hartmut Neven, Sergio Boixo, Cody Jones, Julian Kelly, Alexandre Bourassa, and Kevin J. Satzinger. Magic state cultivation on a superconducting quantum processor, 2025.

[RKP24] Mason L. Rhodes, Michael Kreshchuk, and Shivesh Pathak. Exponential improvements in the simulation of lattice gauge theories using near-optimal techniques. *PRX Quantum*, 5:040347, Dec 2024.

[RLTC21] Alexis Ralli, Peter J. Love, Andrew Tranter, and Peter V. Coveney. Implementation of measurement reduction for the variational quantum eigensolver. *Phys. Rev. Res.*, 3:033195, Aug 2021.

[RS16] Neil J. Ross and Peter Selinger. Optimal ancilla-free clifford+t approximation of z-rotations, 2016.

[RW] Alexis Ralli and Tim Weaving. Symmer.

[RWL25] Alexis Ralli, Tim Weaving, and Peter J. Love. Noncontextual pauli hamiltonians, 2025.

[RWS+17] Markus Reiher, Nathan Wiebe, Krysta M. Svore, Dave Wecker, and Matthias Troyer. Elucidating reaction mechanisms on quantum computers. *Proceedings of the National Academy of Sciences*, 114(29):7555–7560, 2017.

[Sch48a] Julian Schwinger. On quantum-electrodynamics and the magnetic moment of the electron. *Physical Review*, 73(4):416, 1948.

[Sch48b] Julian Schwinger. Quantum electrodynamics. i. a covariant formulation. *Physical Review*, 74(10):1439, 1948.

[Sch14] Matthew D. Schwartz. *Quantum Field Theory and the Standard Model*. Cambridge University Press, 3 2014.

[Ser19] Kamil Serafin. *Bound states of heavy quarks in renormalization group procedure for QCD*. PhD thesis, Warsaw U., 2019.

[SGL25] Kamil Serafin, Carter M. Gustin, and Peter J. Love. Second-order renormalized hamiltonian of yukawa theory. *Phys. Rev. D*, 112:096003, Nov 2025.

[SGRMG24] Kamil Serafin, María Gómez-Rocha, Jai More, and Stanislaw D Głazek. Dynamics of heavy quarks in the fock space. *Physical Review D*, 109(1):016017, 2024.

[SGS+25] William A. Simon, Carter M. Gustin, Kamil Serafin, Alexis Ralli, Gary R. Goldstein, and Peter J. Love. Ladder Operator Block-Encoding. *Quantum*, 9:1953, December 2025.

[Sho94] Peter W Shor. Algorithms for quantum computation: discrete logarithms and factoring. In *Proceedings 35th annual symposium on foundations of computer science*, pages 124–134. Ieee, 1994.

[Sho95] Peter W. Shor. Scheme for reducing decoherence in quantum computer memory. *Phys. Rev. A*, 52:R2493–R2496, Oct 1995.

[SMK+20] Nicolas P. D. Sawaya, Tim Menke, Thi Ha Kyaw, Sonika Johri, Alán Aspuru-Guzik, and Gian Giacomo Guerreschi. Resource-efficient digital quantum simulation of d-level systems for photonic, vibrational, and spin-s hamiltonians. *npj Quantum Information*, 6(1), June 2020.

[Sop97] Davison E. Soper. Parton distribution functions. *Nuclear Physics B - Proceedings Supplements*, 53(1–3):69–80, February 1997.

[SP00] Sergio Szpigel and Robert J Perry. The similarity renormalization group. *arXiv preprint hep-ph/0009071*, 2000.

[SRRJ+25] Pedro Sales Rodriguez, John M. Robinson, Paul Niklas Jepsen, Zhiyang He, Casey Duckering, Chen Zhao, Kai-Hsin Wu, Joseph Campo, Kevin Bagnall, Minho Kwon, Thomas Karolyshyn, Phillip Weinberg, Madelyn Cain, Simon J. Evered, Alexandra A. Geim, Marcin Kalinowski, Sophie H. Li, Tom Manovitz, Jesse Amato-Grill, James I. Basham, Liane Bernstein, Boris Braverman, Alexei Bylinskii, Adam Choukri, Robert J. DeAngelo, Fang Fang, Connor Fieweger, Paige Frederick, David Haines, Majd Hamdan, Julian Hammett, Ning Hsu, Ming-Guang Hu, Florian Huber, Ningyuan Jia, Dhruv Kedar, Milan Kornjača, Fangli Liu, John Long, Jonathan Lopatin, Pedro L. S. Lopes, Xiu-Zhe Luo, Tommaso Macrì, Ognjen Marković, Luis A. Martínez-Martínez, Xianmei Meng, Stefan Ostermann, Evgeny Ostroumov, David Paquette, Zexuan Qiang, Vadim Shofman, Anshuman Singh, Manuj Singh, Nandan Sinha, Henry Thoreen, Noel Wan, Yiping Wang, Daniel Waxman-Lenz, Tak Wong, Jonathan Wurtz, Andrii Zhdanov, Laurent Zheng, Markus Greiner, Alexander Keesling, Nathan Gemelke, Vladan Vuletić, Takuya Kitagawa, Sheng-Tao Wang, Dolev Bluvstein, Mikhail D. Lukin, Alexander Lukin, Hengyun Zhou, and Sergio H. Cantú. Experimental demonstration of logical magic state distillation. *Nature*, 645(8081):620–625, 2025.

[Suz76] Masuo Suzuki. Generalized trotter's formula and systematic approximants of exponential operators and inner derivations with applications to many-body problems. *Communications in Mathematical Physics*, 51(2):183–190, 1976.

[Sym70] Kurt Symanzik. Small distance behaviour in field theory and power counting. *Communications in Mathematical Physics*, 18:227–246, 1970.

[Sze04a] M. Szegedy. Quantum speed-up of markov chain based algorithms. In *45th Annual IEEE Symposium on Foundations of Computer Science*, pages 32–41, 2004.

[Sze04b] Mario Szegedy. Spectra of quantized walks and a $\sqrt{\delta\epsilon}$ rule, 2004.

[Tay91] Richard E Taylor. Deep inelastic scattering: The early years. *Reviews of Modern Physics*, 63(3):573, 1991.

[Tom46] Sin-itiro Tomonaga. On a relativistically invariant formulation of the quantum theory of wave fields. *Progress of Theoretical Physics*, 1(2):27–42, 1946.

[Tro59] Hale F Trotter. On the product of semi-groups of operators. *Proceedings of the American Mathematical Society*, 10(4):545–551, 1959.

[VHJ+22] James P. Vary, Mengyao Huang, Shreeram Jawadekar, Mamoon Sharaf, Avaroth Harindranath, and Dipankar Chakrabarti. Critical coupling for two-dimensional ϕ^4 theory in discretized light-cone quantization. *Phys. Rev. D*, 105:016020, Jan 2022.

[Weg94] Franz Wegner. Flow-equations for hamiltonians. *Annalen der physik*, 506(2):77–91, 1994.

[Wei66] Steven Weinberg. Dynamics at infinite momentum. *Phys. Rev.*, 150:1313–1318, Oct 1966.

[Wil71] Kenneth G Wilson. Renormalization group and critical phenomena. i. renormalization group and the kadanoff scaling picture. *Physical review B*, 4(9):3174, 1971.

[Wil74] Kenneth G. Wilson. Confinement of quarks. *Phys. Rev. D*, 10:2445–2459, Oct 1974.

[Wil83] Kenneth G. Wilson. The renormalization group and critical phenomena. *Rev. Mod. Phys.*, 55:583–600, Jul 1983.

[Wil90] Kenneth G Wilson. Ab initio quantum chemistry: A source of ideas for lattice gauge theorists. *Nuclear Physics B-Proceedings Supplements*, 17:82–92, 1990.

[Wój12] Krzysztof Piotr Wójcik. Application of a numerical renormalization group procedure to an elementary anharmonic oscillator, 2012.

[YLB+18] Yi-Bo Yang, Jian Liang, Yu-Jiang Bi, Ying Chen, Terrence Draper, Keh-Fei Liu, and Zhaofeng Liu. Proton mass decomposition from the qcd energy momentum tensor. *Phys. Rev. Lett.*, 121:212001, Nov 2018.

[Yuk55] Hideki Yukawa. On the interaction of elementary particles. i. *Progress of Theoretical Physics Supplement*, 1:1–10, 01 1955.

[Zee16] Anthony Zee. *Group Theory in a Nutshell for Physicists*. Princeton University Press, USA, 3 2016.

Acronyms

BLFQ Basis Light-front Quantization.

DGLAP Dokshitzer-Gribov-Lipatov-Alterelli-Parisi.

DIS Deeply Virtual Compton Scattering.

DLCQ Discretized Light-Cone Quantization.

DVCS Deeply Virtual Compton Scattering.

GPD Generalized Parton Distribution Function.

LCO Linear Combination of Operators.

LCU Linear Combination of Unitaries.

PDF Parton Distribution Function.

QCD Quantum Chromodynamics.

QEC Quantum Error Correction.

QED Quantum Electrodynamics.

QFT Quantum Field Theory.

QPE Quantum Phase Estimation.

QSP Quantum Signal Processing.

QSVT Quantum Singular Value Transformation.

RGPEP Renormalization Group Procedure for Effective Particles.

SRG Similarity Renormalization Grouop.

Appendix A

Lebesgue's dominated convergence theorem

Theorem A.0.1 *If* $\left\{f_n(x)\right\}$ *is a set of measurable functions on* $\mathcal{S}$ *that converges pointwise to a function* f*, i.e.*

$$\lim_{n\to\infty} f_n(x) = f(x),$$

and $\exists\ g(x)$ *such that*

$$|f_n(x)| \leq g(x)\ \forall n$$

and

$$\int_{\mathcal{S}} dx g(x) < \infty,$$

then

$$\lim_{n\to\infty} \int_{\mathcal{S}} dx f_n(x) = \int_{\mathcal{S}} dx \lim_{n\to\infty} f_n(x).$$

Appendix B

OpenParticle

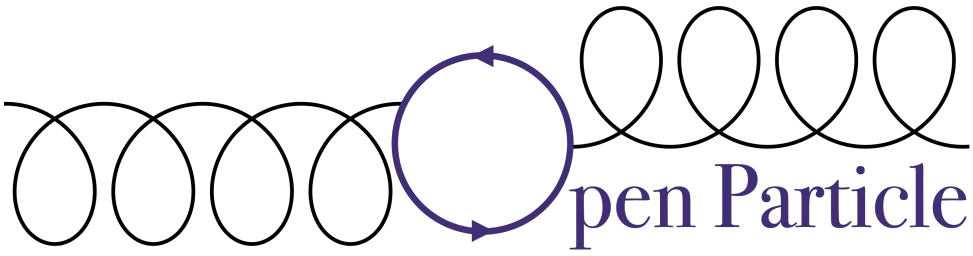

Figure B.1: **OpenParticle Logo**

OpenParticle [GSS+25] is an open source software package designed to solve problems in light-front quantum field theory, and is used in the results throughout this thesis. The main class in this package is the `ParticleOperator()` class, which instantiates products of (anti)fermionic and bosonic ladder operators. For example,

$$b_0^\dagger d_1 a_2 \leftrightarrow \texttt{ParticleOperator('b0^ d1 a2')}. \tag{B.1}$$

The main method in the `ParticleOperator()` class is `.normal_order()`, which reorders an operator such that all creation operators are to the left of annihilation operators by imposing commutation relations.

A child class of `ParticleOperator()` is the `Fock()` class, which stores information about Fock states. For example, given a Fock state with a fermion in mode

0, an antifermion in mode 1 and a two bosons in mode 1, we can represent this as

$$|0_f; 1_{\bar{f}}; 1_b^2\rangle \leftrightarrow \texttt{Fock([0], [1], [(1, 2)])}. \tag{B.2}$$

Under the hood, the Fock object is actually stored as a `ParticleOperator()` as the product of ladder operators that after acting on the vacuum $|\rangle \leftrightarrow$ `Fock()`, will output the Fock object. For example, `Fock([0], [1], [(1, 2)])` is stored as `ParticleOperator('b0^ d1^ a1^ a1^)`.

Lastly, a `ParticleOperator()` can be mapped to Pauli operators with the method `.to_paulis()`. This returns a Symmer [RW] `PauliwordOp()` object. The mappings currently available are Jordan-Wigner for fermions and standard binary for bosons.

Appendix C

Compiling Toffoli Gates

The Toffoli gate is an extremely common quantum gate composed of two-controls and a target, shown in Fig. 1.4. In the Clifford+T gateset, the Toffoli gate is not universal and must be decomposed. Furthermore, general $n-$control gates must be decomposed into Toffoli gates, shown in Fig. C.1. Since many quantum algorithms utilize n-control gates, the scheme chosen for compiling Toffoli gates can have a significant impact on the overall resource estimates of a quantum algorithm.

We compile Toffoli gates with the 'right/left elbow' approach discussed in detail in [BGB$^+$18] and [Gid18]. In comparison to the textbook decomposition of Toffolis (see Fig. 1.4) which requires 7 T-gates, by using "clean ancillae", i.e. ancilla qubits that act like scratch paper and can be used when needed, only 4 T-gates are needed.

The indexing gate used in the SELECT uniatry consists of n-controlled gates in a specific pattern. The work of Ref. [BGB$^+$18] shows that when decomposing the control stucture into elbows, cancellations into CNOT gates can simplify the structure of the cirucit.

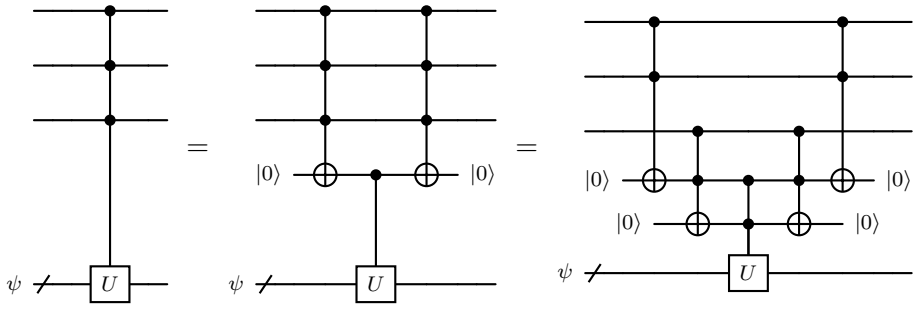

Figure C.1: **Multi-Controlled Operations** Operations with multiple controls are referred to as *multi-controlled operations*. An N-controlled operation can be decomposed into $2(N-1)$ Toffoli gates using $N-1$ clean ancillae. [SGS+25]

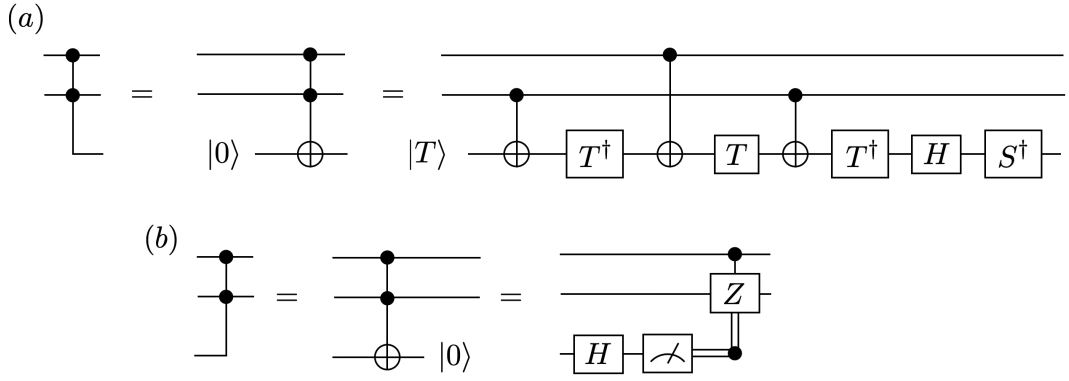

Figure C.2: **Elbows** In (a), a compilation scheme for a Toffoli gate acting on a clean ancillae is shown that uses four T gates. This is sometimes referred to as a "left-elbow". In (b), a compilation scheme for a Toffoli gate that uncomputes a clean ancillae is shown that uses a measurement and classically conditioned operation. This is sometimes referred to as a "right-elbow".

Appendix D

Groups and Representation Theory

Quantum Field Theories are deeply related to group theory. Throughout this thesis, various groups such as $SO(3)$, $SU(2)$, $SU(3)$, and $SO(3,1)$ are referenced. Understanding these groups and their representations is necessary for the work presented here. Much of this appendix follows closely from "Lie Algebras in Particle Physics" by Howard Georgi [Geo82].

D.1 Group Theory

Definition D.1.1 (Group) *A group G is a set of elements $\{g_i\}$ with a rule assigning to every ordered pair of elements, a third element satisfying*

1. *If $g_i, g_j \in G$, then $g_i \cdot g_j \in G$*
2. *For $g_i, g_j, g_k \in G$, $g_i \cdot (g_j \cdot g_k) = (g_i \cdot g_j) \cdot g_k$*
3. *$\exists I \in G$ such that $g_i \cdot I = I \cdot g_i \in G$*
4. *$\forall g_i, \exists g_i^{-1} \in G$ such that $g_i \cdot g_i^{-1} = I$*

The two main types of groups are finite groups, groups such that the number of elements in G is finite, and Lie groups. Additionally, groups are classified as

Abelian or non-Abelian.

Definition D.1.2 (Abelian) *An Abelian group G is one whose group elements commute, i.e. $g_i \cdot g_j = g_j \cdot g_i$.*

D.1.1 Representation Theory

Definition D.1.3 (Representation) *A representation of a group G is a map D of the elements $g_i \in G$ to linear operators on a vector space V i.e. $D : G \to GL(V)$ satisfying*

1. $D(I) = \mathbb{1}$
2. $D(g_i)D(g_j) = D(g_i \cdot g_j)$.

Representations can be classified as either *reducible* or *irreducible*. Given an arbitrary representation $D(g_i)$ it may be possible to construct another representation in two ways. The first is by a similarity transformation $D'(g_i) = S^{-1}D(g_i)S$ (if $\exists$ such a S). The second is by taking a direct product of representations $D(g_i) \oplus D'(g_i)$. These two representations are reducible.

Irreducible representations are those that are not reducible, i.e. not a direct sum, or cannot be transformed under some S. There are an infinite number of reducible representations, so the goal of representation theory is to find all irreducible representations of a given group.

D.1.2 Lie Groups

Lie groups are groups G whose group elements $g_i \in G$ depend on a continuous set of parameters, i.e. $g_i(\theta)$. Any group element can be represented as

$$D(\theta) = e^{i\theta_a X_a}, \tag{D.1}$$

where X_a's are the *generators* of the group G belonging to the group's Lie algebra, $\mathfrak{g}$. Two examples are shown next, $SO(2)$, an Abelian group, and $SO(3)$, a non-Abelian group.

D.1.2.1 $SO(2)$

The group $SO(2)$ is defined as:

$$SO(2) = \Big\{ O \in GL(2) : O^T O = \mathbb{1}, \det O = 1 \Big\}. \tag{D.2}$$

Any matrix $R(\theta) \in SO(2)$ can be written in general as

$$R(\theta) = \begin{pmatrix} \cos\theta & \sin\theta \\ -\sin\theta & \cos\theta \end{pmatrix} \tag{D.3}$$

For infinitesimal rotations:

$$\begin{pmatrix} \cos d\theta & \sin d\theta \\ -\sin d\theta & \cos d\theta \end{pmatrix} = \begin{pmatrix} 1 & d\theta \\ -d\theta & 1 \end{pmatrix} + \mathcal{O}\Big(\theta^2\Big) = \mathbb{1} + d\theta \begin{pmatrix} 0 & 1 \\ -1 & 0 \end{pmatrix} + \mathcal{O}\Big(d\theta^2\Big).$$

This motivates a form of R for infinitesimal $d\theta$: $R(d\theta) \approx \mathbb{1} + A$, where $A = \theta\mathcal{J}$. To satisfy $R^T R = \mathbb{1}$:

$$R^T R \approx (\mathbb{1} + A^T)(\mathbb{1} + A) = \mathbb{1} + A + A^T + \mathcal{O}\Big(A^2\Big).$$

From this, $R^T R = \mathbb{1}$ if and only if $A^T = -A$.

There exists only one 2×2 matrix that satisfies this:

$$\mathcal{J} = \begin{pmatrix} 0 & 1 \\ -1 & 0 \end{pmatrix}.$$

For finite θ, $R(\theta) = \lim_{N\to\infty} R(d\theta/N)^N = \lim_{N\to\infty}(\mathbb{1} + d\theta/N\mathcal{J})^N$. From this, it follows

$$R(\theta) = e^{\theta\mathcal{J}}. \tag{D.4}$$

It's important to note $\mathcal{J} \in \mathfrak{so}(2)$ and since $SO(2)$ is Abelian, its irreducible representation is one dimensional[1]. The representation above in Eq. D.3 is reducible

[1] See Theorem 1.7 in Georgi

becuase we know all of $SO(2)$'s representations must be one-dimensional. In fact, $\exists S$ such that

$$S^{-1}R(\theta)S = \begin{pmatrix} e^{i\theta} & 0 \\ 0 & e^{-i\theta}, \end{pmatrix} \tag{D.5}$$

where $e^{\pm i\theta}$ are two one-dimensional representations of $SO(2)$.

D.1.2.2 $SO(3)$

The group $SO(3)$ is defined as

$$SO(3) = \Big\{ O \in GL(3) : O^T O = \mathbb{1}, \det O = 1 \Big\}. \tag{D.6}$$

Using the motivation from the group $SO(2)$, it is assumed that an element $R(\theta) \in SO(2)$ can be written as $R(d\theta) = \mathbb{1} + A + \mathcal{O}\Big(d\theta^2\Big)$. To satisfy $R^T R = \mathbb{1}$, again it is necessary that $A^T = -A$. There are three 3×3 matrices that satisfy this:

$$\mathcal{J}_x = i \begin{pmatrix} 0 & 0 & 0 \\ 0 & 0 & 1 \\ 0 & -1 & 0 \end{pmatrix}, \qquad \mathcal{J}_y = i \begin{pmatrix} 0 & 0 & -1 \\ 0 & 0 & 0 \\ 1 & 0 & 0 \end{pmatrix}, \qquad \mathcal{J}_z = i \begin{pmatrix} 0 & 1 & 0 \\ -1 & 0 & 0 \\ 0 & 0 & 0 \end{pmatrix}, \tag{D.7}$$

where i is used because of convention.

Any finite rotation can now be generated via

$$R(\theta) = e^{i\theta_l \mathcal{J}_l}. \tag{D.8}$$

The non-Abelianity of $SO(3)$ can be seen by considering $RR'R^{-1}$. If rotations commute, then the following is true: $RR'R^{-1} = RR^{-1}R' = \mathbb{1}R' = R'$. By expliclty computing $RR'R^{-1}$ and comparing the result to R', the measure of commutivity can be determined:

$$RR'R^{-1} \approx (\mathbb{1} + A)(\mathbb{1} + B)(\mathbb{1} - A) \approx \mathbb{1} + B + AB - BA.$$

If these matrices commute, then $RR'R^{-1} = R' \approx \mathbb{1} + B$. It follows that $AB - BA \equiv$

$[A, B]$, the commutator measures the extent the rotation matrices don't commute. Computing the commutators of the three generators of $SO(3)$ in equation D.7 gives the *Lie algebra*, $\mathfrak{so}(3)$:

$$[\mathcal{J}_i, \mathcal{J}_j] = i\epsilon_{ijk}\mathcal{J}_k. \tag{D.9}$$

D.1.3 Representation of Lie Algebras

Representations of Lie groups can be obtained by exponentiating representations of the corresponding Lie algebra [2].

Theorem D.1.1 (Irreducible Representations of $\mathfrak{su}(2)$) *The irreducible representations of $\mathfrak{su}(2)$ are $(2j+1)$-dimensional, where j is a non-negative half-integer.*

Theorem D.1.2 (Irreducible Representations of $\mathfrak{so}(3)$) *The irreducible representations of $\mathfrak{so}(3)$ are $(2j+1)$-dimensional, where j is a non-negative integer.*

[2] pg. 203 "Since we know that rotations are given by exponentials of linear combinations of the $\mathcal{J}$'s, this would lead to matrices representing the rotation group" [Zee16].